Universidade de Aveiro
2020

Departamento de Eletrónica,
Telecomunicações e Informática

JESSICA BARTHOLDY SANSON

ESTUDO DE FORMAS DE ONDA E CONCEÇÃO DE ALGORITMOS PARA OPERAÇÃO CONJUNTA DE SISTEMAS DE COMUNICAÇÃO E RADAR

WAVEFORMS AND ALGORITHMS DESIGN FOR USE IN DUAL COMMUNICATION/RADAR SYSTEMS

Universidade de Aveiro
2020

Departamento de Eletrónica,
Telecomunicações e Informática

JESSICA BARTHOLDY
SANSON

ESTUDO DE FORMAS DE ONDA E CONCEÇÃO DE ALGORITMOS PARA OPERAÇÃO CONJUNTA DE SISTEMAS DE COMUNICAÇÃO E RADAR

WAVEFORMS AND ALGORITHMS DESIGN FOR USE IN DUAL COMMUNICATION/RADAR SYSTEMS

Tese apresentado à Universidade do Minho, Universidade de Aveiro, e Universidade do Porto para cumprimento dos requisitos necessários à obtenção do grau de Doutor em Telecomunicações no âmbito do programa doutoral MAP-tele, realizado sob a orientação científica do Doutor Atílio Manuel da Silva Gameiro, professor associado do Departamento de Eletrónica, Telecomunicações e Informática da Universidade de Aveiro, e sob a coorientação científica do Doutor Daniel Filipe Marques Castanheira, investigador do Instituto de Telecomunicações de Aveiro.

Apoio financeiro da FCT e do FSE no âmbito do III Quadro Comunitário de Apoio. Bolsa FCT ref. PD/BD/128198/2016.

o júri

presidente	Prof. Doutor Vasile Staicu Professor Catedrático, Universidade de Aveiro
vogais	Prof. Doutor Rui Miguel Henriques Dias Morgado Dinis Professor Associado, Universidade Nova Lisboa
	Prof. Doutor Aníbal João de Sousa Ferreira Professor Associado, Universidade do Porto
	Prof. Doutor João Nuno Pimentel da Silva Matos Professor Associado, Universidade de Aveiro
	Prof. Doutor Atílio Manuel da Silva Gameiro Professor Associado, Universidade de Aveiro (orientador)
	Prof. Doutor Marco Alexandre Cravo Gomes Professor Auxiliar, Universidade de Coimbra

agradecimentos

This work was supported by Fundação para a Ciência e a Tecnologia under Ph.D. Grant PD/BD/128195/2016. This scholarship was awarded within the MAP-tele Doctoral Program in Telecommunications. This work was also supported by the European Regional Development Fund (FEDER), through the Competitiveness and Internationalization Operational Programme (COMPETE 2020) of the Portugal 2020 framework, Project, RETIOT, POCI-01-0145-FEDER-016432 and ORCIP-CENTRO-01-0145-FEDER-022141.

First of all, I would like to thank my advisors Prof. Dr. Atilio Gameiro, Dr. Daniel Castanheira and Prof. Dr. Paulo Monteiro, for their candor and their unwavering dedication to helping me in all aspects related to my work during these four years.

I would also like to thank: the Mobile Networks group for the interesting and fruitful discussions regarding this work; the staff at Instituto de Telecomunicações, Polo de Aveiro, including Hugo Mostardinha, Paulo Gonçalves, Nuno Silva, Yannick Sucá, Suzana Condesso, and Dª Elisabete, for their continuous and dependable support; the Department of Electronics, Telecommunications and Informatics and the University of Aveiro for providing a unique environment for personal growth, learning, and creative thinking; and the Instituto de Telecomunicações for providing world-class research facilities, tools and equipment.

I also have to give thanks to my cats, Tesla and Lunastra, for always being cute cats and great companions.

I want to thank my fiancé's family for being like a second family to me in Portugal.

I also want to thank my family and friends, with all my heart, for their unconditional love and support.

And finally, I want to thank my fiancé Pedro for the support, love, companionship, affection, patience, care and dedication in making me happy every day. I also want to thank him not only as my fiancé, but also as my work colleague, for the long technical discussions and laboratory assistance during my Ph.D.

palavras-chave OFDM, Radar, RadCom.

resumo

O foco desta tese é o processamento de sinais e desenvolvimento de algoritmos que podem ser utilizados para a habilitar a função de radar nos sistemas de comunicação. OFDM (Orthogonal Frequency Division Multiplexing) é uma forma de onda com modulação multi-portadora, popular em sistemas de comunicação. Para sistemas de radar, O OFDM melhora a resolução e fornece eficiência espectral, além disso sua diversidade de frequências melhora o desempenho na detecção do radar. Essa tese tem como objetivo utilizar formas de onda multi-portadoras para sistemas de radar, possibilitando a operação simultânea de funções de radar e de comunicação num mesmo dispositivo. A tese esta dividida em duas partes. Na primeira parte da tese são realizados estudos da adaptabilidade de outras formas de onda multi-portadora para funções de radar. Nos dias atuais, muitos estudos sobre o uso do sinal OFDM para funções de comunicação e radar vêm sendo realizados, no entanto, outras formas de onda mostram-se possíveis candidatas a aplicações em sistemas de comunicação, e assim, avaliações para funções de sistema de radar se tornam necessárias. Nesta tese, com a intenção de demonstrar que formas de onda multi-portadoras alternativas podem superar o OFDM nos sistemas de Radar/comunicação (RadCom), propomos a adaptação das seguintes formas de onda: FBMC (Filter Bank Multicarrier); GFDM (Generalized Frequency Division Multiplexing); e UFMC (Universal Filtering Multicarrier) para funções de radar. Também produzimos uma análise de desempenho dessas formas de onda sobre o aspecto da estimativa de parâmetros-alvo, ruído de fundo, interferência entre sistemas e parametrização do sistema. Na segunda parte da tese serão explorados técnicas de processamento de sinal de forma a solucionar algumas das limitações do uso de formas de ondas multi-portadora para sistemas RadCom. Os sistemas de radar baseados no OFDM são candidatos promissores para futuras redes de transporte inteligentes, porque combinam funções de estimativa de alvo com funções de rede de comunicação em um único sistema. Explorando a funcionalidade dupla habilitada pelo OFDM, nesta tese, apresentamos métodos cooperativos de alta resolução para estimar o posição, velocidade e direção dos alvos. A estimativa de parâmetros de alta resolução é um requisito importante para sistemas de radar automotivo, especialmente em cenários de múltiplos alvos que exigem melhor desempenho de separação de alvos. Ao explorar a cooperação entre veículos, os estudos apresentados nesta tese também permitem o rastreamento distribuído de alvos. O resultado é um rastreamento multi-alvo altamente preciso em toda a rede de veículos cooperativos, levando a melhorias na confiabilidade e segurança do transporte.

keywords OFDM, Radar, RadCom.

abstract The focus of this thesis is the processing of signals and design of algorithms that can be used to enable radar functions in communications systems. Orthogonal frequency division multiplexing (OFDM) is a popular multicarrier modulation waveform in communication systems. As a wideband signal, OFDM improves resolution and enables spectral efficiency in radar systems, while also improving detection performance thanks to its inherent frequency diversity. This thesis aims to use multicarrier waveforms for radar systems, to enable the simultaneous operation of radar and communication functions on the same device. The thesis is divided in two parts. The first part, studies the adaptation and application of other multicarrier waveforms to radar functions. At the present time many studies have been carried out to jointly use the OFDM signal for communication and radar functions, but other waveforms have shown to be possible candidates for communication applications. Therefore, studies on the evaluation of the application of these same signals to radar functions are necessary. In this thesis, to demonstrate that other multicarrier waveforms can overcome the OFDM waveform in radar/communication (RadCom) systems, we propose the adaptation of the filter bank multicarrier (FBMC), generalized frequency division multiplexing (GFDM) and universal filtering multicarrier (UFMC) waveforms for radar functions. These alternative waveforms were compared performance-wise regarding achievable target parameter estimation performance, amount of residual background noise in the radar image, impact of intersystem interference and flexibility of parameterization. In the second part of the thesis, signal processing techniques are explored to solve some of the limitations of the use of multicarrier waveforms for RadCom systems. Radar systems based on OFDM are promising candidates for future intelligent transport networks. Exploring the dual functionality enabled by OFDM, we presents cooperative methods for high-resolution delay-Doppler and direction-of-arrival estimation. High-resolution parameter estimation is an important requirement for automotive radar systems, especially in multi-target scenarios that require reliable target separation performance. By exploring the cooperation between vehicles, the studies presented in this thesis also enable the distributed tracking of targets. The result is a highly accurate multi-target tracking across the entire cooperative vehicle network, leading to improvements in transport reliability and safety.

Contents

List of Figures

List of Tables

List of Abbreviations

DoA	Direction-of-Arrival 5, 7, 8, 10, 11, 19–21, 117–122, 124, 127–134, 136, 140, 164, 165, 167–169, 180, 181
DVB	Digital Video Broadcast 15, 16
ESPRIT	Estimation of Signal Parameters via Rotational Invariance Techniques 7, 117, 118, 121–125, 140
FBMC	Filter Bank Multicarrier 5–7, 10, 11, 22, 23, 42, 57–70, 72–74, 78, 98, 101, 109–112, 179, 180
FMCW	Frequency-Modulated Continuous-Wave 28, 29
FS	Frequency Spreading 60
FSK	Frequency Shift Keying 28
GFDM	Generalized Frequency Division Multiplexing 5–7, 9, 11, 22, 23, 77–95, 98, 109–112, 179, 180, 183, 184
ICI	Inter Carrier Interference 37, 80, 98
IDFT	Inverse Discrete Fourier Transform 17, 30, 34, 60, 62, 64, 99, 100, 140
IoT	Internet of Things 3, 4, 14, 59, 98, 111
ISI	Inter Symbol Interference 31, 37, 80
ISM	Industrial Scientific, and Medical 50, 51
ITS	Intelligent Transport System 16, 17
LIDAR	Light Detection And Ranging 158, 159
LTE	Long Term Evolution 14
MF	Matched Filter 82–84, 88, 89
MIMO	Multiple-Input and Multiple-Output 2, 5, 7, 8, 10, 11, 13, 14, 18, 19, 21, 23, 25, 37, 58, 59, 61, 62, 79, 98, 109, 117–119, 124, 127, 128, 131, 133, 157, 159, 170, 175, 176, 180
Min-Norm	Minimum Norm 7, 117, 118, 120–125, 140, 180
MMSE	Minimum Mean Square Error 82, 83

SAR	Synthetic Aperture Radar 2
SFCW	Stepped-Frequency Continuous-Wave 28, 29
SIR	Signal-to-Interference Ratio 73, 92, 105, 106
SISO	Single-Input Single-Output 159, 167, 168, 170
SNR	Signal-to-Noise Ratio 18, 28, 47, 48, 51, 83, 124, 125, 128, 132–134, 137, 153–155, 176
UFMC	Universal Filtering Multicarrier 5–7, 11, 22, 23, 78, 97–107, 109–112, 179, 180
V2I	Vehicle-to-Infrastructure 16
V2V	Vehicle-to-Vehicle 3, 16, 42
V2X	Vehicle-to-Everything 16
VSA	Vector Signal Analyzer 71, 87, 88, 103, 150, 151, 172
VSG	Vector Signal Generator 71, 87, 88, 103, 150, 151, 172
WAVE	Wireless Access in Vehicular Environments 17
ZF	Zero Forcing 82, 83, 88, 89

List of Frequently Used Symbols

$\mathbf{A}(\theta)$	Steering matrix
$\mathbf{A}(\theta_k)$	Steering matrix of the k-th target
$\mathbf{a}_R(\theta_k)$	Steering vector for receiver antennas of the k-th target
$\mathbf{a}_T(\theta_k)$	Steering vector for transmitter antennas of the k-th target
B_W	Bandwidth
c	Speed of light
$\mathbf{D}$	Channel information matrix
$\mathbf{D}_{DoA}$	Channel information matrix relative the direction-of-arrivel estimation
Δf	Subcarrier spacing
Δr	Range resolution
Δv	Velocity resolution
$\mathbf{D}_q$	Channel information matrix of the q-th receiving antenna
d_r	Inter-antenna distance of the receiving antennas
d_t	Inter-antenna distance of the transmitting antennas
f_c	Carrier frequency
f_D	Doppler shift
$f_{D,k}$	Doppler shift realative to the velocity of the target k
K	Number of Targets

λ	Wavelength
$\mathbf{\Lambda}_n$	Diagonal matrices containing the smallest $M_T \times M_R - K$ eigenvalues of a covariance matrix
$\mathbf{\Lambda}_s$	Diagonal matrices containing the largest K eigenvalues of a covariance matrix
M	Number of symbols
M_R	Number of receive antennas
M_T	Number of transmit antennas
N	Number of subcarriers
N_{M_T}	Number of subcarriers allocated to each transmitting antenna
r	Range
$\mathbf{R}_{com}$	Communication covariance matrix relative the direction-of-arrivel estimation
r_k	Range of the k-th target
R_{max}	Unambiguous range
$\mathbf{R}_{radar}$	Radar covariance matrix relative the direction-of-arrivel estimation
$\mathbf{R}_{radcom}$	RadCom covariance matrix relative the direction-of-arrivel estimation
$\mathbf{S}$	Symbols transmited matrix
$\hat{\mathbf{S}}$	Symbols received matrix
$\hat{\mathbf{S}}_q$	Symbols received matrix of the q-th receiving antenna
T	Symbol duration
τ	Delay
T_{CP}	Cyclic prefix duration
θ	Azimuth angle / direction from the signal
θ_k	Azimuth angle / direction from the signal of the k-th target
$\mathbf{U}_n$	Noise subspace with the smallest $M_T \times M_R - K$ eigenvectors of the covariance matrix

$\mathbf{U}_s$	Signal subspace consisting of the largest M_R eigenvalues of the covariance matrix
v	Relative velocity
v_k	Relative velocity of the k-th target
V_{max}	Unambiguous velocity
$\mathbf{Z}$	2D (range and velocity) spectrum
$\mathbf{Z}_{com}$	2D (range and velocity) spectrum of the communication signal
$\mathbf{Z}_{radar}$	2D (range and velocity) spectrum of the radar
$\mathbf{Z}_{radcom}$	2D (range and velocity) spectrum of the RadCom

Notation and Mathematical Operations

Notation

$\mathbf{X}$	Uppercase bold denotes a matrix
$\mathbf{x}$	Lowercase bold denotes a vector
x	Lowercase math denotes a scalar

Mathematical Operations

$(\cdot)^*$	Complex conjugate
$(\cdot)^H$	Conjugate transpose
$(\cdot)^T$	Transpose
$\circledast$	Circular convolution
$\mathbf{0}_n$	$n \times n$ Zero matrix
$\mathbf{I}_n$	$n \times n$ Identity matrix
$\mathrm{DFT}(\cdot)$	Discrete Fourier Transform
$\mathrm{IDFT}(\cdot)$	Inverse Discrete Fourier Transform
$abs(x)/max(abs(\mathbf{x}))$	Normalization operation
$abs\{\cdot\}$	Element-wise absolute value function
$dig\{\cdot\}$	Diagonal matrix operator

$max(\mathbf{x}, \mathbf{y})$	Vector operator with the largest elements taken from $\mathbf{x}$ or $\mathbf{y}$
$max\{\mathbf{x}\}$	Maximum-value element of vector $\mathbf{x}$
$res\{\cdot\}_{n\times m}$	Reshaping vector of size nk in a $n \times m$ matrix
$vec\{\cdot\}$	Vector operator
$\text{circshift}\{n, \mathbf{x}\}$	Circular shift by n samples of $\mathbf{x}$
$\text{rect}(\cdot)$	Rectangular function
$x \; mod \; y$	Modulus after division of x by y

CHAPTER 1

Introduction

This thesis deals with joint operation of communications and radar for future wireless systems. This chapter begins by introducing the multicarrier radar/communication system. Following this, the main aspects and challenges that motivate this thesis are presented. Subsequently, we elaborate the scope of our research and present in detail our contributions to this field, as well as the scientific publications resulting from the developed work. Lastly, we present the outline of this thesis.

1.1 Radar and communication functionalities integration: an overview

Radar detection and wireless communications are among the most prominent radio applications. However, they were studied and developed independently in most cases. Radar & communication (RadCom) system uses the same hardware and signals to perform target detection/tracking and data communication simultaneously [6]. By integrating radar and communication functionalities into one single device, these systems are expected to provide advantages in terms of cost, size and occupied spectrum. RadCom systems have the potential to be employed for area surveillance, search and rescue, and intelligent transportation [7].

The integration of radar and communications will be important for beyond Fifth Generation (5G) systems, where a radar component will add a sensing tool to a telecommunications network. In fact, different technologies and applications can use integrated communication and radar signals. In [8–10] for example, passive radars are used for air, vehicular and even naval traffic control. The use of communication signals for Synthetic Aperture Radar (SAR) was considered in [11, 12]. In [13–15], the authors used an intrapulse radar-embedded communication procedure based on the remodulation of the incident radar signaling, in covert communication for defence-related application. The use of communication signals of mobile personal devices operating as mobile radars for internal mapping has been proposed in [16]. In [17], the use of radar and communication with the same signal for vehicles are considered in transportation systems.

Orthogonal Frequency Division Multiplex (OFDM) can be used to perform radar and communication functions without degrading the performance of any of its subsystems (radar image and data transmission). The use of OFDM for radar was first proposed in [18], and preliminary studies of the integration of radar and communication functionalities were carried out in [19]. A major step in the implementation of OFDM based RadCom systems was presented in [20], where a more efficient and simpler radar processing algorithm was proposed—the direct processing of the modulated symbols instead of the baseband signal. A review of RadCom technology based on OFDM is provided in [21]. OFDM can be used to perform radar and communication without degrading the performance of any of the subsystems as shown in [4, 22–28].

Current radar applications have an important role in many fields where the need for the position, range, and velocity information of objects is crucial. OFDM is suitable for dual use, because the subcarriers can be assigned dynamically to each of the applications as needed. Studies to optimally allocate subcarriers and available energy resources, taking into account restrictions on the performance of radar and communication functions, can be seen in [29–32]. Examples of the use of OFDM in RadCom systems can be seen in [4, 22–28, 33, 34].

The use of RadCom based on Multiple-Input and Multiple-Output (MIMO) systems, already widely used in current communications systems such as Fourth Generation (4G), has been considered. These systems take advantage of the use of multiple transmitting antennas and multiple receiving antennas to exploit the spatial properties of the radio channel, thus increasing the channel capacity in the communication system and adding more benefits from beamforming, both for the communication system (reducing multi-user interference) and radar (to determine the target's position) [19, 35–37].

1.2 Motivation

As referred in the previous section, radar detection and wireless communications have traditionally been studied and developed separately. With the advent of the Internet of Things (IoT) and machine-type communications, it is expected that in the future reflectometry-based techniques will be an important part of the IoT, and radar techniques will be an important enabler of applications such as localization, surveillance etc.

Another point is that the high demand for wireless communications and massive civilian application of radar techniques (automotive being the most important), puts high demands on spectrum, and unless we merge the two technologies we will end up with a fight between radar and wireless communications for spectrum. These two aspects, the expected importance of reflectometry-based techniques in future services and restrictions in the available spectrum, provided the main impetus for the proposal of this thesis.

In the next paragraphs we will detail a little more these aspects.

Examples of joint use

A direct method to improve traffic safety could be conceived from the use of automotive radar along Vehicle-to-Vehicle (V2V) communication. Thus, radio waves used to establish communications between vehicles and infrastructure could be used to detect other cars or obstructing objects. The joint use of radar and communication could also benefit other applications, such as area surveillance and search and rescue.

Economic aspects

In addition, the joint operation of radars and communication systems has positive economic aspects, since both share the same hardware and electromagnetic spectrum, resulting in an economy of devices [38]. The integration of radar operations in cellular networks will open doors for a wide range applications based on refractometry. Thus, research that aims at improving the joint use of radar and communication, has a great importance in the current automotive, smart cities and IoT scenarios.

Enabling techniques

A series of radar applications with communications is already considered viable due to recent advances in digital signal processing, OFDM has become a main candidate due to its orthogonality and ease of implementation, in addition to providing better range resolution [39], spectral efficiency [40], a multicarrier OFDM signal also increases the frequency diversity for the radar system [41]. Accordingly, an OFDM radar may better discriminate a target when other common processing is not effective. This makes OFDM a good choice for such a fusion of systems, particularly in the field of vehicular technology.

Some challenges

Several methods of processing OFDM radar signals with communications systems have been proposed so far, but there are still some problems to be solved that can enable its growth on the radar. Studies for improving target estimates in multi-path environments are important since the radar system is based primarily on signal reflection [42] and within a multi-path environment, where a given transmitted signal not only arrives at the receiver via the line of sight, but also on reflected paths that interact in complex ways with objects (vehicles, people, trees), the correct estimate of the target's position is compromised. Due to the importance of the Doppler estimation, researchers are investigating how to improve it in the case of OFDM radar [43, 44]; for example, in [45] the use of subspace-based methods is considered instead of the usual Discrete Fourier Transform (DFT) [46]. Comparisons and initial evaluations of the use of other waveforms are presented in [47] and [48], but more analyses are still necessary to evaluate their real performance and the possibility of their implementation in real environments. Improvements to problems of canceling interference in a multi-user access environment are fundamental [35, 49], since in the multi-user scenario, the OFDM signal reflected in the receiver contains not only samples of the reflected target, but also interference and noise signals. The importance of this interference cancellation is not only to recover useful data correctly, but also allow a reliable radar estimate.

1.3 Objectives

The main objective of this thesis is the development, study and analysis of signal processing techniques for multicarrier technology (OFDM-type waveforms) targeting the unification of radar and communication technologies. The use of multicarrier waveforms will allow the use of the same signal and device for both radar and communications functions. The flexibility provided by OFDM allows for the dynamic allocation of resources to the communication and radar domains as needed. Motivated by the increasing demands on the performance of automotive radar, the focus of this thesis is the automotive radar/communication system.

Two of the key requirements for future radar and communications systems are flexibility and reconfigurability. However, as described before, it should be noted that despite the benefits brought by the OFDM waveform several problems remain to be solved. Therefore, our main objective is to develop new signal processing techniques to overcome some of these limitations. Namely, the specific objectives of this work were:

- To align with research in communications systems, study alternative candidate multicarrier waveforms for RadCom, such as Universal Filtering Multicarrier (UFMC), Generalized Frequency Division Multiplexing (GFDM) and Filter Bank Multicarrier (FBMC) to investigate their main benefits and drawbacks.

- Study methods to mitigate the interference caused by the presence of other radar sensors (inter-system interference), that is a limiting factor for radar performance.

- Propose new signal processing techniques to overcome the main limitations of the multicarrier waveforms, such as low resolution versus high bandwidth needed, problems for correctly distinguishing targets and others. Take advantage of the communication capability of the multi-carrier waveforms (OFDM) in the system's radar functions, to improve radar operations.

- Study techniques for high resolution estimation of Direction-of-Arrival (DoA) for multicarrier MIMO radars.

- Study and extend the techniques developed for target tracking problems.
- Validate the signal processing methods developed with real measurements at 24 GHz (frequency band for automotive radar).

1.4 Main Contributions

At the present time many studies have been carried out to jointly use the OFDM signal for communication and radar functions, but other waveforms have shown to be possible candidates for communication applications. Therefore, studies on the evaluation of the application of these same signals for radar functions are necessary. In this research, with the intention of demonstrating that alternative multicarrier waveforms can provide increased performance in comparison to the OFDM waveform in RadCom systems, we propose the adaptation of the FBMC, GFDM and UFMC waveforms for radar functions. We have also produced a performance analysis of these alternative waveforms on the aspect of estimating target parameters, background noise, inter-system interference and system parameterization. Also in this research, techniques are proposed to improve the estimation and tracking of targets based on the cooperation of the radar and communication functions of the Radcom system. The following is a brief summary of our contributions to the state of the art in alternative multicarrier waveforms and radar estimation and tracking for RadCom systems.

1.4.1 Alternative multicarrier radar

FBMC radar

We adapted the radar processing of the OFDM signal to be applied in a new FBMC scheme, which is shown to be superior to the OFDM system, since it presents a much higher spectral efficiency. We also evaluated the application FBMC waveform to mitigate inter-system interference in combined radar/communication systems, one limiting factor of the radar's performance. The analysis of FBMC radar is verified with simulations and real measurements at 24 GHz. The results show that FBMC is less affected by inter-system interference than OFDM.

GFDM radar

We proposed the usage of GFDM, a non-orthogonal multicarrier waveform, for radar functions. We presented a novel method that cancels the effect of interference caused by the non-orthogonality of the GFDM waveform in the radar processing, thus not affecting the performance of the radar. This method is validated with simulations and practical measurements at 24 GHz. We also presented GFDM as a solution to mitigate inter-system interference in RadCom systems.

UFMC radar

The use of UFMC signal is presented for radar applications. The UFMC radar presents a superior performance of interference and background noise when compared to the OFDM radar. The analysis of UFMC radar is verified with simulations and real measurements at 24 GHz.

Performance comparison for radar multicarrier waveforms

We compared the FBMC, GFDM, UFMC and OFDM waveforms for radar functions. We have also produced a performance analysis of these alternative waveforms on the aspect of estimating target parameters, background noise, inter-system interference and system parameterization.

1.4.2 Radar estimation and tracking

Comparison of DoA estimation algorithms for MIMO OFDM radar

We compared the performance of the most popular techniques for the DoA estimation in OFDM radar systems. The performance of the Multiple Signal Classification (MUSIC), Estimation of Signal Parameters via Rotational Invariance Techniques (ESPRIT), Minimum Norm (Min-Norm) and Minimum Variance Distortional Response (MVDR) was evaluated using two different metrics; resolution and the probability of target distinction.

High-resolution DoA estimation of closely-spaced and correlated targets

We proposed a new concept of high-resolution DoA estimation in MIMO RadCom systems. High-resolution DoA estimation is an important requirement for automotive radar systems, especially in multi-target scenarios that require higher target separation performance. We presented a subspace-based procedure for high-resolution DoA estimation for closely spaced targets in uncorrelated and partially correlated signals, and allows better DoA estimation in coherent signals. This procedure integrates the use of the radar signal together with the communication signal received from another user (one of the targets to be estimated).

High-resolution delay-Doppler estimation using received communication signal

Exploring the dual functionality enabled by OFDM, we proposed a new cooperative method for high-resolution delay-Doppler estimation. The subspace-based method exploits the combination of both the radar and received communication signals to estimate target parameters. The procedure achieves high-resolution delay-Doppler estimation for both uncorrelated, partially correlated and coherent signals, and enables a significant reduction in the required bandwidth when compared to previous approaches which did not exploit the knowledge of the communication signals. Laboratory measurements at 24 GHz and simulation results demonstrate the efficacy of the proposed method for the estimation of multiple targets.

Cooperative method for distributed target tracking with fusion information

We proposed a new method for distributed target tracking for MIMO RadCom systems. The method employs a cascading information-fusion approach. First, the ego-vehicle performs a multi-target estimation by fusing the radar signals reflected by the targets with the communication signals it receives. Then, the ego-vehicle performs a tracking process, fusing its estimates with the estimates made by other in-network vehicles. By exploring the cooperation between vehicles, the method enables the distributed tracking of targets. The result is a highly accurate multi-target tracking across the entire cooperative vehicle network, leading to improvements in transport reliability and safety. This method is validated with Multi-target tracking results of laboratory measurements at 24 GHz and in simulated environments.

1.5 Publications

From November 2016 to October 2020, this Ph.D. work produced the following contributions:

Papers in Journals

[J1] **J. Sanson**, D. Castanheira, A. Gameiro, and P. Monteiro, "Cooperative Method for Distributed Target Tracking for OFDM Radar with Fusion of Radar and Communication Information," in IEEE Sensors Journal, pp 1-15, Set. 2020.

[J2] **J.Sanson**, P. Tome, D. Castanheira, A. Gameiro, and P. Monteiro, "High-Resolution Delay-Doppler Estimation Using Received Communication Signals for OFDM Radar-Communication System," in IEEE Transactions on Vehicular Technology, pp 1-12, Set. 2020.

[J3] **J. Sanson**, A. Gameiro, D. Castanheira and P. Monteiro, "Non-Orthogonal Multicarrier Waveform for Radar with Communications Systems: 24 GHz GFDM RadCom," in IEEE Access, pp 128694-128705, Set. 2019.

[J4] A. Gameiro, D. Castanheira, **J. Sanson**, and P. Monteiro, "Research challenges, trends and applications for future joint radar communications systems," Wireless Personal Communications, pp. 81–96, May 2018.

Papers in Conferences

[C1] **J. Sanson**, D. Castanheira, A. Gameiro, and P. Monteiro, "Fusion of radar and communication information for tracking in OFDM automotive radar at 24 GHz," in Proc. IEEE MTT-S International Microwave Symposium, Los Angeles, CA, USA, pp 1-4 Jun. 2020.

[C2] J. Sanson, A. Gameiro, D. Castanheira and P. P. Monteiro, "High-Resolution DOA Estimation of Closely-Spaced and Correlated Targets for MIMO OFDM Radar-Communication System", in Proc. IEEE International Symposium on Phased Array Systems and Technology, Boston, MA, USA, pp 1-5, Oct. 2019.

[C3] J. Sanson, A. Gameiro, D. Castanheira and P. Monteiro, "Inter-System Interference Reduction in RadCom Systems - Filter Bank Multicarrier Radar", in Proc. European Radar Conference, Paris, France, pp 77-80, Oct. 2019.

[C4] J. Sanson, A. Gameiro, D. Castanheira and P. Monteiro, "24 GHz Quadrature Amplitude Modulation (QAM)-FBMC Radar with Communication System (RadCom)", in Proc. Asia-Pacific Microwave Conference, Kyoto, Japan, pp 1-3, Aug. 2018.

[C5] J. Sanson, A. Gameiro, D. Castanheira and P. Monteiro, "Comparison of DoA Algorithms for MIMO OFDM Radar", in Proc. European Radar Conference, Madrid, Spain, pp 1-4, Set. 2018.

[C6] J. Sanson, P. Tomé, and P. Georgieva, "Enabling MIMO beaforming through compressed Channel State Information (CSI) feedback based on principal component analysis", in Proc. Portuguese Conf. Pattern Recognition, Amadora, Portugal, pp. 13–14, Oct. 2017.

1.6 Thesis Outline

This document is organized in thirteen chapters. In Chapter 1 the motivation and main contributions of the Ph.D. thesis are presented. Later in Chapter 2 an overview of the current state of the art for RadCom systems is realized. Chapter 3 first reviews the basic concepts of radar systems and OFDM waveform, then the corresponding radar estimation model is presented, and finally the MIMO OFDM radar model is explained. In Chapter 4 the main parameters for RadCom system are discussed and optimized by taking into account the constraints present in the possible application environments.

Chapter 4 concludes the theoretical discussion of this thesis. The following chapters present in detail the work done during this thesis, being divided into two parts. In Part I we study other multicarrier waveforms—most of them 5G candidate waveforms—as an alternative to OFDM to RadCom systems. Part I of the thesis includes Chapters 5, 6, 7 and 8. Chapters 5, 6 and 7 refer to the adaptation of the FBMC, GFDM and UFMC waveforms to RadCom systems, respectively. Chapter 8 compares all waveforms presented in previous chapters and provides concluding remarks about their suitability for RadCom systems.

In Part II new techniques are developed with the aim of improving the resolution of parameter estimation and target tracking techniques available in the literature. Part II includes Chapters 9, 10, 11 and 12. Chapter 9 presents the comparison of the most popular DoA estimation methods for a MIMO OFDM radar system. Based on these methods, Chapter 10 introduces a subspace-based procedure for high-resolution DoA estimation for closely spaced targets in uncorrelated and partially correlated signals. Also to improve the resolution estimation in the radar system, the Chapter 11 presents a high-resolution delay-Doppler estimation method. Chapter 12 integrates all parameter estimation algorithms and presents a new cooperative method for distributed target tracking in MIMO OFDM radar systems.

Finally, in Chapter 13, we summarise the main contributions of the thesis and discuss some possible research topics.

CHAPTER 2

Joint Radar-Communication - State of the Art

THIS chapter describes the state of the art for the joint radar and communications topic. First, a brief overview of the current state of art of communication systems is performed, for later the use of radar with communications systems can be presented next. Extending the discussion of the state of the art on radars integrated with communication systems, studies conducted with MIMO systems for RadCom are presented, and finally, an overview on the use of other waveforms for RadCom systems is carried out.

2.1 Wireless communication systems

In the last century, the revolution in the wireless telecommunications sector has profoundly changed communication, by providing new media for long-distance communication. Everything started with the First Generation (1G) of cellular communications. Second Generation (2G) mobile systems were very successful in the previous decades. Their success has led to the development of Third Generation (3G) mobile systems. 3Gsystems were designed to provide higher data rate services [50]. Subsequently, increasing demands on mobile networks have fueled the need to develop 4G networks, which is OFDM based, including Long Term Evolution (LTE) [51]

With the maturing of 4G standardization and worldwide deployment, data-intensive wireless services have grown in an unprecedented way, representing great pressure on today's wireless systems, which already use advanced technologies, such as MIMO, multiple user diversity, link adaptation, turbo codes, etc. To meet this increased demand, the 5G wireless system is undergoing intensive development, and research on 5G communication technologies has emerged in the academic and industrial communities. Several organizations from different countries and regions have launched initiatives and programs for potential 5G technologies [52].

To allow very high data rates 5G technologies include a millimeter waves component [53]. The use of millimeter waves provides significantly amount of additional spectrum and increasing data capacity. This new technology will allow the exploration of polarization and new spatial processing techniques such as adaptive beamforming and Massive MIMO. Massive MIMO is a new technology that together with the use of the millimeter wave will increase data rates in 5G. According to [54] this technique proposes the use of a very high number of antennas to multiplex data to a smaller number of terminals using the same time frequency resource, concentrating radiated energy to desired directions, minimizing intra and intercellular interference.

5G integrates connectivity and managed services with the IoT, virtual network functions, among others. As Guinard et al. describe in [55], 5G technologies will enable advances in communication systems in IoT, creating new opportunities to develop applications that better integrate the physical world in real time. IoT is a novel networking paradigm and topic of technical, social, and economic importance. Many consumer products, durable goods, vehicles, industrial components, sensors and other everyday objects are being combined with Internet connectivity [56]. However, these new technologies lead to an even greater limitation on the available spectrum. As most IoT technology rely on control and monitoring, reflectometry techniques are required, therefore the integration of sensing and communication functions is extremely important for IoT. For these reasons, the efficient use of spectrum is becoming increasingly important, as a result of this factor, several researches for the joint operation of radar and communication systems have been carried out in recent years [4, 22–28, 33, 34].

2.2 Communication signal used for radar functions

After the use of OFDM in radar was first proposed in [57], preliminary studies on the integration of radar and communication functionalities were carried out in [19]. An initial approach to radar processing is presented in [22] . This method uses the conventional direct matched filtering approach to compute the correlation between transmitted and received signals in an integrated Ultra Wideband OFDM system. A major step in the applicability of the radar system was made in [58], where a more efficient and simpler approach to OFDM radar processing was proposed. This processing technique works directly on the modulated symbols instead of the baseband signal, overcoming the disadvantages of the conventional correlation-based processing that had been proposed until now. Subsequently, in [42], the author proposes a method to remove the influence of communication data on multipath and multiuser environments, and the range resolution has been improved. Based on the mode of operation and the architecture of the system, two distinct modes of radar systems that use communication signals are being studied, passive radar and active radar. In the following sections the two modes will be presented and discussed.

2.2.1 Passive radar: communication signals used as illuminators

The passive radar concept exploits existing transmissions from third party systems as radar illuminators, and process the reflections from the targets to estimate the targets parameters [59]. This type of radar system has a bistatic operation, i.e. the radar system consists of a transmitter and a receiver separated by a considerable distance. This represent an example of radar system that may rely on communication signals. In fact many current communication systems can be used as passive radar sources, including frequency modulated radio, cellular base stations, satellite systems, Digital Audio Broadcasting (DAB) and Digital Video Broadcast (DVB). DVB and DAB transmissions use modulated OFDM signals that can be treated as a special form of radar signal, providing a particularly attractive opportunity for passive radar. Research has shown that digital broadcast communication stations such as DAB or DVB are very promising illuminators, due to their ability to establish a distributed radar network at a single frequency. This passive radar system exploits the digitally synchronized (in the single frequency network) signals of the different transmitters, to detect and track a specific target forming a wide coverage area [60].

The signals of these communication systems are built on a model that includes the data structure, protection intervals and pilot information that is used by a receiver to achieve channel synchronization and estimation [61]. DVB and DAB transmissions typically have high levels of radiated power with sufficient bandwidth for reasonable range accuracy. This allows good and consistent range compression and Doppler estimation of targets without loss of communication data [61].

In [9] the use of DVB signals is studied as a radar system for the application of traffic density monitoring in urban areas. Proposals for applications using personal mobile radars in mobile devices can be seen in [16], where the idea of putting antenna arrays in smartphones or tablets is presented, thus achieving a high-definition, low-cost personal mobile radar, allowing the construction of high-definition interior mappings, new applications to help blind people or Three-Dimension (3D) environmental mapping. Passive radar systems using OFDM signals can also be used to detect and track flying targets operating as surveillance area systems [62].

2.2.2 Active radar with data communication

The concept of passive radar systems based on independent communications signals has a strong limitation, since the radar does not control the transmission. To overcome this limitation, and control both radar and communication functions, an active radar system can be co-designed to optimize the performance of both functions. The unmanned aerial vehicle flight system [63] is an example of a scenario for future application for this technology. The most typical scenario for this application and that will be discussed in more detail in this thesis is Intelligent Transport System (ITS) [64], shown in the Figure 2.1 [65].

The ITS is an advanced system defined by the European Telecommunications Standards Institute and encompasses a wide range of technologies, supporting the essential features, which include telematics and all types of communications in vehicles, such as Vehicle-to-Infrastructure (V2I), V2V, and Vehicle-to-Everything (V2X). The evolution of the automotive radar has already been discussed in [65].

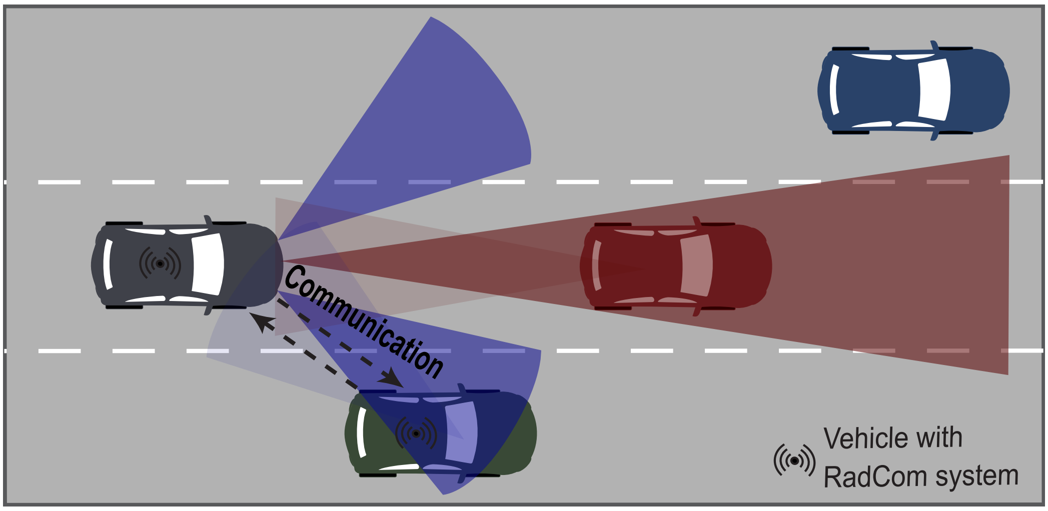

Figure 2.1: Automotive radar in an ITS with vehicles equipped with RadCom systems.

The smart cars/smart vehicles concept is presented as one of the most promising solutions to improve safety, security, efficiency and optimize traffic. For example, the use of this technology reduces the high mortality rate that occurs on roads, since radar offers the possibility of seeing long distances in front of the car in low visibility conditions [66]. Vehicle-vehicle or vehicle to infrastructure networks can improve driver visibility, provide knowledge of road condition or only improve the reaction time in a possible accident through automatic controls, as can be confirmed in publications such as the European standard for ITS [67] or the IEEE 802.11p International Standard [68], which is part of Wireless Access in Vehicular Environments (WAVE). The use of this radar system in multi-user environments may cause interference. As this is an ad hoc mobile network as in ITS, an appropriate and robust multi-user access strategy is required to deal with this limitation. In [69] the authors proposed to separate users in the frequency domain through OFDM sub-carriers as in Orthogonal Frequency-Division Multiple Access (OFDMA). However, instead of using equally spaced sub-carrier sets, the idea is that each user chooses a random set of sub-carriers with the same probability. When two or more OFDM radars have overlapping subcarriers by chance, due to randomly selected subsets, interfering sub-carriers are removed prior to further processing, as shown in Figure 2.2. Its spacing will be arbitrary, which greatly reduces the chances of two users choosing exactly the same set.

However in [70], Sit *et al.* have shown that the selection of only uninterrupted sub-carriers for radar processing using the classic DFT and Inverse Discrete Fourier

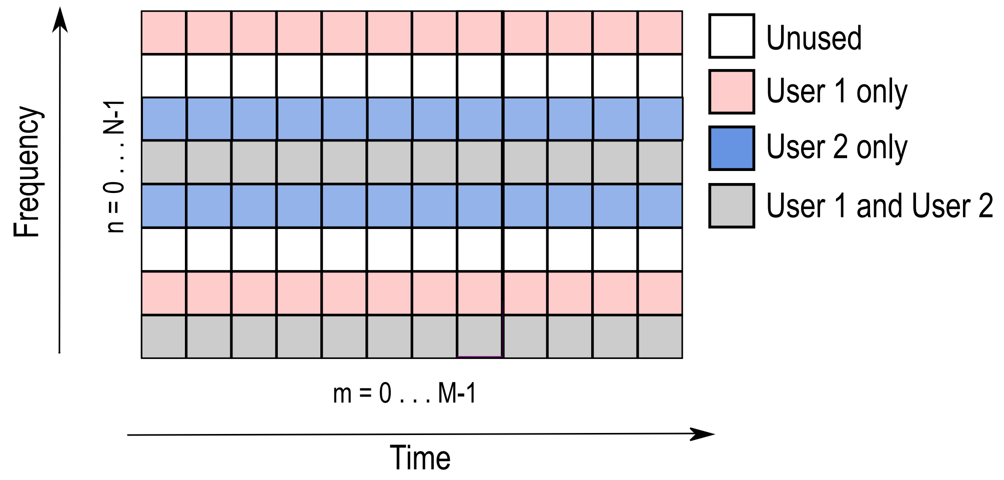

Figure 2.2: Received OFDM frame with interfering sub-carriers

Transform (IDFT) method will lead to degraded performance, failing to detect a weak target that has the same velocity as a strong target. To overcome this, the authors proposed a combined DFT and Compressed Sensing (CS) detection technique for range and Doppler estimation, providing a much better Signal-to-Noise Ratio (SNR) output than the conventional method. Other studies dealing with techniques based on MIMO systems for the cancellation of interference can be seen in [7, 35–37]. A discussion on the use of MIMO techniques for RadCom systems will be conducted in the next section.

2.3 MIMO Technology

The MIMO technology was first used for wireless communication systems. Recently, in [71] initial proposals were made for an MIMO radar. This concept differs from the MIMO communication system, where independent or dependent information streams are transmitted simultaneously through parallel sub-channels, thereby increasing the transfer rate or decreasing the Bit Rrror Rate (BER). The communication system only uses the channel matrix to retrieve the information transmitted from the received signal. On the other hand, a MIMO radar uses the channel information to extract the targets parameters, for example to determine the number, locations and velocity of targets [72].

Accordingly to the literature MIMO radar may be divided into two categories:

MIMO radar with collocated antennas and MIMO radar with widely separated antennas. Transmission and reception with collocated antennas lead to higher resolution, greater sensitivity to detect slow moving targets, and better identification. In this system, the target is modeled as a point without spatial properties [73]. With widely separated antennas, the MIMO radar has the ability to improve radar performance by exploiting the diversity of the radar cross-section, computing Doppler's estimates from multiple directions, thus enabling high-resolution target location [74].

In [72], Wu et al. proposed a new MIMO radar that uses the OFDM waveform. The author has shown that with the OFDM, the frequency selective fading problem can be solved using frequency diversity, and meanwhile the signal orthogonality required for a MIMO radar is still valid. In addition, transmitter waveforms designed for a single narrowband MIMO radar can be applied directly to each sub-band of the MIMO OFDM radar.

For RadCom applications, the processing of multiple antennas is of particular interest, since for the radar function it is possible to estimate the azimuthal positions of the scattering objects through a linear antenna array, and for the communication function it improves the signal-to-noise ratio and the determination of the directions of the transmitters [4].

The additional degrees of freedom provided by the transmission of orthogonal waveforms can potentially improve the performance of a radar system because it provides antenna beams with significant improvements in the accuracy of angular estimate [75]. In [76] the author shows that in a MIMO radar system with M_T transmitting antennas and M_R receiving antennas is equivalent to a virtual array with $M_T M_R$ elements (equivalent to $M_T M_R$ channels) for direction estimation processing—if the N_T transmitted waveforms are perfectly orthogonal (system illustrated in Figure 2.3).

In [1] the author uses the MUSIC algorithm for DoA estimation in a MIMO OFDM radar system. This is done by exploring the phase difference between several pairs of transmit-receive antennas along with the use of orthogonal transmission signals. The accuracy of the angle resolution increases as more pairs of transmitting and receiving antennas are used as can be seen in Figure 2.4 and Figure 2.5, which show the author's results, for a 2×2 array and for a 4×4 array respectively.

Proposals for a 3D radar concept can be seen in [77], where the author

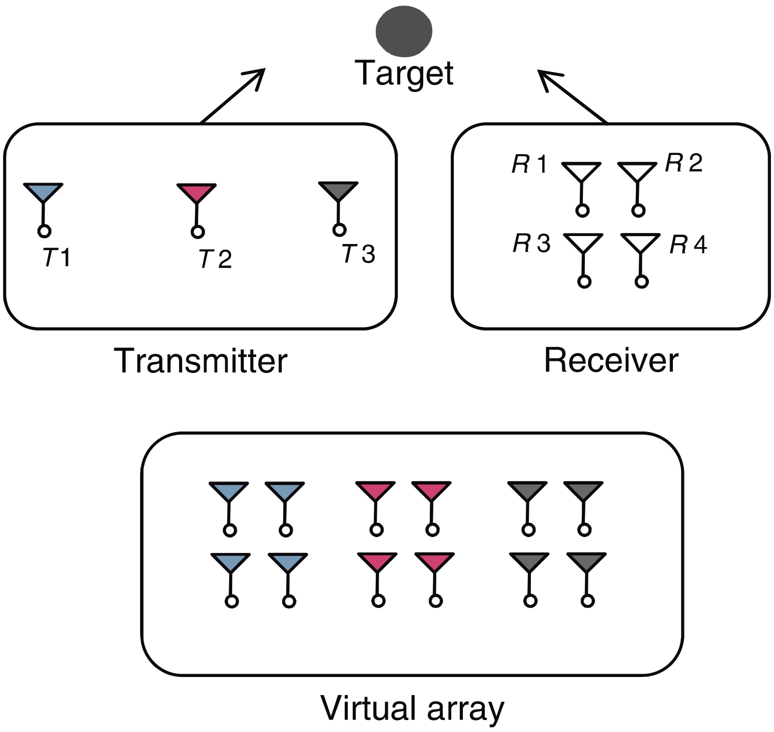

Figure 2.3: MIMO radar system with virtual array.

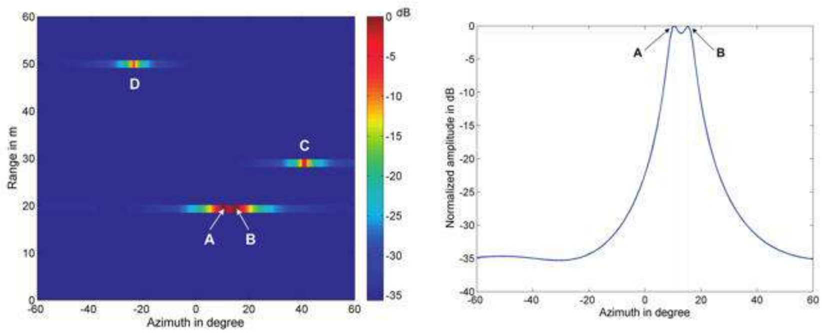

Figure 2.4: 2×2 **MUSIC DoA estimation [1].**

combines the OFDM-based signal model with a DoA algorithm along with the virtual antenna geometry to perform a 3D radar sensor to enable a radar image with range, azimuth and elevation (shown in the Figure 2.6). Other studies that address this concept can be seen in [78], where the 3D estimation algorithm is used with another algorithm for Two-Dimension (2D) (azimuth and range) and velocity estimation. In [79] a 3D estimation model with co-located antennas was used. In [80] the 3D signal extraction methods employ the CS theory, for sparse 3D signals analysis. Anticipated applications include traffic monitoring, unmanned vehicles and even robotic vision.

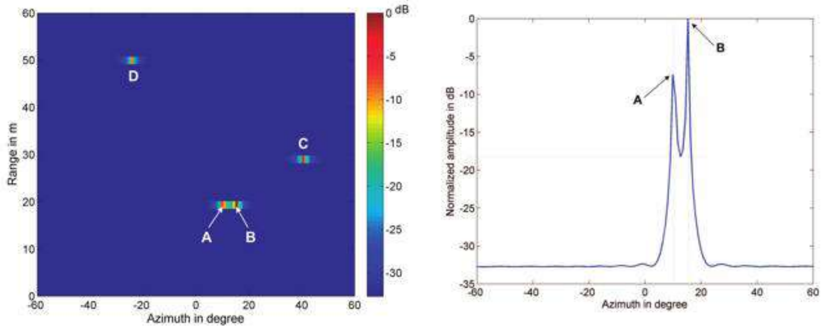

Figure 2.5: 4×4 **MUSIC DoA estimation [1].**

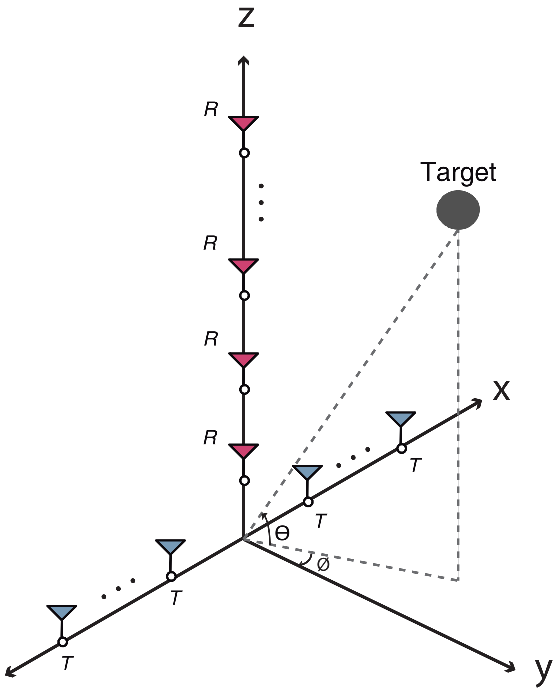

Figure 2.6: Antenna geometry for 3D radar imaging.

In [81] the use of MIMO OFDM is explored to perform angle estimation for object positioning, exploring spatial diversity, to allow access and communication for multiple users. In this chapter the author analyzes the use of spectrally-interleaved OFDM radar and demonstrates that the DoA estimate depends on the characteristics of the physical antenna array. Therefore, in assigning the subcarrier to multiple users, the subcarrier mapping must be chosen so that the resulting virtual antennas have a contiguous linear phase rotation on the virtual antennas. According to [81], this can be done by allocating at least two adjacent subcarriers to a user. This work was extended in [35], where an inter-carrier interference cancellation technique was proposed. In the technique presented, the OFDM transmission frame is adapted to include the use of training symbols as pilot symbols for estimating frequency and channel displacement coefficients. The use of this technique showed a 45 dB improvement in the original radar image. Studies of a different approach with the use of non-equidistant dynamic interleaving of OFDM subcarriers can be seen in [82].

2.4 On the potential of other 5G waveforms for RadCom

The OFDM is a well-known waveform, well studied and widely applied in communication systems. The literature has already shown that OFDM can work very well for joint radar and communications applications, analyzing their performance in various applications and scenarios [9, 60, 62, 63]. However, OFDM has some drawbacks, high out-of-band emissions, susceptibility to Doppler spread, loss of spectral efficiency due to the use of a cyclic prefix, and the need for frequency synchronization to preserve the orthogonality between subcarriers. To overcome some of the limitations found in the OFDM signal, several alternative waveforms have been extensively studied in the literature in recent years in communication systems, such as UFMC, GFDM and FBMC [83]. One of the pioneering studies analyzing other 5G waveforms for RadCom systems was in [47], where the authors showed that FBMC signals can be used for radar processing. In [47] the radar detection performance was shown to be lower than the OFDM one, but all the benefits of FBMC signals to the data communication system were retained.

2.4.1 FBMC

The FBMC as well as OFDM divides the spectrum into several orthogonal subbands, but different from OFDM that filters the entire band, FBMC applies a filter to each subcarrier individually. Thus with the appropriate filter banks, sidelobes are much weaker and, as a result, the problem of inter-carrier interference is attenuated [84]. However, the subcarrier filters are very narrow and require long filters, as a result, individual symbols overlap in time. To achieve orthogonality, Offset Quadrature Amplitude Modulation (OQAM) can be used as the modulation scheme [83].

FBMC has better spectral efficiency than OFDM, but its applicability in MIMO networks is not trivial and may be very limited. Also for many applications, FBMC may be more complex than OFDM [85]. The study analyzing the use of FBMC waveform in radar systems was carried out in [47], where the author proved that it is possible to perform radar functions together with communication using FBMC.

2.4.2 UFMC

UFMC is a 5G waveform that can be considered as an OFDM enhancement. It differs from FBMC in that instead of filtering each subcarrier individually, UFMC divides the signal into several sub-bands and filters them. The filtering operation leads to lower leakage than OFDM. The transmitted signal does not use a Cyclic Prefix (CP), although it can be used to improve protection against inter symbol interference, but there is still a spectral efficiency loss due to the transient time of the modulated filter [83]..

The UFMC waveform is an attractive option for radar systems. It shows a higher spectral efficiency when compared to OFDM, the pulse modeling function improves performance in multiuser asynchronous scenarios, and also preserves compatibility with well-known OFDM algorithms (channel estimation, MIMO detectors, etc.) [85].

2.4.3 GFDM

The GFDM waveform is based on the time-frequency filter of a data block, which leads to a flexible waveform similar to OFDM. In GFDM, a circular filtering operation is applied to a group of QAM symbols in the time domain on a subcarrier basis, solving the UFMC long filter problem [86].

The main difference between this technique and OFDM is that the modulation is not orthogonal, so it is necessary to implement an interference cancellation scheme, which improves performance, but severely increases the receiver complexity. Other option is the use of OQAM which allows the use of less complex linear receivers. GFDM provides better control of out-of-band emissions and reduces Peak to Average Power Ratio (PAPR) [83]. No feasibility studies have yet been carried out for radar systems using this waveform.

CHAPTER 3

Multicarrier waveforms for Joint radar and communications

This chapter describes the joint radar and communications concept when multicarrier waveforms are considered. First, the basic concepts of how the radar device works, such as estimating functions and basic waveforms, are presented. Subsequently, the fundamentals of OFDM radar are exposed. Finally, the MIMO OFDM radar model for the RadCom system is presented.

3.1 Fundamentals of radar

The Radar is an active electromagnetic sensor used to monitor and detect objects (or targets), such as missiles, ships, people and even the natural environment. It allows a particular class of objects to be detected and located without being hampered by night, fog, clouds, smoke, distance and most other obstacles to common vision [87]. The radar can also measure the range of objects and the instantaneous velocity of targets.

Radar works by transmitting radio waves from a transmitter, which are reflected by objects seen by the radar and received in a radio receiver, usually located, for convenience, in the same location as the transmitter (system shown in the Figure 3.1). The properties of the received echoes are processed to determine the presence of targets (detection), location and velocity [88]. The radar is designed to extract information about targets, basic radar operation involves three main tasks: range, relative velocity and directional estimation.

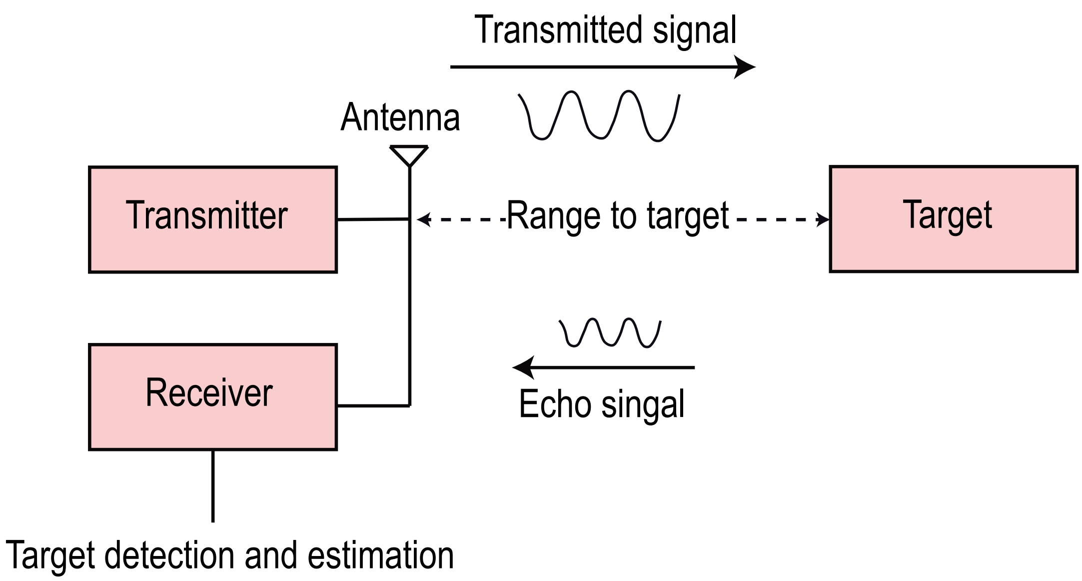

Figure 3.1: Basic radar system.

3.1.1 Range estimation

Range estimation is critical for radars. Due to the modulation of the transmitted signal, the time difference between the emission of the illumination signal and the detection of the signal reflected by the target can be measured as a delay τ. The range is determined based on the round trip time delay that the waves take to propagate to from the target, and is given by

$$r = \frac{c\tau}{2}, \tag{3.1}$$

where c is the speed of light ($c = 3 \times 10^8 m/s$), r is the range in meters, τ is in seconds and the factor $1/2$ is used to explain the round-time delay.

The shape of the waves (signals) that a radar transmits is important for the estimation of the return signal delay. For example, a pulsed radar transmits and receives a pulse train (Figure 3.2), the Pulse Repetition Interval (PRI) is T. The inverse of the PRI is the Pulse Repetition Frequency (PRF), which is denoted by f_r [2].

$$f_r = \frac{1}{PRI} = 1/T. \tag{3.2}$$

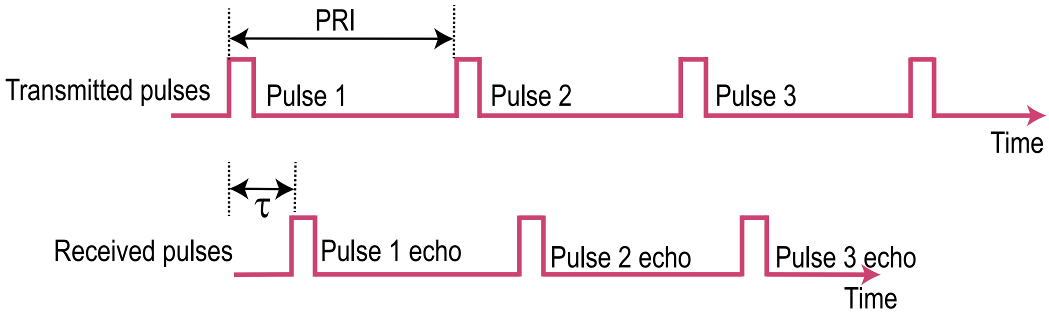

Figure 3.2: Train of transmitted and received pulses [2].

The Range resolution Δr is a radar metric that describes its ability to detect targets close to each other as distinct objects. Radar systems are typically designed to operate between a minimum range R_{min} and a maximum range R_{max}. The targets separated by at least Δr will be completely resolved in the range.

3.1.2 Velocity estimation

Radars use the Doppler frequency to extract the target relative velocity (range rate) as well as to distinguish between moving or stationary targets. The Doppler phenomenon describes the change in the central frequency of an incident wave due to the target motion in relation to the radiation source [89]. With the existence of relative motion v between two cars, from the initial position $r(0)$, the reflected waves are delayed by

$$\tau = \frac{2(r(0) + vt)}{c}. \tag{3.3}$$

The relative velocity time causes a frequency shift in the received wave, shown in the Figure 3.3, known as the Doppler shift, given by

$$f_D = \frac{2v}{\lambda}. \tag{3.4}$$

The Doppler shift is inversely proportional to the wavelength λ ($\lambda = c/f_c$), and its signal is positive or negative, depending on whether the target is approaching

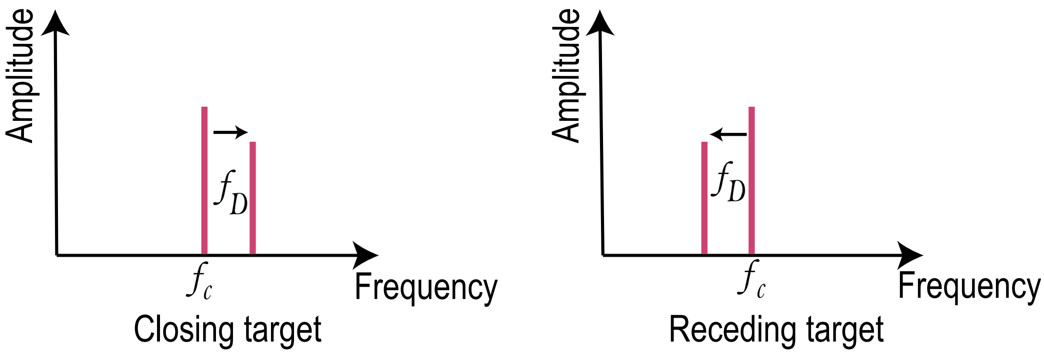

Figure 3.3: Spectra of received signal showing Doppler shift [2].

(relative velocity negative) or moving away (relative velocity positive) from the radar. If the radar velocity resolution is Δv, then two targets with a separation in velocity of at least Δv will be resolved by the radar.

3.1.3 Radar waveforms

The waveform is a determining factor in the performance and application of a radar system. Two fundamental waveforms are the pulse and the continuous waveform (CW), other modulated radar waveforms include Frequency-Modulated Continuous-Wave (FMCW), Stepped-Frequency Continuous-Wave (SFCW), OFDM and Frequency Shift Keying (FSK). The transmit waveform and respective detection principle are shown in the Table 3.1 [89] for main waveforms used for radar and its characteristics.

Table 3.1: Radar waveforms - Transmit Waveform and Detection Principle

Waveform Type	Transmit Waveform	Detection Principle
CW	$e^{2\pi j f_c t}$	Conjugate mixing
Pulsed CW	$\prod(T_p)e^{2\pi j f_c t}$	Correlation
FMCW	$e^{2\pi j(f_c+0.5Kt)t}$, $K = B_W/T$	Conjugate mixing
SFCW	$e^{2\pi j f_n t}$,$fn = f_c + (n-1)\Delta f$	Inverse Fourier transform
OFDM	$\sum_{n=0}^{N-1} S(n)e^{2\pi j(f_c+n\Delta f)t}$	Frequency domain channel estimation

Range and velocity resolution, angular direction, SNR and the probability of target detection are determined, in part, by the nature of the waveform [89]. The Doppler resolution, for example, allows one to distinguish stationary distortions from moving targets. The resolution of the waveforms discussed above are shown in the table 3.2 [89], along with some additional comments.

Table 3.2: Radar waveforms - Resolution

Waveform Type	Resolution	Comments
CW	$\Delta v = 1/t_{total}$	No range information
Pulsed CW	$\Delta r = cT_p/2,\ \Delta v = 1/T_p$	Range-Doppler performance trade-off
FMCW	$\Delta r = c/2B_W,\ \Delta v = 1/MT$	Both range and Doppler information
SFCW	$\Delta r = c/2B_W,\ \Delta v = 1/MT$	Δf decides maximum range
OFDM	$\Delta r = c/N\Delta f,\ \Delta v = 1/MT$	Suitable for vehicular communication

In tables 3.1 and 3.2 we use the following notation:

- B_W denotes bandwidth of the radar;
- t_{total} is the amount of time for which data is captured;
- N stands for a number of samples in CW and number of subcarriers in OFDM;
- $\prod(T_p)$ is a rectangular pulse of duration T_p
- T is the duration of a symbol for OFDM and of a block for FMCW/SFCW.
- M is the number of FMCW/SFCW blocks or OFDM Symbols;
- $\mathbf{S}(n)$ is an arbitrary sequence;
- Δf is a carrier/frequency separation in OFDM/SFCW.

3.2 OFDM modulation basics

OFDM is a special case of multicarrier transmission, where a single data stream is transmitted in several subcarriers. In this way, the bandwidth of the subcarriers becomes small compared to the channel coherence bandwidth, thus the subcarriers experience flat fading, which enables the applicability of a simple equalization techniques, since the observation period is made for a long period of time compared to the dispersive channel delay propagation. The carriers frequencies are orthogonal and if a cyclic prefix is introduced, then orthogonality is maintained in a dispersive channel. Thus, the Subcarrier spectra may overlap without mutual influence between the subcarriers [90].

The representation of a simple point-to-point OFDM system is shown in Figure 3.4, where the message is modulated, so the symbols are converted from serial to parallel and the codes are distributed on the subcarriers. Once subcarriers are assigned, an IDFT is commonly used. The discrete signal resulting from the IDFT is then converted from parallel to serial and transmitted. The receiver works as the transmitter, but in the opposite way.

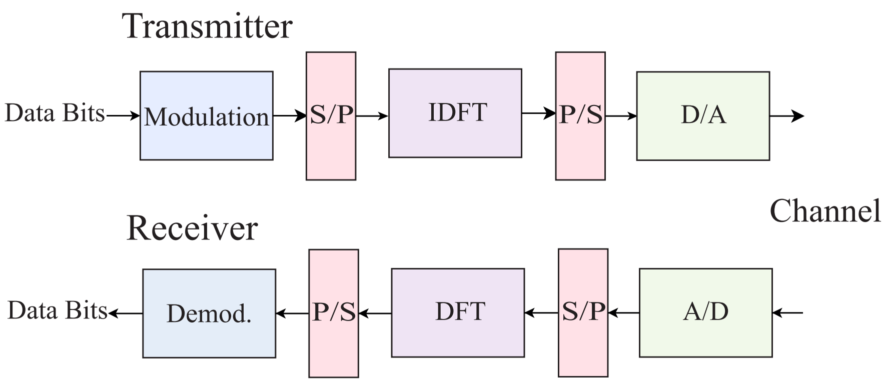

Figure 3.4: Simplex point-to-point OFDM [3].

The complex envelope of the transmitted OFDM, graphically illustrated in Figure 3.5, can be expressed as

$$x(t) = \sum_{m=0}^{M-1} \sum_{n=0}^{N-1} \mathbf{S}(m,n) e^{j2\pi n \Delta f t} \mathrm{rect}\left(\frac{t - mT}{T}\right), \tag{3.5}$$

where N is the number of subcarriers, M is the number of OFDM symbols, Δf is the subcarrier spacing, T is the symbol duration. $\mathbf{S}(m,n)$ is the transmitted data at subcarrier n and symbol m, modulated with a digital modulation technique, for example, QAM or Phase Shift Keying (PSK) [58].

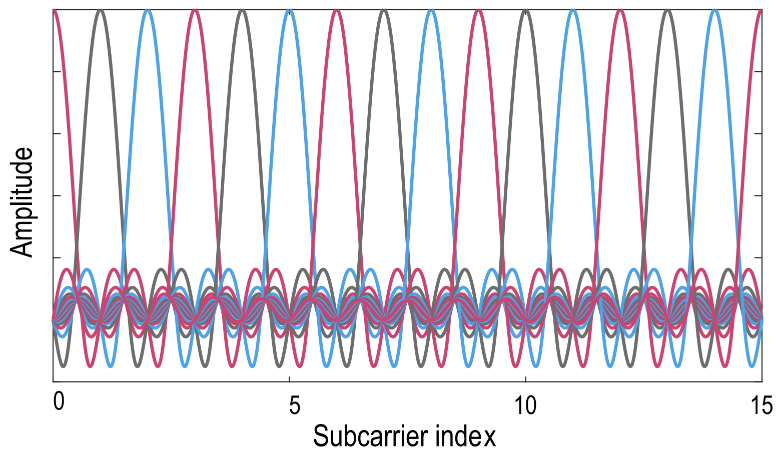

Figure 3.5: Consecutive OFDM Subcarriers

The subcarrier orthogonality of the frequency division is achieved by choosing a constant subcarrier distance Δf equal to the inverse OFDM symbol duration T, given by

$$\Delta f = \frac{1}{T}. \tag{3.6}$$

For a clear understanding of the definitions of subcarriers and symbols, the signal is represented in the time-frequency grid in Figure 3.6.

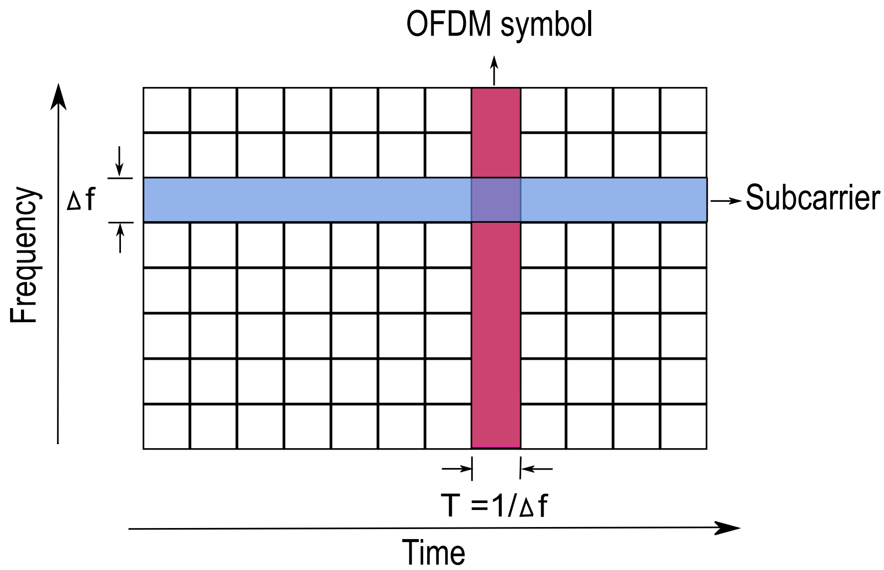

Figure 3.6: Time-frequency grid of transmit OFDM signal

The guard interval is introduced to the OFDM signal to remedy the effects of multipath reflection onto the signal. The received signal consists of several copies of the transmitted signal each with a different delays, amplitudes and phases. The multipath may lead to Inter Symbol Interference (ISI), i.e. the received OFDM symbol is distorted by the previously transmitted OFDM symbol. To prevent ISI and guarantee the circular condition in the channel matrix, a guard interval can be implemented using a CP. The CP is simply a replica of a piece of length T_{CP} from the end of the symbol. The duration of the cyclic prefix should cover the longest expected channel delay [91].

3.3 OFDM RadCom concept

The idea of using OFDM signals for radar was first proposed by Levanon in [57]. The flexibility provided by OFDM signals leads to a wide variety of techniques that improve the various aspects of radar performance. In the referred chapter, Levanon showed that OFDM-type signals are suitable for radar applications and the possibility of integration with communication systems has been demonstrated in [92] and [22].

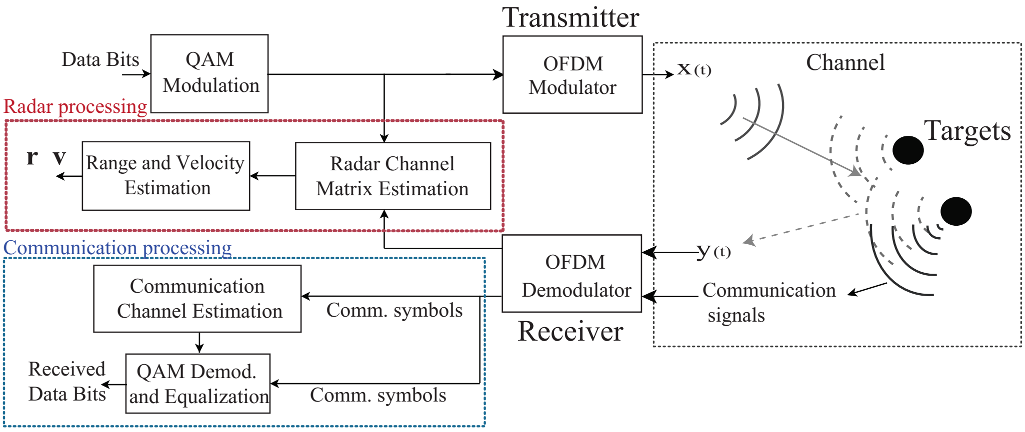

Figure 3.7: Simplified block representation of the RadCom system structure. The encoded data is transmitted by the RadCom system using OFDM modulation. The transmitted signal is then reflected by the targets and received back by the same RadCom system to estimate the range and velocity of targets. The system also receives and processes communication signals transmitted from other devices (e.g., other vehicles).

A block diagram depicting the operation of a RadCom system is shown in Figure 3.7. Before reaching the radar, the OFDM signal transmitted by the radar is reflected by the K targets, so for target k the signal suffers from delay $\tau_k = \frac{2r_k}{c}$ proportional to the range of the target (r_k), and a Doppler frequency shift $f_{D,k} = \frac{2v_k f_c}{c}$ proportional to the velocity v_k of the target. The received OFDM signal [20] is given by

$$y(t) = \sum_{k=1}^{K} x\left(t - \tau_k\right) e^{j2\pi f_{D,k} t} = \tag{3.7}$$

$$\sum_{k=1}^{K} \sum_{m=0}^{M-1} \sum_{n=0}^{N-1} \mathbf{S}(m,n) e^{j2\pi (n\Delta f + f_{D,k})(t-\tau_k)} + \tilde{\eta}(t), \tag{3.8}$$

where $\tilde{\eta}$ is an Additive White Gaussian Noise (AWGN) with zero mean and variance σ_n.

Considering that the transmitted signal has a bandwidth $B_W \ll f_c$, we can consider that each subcarrier experiences the same Doppler shift $f_{D,k}$. In addition, $f_{D,k} \ll f_c$, therefore, the term relative to the coupling between Doppler effect $f_{D,k}$ and the delay τ_k, $e^{(-j2\pi f_{D,k}\tau_k)}$ is insignificant and can be ignored [93]. The received OFDM signal can be rewritten by

$$y(t) = \sum_{k=1}^{K} \sum_{m=0}^{M-1} \sum_{n=0}^{N-1} \mathbf{S}(m,n) e^{j2\pi t f_{D,k}} e^{j2\pi n \Delta f (t-\tau_k)} + \tilde{\eta}(t). \tag{3.9}$$

The received OFDM symbols $\hat{\mathbf{S}}$ [58] can be defined as

$$\hat{\mathbf{S}}(m,n) = \mathbf{S}(m,n) \sum_{k=1}^{K} g_k e^{j2\pi T f_{D,k} m} e^{-j2\pi n \Delta f \tau_k} + \tilde{\eta}. \tag{3.10}$$

We can observe that the distortions due to the channel are completely contained in the received modulation symbol $\hat{\mathbf{S}}$. Thus, comparing the transmitted signal $\mathbf{S}$ with the received soft-side signal $\hat{\mathbf{S}}$, disregarding the noise, would generate the frequency domain channel matrix $\mathbf{D}$

$$\mathbf{D_r}(m,n) = \frac{\hat{\mathbf{S}}(m,n)}{\mathbf{S}(m,n)} = \sum_{k=1}^{K} e^{j2\pi T f_{D,k} m} e^{-j2\pi n \Delta f \tau_k} + \tilde{\eta}. \tag{3.11}$$

The estimate of the round trip delay and the Doppler shift (and hence the distance and the relative velocity of the targets) is transformed into a spectral estimation problem, since the distance and velocity information can be calculated from the channel matrix $\mathbf{D}$, using the phase difference between the transmitted and received symbols [45].

3.3.1 Range and doppler estimation

The range and velocity parameters can be obtained from a Two-Dimension Discrete Fourier Transform (2D-DFT). Considering the case corresponding to range estimation, for a target at the distance r of the radar, the channel matrix of the corresponding channel is given by

$$\mathbf{D}(n) = e^{-j2\pi n \Delta f \tau_k}. \tag{3.12}$$

The impulse response of the channel containing the range profile of the object can then be determined by taking an IDFT, given by

$$\mathbf{Z}(p) = \mathrm{IDFT}[\mathbf{D}(n)] \quad , p = 0, 1..., N-1. \tag{3.13}$$

Considering now, the case corresponding to velocity estimation, the signal from a target moving with a relative velocity v will experience double the amount of Doppler shift according to

$$\mathbf{D}(m) = e^{j2\pi T f_D m}. \tag{3.14}$$

It can be assumed that Doppler affects all subcarriers in the same way, since the system bandwidth is much smaller than the carrier frequency. Thus, for an object with a nonzero relative velocity for the radar, taking the DFT through the time axis of the corresponding channel transfer function, the Doppler term can be estimated [93] by

$$\mathbf{Z}(q) = \mathrm{DFT}[\mathbf{D}(m)] \quad , q = 0, 1..., M-1, \tag{3.15}$$

or jointly the two estimates, can be calculated by a DFT of length M in each line of $\mathbf{D}$ and an IDFT of length N in each column, such as

$$\mathbf{Z}(p, q) = \mathrm{IDFT}[\mathrm{DFT}[\mathbf{D}]]. \tag{3.16}$$

In the Figure 3.8 is demonstrated how the method works. For every reflective target, we have a peak in $|Z(p,q)|^2$ at index (p,q) [93], so

$$r = \frac{pc}{2\Delta f N}, \quad , p = 0, 1..., N-1, \tag{3.17}$$

$$v = \frac{qc}{2v f_c T M} \quad , q = 0, 1..., M-1. \tag{3.18}$$

3.3.2 Range and doppler resolution

One of the performance measures of a radar system is the resolution limit for the most important parameters (range and velocity). The range resolution Δr depends only on the total bandwidth occupied by the transmitted signal, and is given by

$$\Delta r = \frac{c}{2B_W} = \frac{c}{2N\Delta f} \ . \tag{3.19}$$

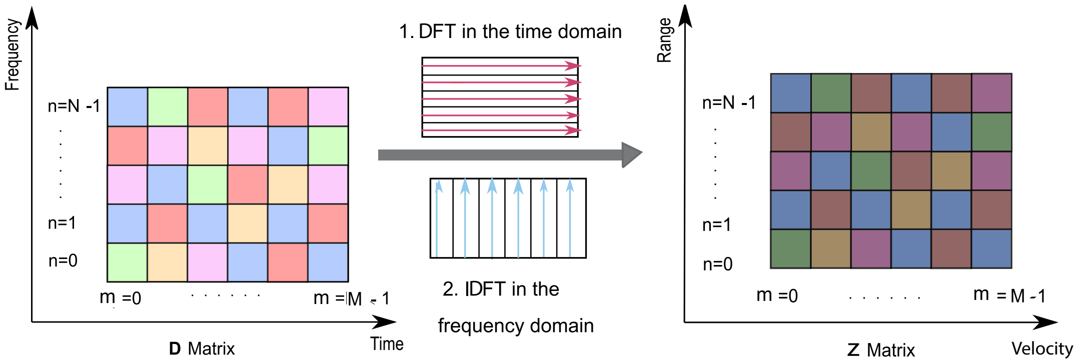

Figure 3.8: Estimate Doppler and range for OFDM radar.

For future applications, the resolution must be small enough to allow the separation of objects such as cars, buildings, etc. Presumably a resolution of about 1 m is sufficient for a large number of applications, then a total signal bandwidth of at least 100-150 MHz would be required, approximately .

The Doppler resolution depends on the number M of evaluated symbols, and the duration of Pulse T [34], being

$$\Delta f_D = \frac{1}{MT}, \tag{3.20}$$

or, in terms of velocity resolution

$$\Delta v = \frac{c}{2Mf_cT} = \frac{c\Delta f}{2Mf_c}. \tag{3.21}$$

In principle, evaluating more OFDM symbols would give a better velocity resolution, but is not practical, since moving objects must remain within a resolution cell during the evaluation [34], given by

$$\Delta R \Delta v = \frac{c^2}{4MNf_c}. \tag{3.22}$$

This is inversely proportional to the total number of samples ($M \times N$) and the carrier frequency (f_c). We also see that the resolution of the range is inversely proportional to Δf and the resolution of velocity directly proportional to Δf, so a high resolution for range implies a low resolution for velocity.

3.3.3 Common limitations

Unambiguous range and velocity limitation

In addition to the individual requirements for the radar application, there are also common limitations that result from the physical properties of the channel. In the case of OFDM radar, propagation has twice the Doppler shift in relation to the propagation of communications systems [58]. The Doppler shift in the radar system can be described as follows

$$f_D = \frac{2v}{\lambda}.$$

To avoid distortion of the orthogonality of the subcarriers, the subcarrier spacing must satisfy the condition

$$\Delta f = 10 f_{D,max}, \tag{3.23}$$

where $f_{D,max}$, max is the maximum Doppler shift. The OFDM radar system also suffers from maximum and unambiguous distance limitations, as the signal travels the distance twice, resulting in an unequivocal maximum measurement distance, given by

$$R_{max} = \frac{c}{2\Delta f} = \frac{cT}{2}. \tag{3.24}$$

Therefore, the duration of the OFDM symbol must be chosen large enough to allow good radar coverage. The OFDM radar system also has maximum unambiguous velocity given by

$$V_{max} = \frac{c}{2 f_c T}. \tag{3.25}$$

In addition to obtaining a sufficiently high signal-to-noise ratio at the radar input, the energy content of the signal being processed must be maximized. In applications where transmission power is limited, to maximize the signal-to-noise ratio the duration of the OFDM symbol must be chosen as long as possible, but should not violate the restrictions resulting from the Doppler effect [58].

Inter-symbol interference

Another important limitation of the OFDM system is the maximum spread for the different propagation components of multiple paths. To avoid the ISI, each OFDM symbol is preceded by a CP. The duration of this CP (T_{CP}) is chosen according to the maximum excess delay, which is the maximum time difference between the arrival of the first and last propagation paths in a multipath environment [34].

For the radar application, it can be assumed that there is a direct coupling between the transmitting and receiving antennas on the same platform. Therefore, the duration of the cyclic prefix must be at least equal to twice propagation time of the longest path between the radar and the object (R_{max}).

Intercarrier interference

The reflected signal received by the radar or the signal received by the communication system is subject to a frequency shift caused by the Doppler effect. If this is not compensated, during demodulation the DFT will recover incorrect values for the phase codes in the signal. Essentially, for each subcarrier, the sampling of the spectrum no longer occurs at the peak, but with a displacement, and so the other subcarriers interfere with the information of the subcarrier to be demodulated [3]. Inter Carrier Interference (ICI) degrades the performance of OFDM systems.

3.4 MIMO OFDM radar

Consider a MIMO radar system with M_T transmitting antennas and M_R receiving antennas illuminating K targets from the directions $\theta_k,\ k = 1, 2, ..., K$. The antennas are assumed to be uniformly spaced with an inter-antenna distance of d_t for the transmitting antennas and d_r for the receiving antennas, shown in Figure 3.9. In a MIMO radar system if an array of elements M_T is used in the transmission and an array of M_R elements is used in the reception, the $M_T M_R$-length array direction vectors are equivalent to the direction vectors that would result from the spatial convolution of the transmit and receive phase centers, providing an increase of the conventional array direction vectors [76]. The corresponding virtual matrix of the system consists of $M_T M_R$ virtual elements if the M_T waveforms are perfectly orthogonal.

The interleaved OFDM structure proposed in [94] is employed in order to obtain simultaneous uncorrelated transmissions from multiple transmitting antennas. In

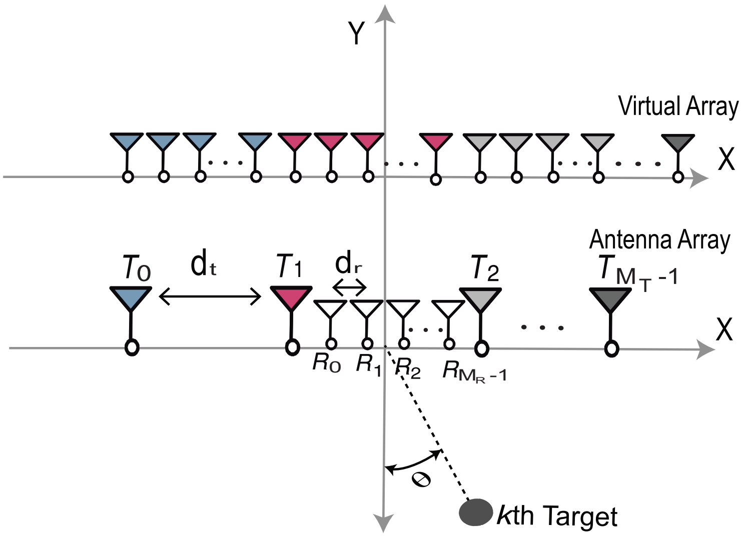

Figure 3.9: Representation of Antenna geometry and the resulting virtual array for a MIMO OFDM radar .

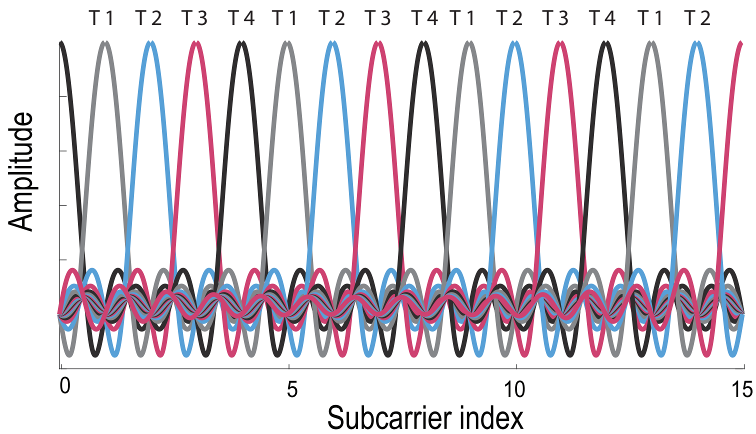

Figure 3.10: Interleaving OFDM signal structure for 4 transmitter antennas.

the interleaved OFDM structure, the subcarriers are assigned to the transmit antennas in order that each antenna radiates only certain subcarriers, as presented in the Figure 3.10. We considered the allocation of N_{M_T} subcarriers to the transmitting antenna p with the set of subcarriers $\{p, p+M_T, p+2M_T, ...N-(M_T-p)\}$, where $p = 0, \ldots, M_T-1$, and $N_{M_T} = N/M_T$. The details of this allocation model can be seen in [94, 95]. The signal transmitted by the p-th transmitting antenna can be described as

$$x_p(t) = \sum_{m=0}^{M-1} \sum_{n_\mu=0}^{N_{M_T}-1} \mathbf{S}(m, p + n_\mu M_T) e^{2\pi j \Delta f (p+n_\mu M_T)t} \\ \mathrm{rect}\left(\frac{t - mT}{T}\right). \tag{3.26}$$

The signal received by the q-th receiving antenna, where $q = 0, ..., M_R - 1$, is the sum of all signals transmitted by the M_T transmitting antennas. Considering then $\mathbf{X}(t) = [x_0(t), ..., x_{M_T-1}(t)]^T$ as the set of signals transmitted by the M_T transmitting antennas, the set of signals $\mathbf{Y}(t) = [y_0(t), ..., y_{M_R-1}(t)]^T$ received by the M_R receiving antennas after the reflection by K targets is given by

$$\mathbf{Y}(t) = \sum_{k=1}^{K} [\mathbf{a}_T(\theta_k) \otimes \mathbf{a}_R(\theta_k)] \, \mathbf{X}\left(t - \frac{2r_k}{c}\right) e^{j2\pi f_{D,k} t} + \boldsymbol{\eta}(t) \tag{3.27}$$

$$= \sum_{k=1}^{K} \mathbf{A}(\theta_k) \mathbf{X}\left(t - \frac{2r_k}{c}\right) e^{j2\pi f_{D,k} t} + \boldsymbol{\eta}(t) \tag{3.28}$$

with $\mathbf{A}(\theta_k) = [\mathbf{a}_T(\theta_k) \otimes \mathbf{a}_R(\theta_k)]$, where $\otimes$ denotes the Kronecker product and $\mathbf{a}_T(\theta_k)$ and $\mathbf{a}_R(\theta_k)$ are the steering vectors of the transmitter and receiver for the k-th target, given by

$$a_T(\theta_k) = \left[1, e^{j2\pi d_t 1 \sin\theta_k/\lambda}, \cdots, e^{j2\pi d_t (M_T-1)\sin\theta_k/\lambda}\right]^T \tag{3.29}$$

$$a_R(\theta_k) = \left[1, e^{j2\pi d_r 1 \sin\theta_k/\lambda}, \cdots, e^{j2\pi d_r (M_R-1)\sin\theta_k/\lambda}\right]^T, \tag{3.30}$$

with λ being the wavelength $\lambda = c/f_c$.

The symbols received by the q-th antenna can be described by the following equation

$$\hat{\mathbf{S}}_q(m, p + n_\mu M_T) = \sum_{k=1}^{K} e^{j2\pi d_t p \sin\theta_k/\lambda} e^{j2\pi d_r q \sin\theta_k/\lambda} \\ \mathbf{S}(m, p + n_\mu M_T) e^{j2\pi f_{D,k} mT} e^{-j2\pi n \Delta f \frac{2r_k}{c}} + \eta_q(m, n). \tag{3.31}$$

For the radar processing, the estimation of the channel information matrix $\mathbf{D}$

of the q-th receiving antenna is given by

$$\mathbf{D}_q(m, p + n_\mu M_T) = \frac{\hat{\mathbf{S}}_{\mathbf{q}}(m, p + n_\mu M_T)}{\mathbf{S}(m, p + n_\mu M_T)}. \tag{3.32}$$

For the estimation of the range and velocity, only one of the matrices $\mathbf{D}_q$ is necessary, however all matrices can be used.

CHAPTER 4

Multicarrier Signal Specifications for Joint Communications and Radar

In this chapter we present relationships and constraints for optimal choice of parameters used in RadCom systems based on multicarrier waveforms. The design strategies for these parameters have already been presented and discussed in [5, 58, 96, 97]. However, it is still quite open to optimizations and variations in the values assigned to the parameters, as optimal parameterization has not yet been found. Specifications for waveform parameters used in radar and communication systems are restricted by several factors related to communication and radar functions. In this chapter we discuss in detail an optimized choice of parameters, taking into account the constraints inherent to RadCom system environments. The optimized choice of parameter present in this chapter are based on the parameterizations for OFDM signals presented at [5]. After the discussion, a parameterization for OFDM RadCom systems is proposed.

4.1 Restrictions on the communication system

The main focus for applications in joint radar and communication systems has been for automotive systems, where the purpose of the communication functions is to provide wireless V2V and vehicle communications for infrastructure. The main factors that can limit and restrict the system related to communication functions are imposed by the characteristics of the type of application and the signal used in the transmission .

The radio channel is characterized by two main characteristics of the system: the maximum multipath distance and the maximum Doppler frequency, which are directly related to the coherence bandwidth B_C and the coherence time T_C of the channel [98]. The main parameters of the RadCom system that are limited by the communication function and need to be designed over these limitations are: cyclic prefix, subcarrier spacing and frame size. The details of this parameterization are described below.

4.1.1 Duration of the cyclic prefix/guard interval

Applications that eventually need to use RadCom systems have multipath channels. The transmitted signal reaches the receiver through several paths with different delays. Consequently, if a short pulse is transmitted, the received signal will contain many echoes with varying spacing and amplitude. This causes intersymbol interference. In order to avoid inter-symbol interference, a prefix can be added to the signal, containing a cyclic repetition with a duration of T_{CP}. This duration must correspond to: The maximum excess delay τ_e, that is the time difference between the first and the last arrival of the same wave [98].

$$T_{CP} > \tau_e \tag{4.1}$$

However for some waveforms, such as FBMC, the system can operate properly without the use of CP and this restriction becomes unnecessary, improving the efficiency of the system. As the cyclic prefix reduces channel throughput, the choice of T_{CP} may represent a trade-off between available data bandwidth and system reliability [96]

4.1.2 Subcarrier spacing

The effects caused in the multipath are also reflected in the frequency domain, resulting in selective frequency fading. There is little we can do to control the multipath in an environment, but we can restrict the spacing of the subcarriers so that the signal is not seriously affected by the multipath. The length of the path or the multipath propagation is called coherence bandwidth. In the literature coherence bandwidth has different definitions, commonly the coherence bandwidth is expressed as the bandwidth at which a complete cycle change occurs [99] and is given by

$$B_C = \frac{1}{\tau_{rms}}, \tag{4.2}$$

where τ_{rms} is the Root Mean Square (RMS) delay spread. One measure for this parametrization is to how probable is the correlation of two signals present at two frequencies separated by Δf. The value of Δf where the envelope autocorrelation of the spectrum falls below a value 'x' is known as coherence bandwidth of 'x' multiplied by 100 in percentage units [96].

The most common values to represent the coherence bandwidth are 50% and 90%, is also commonly still used the corresponding 25% percent. In the coherence bandwidth of 50% correlation between end frequencies, the channel varies by 3 dB [99], and is defined by

$$B_{C,50\%} = \frac{1}{5\tau_{rms}}. \tag{4.3}$$

For 90% correlation has 0.5 dB channel variation:

$$B_{C,90\%} = \frac{1}{50\tau_{rms}}. \tag{4.4}$$

The 1/3 cycle criteria can be used to define the flat channel [99], which corresponds to 25% correlation with a variation of about 6 dB in the channel, the $B_{C,25}$ of 25% correlation is

$$B_{C,25\%} = \frac{1}{3\tau_{rms}}. \tag{4.5}$$

The notions of flat fading and frequency selective fading are important for relating coherence bandwidth to multicarrier waves. The fading can be classified according to the ratio of the coherence bandwidth to the channel bandwidth. In the case of flat fading, the signal bandwidth is small compared to the channel variations. As a result, the signal amplitude varies, but the signal is not distorted. On the other hand, for frequency selective fading, the signal bandwidth is large compared to the channel variations, and the signal presents low amplitude variations however it is distorted. One advantage of multicarrier waves is that the spacing of the subcarrier can be selected so that each carrier experiences flat fading [96].

Interference between frequency components also determines the coherence time. In particular, the doppler spread B_D and the coherence time are inverse. The Doppler spread is an additional restriction on the spacing of the subcarriers [96]. To avoid the scenario where a spread Doppler signal leaks to adjacent carriers and causes interference, the spacing of the subcarriers must be much greater than the maximum Doppler spread.

$$B_D \ll \Delta f \ll B_C, \tag{4.6}$$

since multicarrier systems are very sensitive to fading, a lower channel boundary is defined as ten times the Doppler [5].

4.1.3 Frame duration

The propagation channel changes due to the relative movement (velocity) of the receiver or transmitter. A metric to characterize this time variation is the coherence time, which describes the interval during which the channel can be considered unchanged. The channel estimates are performed and used to correct the effect of flat fading in individual subcarriers. These estimates are obtained from training sequences in the packet header [96]. In order for the equalizer to perform the equalization process without any update during one packet, the maximum packet size must be less than the channel coherence time, so that equalizations remain valid.

4.2 Limitations on the radar system

The limits of the perspective of the radar function refer mainly to the minimum resolutions required for proper targeting operation and the minimum ambiguity values of range and velocity. For this, the choice of the bandwidth, the number of subcarriers, the duration of the symbol and the number of evaluated symbols must be designed in such a way that the ambiguity and radar resolution profiles cover the requirements of the desired application.

4.2.1 Bandwidth

In the transmitted multicarrier pulse with a bandwidth B_W, the received complex signal will have the same bandwidth and can be sampled as $f_s = B_W$ [3]. The size of the estimation interval cell is then given by $c/2B_W$. As a result, if we want to project the resolution range, we will adjust the bandwidth to comply with

$$B_W \geq \frac{c}{2\Delta r}, \tag{4.7}$$

where Δr is the range resolution. The range resolution does not depend on the waveform employed or the particular parameterization of the system, it depends only on the total bandwidth occupied by the transmitted signal. The resolution must be small enough to allow the separation of the desired objects, such as cars, buildings, etc.

4.2.2 Pulse duration

In cases where the radar system uses the same antennas for transmission and reception, the pulse duration is limited, therefore, considering the distance to be detected R_{max} [3], the pulse length will have a limit of

$$T \geq \frac{2BR_{max}}{c}. \tag{4.8}$$

The maximum unambiguous velocity of the targets also limits the duration of the symbol. For reliable radar operation, after setting the maximum relative velocity we have to define a symbol duration, given by

$$T \geq \frac{c}{2f_c V_{max}}. \tag{4.9}$$

4.2.3 Number of subcarriers

The radar is also affected by the Doppler effect. In the case of radar, propagation has twice the Doppler shift in relation to the propagation of communications systems [58]. The Doppler shift in the radar system can be described as

$$f_D = \frac{2v}{\lambda}.$$

To avoid distortion in the orthogonality of the subcarriers, a reasonable condition for the spacing of the subcarrier is given by

$$\Delta f \gtrsim 10 f_D. \tag{4.10}$$

The radar system also suffers from maximum unambiguous distance limitations, considering that the signal travels the distance twice, resulting in an unequivocal maximum measurement distance of

$$R_{max} = \frac{c}{2\Delta f} = \frac{cT}{2}. \tag{4.11}$$

The minimum bandwidth value B_{min} is determined by the minimum resolution, and in addition we have the limitations imposed by the channel and by the R_{max} to design the number of subcarriers. Therefore, we must choose the appropriate value for N, a reasonable condition is given by

$$N \gtrsim \frac{B_{min}}{\Delta f}. \tag{4.12}$$

4.2.4 Number of symbols

The Doppler resolution depends on the number M of evaluated symbols, and the duration of Pulse T [34], being

$$\Delta f_D = \frac{1}{MT}, \tag{4.13}$$

or, in terms of velocity resolution

$$\Delta v = \frac{c}{2Mf_cT} = \frac{c\Delta f}{2Mf_c}. \tag{4.14}$$

It can be said that the radar system performs better if it occupies a high bandwidth, which can be achieved by increasing the distance of the subcarrier or the number of subcarriers; and if it occupies a longer period of time, which is achieved by increasing the length of a symbol (which would decrease the spacing of the subcarriers and thus the range resolution) or also by adding more OFDM symbols to a frame, so

$$M \geq \frac{c}{2\Delta v f_c T}. \tag{4.15}$$

Thus, in principle, the evaluation of a greater number of OFDM symbols would impart a better velocity resolution, but is not practical, since moving objects must remain in a resolution cell during the evaluation [34], given by

$$\Delta R \Delta v = \frac{c^2}{4MNf_c}. \tag{4.16}$$

This is inversely proportional to the total number of samples ($M \times N$) and the carrier frequency (f_c).

4.3 Physical system and regulatory restrictions

In addition to the parameters imposed by the applications for the RadCom system, there are also hardware limitations and regulatory restrictions due to the fact that radio activity is regulated.

The two major factors of the physical system to be weighted in the parameter choices are the signal power limits and the current hardware technologies. In relation to regulatory restrictions, the limits imposed by the legislation restrict the values that can be chosen for the parameters in the implementation of the commercial application system. For example, the choice of the center frequency f_c, the available bandwidth B_W and the maximum transmission power P_{max} are restricted and are regularized [5]. This restricts quite effectively the great values that could be found fulfilling the other constraints and can be further modified as new regulatory standards are chosen. A discussion of these three decisive factors in the choice of RadCom system parameters will be developed next.

4.3.1 Power limitations

In practical systems receivers and transmitters are always limited in their energy consumption, effectively limiting the SNR in the receiver. Both radar and communication systems require a minimum SNR at the reception to operate accurately, but they have a maximum power limit that can be transmitted at the transmitter.

It is then necessary to optimize the system values so that a signal transmitted with power P_t arrives at the receiver with a minimum received power P_r which allows the system to have a desirable SNR for the correct operation of the desired function. In a free space scenario, for communication systems a received power P_r

in a distance of r [100] is given by

$$P_{r,comm} = \frac{P_t G_r \lambda^2}{(4\pi)^3 r^2}, \tag{4.17}$$

and for the radar [97, 100] is

$$P_{r,radar} = \frac{P_t G_r \lambda^2 \sigma_{RCS} NM}{(4\pi)^3 r^4}, \tag{4.18}$$

where σ_{RCS} is the radar cross section of the target.

Assuming an existing SNR value, we have that the maximum distance R_{det} [97, 100] for which a target can be detected given by

$$R_{det} = \left[\frac{P_t G_r \lambda^2 \sigma_{RCS} NM}{(4\pi)^3 SNR P_N}, \right]^{\frac{1}{4}} \tag{4.19}$$

since the SNR of the radar signal is given by

$$SNR_{radar} = \frac{P_r}{P_N} = \frac{P_t G_r \lambda^2 \sigma_{RCS} NM}{(4\pi)^3 R_{det}^4 P_N}, \tag{4.20}$$

P_N is the noise power in the radar receiver defined by

$$P_N = \kappa_B T_0 NF B_W, \tag{4.21}$$

where κ_B is Boltzmann's constant (1.38×10^{-23} watt-sec/K); T_0 is the standard temperature (290 K); NF is the noise figure of the receiver subsystem (unitless). The noise figure, NF, is a method to describe the receiver noise (the noise figure is often given in dB, it must be converted to linear unit)[100]. In [97] the author has shown that the minimum SNR needed to detect a target is

$$SNR_{min} = \frac{P_r}{P_N} = \ln(1 - (1 - p_{FA})^{\frac{1}{NM}})), \tag{4.22}$$

where p_{FA} is the probability of a false alarm during the processing of a single frame with only noise present. To obtain a sufficiently high signal for the noise ratio for the radar processor, the energy content of the signal to be processed must be maximized [5]. At the receiver, for example, in an OFDM system, the symbol energy (E_s) per noise power density (N_0) is given by

$$\frac{E_s}{N_0} = \frac{P_r}{B_W N_0}. \tag{4.23}$$

For practical applications where transmission power is limited, this means that the integration time of the processor should be chosen as long as possible. Thus the minimum values for bandwidth B_W [5] can be found through the following function

$$B_W \leq min\left[\frac{P_t G_r \lambda^2 \sigma_{RCS}}{(E_b/N_0)_{radar} N_0 (4\pi)^3 R_{det}^4}, \frac{P_t G_r \lambda^2}{(E_b/N_0)_{com} N_0 (4\pi)^2 r^2}\right], \tag{4.24}$$

where E_b is the bit energy. As shown in [5], the lower the bandwidth value B the better the signal-to-noise ratio in the system.

4.3.2 The PAPR Problem

The multicarriers signals have the coherent superposition of a large number of modulated subcarriers, the magnitude of the composite signal is time-varying. The magnitude of the time variable baseband signal is a problem for the Radio Frequency (RF) power amplifier after the baseband signal has been converted to the frequency of the RF carrier in the transmitter [101]. High PAPR signals lead to the requirement for high dynamic range RF power amplifiers. The PAPR is defined as

$$\text{PAPR} = \frac{\max[|x(t)|^2]}{\text{mean}[|x(t)|^2]}, \tag{4.25}$$

when the signal changes from a low instantaneous power level to a high instantaneous power level, large signal amplitude oscillations are encountered, causing distortions [101].

Distortion can become another source of noise that can fall in and out of the band. In-band distortion cannot be reduced by filtering and results in degraded performance, increasing the probability of bit error, while out-of-band reduces spectral efficiency, since the power density spectrum is significantly extended. Therefore, during design of the RadCom systems, we need to mitigate these variations [3].

In most current multichannel systems expensive highly linear amplifiers are used and/or a large back-off power is chosen to maintain quasi-orthogonality. However for RadCom applications that are focused primarily on automotive technologies, it is desirable to apply inexpensive amplifiers operating with a reasonably small power back-off in order to maintain energy efficiency. Therefore, low PAPR values are very important [98].

For the choice of a value N that helps to reduce the value of PAPR, we must choose a value of $2 \ln N$, always looking for the lowest possible N value, as discussed in [5], this will reduce the PAPR. It is also possible that in future technologies compensation techniques can be used to mitigate these problems, such as pre-distortion technique. Pre-distortion technique is a popular compensation technique applied on the transmitter side, in which the transmitted data symbols or the input signal of the amplifier are pre-distorted so that the amplifier output signal is less distorted [98].

4.3.3 Sampling Limitation

The hardware technologies that can be implemented in the system need to be taken into account when choosing the parameters. First of all, for the modulation process in subcarriers we know that all the signal needs to be converted to digital, so the higher the bandwidth, the more costly and complex it will be for the physical system to carry out the process. Therefore the value of $N\Delta f$ must be as low as possible, being within the acceptable value for the desired range resolution.

4.3.4 Regulations

The major challenge of the RadCom system parametrization is to make all other requirements from the point of view of radar and communication functions can be achieved within the technical limits allowed for the signal. RadCom systems can operate in the license-free Industrial Scientific, and Medical (ISM) frequency bands that are defined by the ITU Radio Regulations [102]. These bands have bandwidth limits and specific availabilities depending on the region of the world, which further restricts the range of optimal values available for RadCom systems. A frequency band that is suitable for both radar and communications is the 24 GHz ISM band, which has a bandwidth of 200 MHz [102].

Table 4.1: Example of system Parameters for OFDM proposed in [4]

PARAMETERS	SYMBOL	VALUE
Carrier frequency	f_c	24 GHz
Number of subcarriers	N	1024
Number of evaluated symbols	M	256
Total signal bandwidth	B	93.1 MHz
Subcarrier spacing	Δf	90.909 kHz
OFDM symbol duration	T	12.375 μs
Range resolution	ΔR	1.61 m
Velocity resolution	Δv	1.97 m/s
Unambiguous range	R_{max}	1659 m
Unambiguous velocity	v_{max}	$\pm$ 253 m/s
Modulation		4-QAM

4.4 Examples of parameter sets

The band chosen for the parametrization was the 24 GHz ISM band, we followed the parametrization models realized in [5] for OFDM signals, a example of parametrization proposed in [4] is presented in the Table 4.1.

4.4.1 OFDM radar parametrization

We will start the parametrization by finding the limits of maximum and minimum values for certain parameters, and then we can optimize them, according to the other restrictions. Starting first with the bandwidth value. We know that the maximum bandwidth we can use in the 24 GHz ISM is 200 MHz with a maximum P_{max} of 20 dBm (100 milliwatts). Then $B \leq 200$ MHz.

Although we have previously seen that a large bandwidth decreases the SNR, we consider an acceptable bit error probability of $P_b = 10^{-3}$ [5]. Then according to, in the case of Binary Phase Shift Keying (BPSK) and Quadrature Phase Shift Keying (QPSK) modulation, the bit error rate before coding for the additive white Gaussian noise is given by

$$P_b = \frac{1}{2}\text{erfc}\left(\sqrt{\frac{E_b}{N_0}}\right), \tag{4.26}$$

so a minimum E_s/N_0 would be 6.8 dB for BPSK and 9.8 dB for QPSK, producing a maximum bandwidth of 258 MHz and 129 MHz. In our system we consider the

Table 4.2: Channel constraints for 24GHz [5]

Parameters	Urban	Highway
RMS excess delay (τ_e)	0.24 μs	0.86 μs
RMS Doppler spread B_D	0.30 kHz	2.72 kHz
Coherence bandwidth $B_C 90\%$	292 kHz	195 KHz
Coherence time (T_C)	0.36 ms	0.03 ms

worst case, with a QPSK modulation, and so we have $B_W < 129$ MHz.

The lower limit will be given by the minimum value required by the desired distance resolution Δr, as the focus application of this technology until the present moment is for automotive radar, we have that a minimum resolution of 2 m may be sufficient to differentiate vehicles [97]. So we have

$$B_W \geq \frac{c}{2\Delta R} = 75\ MHz, \tag{4.27}$$

for choose B_W we have the following limits $75\ MHz \leq B_W \leq 129\ MHz$. Let us now find the values for Δf and N. We have Δf need to be $\Delta f \geq 10 f_D$, and smaller than the coherence band B_C of the channel, the specifications of the channels considered for application are shown in the table 4.2, as presented in [5], for the two most typical scenarios of automotive radar applications, called " Urban "and" Autobahn "scenarios. In the simulation performed by the author [5],an urban environment was considered with a high density of both parking and moving vehicles, and the highway scenario, with vegetation being the main source of scattering; one vehicle acts as transmitter and another as receiver.

We have seen that $\Delta f < B_C$ to be within the coherence band of 90%. For the lower limit, we consider the maximum relative velocity 270 km/h, which generates a $F_D = 12.015$ KHz, providing a minimum limit for $\Delta f = 10F_D = 120,15$ KHz. Thus we have 195.31 KHz> $\Delta f \geq 120,15$ KHz. However, the value of Δf can not be defined only for this reason, since $T = 1/\Delta f$, we need to find the limits for the duration of the symbol, to properly restrict the value of Δf.

We know that the duration of the symbol limits the maximum detectable distance ($R_{max} = cT/2$), so we need to make sure that the symbol duration is in accordance with that value. According to [5] if we assume that due to the high attenuation of the scattering process the maximum detectable distance is 200 m, a maximum limit of 200 m is acceptable, which gives us $T > 1.33$ μs or $\Delta f < 750$ kHz. The duration of the symbol also limits the maximum unambiguous velocity, as we consider 270 km/h (75 m/s) as a maximum acceptable value, we will have

$$T \geq \frac{c}{2\Delta R f c} = 0.83\mu s. \tag{4.28}$$

Finally for the communication system, we need the duration of the symbol to be less than the coherence time, so we have that $T < 0.03$ ms. However, the duration of the symbol in OFDM also has a contribution portion of the cycled prefix period T_{CP} that must be greater than the delay time, considering table 4.2 and that $T_{CP} > \tau_e$, we assume that process is maximum detectable distance is 200 m, so we can calculate the maximum delay of the system, thus obtain the value $T_{CP} > 1.33$ μs (in the communications function this corresponds to a maximum delay difference between the propagation paths of 400 m).

$$T = T_{OFDM} + T_{CP} \tag{4.29}$$

Table 4.3: OFDM System Parameters

PARAMETERS	SYMBOL	VALUE
Carrier frequency	f_c	24 GHz
Number of subcarriers	N	1024
Number of evaluated symbols	M	256
Total signal bandwidth	B	113.92 MHz
Subcarrier spacing	Δf	111.25 kHz
OFDM elementary symbol duration	T_{OFDM}	9.00 μs
Cyclic prefix duration	T_{CP}	2.25 μs
OFDM symbol duration	T	11.25 μs
Range resolution	ΔR	1.316 m
Velocity resolution	Δv	2.171 m/s
Unambiguous range	R_{max}	1347 m
Unambiguous velocity	v_{max}	± 278 m/s
Modulation		4-QAM

By setting all the lower and maximum limits for the parameters, we will now choose an optimized value for each parameter. For bandwidth we try to use as little as possible to maximize the duration of the symbol. For the choice of the value of N, we must for a lower value of PAPR to obtain the smallest value of N and that is a power of two, since the DFT can then be implemented in a particularly efficient way. Considering the minimum value for Δf, we can choose a Δf to correspond to the minimum Δr resolution of 2 m, we have the lowest possible value for $N = 1024$, thus providing us with a band of 124 Mhz and a resolution of 1.4 m. To choose the number of symbols we have to define the desired value of velocity resolution and M. From this we calculate the other values and construct the Table 4.3. With an optimized parameterization for the OFDM for both the radar system and the communication system.

Note that the frame length was equal to 2.9 ms, greater than the coherence time of the channel, but this can be solved, as proposed in [5], to send two OFDM symbols for synchronization, gain control and equalization and then send one OFDM symbol for re-equalization every T_C. In addition, as explained in [5], since the frame is very large, it needs a large amount of data, this amount of data has to be transmitted, if necessary by padding the frame with random bits or increasing the channel coding rate.

PART

I

MULTICARRIER RADAR

CHAPTER 5

FBMC Radar

At the present time many studies have been carried out to jointly use the OFDM signal for communication and radar functions, but other waveforms have been shown to be better candidates than OFDM for communications applications. Therefore studies on evaluation of the application of these same signals to radar functions may be necessary. In this chapter, we adapted the radar processing of the OFDM signal to be applied in a new FBMC scheme, which is shown to be much superior to the OFDM system. FBMC radar presents the same BER performance in multipath channels, a much higher spectral efficiency and as shown here, better performance in radar targeting. In this chapter we also evaluate the application of FBMC to mitigate inter-system interference in RadCom systems, one limiting factor of the radar's performance. First in Section 5.2 we will briefly outline the FBMC waveform. In the Section 5.3 we present the OQAM-FBMC radar. Following this, in Section 5.4, we present the adaptation of OFDM radar processing techniques to the QAM-FBMC transmission scheme. In Section 5.5, we describe our radar measurement setup and we compare the performance of the FBMC and OFDM radars for a scenario with one user and another with multiple users, where an evaluation with measurements of interference is performed. In order to better quantify the inter-system interference of both systems, we simulate the systems with noiseless environment. Finally, in Section 5.5.4 we present the summary.

5.1 Introduction

Most current RadCom systems use OFDM signals, which requires a CP that lowers the spectral efficiency. Moreover, the use of rectangular pulses in OFDM generates high Strong Out-of-Band (OOB) emissions, which lead to inter-system interference in adjacent frequency bands. For this reason, guard bands are required; these, in addition to decreasing spectral efficiency, worsen the range resolution of the radar.

The interference caused by OOB emissions appears as additive noise for OFDM radar and cannot be filtered by conventional methods [103]. A possible solution to reduce such interference in RadCom systems is the use of other multicarrier waveforms with very low OOB emission such as FBMC. The FBMC waveform eliminates the use of guard bands and CP, provides low OOB emission, and has high spectral efficiency. OQAM-FBMC is the best-known implementation of FBMC, where the modulated symbols are mapped separately in the real and imaginary parts and are offset in time by the symbol duration. In [47] the authors consider the use of OQAM-FBMC for radar as an extension of OFDM, but the methods have several disadvantages. Namely, retaining self-interference (caused by the non-orthogonality of FBMC) in the radar estimates; also, its implementation in MIMO radar systems is difficult. This is what makes it a weak candidate for the uses in radar, since the doubled rate of transmission makes the resolution of the velocity fall by half, and the self-interferences remain in the estimates of targets made by the radar, and it is very difficult to implement in RADAR MIMO systems [47].

A new FBMC signal scheme with QAM modulation has been recently proposed in [104]. This scheme supports complex value QAM symbols instead of real-valued symbols, and thus the transmission rate in QAM-FBMC is the same as in the OFDM. It also has a BER, even in multipath systems, equivalent to that found in OFDM, it does not suffer from remaining intresting interferences and also presents no difficulty to be implemented in MIMO systems. Initial analysis of this technique for communication systems can be seen in [105]. Motivated by these attractive features, we adopt a QAM-FBMC system to be adapted for use in radar systems and evaluate the reduction of inter-system interference with the use of QAM-FBMC.

5.2 FBMC waveform

In FBMC system, a set of parallel symbols are transmitted through a bank of synthesis filters and the receiver side the data symbols are recovered through a bank of analysis filters. Each filter is based on the specially designed prototype filter. in the case of the FBMC, the filters are designed to reduce the side lobes. The FBMC, as well as the OFDM, divided the spectrum into several subbands, but different from the OFDM that filters the whole band, this technique applies filtering functionality to each of the subcarriers. Thus, the sidelobes are much weaker and, therefore, the problem of inter-carrier interference is attenuated [84]. FBMC reduces guard band overhead and eliminates the use of CP. Having thus improved spectral efficiency. However, the subcarrier filters are very narrow and require long filter time constants, as a result, individual symbols overlap in time.

FBMC may be one of the candidates for the post-OFDM waveform for IoT applications, since it can use the spectrum efficiently under various environments. However, in order not to compromise spectral efficiency, conventional FBMC systems generally double the rate of transmission symbols compared to OFDM, due to adopting the OQAM [106], but new FBMC modulation techniques have been proposed in [104], where the modulation adopts is the QAM, and the transmission rate remains the same as OFDM. In the following subsections we will discuss in detail each of these FBMC modulation techniques.

5.2.1 OQAM-FBMC

The most popular method of FBMC [106]: OQAM-FBMC, has only real-value data (pulse amplitude modulation signals), in which the modulation symbols are mapped separately with the symbol shift duration (shown in Figure 5.1). OQAM is necessary since the prototype filter satisfies the orthogonality of the subcarriers only in the real field. And so to compensate for the data rate, the transmission rate in OQAM-FBMC is twice as fast as in OFDM without CP. This method also has self-interference and implementation in MIMO networks is not trivial and may be very limited [107].

Several architectures of FBMC receivers have been studied in the literature,

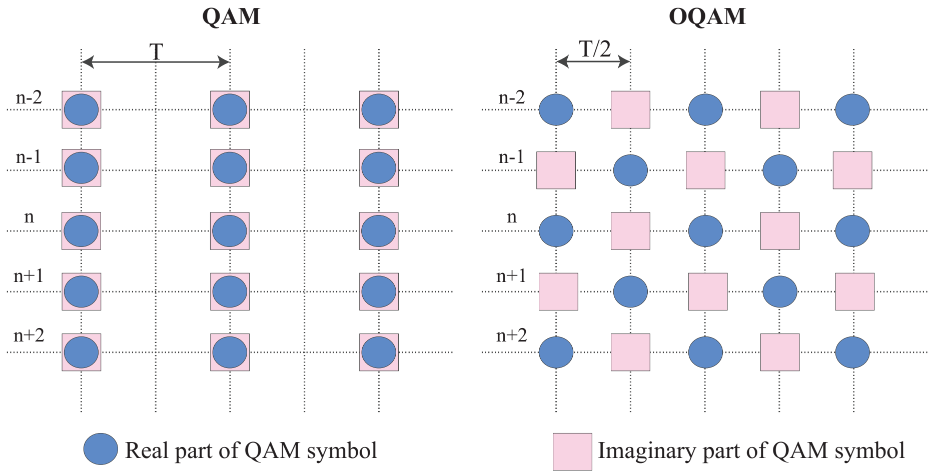

Figure 5.1: QAM and OQAM symbol mapping on carriers.

the most important are Polyphase Networks (PPN) [108] and the Frequency Spreading (FS) implementations [109]. In the classical PPN approach (figure 5.2), the OQAM symbols feed an N size DFT and then a PPN. The receiver applies the corresponding filtering before an N-size DFT and then the equalization is performed [83].

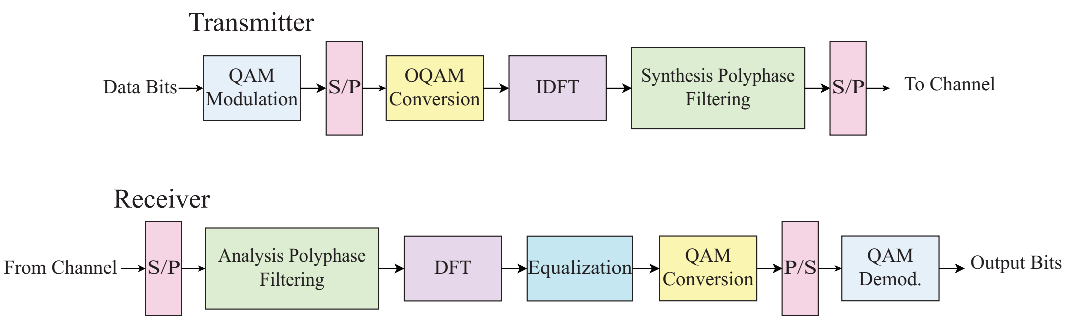

Figure 5.2: PPN OQAM-FBMC model.

In the alternative scheme proposed by Bellanger [109] the filter bank is generated by Frequency Spreading (Figure 5.3), the OQAM symbols are filtered in the frequency domain. The filters are characterized by the overlapping factor, L which is the number of multicarrier symbols that overlap in the time domain. The prototype filter order can be chosen as $2L-1$. The result then feeds an IDFT of size LN, followed by an overlay and sum operation. On the receiver side, a sliding window selects LN points for each set of $N/2$ sample. A DFT of size KN is applied followed by filtering by the corresponding filter [83].

The time domain OQAM-FBMC transmitted signal composed by N subcarriers

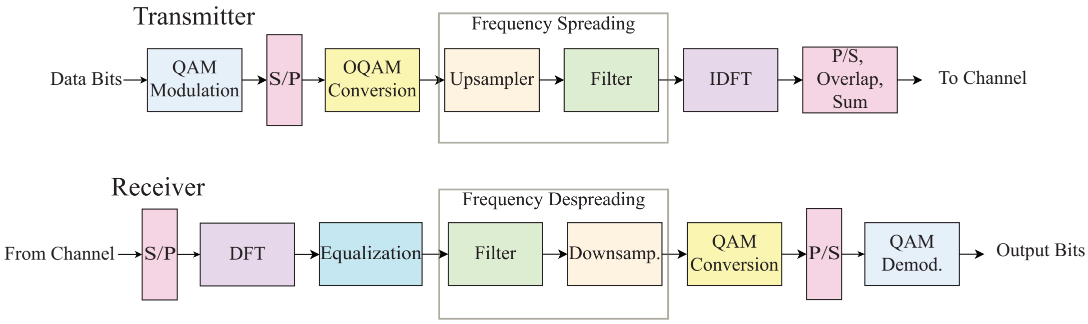

Figure 5.3: FS OQAM-FBMC model.

and M symbols is expressed by:

$$x(t) = \sum_{m=0}^{M-1} \sum_{n=0}^{N-1} a(m,n)\theta(m,n)g(t - mT/2)e^{2\pi jn\Delta f(t-mT/2)} \tag{5.1}$$

where $a(m,n)$ is Pulse Amplitude Modulation symbol, with $a(2m,n) = \Re(\mathbf{S}(m,n))$ and $a(2m+1,n) = \Im(\mathbf{S}(m,n))$ ($\Re(x)$ being the real part of x, and $\Im(x)$ the imaginary part of x), and $\theta(m,n) = j^{(n+m)}$ is the additional phase term [47].

The demodulation of FBMC signals is performed analogously to OFDM by performing the inverse transmitter operations:

$$b(m,n) = g^*(-t)y(t)e^{-2\pi jn\Delta ft} \tag{5.2}$$

So the received data $\hat{\mathbf{S}}(m,n)$ is:

$$\hat{\mathbf{S}}(m,n) = \Re\{\theta(m,n) * b(2m,n)\} + j * \Im\{\theta(m,n) * b(2m+1,n)\} \tag{5.3}$$

where two successive samples of $b(m,n)$ are used to form a complex-valued received data estimate $\hat{S}(m,n)$.

5.2.2 QAM-FBMC

The orthogonality in the real domain achieved in the OQAM-FBMC system can be easily broken by complex channel or MIMO technologies, therefore, OQAM-FBMC has an inevitable self-interference problem. To solve this problem A new FBMC signal scheme with QAM modulation has been recently proposed in [104].

This scheme supports complex value QAM symbols instead of real-valued symbols, and thus the transmission rate in QAM-FBMC is the same as in the OFDM. It also has a BER, even in multipath systems, equivalent to that found in

OFDM, it does not suffer from remaining self-interferences and also presents no difficulty to be implemented in MIMO systems. Initial analysis of this technique for communication systems can be seen in [105]. The QAM-FBMC filter design performed in [104], partially satisfies the generalized Nyquist criterion and the fast fall rate condition, optimizing overall filter coefficients

The architecture of the QAM-FBMC transceiver is shown in Figure 5.4. In this architecture the filter coefficients in the time domain are designed pulse shaping filter, and frequency domain filter coefficients are given with up-sampling between subcarriers. Initially the modulated symbols for N subcarriers are divided into even subcarrier symbols and odd subcarrier symbols. Then an IDFT is applied and the symbols are repeated. Finally then, the symbols are filtered by $B(B \geq 2)$ prototype filters through windowing (elemental multiplication) and summed. At the reception the reverse process is performed, with the additional equalization performed. The QAM-FBMC symbol interval is the same as the duration of OFDM symbols without CP, but the symbols overlap each other [105].

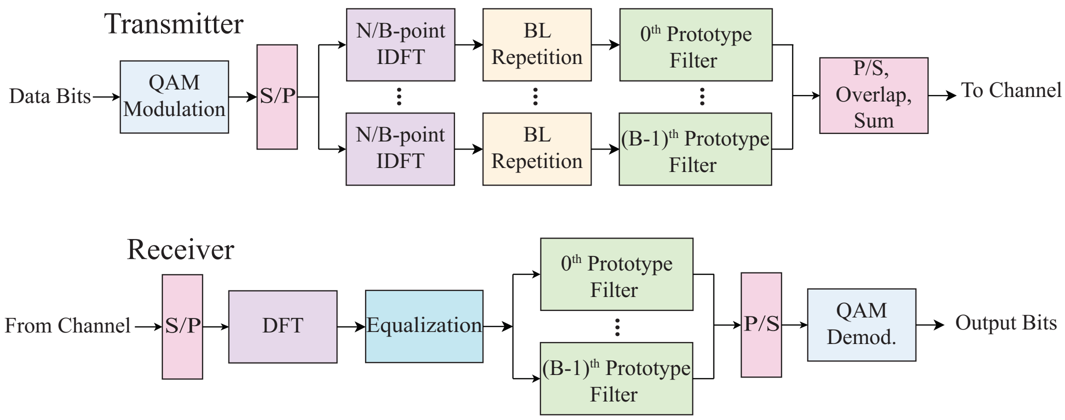

Figure 5.4: QAM-FBMC transceiver.

In the QAM-FBMC system proposed in [104] the discrete-time transmit signal $x(q)$ of the QAM-FBMC system is represented as the sum of complex QAM data symbols $\mathbf{S}(m,d)$ on the d-th subcarrier with $n = Bd + b$, where $b = 0, ..., B-1$ and the m-th symbol as

$$x(q) = \sum_{m=0}^{M-1} \sum_{b=0}^{B-1} p_{b,0}(q - mN) \sum_{d=0}^{\frac{N}{B}-1} \mathbf{S}(m,d) e^{j\frac{2\pi q}{N/B}d}. \tag{5.4}$$

The FBMC symbol duration Q is defined by $Q = LM$, with L as an up-sampling factor and the index q is given by $0 \leq q < Q$. For simplification of the equation we now turn to the representation of the system in block processing form. Figure 5.5 shows a simplified representation of the structure of the QAM-FBMC transceiver systems. We define the transmitted data symbol vector of length N in the m-th QAM-FBMC symbol as $\mathbf{S}[m]$ with the n-th element $\mathbf{S}(m,n)$ [104]. Then we can rewrite the m-th transmitted symbol vector $\mathbf{x}[m]$ as follows

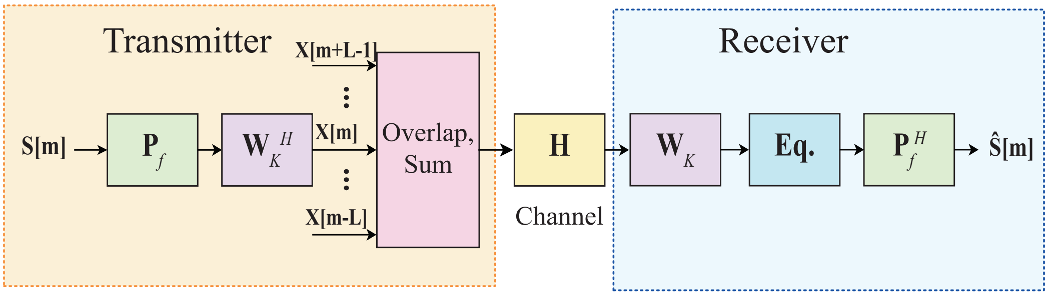

Figure 5.5: Simplified block representation of QAM-FBMC transceiver system structure—Eq. denotes equalizer.

$$\mathbf{x}[m] = \mathbf{W}_Q^H \mathbf{P}_f \mathbf{S}[m], \tag{5.5}$$

where $\mathbf{P}_f$ is the $Q \times N$ frequency domain filter coefficient matrix in which the n-th column is given by Q-point DFT of the corresponding shifted filter of the prototype filter $p_{b,0}$, and $\mathbf{W}_Q$ is the Q-point DFT matrix. Using the equation (5.5) and the overlap and sum structure of the transmitted symbols [110], the 0-th received symbol vector of length Q is represented by

$$\mathbf{y}[0] = \sum_{m=-L}^{L-1} \mathbf{T}[m]\mathbf{H}[m]\mathbf{x}[m] + \tilde{\eta}, \tag{5.6}$$

where the $\tilde{\eta}$ is the AWGN vector. The channel matrix $\mathbf{H}[m]$ is a Toeplitz matrix with size $(Q+N)\times Q$, and each column of the matrix is given by the circular shift of the channel impulse response $[\mathbf{H}]_{(:,\mathrm{k})} = \mathrm{circshift}\left\{[h_0 \cdots h_{L_c-1}\mathbf{0}_{K+N-L_c}]^T, n-1\right\}$,where L_c is the length of time domain channel taps. The shift-and-slice matrix $\mathbf{T}[q]$ with size $Q \times (Q+N)$ [110] and $\mathbf{I}$ as identity matrix, is defined as

$$\mathbf{T}[m] = \begin{cases} \begin{bmatrix} \mathbf{0} & \mathbf{I}_{Q+N+mN} \\ \mathbf{0} & \mathbf{0} \end{bmatrix}, & m < 0 \\ \begin{bmatrix} \mathbf{I}_Q & \mathbf{0} \end{bmatrix}, & m = 0\,, \\ \begin{bmatrix} \mathbf{0} & \mathbf{0} \\ \mathbf{I}_{N-mN} & \mathbf{0} \end{bmatrix}, & m > 0 \end{cases} \tag{5.7}$$

which is used to model the interferences to the 0-th received symbol from neighboring symbols. The summation index from the $-(L-1)$ to the $(L-1)$ is interpreted in interferences from adjacent symbols by the QAM-FBMC overlap and sum structure shown in the Figure 5.6, where the comparison of the overlap of the OQAM system with the QAM is performed, see that the OQAM-FBMC comparing to QAM-FBMC transmission requires two times faster transmission, which causes two more times overlap in time domain. The $-L$ term should be included by the tails of causal channel [110].

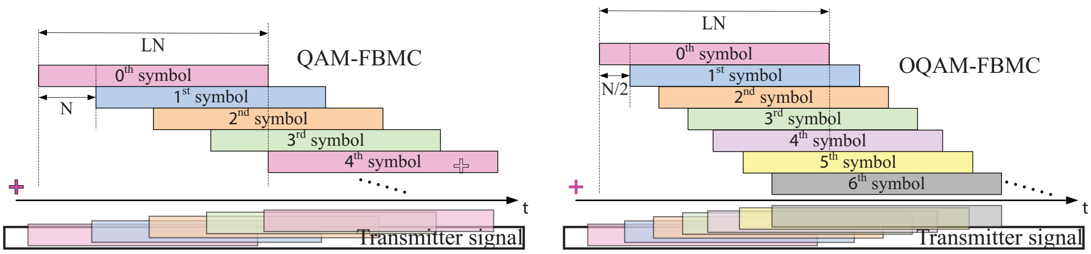

Figure 5.6: Overlap and sum structure comparison of OQAM-FBMC and QAM-FBMC.

Let the 0-th received QAM-FBMC symbol in frequency domain is $\mathbf{y}[0]$, which is the Q-point DFT output. If we apply the appropriate channel equalizer $\mathbf{G}[0]$, then the estimated data symbol vector of the 0-th symbol can be written as

$$\hat{\mathbf{S}}[0] = \mathbf{P}_f^H \mathbf{G}[0] \mathbf{W}_Q \mathbf{y}[0] \tag{5.8}$$

$$= \mathbf{P}_f^H \mathbf{G}[0] \mathbf{W}_Q \sum_{m=-L}^{L-1} \mathbf{T}[m]\mathbf{H}[m]\mathbf{x}[m] + \tilde{\eta}, \tag{8}$$

The filter bank used for QAM-FBMC is shown in the table 5.1 for the construction of the filter coefficients $p_b[q]$. We apply a Q-point IDFT to the elements

Table 5.1: Filter coefficients in the frequency domain

	$Q_0[q]$		$Q_1[q]$	
filter	Real	Imag	Real	Imag
$P_b[0]$	+1.0000		+1.0000	
$P_b[1]$	-0.5005	+0.4286	+0.0995	-0.6281
$P_b[2]$	+0.5677	-0.5077	-0.5738	+0.4537
$P_b[3]$	-0.0287	-0.1000	+0.6079	-0.7773
$P_b[4]$	+0.3053	-0.5326	-0.2960	+0.5131
$P_b[5]$	-0.9982	-0.1158	-0.0425	+0.0581
$P_b[6]$	+0.2990	+0.1010	+0.0478	-0.3231
$P_b[7]$	-0.2697	+0.3972	-0.3200	-0.0565
$P_b[8]$	+ 0.0848	+0.1466	+0.0775	+0.1336
$P_b[9]$	-0.1223	-0.2905	-0.4873	-0.0060
$P_b[10]$	-0.0231	+0.3285	+0.2316	+0.2267
$P_b[11]$	+0.1325	+0.0146	+0.0706	-0.0493
$P_b[12]$	+0.0121	+0.0128	-0.0184	-0.0137
$P_b[13]$	-0.0727	+0.0011	-0.0641	-0.1362
$P_b[14]$	+0.1139	-0.1402	+0.1672	+0.0884

$P_b[q]$, that has conjugate symmetric filter coefficients(i.e.,$P_b[q] = P_b[Q-q]^*$), and the coefficients are defined as

$$P_b[q] = 0, N_{tap} \leq q \leq Q - N_{tap} \tag{5.9}$$

where N_{tap} is the one-sided number of non-zero filter taps.

5.3 OQAM-FBMC radar

The adaptation of the FBMC-OQAM was proposed in [47], where the authors show that using the complex symbols $\mathbf{S}(m,n)$ of $\mathbf{S}$ matrix transmission is not a viable option because the real and imaginary parts are not transmitted at the same time due to OQAM modulation. They describe a transmission frame using the real-valued pulse amplitude modulation symbols. The resulting matrix $\bar{\mathbf{S}}$ has elements $a(n,m)$ with respective self-interference estimates resulting from the packaging of the symbols in the time-frequency plane of the FBMC-OQAM modulation.

The influence of previous and subsequent symbols is determined by the length

Table 5.2: Impulse Response for a Phydyas Filter

	$m-4$	$m-3$	$m-2$	$m-1$	m	$m+1$	$m+2$	$m+3$	$m+4$
$n-1$	+0.005j	-0.043j	+0.125j	-0.206j	+0.239j	-0.206j	+0.125j	-0.043j	+0.005j
n	0	+0.067j	0	+0.564j	1	-0.564j	0	-0.067j	0
$n+1$	-0.005j	-0.043j	-0.125j	-0.206j	-0.239j	-0.206j	-0.125j	-0.043j	-0.005j

of the impulse response of the filter. the Table 5.2 shows values of the impulse response $A_{\Delta m \Delta n}$ for a PHYDYAS filter. Then the elements of the modified transmission matrix $\bar{\mathbf{S}}$ according to [47] are

$$\bar{\mathbf{S}}(m,n) = a(m,n) + \sum_{(\Delta m \Delta n) \in \Omega} a(m+\Delta m, n+\Delta n) A_{\Delta m \Delta n}, \tag{5.10}$$

where Ω is the set of symbol positions $(\Delta m \Delta n)$ contributing to the self-interference.

For the receive matrix $\hat{\bar{\mathbf{S}}}$, the authors omit the real part in the demodulator and use the output of the phase corrected analysis filter bank, since their respective real-symbol estimates are not very useful, because they no contain the required phase information.

$$\hat{\bar{\mathbf{S}}}(m,n) = \theta(m,n)^* b(m,n) \tag{5.11}$$

With the two equivalents found $\bar{\mathbf{S}}$ and $\hat{\bar{\mathbf{S}}}$, the equivalent $\mathbf{D}$ matrix is now estimated and can proceed with the same known radar algorithms for the OFDM radar.

$$\mathbf{D}(m,n) = \frac{\hat{\bar{\mathbf{S}}}(m,n)}{\bar{\mathbf{S}}(m,n)} \tag{5.12}$$

The only difference is that there are twice as many points in time, which means that the phase due to a Doppler shift is reduced by taking half of the velocity resolution [47].

5.4 QAM-FBMC radar

Based on the OFDM radar processing, we propose the corresponding representation to QAM-FBMC. In order to apply the radar processing technique to the FBMC signal, an equivalent $\mathbf{D}$ matrix needs to be found, since, unlike in conventional OFDM processing, in the QAM-FBMC we have phase changes and interferences in addition to those caused by the channel. In the receiver side, in order to process the signal for the radar, the matrix of received symbols $\hat{\mathbf{S}}_{FBMC}$ is

$$\hat{\mathbf{S}}_{FBMC}[0] = \mathbf{P}_f^H \mathbf{W}_Q \mathbf{y}[0] = \mathbf{P}_f^H \mathbf{W}_Q \sum_{k=-L}^{L-1} \mathbf{T}[m]\mathbf{H}[m]\mathbf{x}[m] + \tilde{\eta}. \tag{5.13}$$

For the matrix of transmitted symbols $\mathbf{S}_{FBMC}$ to be used in the processing of the radar, we have to consider the interference between the symbols. Due to the overlap and the sum of the transmission structure, the interference of adjacent symbols in the FBMC transmission $(2L-1)$ is included in the received signal and since QAM-FBMC has no CP, inter-symbol interference is present. For this reason, the simple division of the modulated symbols transmitted by the received ones as it happens in OFDM is not possible. In spite of this, we can calculate the interference on the modulated symbols since we know the filter bank, the overlapping factor and the modulated data. Thus, we can build a new matrix of transmitted symbols $\boldsymbol{S}$, which will already have interferences. For the estimation of the elements of $\mathbf{S}_{FBMC}$, we first calculate the interference suffered by the previous and subsequent symbols on the transmitted FBMC signal $\mathbf{x}[m]$ through a shift-and-slice matrix $\bar{\mathbf{T}}[m]$ based on the matrix $\mathbf{T}[m]$ used to calculate the interference in the received signal. The matrix $\bar{\mathbf{T}}[m]$ has dimensions $Q \times Q$, and is defined as

$$\bar{\mathbf{T}}[m] = \begin{cases} \begin{bmatrix} \mathbf{0} & \mathbf{I}_{Q+mN} \\ \mathbf{0} & \mathbf{0} \end{bmatrix}, & m < 0 \\ \begin{bmatrix} \mathbf{I}_Q \end{bmatrix}, & m = 0\,, \\ \begin{bmatrix} \mathbf{0} & \mathbf{0} \\ \mathbf{I}_{N-mN} & \mathbf{0} \end{bmatrix}, & m > 0 \end{cases} \tag{5.14}$$

a DFT is applied and the signal is finally filtered with $\mathbf{P}_f^H$, pre-calculating the interferences introduced by the filter banks in the transmitted signal. Thus the elements of the transmission matrix $\mathbf{S}_{FBMC}$, are given by

$$\mathbf{S}_{FBMC}[0] = \mathbf{P}_f^H \mathbf{W}_Q \sum_{m=-L}^{L-1} \bar{\mathbf{T}}[m]\mathbf{x}[m] + \tilde{\eta}, \tag{5.15}$$

in summary, with the new matrices of transmitted and received symbols, $\mathbf{S}_{FBMC}$ and $\hat{\mathbf{S}}_{FBMC}$, the $\mathbf{D}$ and $\mathbf{Z}$ matrices can be obtained and used to estimate the range and velocity of the targets. This estimation process is equal to the one performed in OFDM radar.

5.4.1 QAM-FBMC radar parameterization

Following the parametrization constraints discussed for OFDM RadCom in [5], the parameters for the OFDM radar used in this chapter are shown in Table 4.3. From these parameters, we may find the equivalent ones for the FBMC waveform. Note that, in order to maintain the same resolution values (for comparative performance purposes), we maintained the same bandwidth B and the total duration of evaluated symbols T_F given by $T_F = MT$ for FBMC.

We have considered a mobile vehicular communications channel in the 24 GHz frequency. We have chosen the number of subcarrier $N = 1024$ to be equal to OFDM, and so once the same bandwidth B_W is maintained, the range resolution will remain the same. However, as FBMC does not have a CP, the period of each FBMC symbol will be shorter than OFDM, so more FBMC symbols need to be evaluated for the same velocity resolution. We have chosen $M = 332$, and the complete parametrization is shown in Table 5.3.

Table 5.3: FBMC System Parameters

PARAMETERS	SYMBOL	VALUE
Carrier frequency	f_c	24 GHz
Number of subcarriers	N	1024
Number of evaluated symbols	M	332
Overlapping factor FBMC	L	4
Total signal bandwidth	B_W	113.92 MHz
Subcarrier spacing	Δf	111.25 kHz
Trans. symbol duration FBMC	T_{FBMC}	9 μs
Duration of evaluated symbols	T_F	3 ms
Range resolution	ΔR	1.316 m
Velocity resolution	Δv	2.171 m/s
Unambiguous range	R_{max}	1347 m
Unambiguous velocity	V_{max}	± 360 m/s
Modulation		4-QAM

5.5 Analysis, comparisons and measurements for FBMC RADAR

5.5.1 Analysis of intrinsic interference and radar resolution

In this subsection, we will present the results obtained in simulations to compare the performance of QAM-FBMC, OQAM-FBMC and OFDM in terms of self-interference remaining on radar images, and also FBMC and OFDM radar in terms of radar resolution. The parameters used for FBMC are present in table 5.3 and the parameters used for OFDM are presented in 4.3. In this subsection a guard band of 128 subcarriers are used for OFDM, in order to demonstrate the effects caused by the use of guard bands in the resolution of radar estimation. We consider a noiseless environment. Three targets were considered, with velocities of $v_1 = 4$ m/s $v_2 = 2$ m/s and $v_3 = 3$ m/s, ranges $r_1 = 8$ m, $r_2 = 10$ m and $r_3=$ 5.6 m and normalized power of $P_1 = 0.56$ $P_2 = 0.3$ and $P_3 = 0.14$.

The results for the same case for the OFDM, OQAM-FBMC and QAM-FBMC signals are shown in the Figures 5.7(a), 5.7(b) and 5.7(c) respectively. When comparing the results we see that the OFDM and QAM-FBMC methods have a better frequency resolution, as expected, since the velocity resolution is dependent on the symbol time, and in the case of OQAM-FBMC we have the symbol time $T_{sym}/2$ [47], thus reducing half the velocity resolution. In addition to this we can see that OQAM-FBMC is the one that presents the most interference, QAM-FBMC does not present this problem, having the same performance as OFDM.

In the Figure 5.7 it is also possible to see that QAM-FBMC not present any additional interference, different from the OQAM-FBMC presented in [47], which shows traces of interference. This demonstrates that the filter bank proposed in [104] for QAM-FBMC modulation also operates satisfactorily in removing self-interference for radar applications.

In Figure 5.8(a) and 5.8(b) we have a zoom in the area of the targets shown in Figure 5.7(a), and Figure 5.7(c) respectively. We can see that the QAM-FBMC for a configuration equivalent to that of OFDM, performs better than OFDM. The QAM-FBMC can distinguish more clearly the 3 targets, presenting a better resolution than OFDM. This occurs because OFDM requires the use of CP and guard bands, which decrease the resolution of the radar system. For the

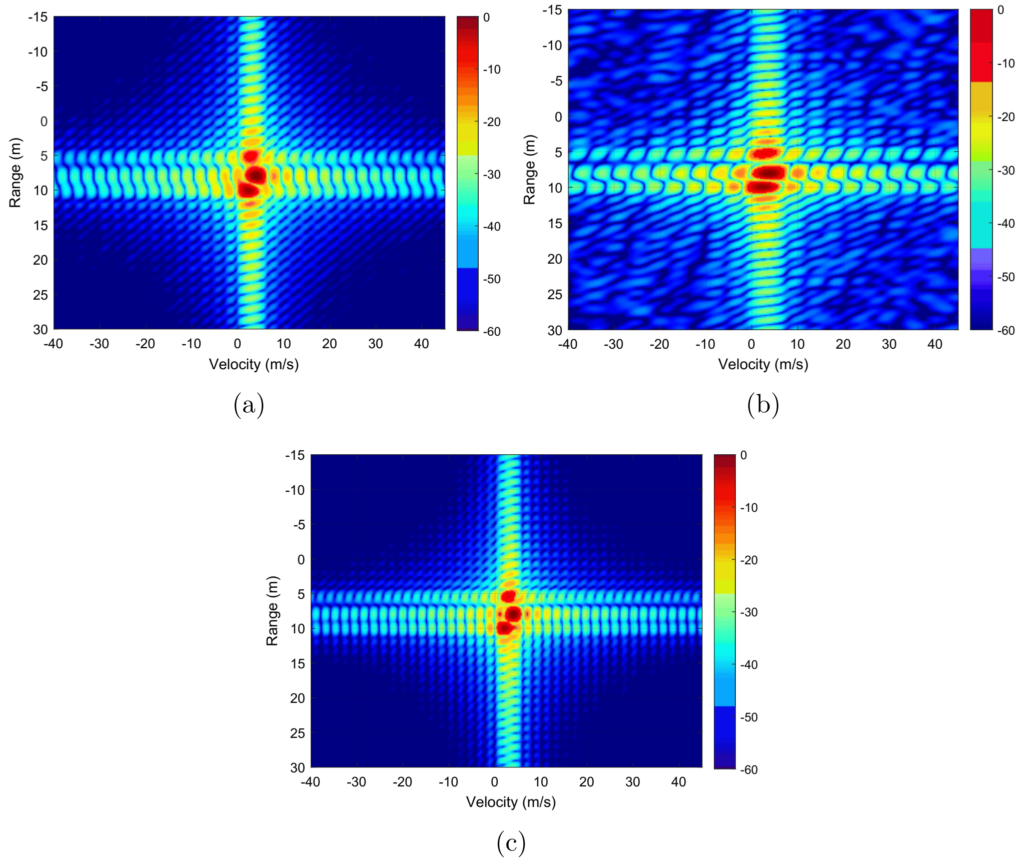

Figure 5.7: Radar image for (a) OFDM, (b)OQAM-FBMC and (c) QAM-FBMC.

same scheme the RadCom QAM-FBMC system presented a velocity resolution of 2.21m/s and a range resolution of 1.61 m, while OFDM had 2.21m/s of velocity and 1.84m of range resolution.

5.5.2 QAM-FBMC radar measurements

In this subsection, we will present the laboratory setup and measurements of a 24 GHz RadCom system, results obtained in the laboratory environment are detailed. We compare the performance of the FBMC and OFDM radars under two different scenarios. In the first scenario, we validate the target estimation capability of the implemented FBMC radar. In the second scenario, we compare the radar systems under the interference from another radar with the same waveform in an adjacent band.

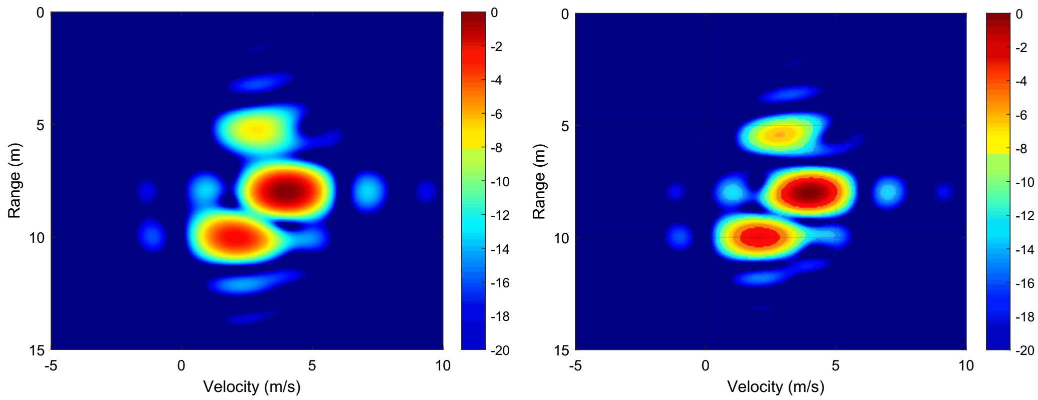

(a) (b)

Figure 5.8: Radar image for (a) OFDM and (b) QAM-FBMC.

Measurement setup

The measurement scenario for the 24 GHz radar system was performed in the laboratory. A pair of A-Info LB-180400-KF 15 dBi horn antennas was used as the radar front-end (one for the transmission and another for the reception). The transmitted waveform had a bandwidth of 113.92 MHz and was synthesized in the baseband using a Keysight M8190A Arbitrary Waveform Generator (AWG). The baseband waveform was then converted to the 24 GHz band using a Keysight E8267D PSG Vector Signal Generator (VSG). The signal at the output of the VSG had an average power of 10 dBm and was fed to the transmitting antenna. The signal received by the receiving antenna was measured using a Keysight N9041B UXA Vector Signal Analyzer (VSA). The measurement setup and scenarios with one and two targets are shown in Figure 5.9. For the scenario with one target, we used a steel sheet with 50×50 cm dimensions at a distance of 2 m (and at an angle of 0°). In the scenario with two targets, the steel target was placed at a distance of 3.5 m (0°) and an additional copper sheet with 30×22 cm dimensions was placed at a distance of 1.5 m (25°).

Two types of measurements were made: one with a single user, and another with two users with inter-system interference. For the measurement of the interference between users, two signals were generated with average powers according to the desired signal-to-interference ratio at the radar input (SIR_{in}). These signals were allocated to adjacent frequency bands (with 113.92 MHz each) and were synthesized by the AWG. The received signal (in baseband) was averaged across 25 consecutive VSA measurements and was filtered by a sharp low-pass filter in

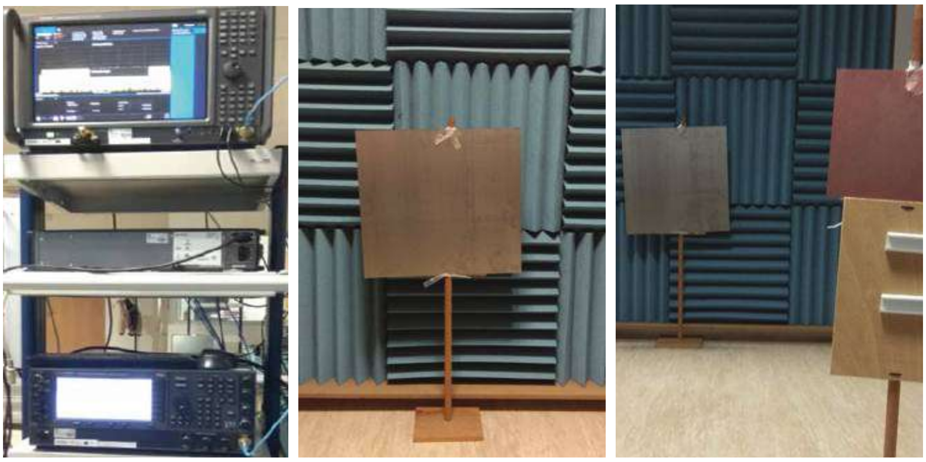

(a) (b) (c)

Figure 5.9: Photograph of the (a) measurement setup, (b) scenario with one target, and (c) scenario with two targets.

order to select the desired user band. In order to remove the delays inherent to the instrumentation setup, the transmitting and receiving antennas were positioned facing one another at a short distance; then, a test signal was transmitted and received, and the delay was measured.

Measurement results

The QAM-FBMC and OFDM radars were implemented with parameters presents in Table 5.3 and Table 4.3, respectively. Figure 5.10 shows the measurements performed with OFDM radar and the proposed QAM-FBMC radar in the scenario with two static targets: one at 1.5 m and the other at 3.5 m. Since the two radars yielded the same range estimations, 1.49 m and 3.46 m, we conclude that QAM-FBMC presents the same performance as OFDM for multiple target estimation.

For the measurement of the inter-system interference in a multi-user environment, the scenario with a single static target at 2 m was used. The interfering signal was scaled so that $SIR_{in} = -30$ dB. Figure 5.11 reveals the resulting radar images for the OFDM and the QAM-FBMC radars. It is visible in the radar images that the OFDM radar suffers much more with the inter-system interference caused by OOB emissions than the QAM-FBMC radar.

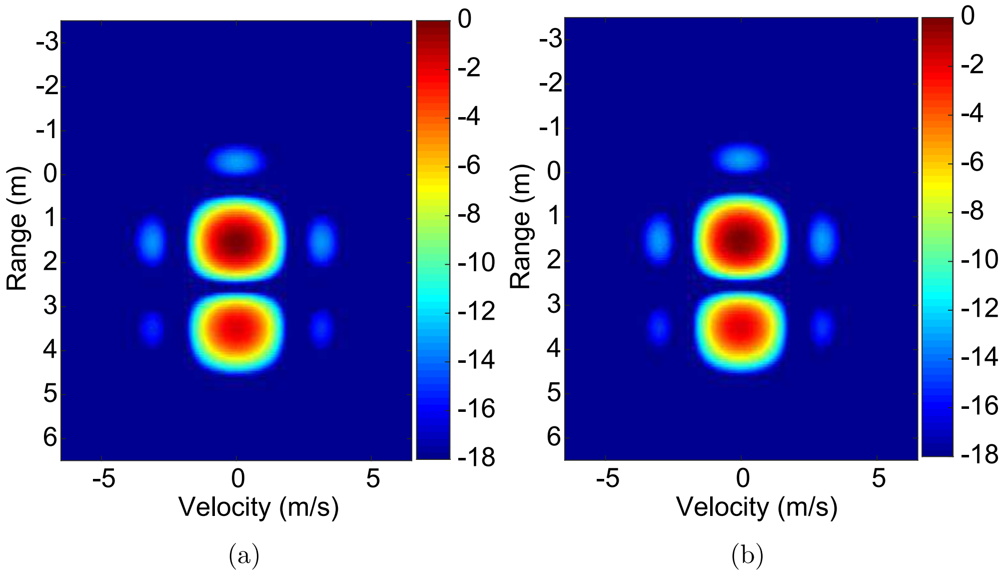

Figure 5.10: Radar image with two targets for (a) OFDM and (b) QAM-FBMC.

5.5.3 Performance evaluation - inter-system interference

In order to better quantify how much the two radars suffer from inter-system interference, we repeated the previous test in a simulated noiseless environment for multiple Signal-to-Interference Ratio (SIR). The SIR is the ratio between the power of the radar signal reflected by the targets (P_{radar}) and the power of the interfering signal (P_{int}), defined by $SIR = P_{radar}/P_{int}$. We define two interference metrics: SIR_{in}, the interference level in the reception before filtering, and SIR_{out}, the remaining interference after filtering with the sharp low-pass filter. We also considered the Normalized Mean Square Error (NMSE). The NMSE measures the difference between the reconstructed signals with interference ($\mathbf{Y}_{int}$) and the received signal without interference ($\mathbf{Y}_{true}$), given by $NMSE = \|\mathbf{Y}_{int} - \mathbf{Y}_{true}\|_2^2/\|\mathbf{Y}_{true}\|_2^2$.

Figure 5.12 displays the level of interference in one band caused by a user in an adjacent band. Through these results, we conclude that the OFDM radar produces an interference level 10 dB higher than the QAM-FBMC radar. To evaluate the changes in the signal due to inter-system interference for the two waveforms, we estimate the NMSE of the radar matrix $\mathbf{Z}$ for different levels of SIR_{in}. The result, illustrated in Figure 5.13, shows that the matrix $\mathbf{Z}$ in the OFDM radar suffered more with the interference, presenting an NMSE of approximately 13 dB more

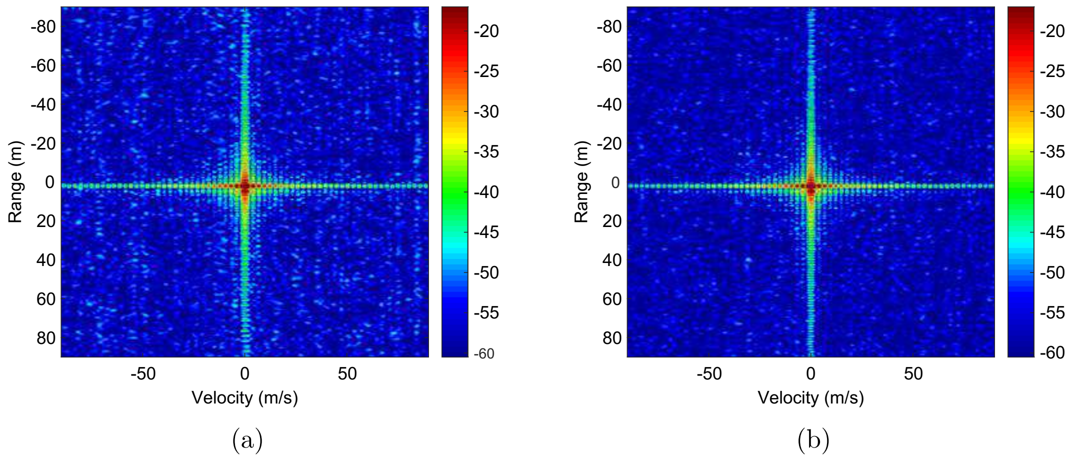

Figure 5.11: Radar image with inter-system interference for (a) OFDM and (b) QAM-FBMC.

than QAM-FBMC for the same levels of interference. In communications systems, the problems of inference between adjacent channels are solved by using guard bands. However, in RadCom systems, the addition of guard bands decreases the radar range resolution. Therefore, the use of a waveform with lower OOB emission such as QAM-FBMC is a more appropriate solution.

5.5.4 Summary

This chapter presents the adaptation of the radar processing of the OFDM signal to be applied in a QAM-FBMC, which improves the spectral efficiency relatively to OFDM. We also verified that the filter design proposed in [104], is also able to remove self-interferences caused by the non-use of CP and non-orthogonality. We also evaluated the application of FBMC for radar operations to mitigate inter-system interference in radar/communication systems, one limiting factor of the radar's performance. We verified that the QAM-FBMC radar presents less inter-system interference than the OFDM radar. For both systems to have the same level of inter-system interference, the OFDM radar requires a very large guard band that dramatically decreases the range resolution. The QAM-FBMC radar system, however, does not require guard bands, and the entire available bandwidth can be used for target estimation. Thus, the QAM-FBMC waveform is a superior candidate for RadCom applications due to its lower inter-system interference and better resolution in the radar system.

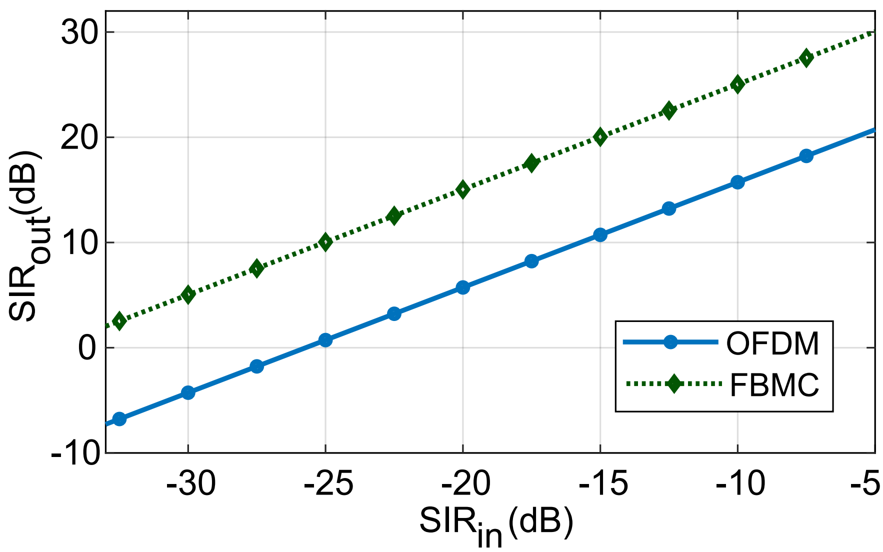

Figure 5.12: Analysis results of SIR estimation over the input SIR.

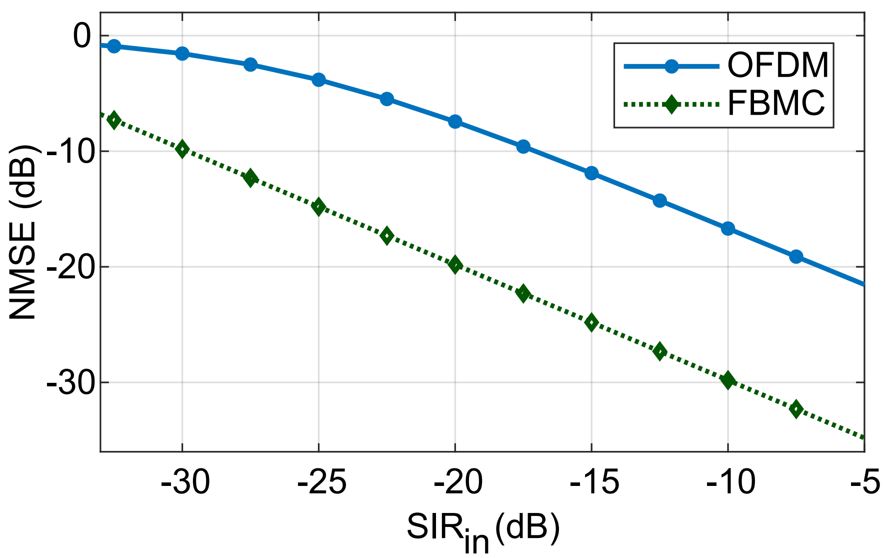

Figure 5.13: Analysis results of NMSE for different input SIR.

CHAPTER 6

GFDM Radar

In this chapter we propose the usage of GFDM, a non-orthogonal multicarrier waveform for radar. We present a method that cancels the effect of interference caused by the non-orthogonality of GFDM waveform in the radar processing, thus not affecting the performance of the radar. We show the viability of GFDM for radar with communications systems and the benefits of using it over OFDM. Finally, we also present GFDM as a solution to mitigate inter-system interference in RadCom systems, thus showing that GFDM may prove to be a better candidate than OFDM for RadCom applications. This chapter is organized as follows. In Section 6.2, we provide a brief outline of the GFDM modulation scheme, from the viewpoint of communication systems. In Section 6.3, the new method for radar processing with GFDM is described. In Section 6.4, the laboratory setup and measurements of a 24 GHz RadCom system are detailed. In Section 6.5, we present the evaluation of the performance of the GFDM radar for two distinct scenarios: one with a single user, where the resolution capacity of the system is analyzed, and another with multiple users, where an evaluation of the interference between users (inter-system interference) is performed. Finally, in Section 6.6 we present the summary.

6.1 Introduction

In RadCom systems, the disadvantages of the OFDM waveform affect not only the communications functions but also the radar. For example, in order to compensate for strong OOB emission in OFDM, guard bands are required, which decrease the range resolution of the radar.

To overcome some of the limitations of OFDM in communications systems, several alternative candidates waveforms have been proposed, such as UFMC, GFDM and FBMC [83]. UFMC, although better contained than OFDM, has higher out-of-band emissions than GFDM and FBMC [111]. FBMC is a spectrally well-contained waveform, with a very high computational complexity [112]. Generalized Frequency Division Multiplexing (GFDM) is a flexible and well-contained spectral multicarrier modulation with low computational complexity [113–115]. GFDM is a block-based multicarrier transmission scheme. The processing of these blocks is based on digital filters that preserve the circular properties of the signals over the time and frequency domains [116]. This process reduces OOB emission, making possible the use of spectrum without severely interfering with established services or other users [117]. Figure 6.1 shows OOB emissions for OFDM and GFDM.

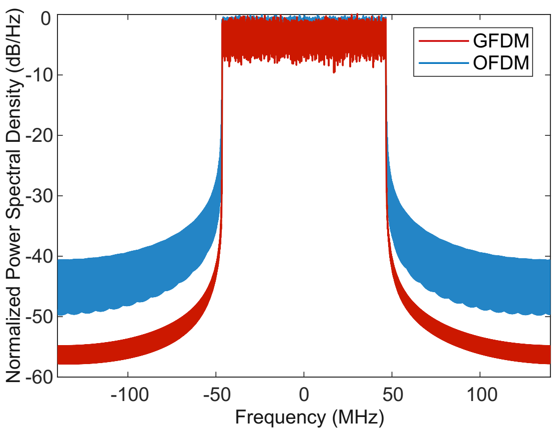

Figure 6.1: OOB emissions for OFDM and GFDM signals.

In GFDM, the transmission data of each block are distributed in time and frequency, and the insertion of CP is done in each block. This increases the spectral efficiency while still providing the means for efficient channel equalization [118]. GFDM blocks are independent of each other, with a structure shaped as desired, so it is possible to adaptively design their structure in order to match the limitations of time and system latency [119]. For example, in real-time applications, the signal length may be reduced to operate under low-latency requirements [117, 120], which makes it an attractive option for applications such as the Internet of Things and radar [113]. Furthermore, GFDM can be easily implemented in multiple-input multiple-output (MIMO) systems [117]. Previous studies have already shown the superiority of the use of GFDM for vehicular communications in relation to OFDM. In [121], it is demonstrated that GFDM can utilize the time and frequency resources more efficiently than OFDM and outperform it particularly under challenging channel conditions for intelligent transportation systems. Motivated by these attractive features, in this chapter, we present a method for radar processing with GFDM, demonstrating the viability of its use in RadCom systems and its benefits over OFDM. We also present GFDM as a solution to mitigate inter-system interference in RadCom systems.

6.2 GFDM waveform

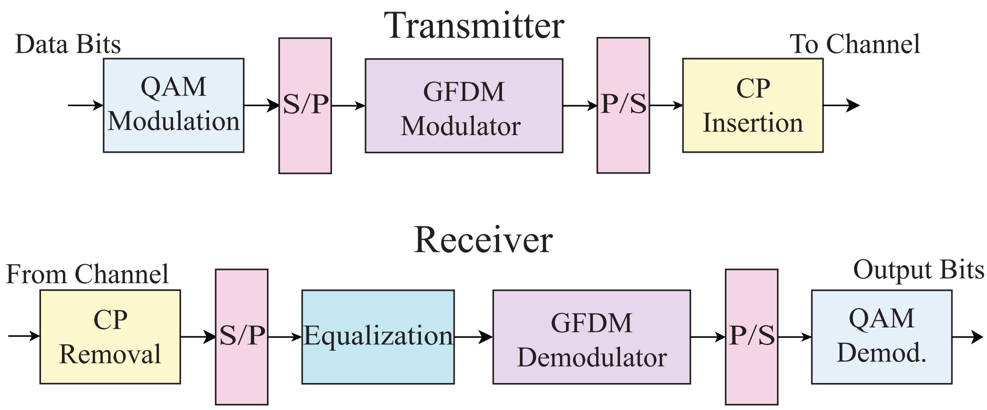

Figure 6.2: GFDM transceiver.

In this section, we present the GFDM waveform and corresponding transceiver, from the viewpoint of a communication system, shown in Figure 6.2. The use of the GFDM waveform for the radar functionality is presented in the following section.

The GFDM block is composed of N subcarriers and M symbols and contains $Q = NM$ complex data symbols. The duration of a GFDM block is $T_{GFDM} = MT + T_{CP}$, where $T = 1/\Delta f$ is the duration of an elementary symbol.

The details of the GFDM modulator are shown in Figure 6.3 [117]. Each GFDM symbol is filtered by its corresponding pulse-shaping filter, which is implemented

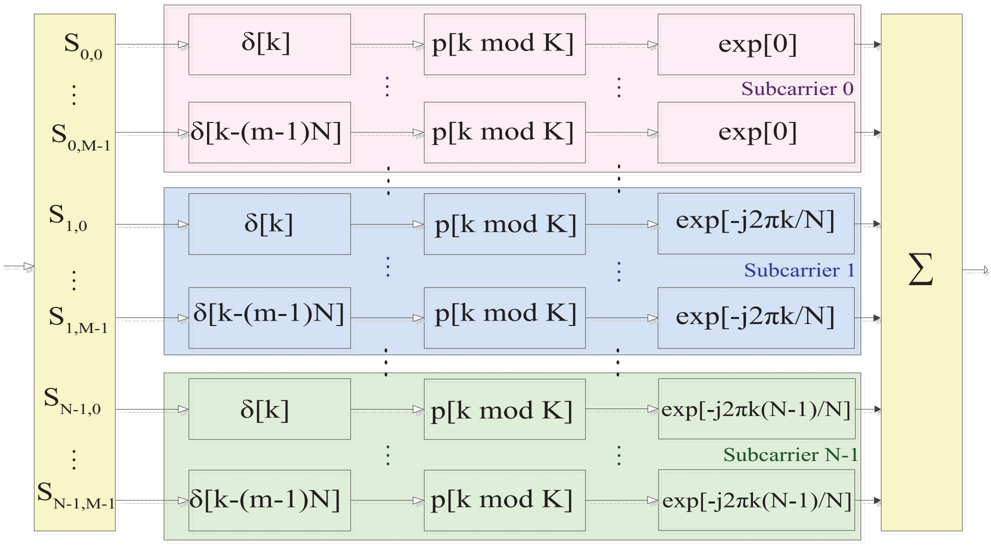

Figure 6.3: GFDM modulator.

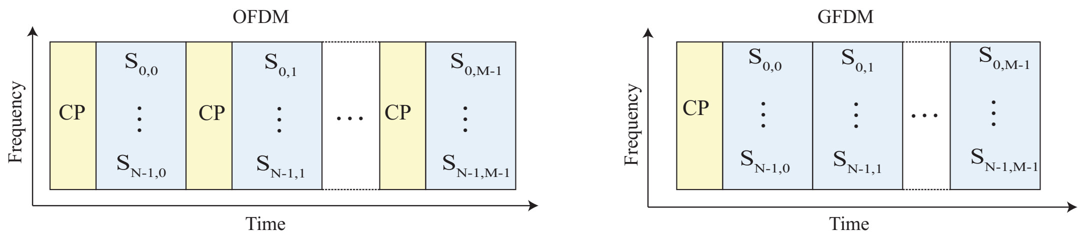

Figure 6.4: Structure of OFDM and GFDM signals composed of N subcarriers and M symbols.

based on a prototype $p[q]$ filter with an offset in time and in frequency, as shown in Figure 6.3 [122].

The subcarrier filtering performed in GFDM results in non-orthogonal subcarriers, which leads to ICI and ISI, denominated by self-interference in the following. Different filters can be used to filter subcarriers, and this choice affects OOB emissions and self-interference [117]. To avoid ISI, a CP is added at the beginning of each block of symbols instead of each symbol as in OFDM [83], as shown in Figure 6.4.

In the receiver, the CP is first removed and each block is equalized to remove the self-interference caused by the non-orthogonality between subcarriers. After equalization, each block is filtered by the same time and frequency translated filters that were used in the transmission stage [117].

The structure of the complex data matrix $\mathbf{S}$ in a GFDM block is

$$\mathbf{S} = \begin{bmatrix} S(0,0) & \dots & S(0,M-1) \\ \vdots & \ddots & \vdots \\ S(N-1,0) & \dots & S(N-1,M-1) \end{bmatrix} \tag{6.1}$$

and the transmitted GFDM signal [117] can be expressed as

$$x(q) = \sum_{m=0}^{M-1} \sum_{n=0}^{N-1} S(n,m) p[(q-mN) \bmod Q] e^{\frac{j2\pi qn}{N}}, \tag{6.2}$$

with $q = 0, \dots, Q-1$. The corresponding pulse shaping filter is

$$p_{n,m}[k] = p[(q-mN) \bmod Q] e^{\frac{j2\pi qn}{N}}. \tag{6.3}$$

Each $p_{n,m}[q]$ is a circularly shifted version of $p_{n,0}[q]$, and the complex exponential performs the frequency shift operation [117].

The transmitted samples can then be represented by

$$x(q) = \sum_{m=0}^{M-1} \sum_{n=0}^{N-1} S(n,m) p_{n,m}[q]. \tag{6.4}$$

This equation can be rearranged in matrix form,

$$\mathbf{q} = \mathbf{A} vec\{\mathbf{S}\}, \tag{6.5}$$

where $\mathbf{x} = [x[1], \dots, x[Q]]^T$ is the $Q \times 1$ transmitted signal, $\mathbf{A}$ is a $Q \times Q$ modulation matrix [117] with a structure according to

$$\mathbf{A} = [\mathbf{p}_{0,0} \quad \dots \quad \mathbf{p}_{N-1,0}, \quad \mathbf{p}_{0,1} \quad \dots \quad \mathbf{p}_{N-1,M-1}], \tag{6.6}$$

with the vector $\mathbf{p}_{n,m} = [p_{n,m}[1], \dots, p_{n,m}[Q]]^T$. The received signal vector can be defined as

$$\mathbf{y} = \mathbf{H_C}\mathbf{x} + \boldsymbol{\eta}, \tag{6.7}$$

where $\boldsymbol{\eta}$ is a complex AWGN vector. The channel matrix $\mathbf{H_C}$ of size $Q \times Q$ is a circular convolution matrix and each column of the matrix [113] is given by the circular shift of the channel impulse response $\mathbf{h}$ with the length (in samples) of L_c

$$[\mathbf{H_C}]_{(:,q)} = \text{circshift}\left\{[h_0, \cdots, h_{L_c-1}, \mathbf{0}_{Q-L_c}]^T, Q-1\right\}. \tag{6.8}$$

In the receiver of the communications system, the zero forcing equalizer (${\mathbf{H_C}}^{-1}$) can be used for channel equalization, although other procedures can be employed. As detailed in [117], the estimated received data matrix $\hat{\mathbf{S}}$ can be obtained by

$$\hat{\mathbf{S}} = res\{\mathbf{C}{\mathbf{H_C}}^{-1}\mathbf{y}\}_{N\times M}, \tag{6.9}$$

where $\mathbf{C}$ is the $Q \times Q$ demodulation matrix of GFDM, which can be, e.g., the Matched Filter (MF), Zero Forcing (ZF), or Minimum Mean Square Error (MMSE) matrices [117], defined below

$$\mathbf{C}_{MF} = \mathbf{A}^H, \tag{6.10}$$

$$\mathbf{C}_{ZF} = \mathbf{A}^H(\mathbf{A}\mathbf{A}^H)^{-1}, \tag{6.11}$$

$$\mathbf{C}_{MMSE_H} = \left(\mathbf{A}^H{\mathbf{H_C}}^H\mathbf{H_C}\mathbf{A} + \mathbf{R}_\eta^2\right)^{-1}\mathbf{A}^H{\mathbf{H_C}}^H. \tag{6.12}$$

where $\mathbf{R}_\eta^2$ is the covariance matrix of the noise. Note that in case of MMSE reception, the channel is jointly equalized in the receiving process.

6.3 GFDM radar

The signal received by the radar, assuming that we have Ω reflective targets and M_B GFDM blocks, is given by

$$y[q] = \sum_{k=1}^{K}\sum_{b=0}^{M_B-1}\sum_{m=0}^{M-1}\sum_{n=0}^{N-1} S_b(n,m)p_{n,m}[q] \\ e^{j2\pi f_{D,k}(Tm+T_{GFDM}b)}e^{-j2\pi n\Delta f\frac{2r_k}{c}} + \tilde{\eta}(m,n). \tag{6.13}$$

where S_b is the data matrix of the GFDM block b, with $b = 0, \ldots, M_B - 1$. The total duration of evaluated symbols in GFDM radar is $T_F = M_B T_{GFDM} = M_B(MT + T_{CP})$

For the estimation of the matrix of received symbols in the radar, contrary to the processing in communications systems, we remove the channel equalization matrix ${\mathbf{H_C}}^{-1}$ in (6.9) in order to preserve the information from the channel. The estimated received symbols are then obtained as

$$\hat{\mathbf{S}}^{\dagger} = res\{\mathbf{Cy}\}_{N\times M}. \tag{6.14}$$

In the radar receiver, the demodulation matrix $\mathbf{C}$ of GFDM needs to be properly chosen. The influence of the shape of the filtered pulse in GFDM leads to a non-orthogonality condition causing inter-symbol and inter-carrier interference in the received symbols. This interference was denominated by self-interference in the previous section.

The use of the MF for the demodulation maximizes the signal-to-noise ratio (SNR) per subcarrier but does not remove the self-interference. The ZF receiver, on the other hand, removes the self-interference at the cost of decreasing the SNR. In addition, there may be instances where $\mathbf{A}$ is poorly conditioned, further deteriorating the SNR. The linear MMSE receiver makes a trade-off between self-interference and noise suppression. However, in the case of MMSE, the channel is equalized together in the receiving process, which impairs the estimation of radar targets. For these reasons, MF and ZF are suitable for radar processing, while MMSE is not [117].

6.3.1 GFDM - ZF/MF radar

Considering the cases of GFDM radar with ZF receiver (GFDM-ZF), and GFDM radar with MF (GFDM-MF) receiver, the radar processing is performed directly with the matrix of transmitted symbols $\mathbf{S}^{\dagger}_{ZF/MF} = \mathbf{S}$, as well as in OFDM. The estimated received symbols are $\hat{\mathbf{S}}^{\dagger}_{ZF/MF} = res\{\mathbf{C}_{ZF/MF}\mathbf{y}\}_{N\times M}$ and then components of estimation matrix $\mathbf{D}$ are

$$D(m+Mb,n) = \frac{\hat{S}^{\dagger}_{b,ZF/MF}(m,n)}{S^{\dagger}_{b,ZF/MF}(m,n)}. \tag{6.15}$$

6.3.2 GFDM - PMF radar

To overcome the aforementioned problems of ZF and MF in GFDM based radar, we propose a self-interference cancelation technique based on the MF approach for GFDM radar, denoted by GFDM-Proposed Matched Filter (PMF). This technique cancels the self-interference in the matrix $\mathbf{D}$ without increasing the background noise, as occurs with GFDM-ZF. Concerning the radar functionalities, our GFDM-PMF allows the optimum performance. The details are presented in the appendix, but basically the technique resorts to the fact that for MF in (6.15), $\hat{\mathbf{S}}^{\dagger}_{MF}$ can be decomposed as interference, noise and intended signal while in the denominator we just have the intended signal. The PMF technique estimates the interference complement and adds it in the denominator. Although we have no interblock interference, inside the blocks the waveforms are non-orthogonal. For all interference between the symbols and subcarrier to be removed, it is necessary to consider the whole GFDM block in the radar processing.

In GFDM-PMF, the MF receiver (the $\mathbf{C}_{MF}$ matrix) is used for the estimation of the received symbols $\hat{\mathbf{S}}^{\dagger}_{PMF}$, therefore

$$\hat{\mathbf{S}}^{\dagger}_{PMF} = res\{\mathbf{C}_{MF}\mathbf{y}\}_{N\times M}. \tag{6.16}$$

The matrix $\mathbf{S}$ is processed in order to estimate the self-interference suffered by the transmitted symbols. This estimation is done by applying the same filtering process the received symbols went through (the two pulse-shaping filters of the transmit and receive stages, $\mathbf{A}$ and $\mathbf{A}^{H}$) to the transmitted symbols ($\mathbf{S}$, cf. the appendix). This results in a matrix $\mathbf{S}^{\dagger}_{PMF}$, defined as

$$\mathbf{S}^{\dagger}_{PMF} = res\{\mathbf{A}^{H}\mathbf{A}vec\{\mathbf{S}\}\}_{N\times M}, \tag{6.17}$$

that incorporates not only the transmitted symbols but the self-interference as well. This way, as shown in the appendix, the self-interference is compensated for when computing the radar estimation matrix $\mathbf{D}$.

Considering, then, M_B GFDM blocks evaluated in the radar estimation, the components of estimation matrix $\mathbf{D}$ for GFDM-PMF are

$$D(m+Mb,n) = \frac{\hat{S}^{\dagger}_{b,PMF}(m,n)}{S^{\dagger}_{b,PMF}(m,n)} \tag{6.18}$$

$$= \sum_{k=1}^{K} e^{j2\pi f_{D,k}(Tm+T_{GFDM}b)} e^{-j2\pi n\Delta f\frac{2r_k}{c}} + \tilde{\eta}(m,n). \tag{6.19}$$

The range and velocity parameters can be obtained from a 2D-DFT as in OFDM radar.

Table 6.1: GFDM System Parameters

PARAMETERS	SYMBOL	VALUE
Carrier frequency	f_c	24 GHz
Number of subcarriers	N	256
Number of GFDM symbols	M	32
Number of evaluated blocks	M_B	41
Total signal bandwidth	B_W	113.92 MHz
Subcarrier spacing	Δf	445 kHz
GFDM elementary symbol duration	T	2.25 μs
Cyclic prefix duration	T_{CP}	2.25 μs
Total block duration	T_{GFDM}	74.25 μs
Duration of evaluated symbols	T_F	3 ms
Range resolution	ΔR	1.316 m
Velocity resolution	Δv	2.171 m/s
Unambiguous range	R_{max}	337 m
Unambiguous velocity	V_{max}	± 1424 m/s
Modulation		4-QAM

6.3.3 GFDM radar parameterization

Following the parametrization constraints discussed for OFDM RadCom in [5], the parameters for the OFDM radar used in this chapter are shown in Table 4.3. From these parameters, we may find the equivalent ones for the GFDM waveform. Note that, in order to maintain the same resolution values (for comparative performance purposes), we maintained the same bandwidth B_W and the total duration of evaluated symbols T_F given by $T_F = MT$ for OFDM and $T_F = MTM_B$ for GFDM. However, a parametrization optimized for the GFDM waveform and its features can also be performed.

As we know $B_{C90\%} = 195.31$ kHz, but in this case, there is no multiple value of 2 below 1024 that provides a band spacing lower than this value, so in the case of GFDM we will work with the $B_{C50\%}$. $B_{C50\%}$ could be approximated to 1931KHz, since GFDM suffers less from interferences, especially out-of-band, there will be considerable losses. We have considered a mobile vehicular communications channel in the 24 GHz frequency range with a coherence bandwidth of $B_{C50\%} =$ 1953 kHz [5], and we have chosen $N = 256$, $M = 32$ and $M_B = 41$. The CP duration of each block is the same as in OFDM, 2.25μs. The complete parametrization is shown in Table 6.1. The pulse-shaping filter used in the GFDM waveform is a raised-cosine (RC) filter with a roll-off factor of 0.5.

It is possible to see in Table 4.3 and Table 6.1 that the GFDM modulation presents a lower unambiguous range than that of OFDM, but still above the maximum value detectable by the radar [5]. In contrast, the unambiguous velocity is much higher.

6.4 Radar measurements

In this section, we will present the laboratory setup and measurements of a 24 GHz RadCom system, results obtained in the laboratory environment is detailed. In the next section (section VI), we will present results obtained by simulation, in order to complement and validate those obtained in the laboratory.

6.4.1 Measurement setup

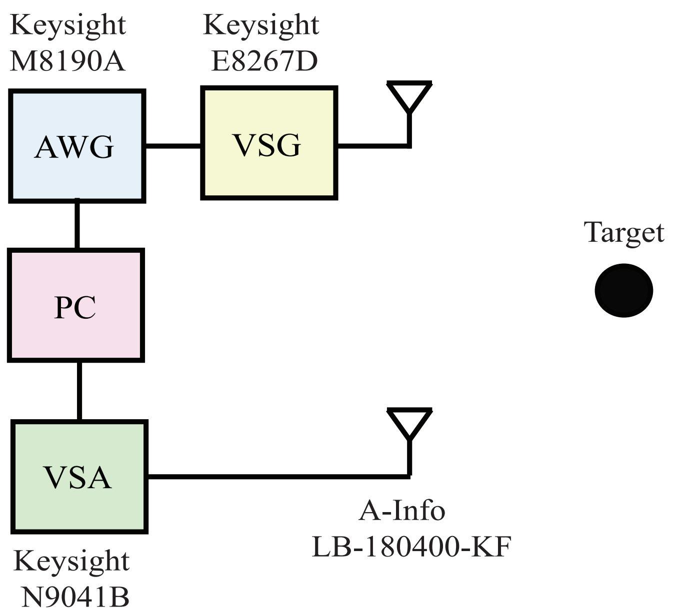

Figure 6.5: Diagram of the measurement setup.

The measurement scenario for the 24 GHz radar system was performed in the laboratory and is schematized in Figure 6.5. The frequency of 24 GHz was considered due to being the frequency, together with 77GHZ, normally used in automotive radars. The radar system front-end consisted of two A-Info LB-180400-KF 15 dBi horn antennas: one for the transmission and another for the reception. The transmitted data was randomly generated with a 4-QAM constellation. The transmitted waveform (OFDM or GFDM) had a bandwidth of 113.92 MHz and was synthesized in the baseband, at a sample rate of 683.52 MSa/s, using a Keysight M8190A AWG. The AWG outputs the in-phase (I) and quadrature (Q) components of the waveform in a differential-pair configuration ($I/\bar{I}$ and $Q/\bar{Q}$). The baseband waveform was then converted to the 24 GHz band using a Keysight E8267D PSG VSG. The signal at the output of the VSG had an average power of 14 dBm and was fed to the transmitting antenna.

(a) (b) (c)

Figure 6.6: Photograph of the (a) measurement setup, (b) scenario with one target, and (c) scenario with two targets.

The signal received by the receiving antenna was measured using a Keysight N9041B UXA VSA. For greater accuracy of measurement, the 10 MHz oscillator of the VSA was used as a reference to synchronize the clocks of all instruments (the AWG, the VSG, and the VSA), and a baseband trigger signal was provided by the AWG to the VSA.

The AWG was connected via USB to a personal computer (PC) and the other instruments were connected through a local area network to the same computer. All instruments were controlled via Matlab, where all signals were generated and processed.

The measurement scenarios are shown in Figure 6.6, with one and two targets, respectively. In the first scenario, we have a copper target with 30×22 cm dimensions at a distance of 2 m (at an angle of 0°) from the radar front-end. In the second scenario, we have two copper targets with 35×22 cm and 30×22 cm dimensions, at a distance of 3.7 m (0°) and 1.5 m (25°) respectively. Only static targets were considered in these scenarios because no moving targets were available.

Two types of measurements were made: one with a single user (radar) without inter-system interference, and another with two users (two radars) with inter-system interference. For the case with interference between users, two signals were generated with a bandwidth of 113.92 MHz and with different average powers according to the desired signal-to-interference ratio at the radar input (SIR_{in}). These signals were allocated to adjacent bands and were synthesized together by the AWG. The received signal (in complex baseband form) was filtered by a sharp low-pass filter in order to select the desired user band. In the multi-user case, the received signal was averaged across 25 consecutive VSA measurements in order to reduce the effects of external noise and to better observe the effects of the inter-system interference. In the single-user case, only one measurement was performed.

The calibration of the system was performed with the transmitting and receiving antennas positioned facing one another at a short distance, thus measuring the total delay of the system (cables, AWG, VSG, VSA and antennas). This delay was then removed from the received signal during radar processing. The transmitting and receiving antennas were 12 cm apart. The coupling between the antennas, measured using a Keysight N5242A Vector Network Analyzer, was below -50 dB in the band of operation, ensuring the leakage interference is negligible.

6.4.2 Measurements

All measurements were done according to the modulation parameters presented in Table 4.3 (OFDM) and Table 6.1 (GFDM). Figure 6.7 shows the resulting radar images for a single static target at a distance of 2 m. Figure 6.7(a) refers to GFDM-MF without the self-interference removal technique, Figure 6.7(b) refers to GFDM-ZF, Figure 6.7(c) refers to GFDM-PMF with the proposed self-interference removal technique, and Figure 6.7(d) refers to OFDM. The estimated range value for OFDM was 1.93 m and for all GFDM techniques was 1.94 m.

In Figure 6.7, the self-interference is evident in the GFDM-MF radar due to the presence of a great amount of visible background noise. In contrast, the GFDM-PMF radar achieves a performance equal to that of the OFDM radar, not presenting any remaining self-interference. Finally, the GFDM-ZF radar removed the self-interference but, due to the ZF processing, it also increased the noise level. We conclude, then, that the proposed GFDM-PMF processing is more

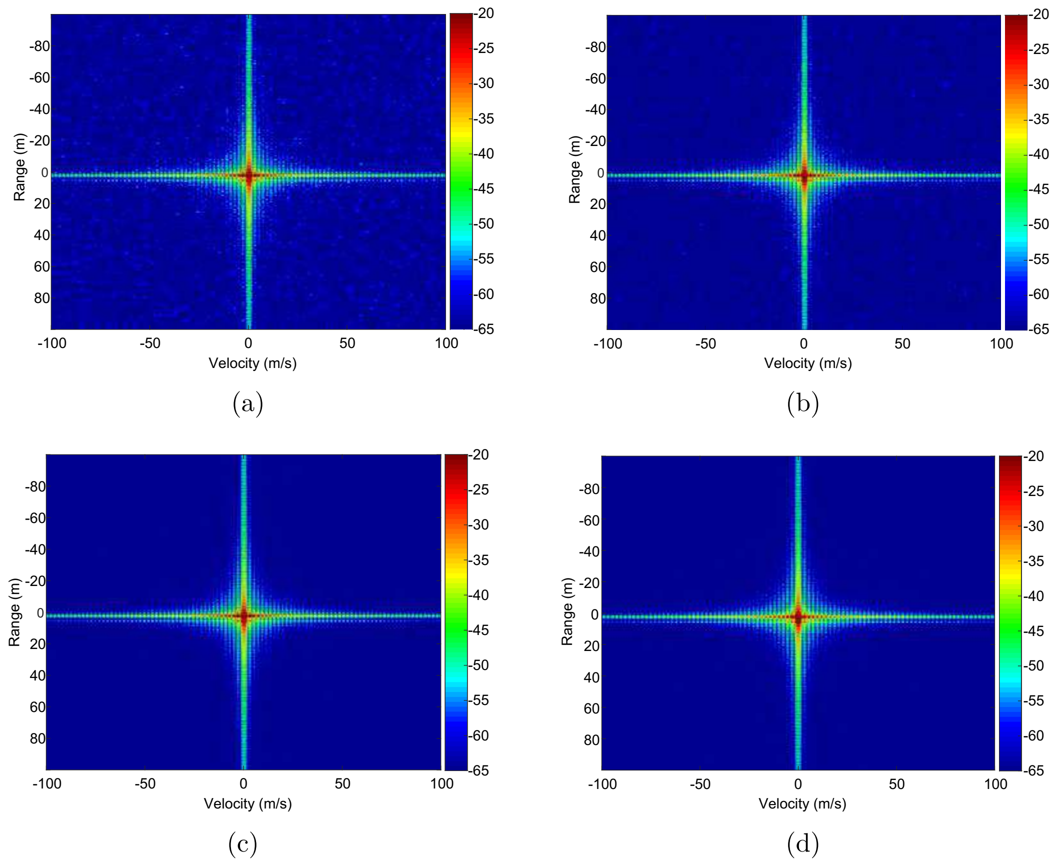

Figure 6.7: Radar image for (a) GFDM-MF, (b) GFDM-ZF, (c) GFDM-PMF, and (d) OFDM.

appropriate for radar than GFDM-ZF and GFDM-MF. Moreover, we conclude that it is feasible to use non-orthogonal waveforms for radar functions: since the transmitted signal is known by the radar system, it is possible to estimate the self-interference and cancel the effects during the radar processing.

Throughout the rest of this thesis, all further measurements related to the GFDM waveform will use the proposed GFDM-PMF radar processing technique.

Figure 6.8 shows the measurements performed with OFDM and GFDM in the scenario with two static targets: one at 1.5 m and the other at 3.7 m. In the radar images, it is possible to verify that GFDM also presents the same performance as OFDM for multiple targets. The estimated range values for GFDM are 1.50 m and 3.67 m, and for OFDM 1.60 m and 3.60 m.

The scenario of a single static target at 2 m was also used to measure the inter-system interference in a multi-user environment. Figure 6.9 shows the radar image for a system with an interference level in the reception (before filtering)

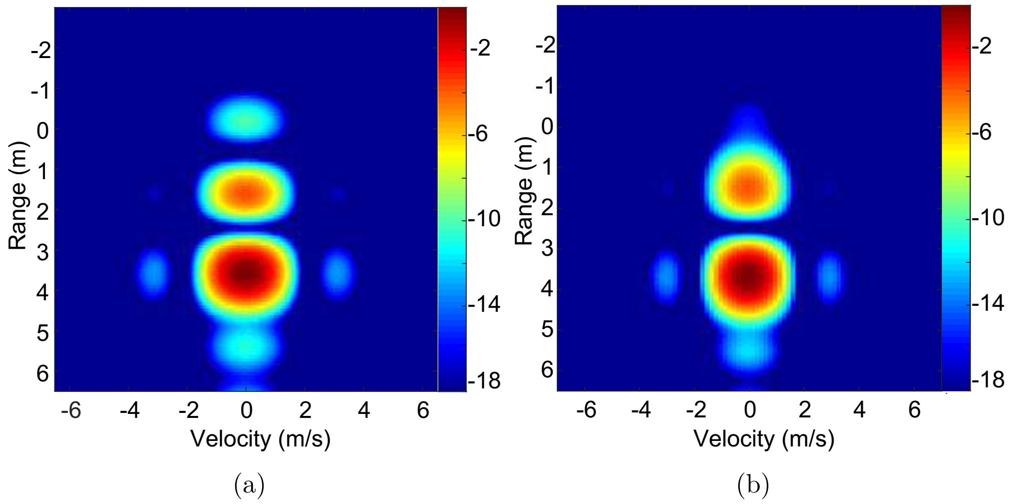

Figure 6.8: **Radar image with two targets for (a) OFDM and (b) GFDM.**

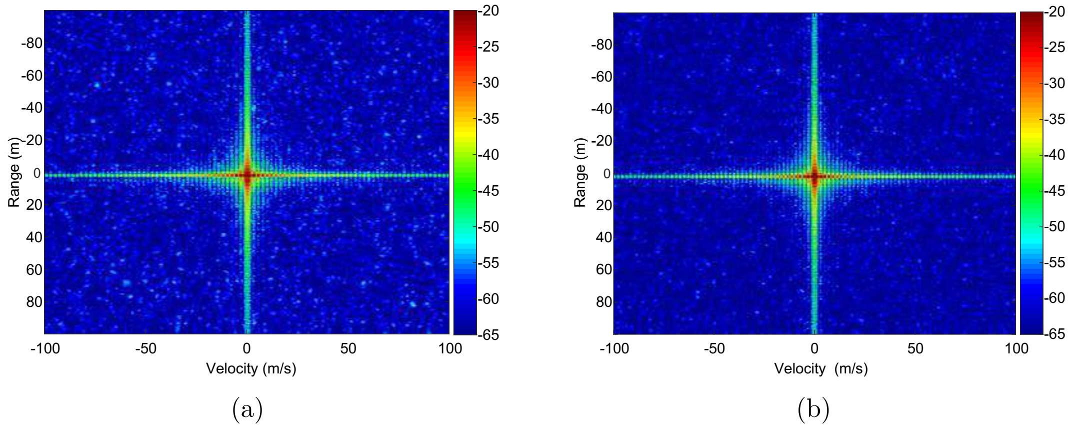

Figure 6.9: **Radar image with inter-system interference for (a) OFDM and (b) GFDM.**

of $SIR_{in} = -20$ dB for the OFDM and GFDM waveforms. In this figure, it is possible to see that the high OOB emission of OFDM causes a higher inter-system interference, resulting in a higher level of background noise (interference) in the radar image. This may cause difficulties in detecting targets with low power signals reflected in a scenario with a large number of radars. On the other hand, since the background interference in the GFDM radar image is much lower, it is expected that in a scenario with multiple radars we are still close to a noise-limited system and targets are detected with much higher probability than in OFDM. We conclude, then, that the GFDM waveform is more appropriate for multi-user

RadCom systems than the OFDM waveform.

6.5 Performance evaluation

In this section, we compare the performance of the GFDM radar with that of the OFDM radar under various simulation environments with parameters presented in Table 4.3 (OFDM) and Table 6.1 (GFDM). First, we consider an environment with a single radar and multiple mobile targets. Then, we consider a noiseless environment with two radars (multiple users) and one target for the estimation of the inter-system interference after filtering in radar processing (SIR_{out}). The proposed GFDM-PMF processing technique was the one used for the GFDM radar. The transmitted data was randomly generated with a 4-QAM constellation.

6.5.1 Single user – range and velocity estimation

Three targets were considered with velocities of $v_1 = 4$ m/s, $v_2 = 2$ m/s and $v_3 = 3$ m/s, ranges of $R_1 = 8$ m, $R_2 = 10$ m and $R_3 = 5$ m, and normalized average power (to unity power) of the received signal in the ratios of $P_1 = 0.56$, $P_2 = 0.3$ and $P_3 = 0.14$. The channel was considered to be noiseless, flat, and with no attenuation.

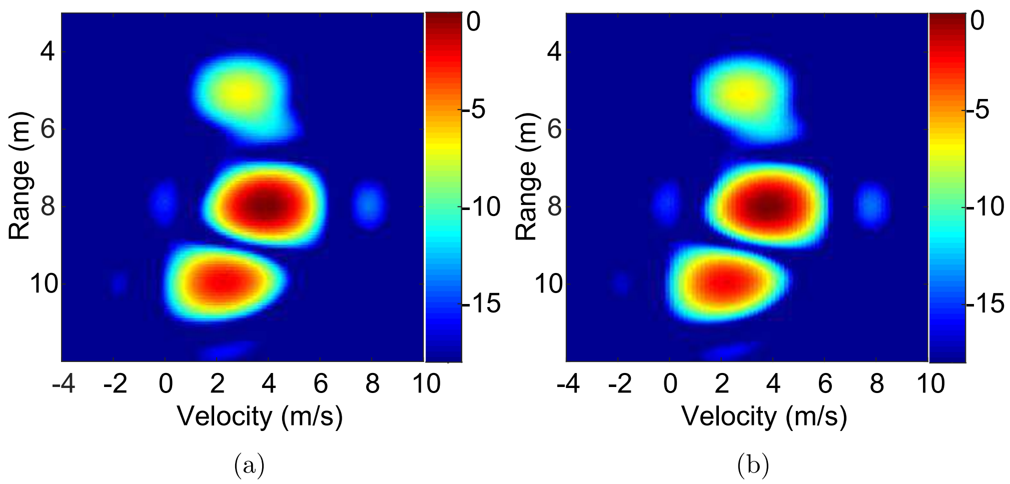

Figure 6.10: Comparison of the (a) GFDM and (b) OFDM radar image with multiple mobile targets.

A comparison between the GFDM and OFDM radars is presented in Figure 6.10. Based on the results shown in this figure, it is possible to verify that the GFDM radar yields the same target velocity estimate as the OFDM radar.

6.5.2 Multiple users – inter-system interference

It is known that OFDM suffers from high OOB emissions and that one of the advantages of GFDM is its lower OOB emissions. It is for these reasons that the GFDM radar system has a much lower inter-system interference than the OFDM radar, as shown in the measurement results presented in Figure 6.9. In this subsection, the proposed GFDM radar is compared to the OFDM radar under the interference from another radar with the same waveform in an adjacent channel (that is, OFDM interfered by OFDM and GFDM interfered by GFDM).

A configuration based on the modulation parameters presented in Table 4.3 (OFDM) and Table 6.1 (GFDM) is used. The radar system with carrier frequency f_c is interfered by a radar with the same waveform with carrier frequency $f_c + B$. Both radars have the same bandwidth B. One target at a distance of $r = 2$ m and with a velocity $v = 0$ m/s is simulated considering a noiseless flat channel with no attenuation. After being received, the signal is filtered by a sharp low-pass filter with bandwidth B.

In order to compare the performance of the GFDM and OFDM radars, we define the ratio between the power of the reflected radar signal and the power of the interfering signal as the signal-to-interference ratio (SIR), given by

$$SIR = \frac{P_{radar}}{P_{int}}, \tag{6.20}$$

where P_{radar} is the power of the reflected radar signal and P_{int} is the power of the interfering signal. We denote SIR_{in} as the SIR of the received radar signal before filtering, and SIR_{out} as the SIR of the received radar signal after filtering.

Moreover, the performance is also compared in terms of the normalized mean square error (NMSE) of the received radar signal after filtering in relation to the signal received by a radar with no interference, defined by

$$NMSE = \frac{\|\mathbf{Y}_{int} - \mathbf{Y}_{true}\|_2^2}{\|\mathbf{Y}_{true}\|_2^2}, \tag{6.21}$$

where $\mathbf{Y}_{true}$ is the received radar signal with no interference and $\mathbf{Y}_{int}$ is the signal with interference.

Figure 6.11 shows the NMSE of the reconstructed signals for the OFDM

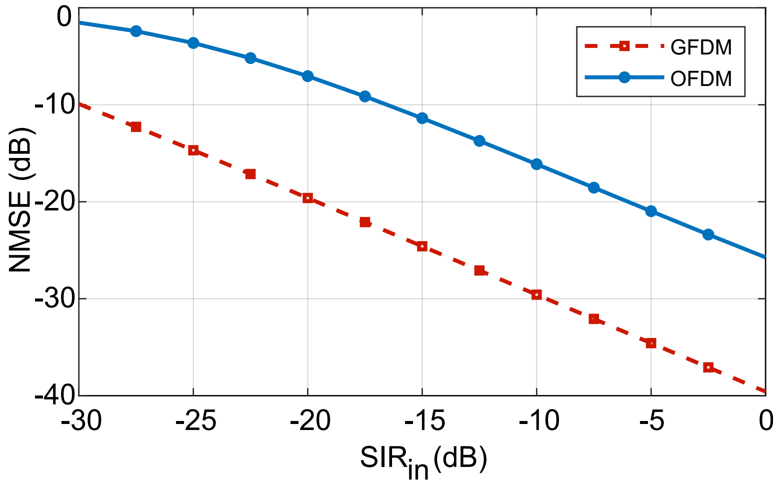

Figure 6.11: Variation of the NMSE of the received radar signal as a function of SIR_{in}.

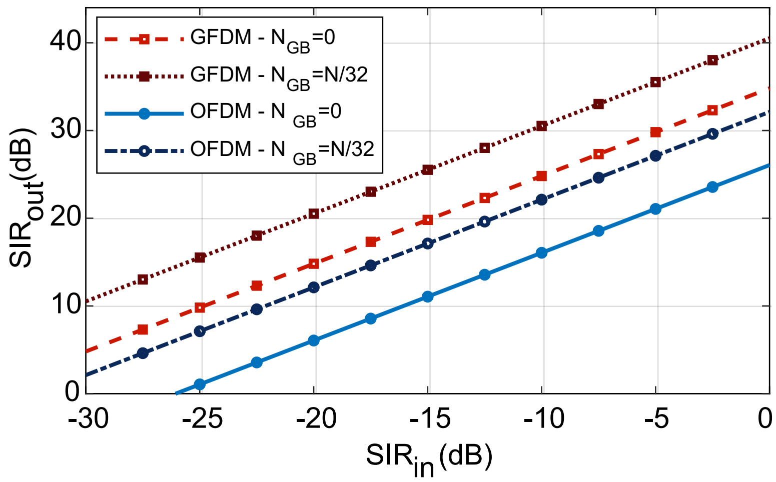

Figure 6.12: Variation of the post-filtered SIR as a function of SIR_{in}.

and GFDM radars for different values of SIR_{in}. Greater interference can be observed in the OFDM radar due to its higher OOB emissions. Figure 6.12 shows the interference after filtering (SIR_{out}) for both radars, with the GFDM radar presenting a SIR_{out} better by approximately 9 dB than that of the OFDM radar.

In Figure 6.12 we also compare the same systems with the addition of guard bands ($N_{GB} = N/32$). This figure demonstrates that, naturally, the two radars show an improvement in SIR_{out} when guard bands are used. However, we note that the OFDM radar with $N_{GB} = N/32$ still has more interference than the GFDM radar without guard bands.

In fact, for the OFDM radar to reach values of SIR_{out} close to the GFDM

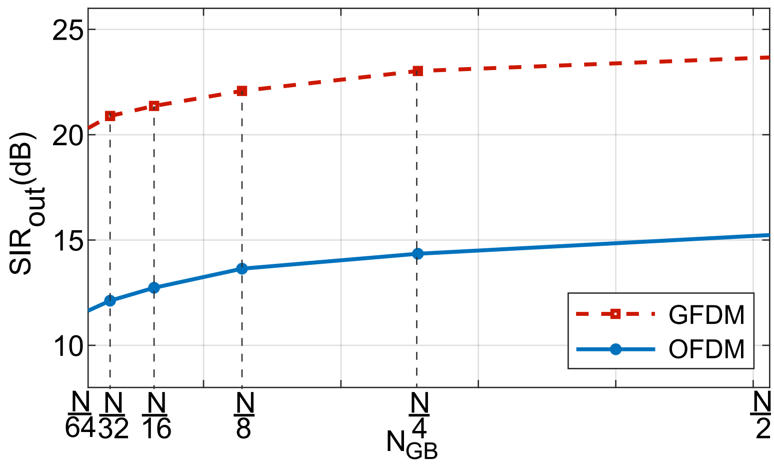

Figure 6.13: Variation of the pos-filtered SIR as a function of the guard bandwidth for $SIR_{in} = -20 =$ dB.

radar's, it requires much wider guard bands. This is shown in Figure 6.13, where a comparison of the SIR_{out} versus the guard bandwidth is done for both radar systems (for SIR_{in} = -20 dB).

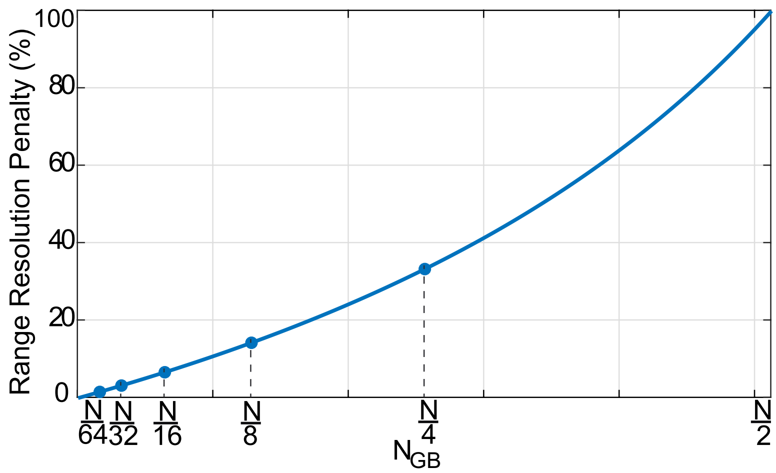

Figure 6.14: Relative decrease in range resolution as a function of the guard bandwidth.

It can be seen from Figure 6.13 that, although the GFDM radar only requires $N_{GB} = N/64$ to achieve $SIR_{out} = 20$ dB, the OFDM radar requires at least $N_{GB} = N/2$ to achieve $SIR_{out} = 15$ dB. The larger number of guard band subcarriers for OFDM causes not only a decrease in spectral efficiency for data transmission, but also a decrease in radar resolution capacity. Figure 6.14 shows the relationship between the number of guards band subcarriers and the radar range resolution penalty, given by:

$$\Delta R \text{ Penalty}(\%) = \frac{\Delta R_{[N_{GB}]} - \Delta R_{[N_{GB}=0]}}{\Delta R_{[N_{GB}=0]}} * 100. \tag{6.22}$$

In order to achieve levels of SIR_{out} equal to 20 dB and 15 dB respectively, the GFDM radar with a guard band of $N/32$ subcarriers would incur a range resolution penalty of only 1.6% ($\Delta R_{[N_{GB}=0]} = 1.316$ m and $\Delta R_{[N_{GB}=N/64]} = 1.336$ m) while the OFDM radar would incur a penalty of 100% ($\Delta R_{[N_{GB}=0]} = 1.316$ m and $\Delta R_{[N_{GB}=N/512]} = 2.632$ m).

6.6 Summary

This chapter presents the processing of the GFDM waveform for radar with simulations and measurements at 24 GHz. The results demonstrate the viability of GFDM for RadCom systems, which combine radar and communications functions. In this chapter, we also demonstrate that the processing of GFDM using the matched filter at the receiver (GFDM-PMF) results in superior radar performance compared to using zero forcing. In fact, the self-interference caused by the non-orthogonality of the GFDM subcarriers is completely mitigated by using the proposed GFDM radar processing technique. It was also verified that in multi-user environments, where interference between users in adjacent channels may occur, the GFDM radar presents less inter-system interference than the OFDM radar. Thus, the GFDM radar requires a narrower guard band and has a better range resolution than the OFDM radar, which makes the GFDM waveform a better candidate for RadCom systems. In this chapter, we also show that, with correct processing, non-orthogonality in multicarrier waveforms is not a problem for radar estimation. This opens the door to further investigations with other non-orthogonal waveforms for RadCom systems. Research with multicarrier waveforms that optimize performance on both integrated functions (radar and data communication) will be performed.

CHAPTER 7

UFMC Radar

In this chapter we will present the latest multicarrier waveform proposed for radar applications in this thesis. UFMC is an orthogonal waveform based on OFDM, and therefore different from the waveforms presented in the last chapters, its implementation for radar applications occurs directly. The use of UFMC signal for radar applications present a superior performance of inter-system interference and background noise when compared to OFDM. The UFMC radar is validated with simulations and real measurements at 24 GHz. The chapter is organized as follows. In Section 7.2, we present the UFMC waveform. In Section 7.2.1, the proposed method for radar processing with UFMC waveform is presented. In Section IV, the laboratory setup and measurements at 24 GHz RadCom system are detailed, also in Section 7.3, we present the evaluation of the performance of the proposed UFMC radar system with a single user, where an evaluation of the inter-system interference is performed. Finally, in Section 7.4 we present the summary.

7.1 Introduction

UFMC is a generalization of FBMC and OFDM. It differs from FBMC in that, instead of filtering each subcarrier individually, UFMC divides the signal into groups of sub-bands and filters each sub-band separately with a filter of size L. The entire bandwidth is divided into B subbands and each subband is allocated with N_{sub} consecutive subcarriers, this subcarrier grouping reduces the length of the filter (when compared to the FBMC). The transmitted signal does not use CP (although it can be used to improve protection against interference between symbols), the filtering operation leads to a lower OOB emission than OFDM and minimizes ICI among adjacent users [83].

The OFDM can be represented as a special case of UFMC with $L = 1$. Within a single subband, the spectral properties for UFMC are similar to filtered OFDM [123]. The UFMC waveform is an interesting option for applicability in radar systems. It shows higher spectral efficiency compared to OFDM, the pulse modeling function improves performance in the multiuser asynchronous scenario, and also preserves compatibility with well known OFDM algorithms (channel estimation and MIMO detectors) [85]. UFMC can be considered as a potential candidate for future wireless systems that need to support a multitude of low-cost devices that will integrate IoT technologies and massive machine communication. To serve these devices, UFMC can be used even with different subcarrier spacings or filter times for users on different sub-bands [124].

UFMC is a highly adaptive modulation scheme that can be easily adjusted for many different aspects of RadCOM systems, such as Doppler and delay propagation characteristics and radar system resolution. Since UFMC is an orthogonal waveform, UFMC does not require specific processing on the radar to remove self-interference, making its implementation for radar applications easier. UFMC presents out-of-band emission bands lower than OFDM at the cost of an DFT with double points in the reception. The UFMC waveform represents an intermediary performance trade-off, since it presents, inferior performance in interference reduction between systems, when compared to the FBMC and GFDM waveforms, but also presents a lower computational complexity when compared to the FBMC and GFDM .

7.2 UFMC waveform

The UFMC transceiver model is shown in figure 7.1. In this architecture the complete band of N subcarriers is divided into B subbands/transmitter blocks with a fixed number of N_{sub} subcarriers in each. The input data packet is distributed in sub packets with the lowest data rate in each transmitter block. Each block transforms the modulated symbols into the time domain through an N-size IDFT, where zeros are entered for unallocated carriers. The IDFT operation is followed by a sub-band filtering operation with a filter of length L—Linear convolution between the IDFT output and the filter impulse response of an output of length $N + L - 1$. Consequently, the signal transmitted by the UFMC is the sum of the B signal blocks. The transmission does not have overlap between the UFMC blocks in the time domain, which means that the transmission of a particular UFMC block starts after the end of the previous one [125]. You can also apply different filters per sub-band, if it is advantageous.

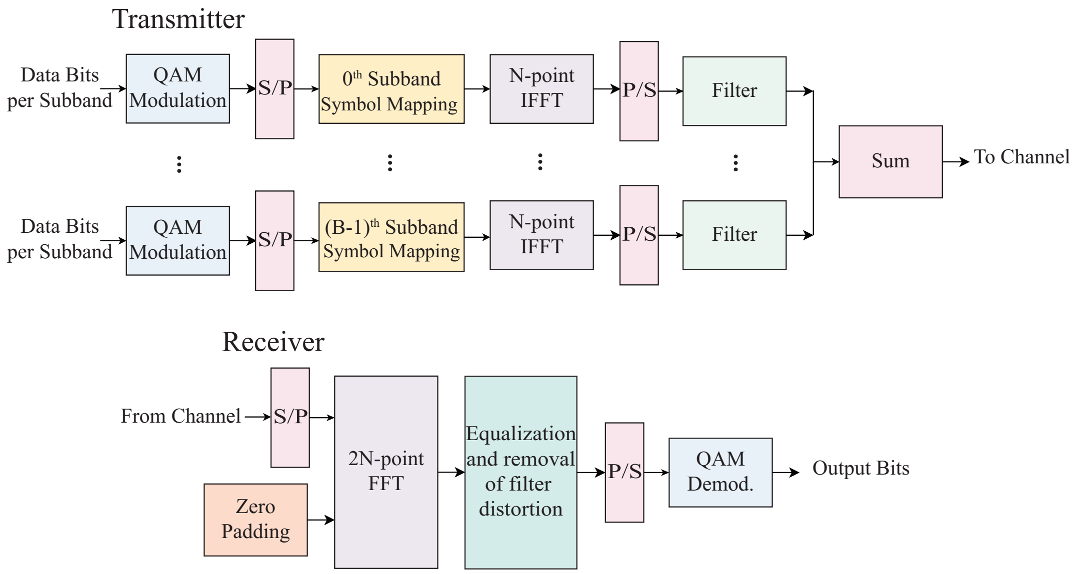

Figure 7.1: UFMC transceiver.

On the receiver side, a 2N-DFT is executed where a zero fill is applied before, since the length of the input signal (ie, the transmitted signal) is $N + L - 1$. Similar to OFDM, channel equalization in the frequency domain can be performed after the decimation of the DFT output by a factor 2 [125]. This prevents the Transmitter filter delay. A window stage can also be entered before the DFT [83].

The time-domain UFMC transmit signal is the superposition of the sub-bandwise filtered components, the input vector $\tilde{\mathbf{S}}(m) = [\tilde{\mathbf{S}}_0(m), ..., \tilde{\mathbf{S}}_{B-1}(m)]$ with $m = 1..M$, where M is the number of transmitted symbols, is formed by the data input $\mathbf{S}(m)$ of size $N_{sub} * B \times M$, divided into B data blocks with N_{sub} subcarriers allocated for each data block. Each $\mathbf{S}_b(m)$ is zeropadde with $N - N_{sub}$ zeros being $\tilde{\mathbf{S}}_b(m) = [\vec{0}_{[1\times(b-1)N_{sub}]}, \mathbf{S}_b^T(m), \vec{0}_{[1\times(N-(b-1))N_{sub}]}]^T$, in order to realize a N-IDFT obtaining $\mathbf{s}_b$ in the time domain, which is then filtered by a filter of length L with impulse response $\mathbf{p}_b$. The output vector of each sub-bands $\tilde{\mathbf{x}}_b$ is added to others, obtaining the output vector $\mathbf{X}(m)$ for each symbol m transmitted [126], which has the following expression

$$x(q, m) = \sum_{b=0}^{B-1} \tilde{x}_b(q, m) = \sum_{b=0}^{B-1}\sum_{n=0}^{N-1} \tilde{s}_b(n, m) p_b(q - n), \tag{7.1}$$

where k = 0, ..., N + L-1. Then, the transmit signal of one UFMC block can be written in matrix-vector form as

$$\underbrace{\mathbf{x}[m]}_{[(N+L-1)\times 1]} = \sum_{b=1}^{B} \underbrace{\mathbf{P}_b}_{[(N+L-1)\times N]} \cdot \underbrace{\tilde{\mathbf{W}}_b^{\mathbf{H}}}_{[N\times N_{sub}]} \cdot \underbrace{\mathbf{S}_b[m]}_{[N_{sub}\times 1]}, \tag{7.2}$$

where $\tilde{\mathbf{W}}_b^{\mathbf{H}}$ is the matrix of the IDFT which includes the relevant columns of the Fourier inverse matrix according to the respective position of the sub-band. $\mathbf{P}_b$ is a toeplitz matrix, composed of the impulse response of the filter, performing linear convolution.

The discrete-time domain received signal at the m-th symbol can be expressed as

$$\mathbf{y}[m] = \mathbf{H}[m]\mathbf{x}[m] + \mathfrak{n}[m] \tag{7.3}$$

, where the AWGN vector $\mathfrak{n}[m]$ with zero mean and variance σ^2 is identically independent complex Gaussian distributed. The channel matrix $\mathbf{H}[m]$ is a Toeplitz matrix with size $(N + L - 1) \times (N + L - 1)$, whose first column is $[h_0, \cdots, h_{L_c-1}, \mathbf{0}_{(N+L-1)-L_c}]^T$, where L_c is the length of the time domain channel taps.

On the receiver side, the UFMC receiver consists of DFT of size $2N$, followed by a downsampler with a factor of 2 and an equalizer. A guard interval of zeros is added to the signal received between IDFT symbols. This prevents the inter symbol interference due to transmitter filter delay [83].

$$\tilde{\mathbf{Y}}[m] = \text{FFT}[\mathbf{y}^T[m], \vec{0}_{[1\times(N-L)]}]^T. \tag{7.4}$$

The receiver can be based on a simple scalar equalization per subcarrier. The symbol estimate is given by

$$\hat{\mathbf{S}}(n,m) = (P(n,m)H(n,m))^{-1}\tilde{y}(n,m), \tag{7.5}$$

with $H(n,m)$ being the complex scalar channel transfer function coefficient and $P(n)$ the filter frequency response of the subband of interest b, belonging to the respective subcarrier n.

7.2.1 UFCM radar

UFMC is a filtering operation that is applied to a group of successive subcarriers instead of FBMC subcarrier filtering. Block filtration brings additional flexibility and can be used to avoid the main disadvantages of FBMC. The UFMC is orthogonal to the complex plain. Thus, complex modulation symbols can be used without any Auto Interference problems, so we can apply the UFMC functions directly to radar processing.

The matrix $\mathbf{S}$ is given by the received symbols without the equalization of the channel. The symbol estimate is given by

$$\hat{\mathbf{S}}_{UFMC}(n,m) = (P(n))^{-1}\tilde{y}(n,m), \tag{7.6}$$

with $P(n)$ being the filter frequency response of the sub-and of interest b, belonging to the respective subcarrier n.

7.2.2 UFMC radar parameterization

From the parameters previously defined for OFDM (Table 4.3), we will find the equivalent for the UFMC waveform. In UFMC, groups of subcarriers (sub-bands) are filtered, so one of the differences in the parameterization of UFMC is that we have to find the number of subbands B and the number of subcarriers in each subband N_{sub}.

The number of symbols will be the same, M=256. We could directly parameterize these parameters as $N_{sub} = 1024$, $B = 1$, $M = 256$, and we would have the same system as OFDM, but we would not be able to benefit from some advantages derived from the application of this waveform. We have to maintain the same bandwidth, thus $BN_{sub}\Delta f = B_W$. We chose the values of $N_{sub} = 64$, $M = 256$ and $B = 16$; the filter of each subband will the length L=16 designed by using the Dolph-Chebyshev window with side-lobe attenuation of 80 dB. The smaller number of subcarriers reduces PAPR problems. The complete parameterization is shown in Table 7.1.

Table 4.3 and Table 7.1 show that UFMC modulation has ambiguous velocity and range values, as well as range and velocity resolution, very similar to those presented by OFDM.

7.3 UFMC radar measurements and performance evaluation

In this section, we will present the laboratory setup and measurements using UFMC waveform for radar functions. We will also present results obtained by simulation, in order to evaluate the inter-system interference.

7.3.1 Measurement setup

The measurement scenario and setup is shown in Figure 7.2. In the scenario, we have two steel sheet targets with 50 × 50 cm dimensions, at a distance of 3.3 m (0°) and 0.6 m (25°). The measurement scenario for the 24 GHz radar system was

Table 7.1: UFMC System Parameters

PARAMETERS	SYMBOL	VALUE
Carrier frequency	f_c	24 GHz
Number of subcarriers	N_{sub}	64
Number of UFMC symbols	M	256
Number of subbands	B	16
Total signal bandwidth	B_W	113.92 MHz
Subcarrier spacing	Δf	111.25 kHz
UFMC symbol duration	T_{UFMC}	9.00 μs
filter length	L	16
Duration of evaluated symbols	T_F	2.4 ms
Range resolution	ΔR	1.316 m
Velocity resolution	Δv	2.6 m/s
Unambiguous range	R_{max}	1347 m
Unambiguous velocity	V_{max}	± 342 m/s
Modulation		4-QAM

(a) (b)

Figure 7.2: Photograph of the (a) measurement setup and (b) the scenario with two targets.

performed in the laboratory. The frequency of 24 GHz was considered. The radar system front-end consisted of two A-Info LB-180400-KF 15 dBi horn antennas: one for the transmission and another for the reception.

The transmitted data was randomly generated with a 4-QAM constellation. The transmitted waveform (OFDM and UFMC) had a bandwidth of 113.92 MHz and was synthesized in the baseband, at a sample rate of 683.52 MSa/s, using a Keysight M8190A AWG. The baseband waveform was then converted to the 24 GHz band using a Keysight E8267D PSG VSG. The signal at the output of the VSG had an average power of 12 dBm and was fed to the transmitting antenna.

The signal received by the receiving antenna was measured using a Keysight N9041B UXA VSA. Thee 10 MHz oscillator of the VSA was used as a reference to synchronize the clocks of all instruments, and a baseband trigger signal was provided by the AWG to the VSA. The AWG was connected to a personal computer and the other instruments were connected through a local area network to the same computer. The calibration of the system was performed with the transmitting and receiving antennas positioned facing one another at a short distance, thus measuring and removing the total delay of the system during the radar processing.

7.3.2 Measurements

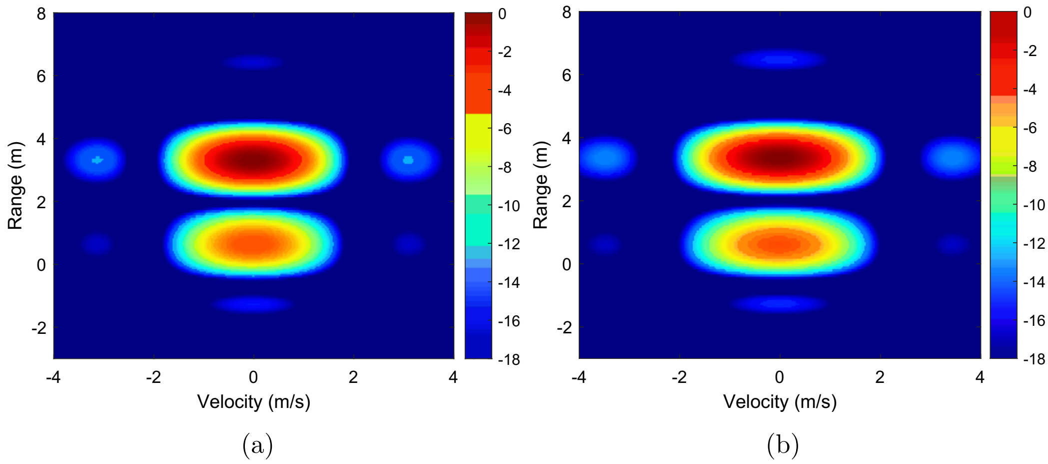

Figure 7.3: Radar image with two targets for (a) OFDM and (b) UFMC.

All measurements were done according to the modulation parameters presented in Table 4.3 (OFDM) and Table 7.1 (UFMC). Figure 7.3 shows the measurements performed with OFDM and UFMC in the scenario with two static targets: one at 0.6 m and the other at 3.3 m. In the radar images, it is possible to verify that UFMC also presents the same performance as OFDM for multiple targets. The estimated range values for both waveforms are 0.62 m and 3.33m.

7.3.3 Performance evaluation

In this section, we compare the performance of the UFMC waveform with OFDM waveform for inter-system interference (interference from another radar with the same waveform in an adjacent channel) in radar image. The performance is evaluated using a simulated scenario with parameters presented in Table 4.3 (OFDM) and Table 7.1 (UFMC). We consider a noiseless environment with two radars (multiple users) and one target for the estimation of the inter-system interference after filtering in radar processing (SIR_{out}). The signals of the two radar systems were generated with a bandwidth of 113.92 MHz and with different average powers according to the desired signal-to-interference ratio at the radar input (SIR_{in}). Theses were allocated to adjacent bands. The received signal (in complex baseband form) was filtered by a sharp low-pass filter in order to select the desired user band. The simulate scenario of a single static target at 0 m is used

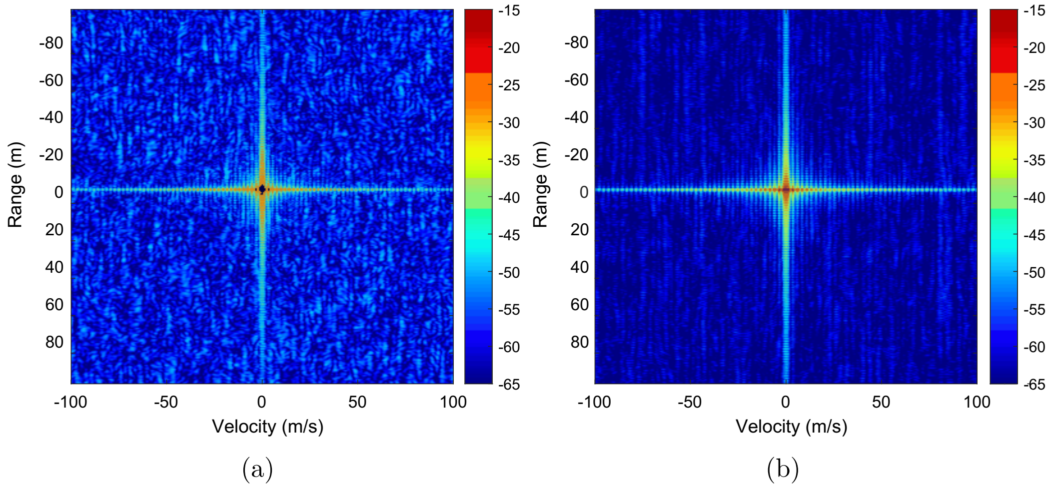

Figure 7.4: Radar image with inter-system interference for (a) OFDM and (b) UFMC.

to measure the inter-system interference in a multi-user environment. Figure 7.4 shows the radar image for a system with an interference level in the reception (before filtering) of $SIR_{in} = -20$ dB for the OFDM and UFMC waveforms. In this figure, it is possible to see that the high OOB emission of OFDM causes a higher inter-system interference, resulting in a higher level of background noise in the radar image. In the radar image with the UFMC waveform, this background noise is reduced.

The performance is compared in terms of the NMSE of the received radar signal after filtering in relation to the signal received by a radar with no interference, defined by

$$NMSE = \frac{\|\mathbf{Y}_{int} - \mathbf{Y}_{true}\|_2^2}{\|\mathbf{Y}_{true}\|_2^2}, \tag{7.7}$$

where $\mathbf{Y}_{true}$ is the received radar signal with no interference and $\mathbf{Y}_{int}$ is the signal with interference.

We also compare the performance in term of SIR (ratio between the power of the reflected radar signal and the power of the interfering signal), given by

$$SIR = \frac{P_{radar}}{P_{int}}, \tag{7.8}$$

where P_{radar} is the power of the reflected radar signal and P_{int} is the power of the interfering signal. We denote SIR_{in} as the SIR of the received radar signal before filtering, and SIR_{out} as the SIR of the received radar signal after filtering. The simulate scenario of a single static target at 2 m with noiseless environment is used in the simulation.

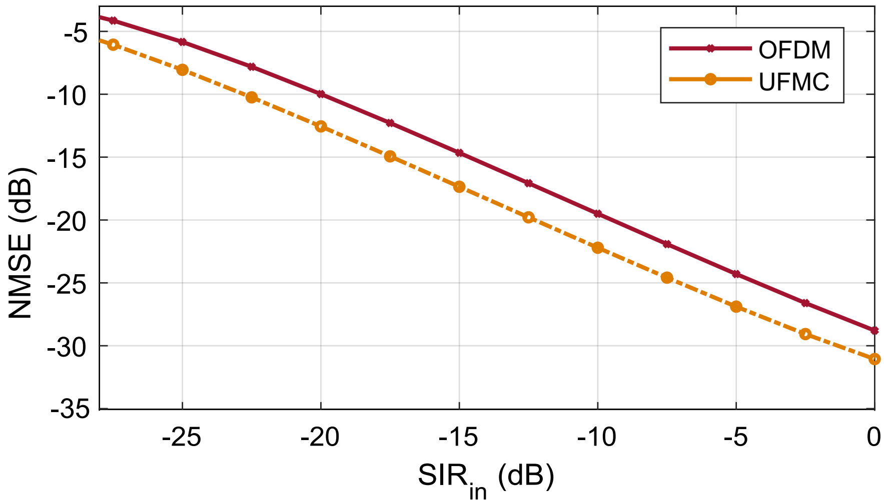

Figure 7.5: Variation of the NMSE of the received radar signal as a function of SIR_{in}.

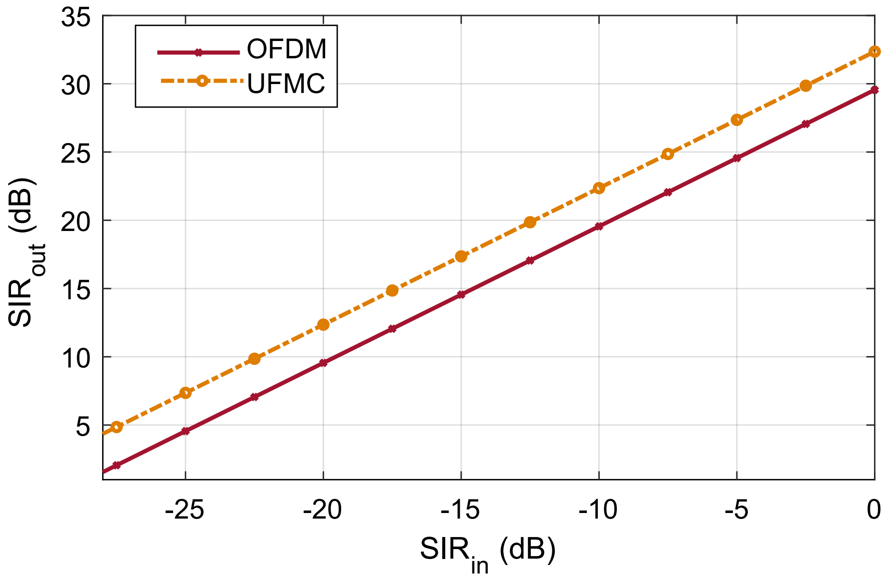

Figure 7.6: Variation of the post-filtered SIR as a function of SIR_{in}.

Figure 7.5 shows the NMSE of the reconstructed signals for the OFDM and UFMC radars for different values of SIR_{in}. Less interference can be seen on the UFMC radar due to lower OOB emissions.

In Figure 7.6 we also compare the same systems for the interference after filtering (SIR_{out}) . This figure demonstrates that, the UFMC radar SIR_{out} is lower than that of the OFDM radar.

7.4 Summary

This chapter presents the processing of the UFMC waveform for radar with simulations and measurements at 24 GHz. The results demonstrate the viability of UFMC for RadCom systems. We verified that in multi-user environments, where interference between users in adjacent channels may occur, the UFMC radar presents less inter-system interference than the OFDM radar.

CHAPTER 8

Multicarrier Waveform Radar - Final Comparisons and Remarks

In this chapter presents a comparison between FBMC, GFDM, UFMC and OFDM waveforms for radar functions. The waveforms are compared by taking into account several aspects. Namely, estimating target parameters, background noise, inter-system interference and system parameterization.

8.1 Final comparisons and remarks

OFDM offers several attractive properties for RadCom systems, such as simple target estimation, low complexity equalization, efficient hardware implementation and easy combination with MIMO systems. With these benefits, the OFDM waveform will remain an important candidate for RadCom systems. OFDM has been extensively studied for the joint radar and communication applications [8, 9, 11, 127–131]. However, OFDM has some disadvantages, such as high OOB emission, leading to the need for frequency guard bands at the two edges of the system bandwidth so that the signal achieves sufficient attenuation to meet the requirements of spectrum mask and adjacent channel leakage ratio. In addition, this high out-of-band emission generates inter-system interference for radar operations, leading to background noise in target estimation images and the guard bands required decrease the range resolution of the radar. OFDM also loses efficiency due to the use of a cyclic prefix, has susceptibility to Doppler spread and the need for frequency synchronization to preserve the orthogonality of the subcarriers [98]. To overcome the problems mentioned above, other waveforms must be evaluated for RadCom systems. The waveform for RadCom systems needs to have efficient spectrum confinement, low out-of-band emission and implementation flexibility.

Table 8.1: Multicarrier radar comparison

	OFDM	UFMC	GFDM	FBMC-QAM
FFT size	1024	1024	256	4096
Symbol	256	256	32 p/block (41 blocks)	332
Filter type	-	Cherbyshev	RC with rolloff 0.5	[104]
Filter length	-	16	1024	4096
Orthogonality	orthogonal	orthogonal	non-orthogonal	non-orthogonal
CP	use	no use	use	no use
Receiver processing	-	-	self-interference cancellation	self-interference cancellation
Range Resolution	1.316 m	1.316 m	1.316 m	1.316 m
Velocity Resolution	2.171 m	2.6 m/s	2.171 m/s	2.171 m/s
Unambiguous Range	1347 m	1347 m	337 m	1347 m
Unambiguous velocity	± 278 m/s	± 342 m/s	± 1424 m/	± 360 m/s

In communications systems, several alternative candidates waveforms have been proposed to replace OFDM, such as UFMC, GFDM) and FBMC [83]. In this thesis, as presented in chapters 5, 6 and 7, we evaluate each of these waveforms for radar functions, and a conclusion that can certainly be drawn is that what is the “best” modulation cannot be easily chosen, as there is no modulation with the best performance in all aspects for RadCom systems. Therefore, the choice of the waveform depends on the priority needs of the application. A brief summary of the parameters for comparing the performance of the previously mentioned multicarrier waveforms for RadCom systems is provided in Table 8.1.

UFMC is a modulation scheme that was designed to perform well in asynchronous transmission scenarios, however although better contained than OFDM, has higher out-of-band emissions than GFDM and FBMC [111]. FBMC is a spectrally well-contained waveform, however due to its long filters, FBMC has

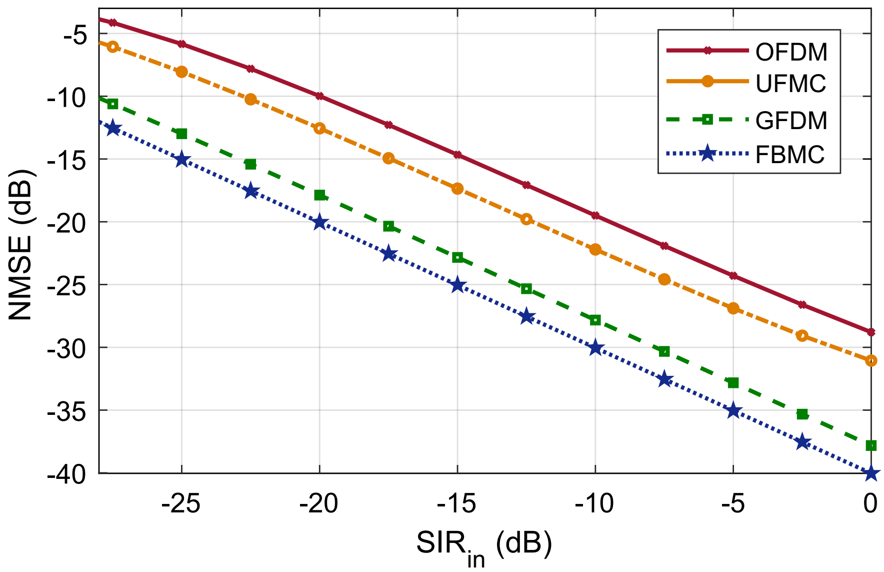

Figure 8.1: Variation of the NMSE of the received radar signal as a function of SIR_{in}.

a low efficiency in situations where small data packets must be transmitted, a typical scenario for automotive systems and IoT, in addition, FBMC has very high computational complexity [112].

UFMC and FBMC do not require the use of a CP, an advantage over the OFDM. Although GFDM uses CP, it exhibits great flexibility, since frequency bands can be added and removed on a communication link quite easily and flexibly. In addition, GFDM well-contained spectral modulation with low computational complexity [113–115]. The latency requirement also plays an important role for automotive RadCom system applications, and in that respect, FBMC is an inappropriate choice, since the long-term impulse response of FBMC filters limits its use in situations of sporadic traffic and low latency.

UFMC and OFDM are orthogonal waveforms, so they do not suffer from self-interference, whereas FBMC and GFDM are non-orthogonal. However, unlike what happens with communication systems, for active radar operations, the interferences caused by non-orthogonality of the waveforms can be totally canceled in the radar processing (as demonstrated in chapters 5, 6 and the 13.2), not being a problem for the system, at the cost of additional processing at the receiver.

Interference between RadCom systems becomes a major problem, especially for automotive system applications, where safety is the focus of the application. Therefore, the robustness of the interference is an aspect of vital importance for the successful implementation of this type of system. In this thesis performance

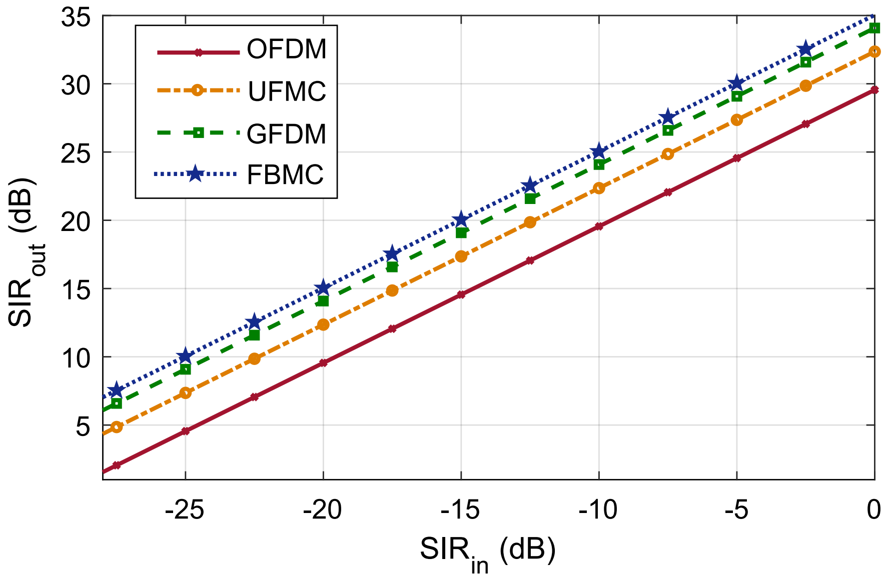

Figure 8.2: Variation of the post-filtered SIR as a function of SIR_{in}.

evaluations on inter-system interference for each waveform were presented in the chapter 5, 6 and 7, the comparative results with all waveforms are shown in Figure 8.1 and Figure 8.2.

Figure 8.1 shows the NMSE of the reconstructed signals for the OFDM, UFMC, GFDM and FBMC radars for different values of SIR_{in}. Figure 8.2 shows the interference after filtering (SIR_{out}). In the Figure 8.1 and Figure 8.2, it is possible to verify that FBMC is the waveform that suffers from the lowest inter-system interference, followed by GFDM, as expected, since both have lower OOB emission values.

In Figure 8.3 we can see the result of this interference in the radar image. Figure 8.3 presents the radar image in a simulation scenario with an interference level in the reception (before filtering) of $SIR_{in} = -20$ dB. It is possible to verify in Figure 8.3, that OFDM presents the image with the highest background noise, and the FBMC the one with the lowest noise, followed by the GFDM and UFMC respectively.

A synthesis graph is shown in Figure 8.4 with all the comparative metrics for choosing the waveform for RadCom applications, the waveforms that homogeneously cover the largest area, is the one that presents a more homogeneous performance. Possibly GFDM would be one of the strongest candidates, GFDM is a solution to mitigate inter-system interference, with an increase in computational complexity lower than FBMC. GFDM has great flexibility, low latency and high

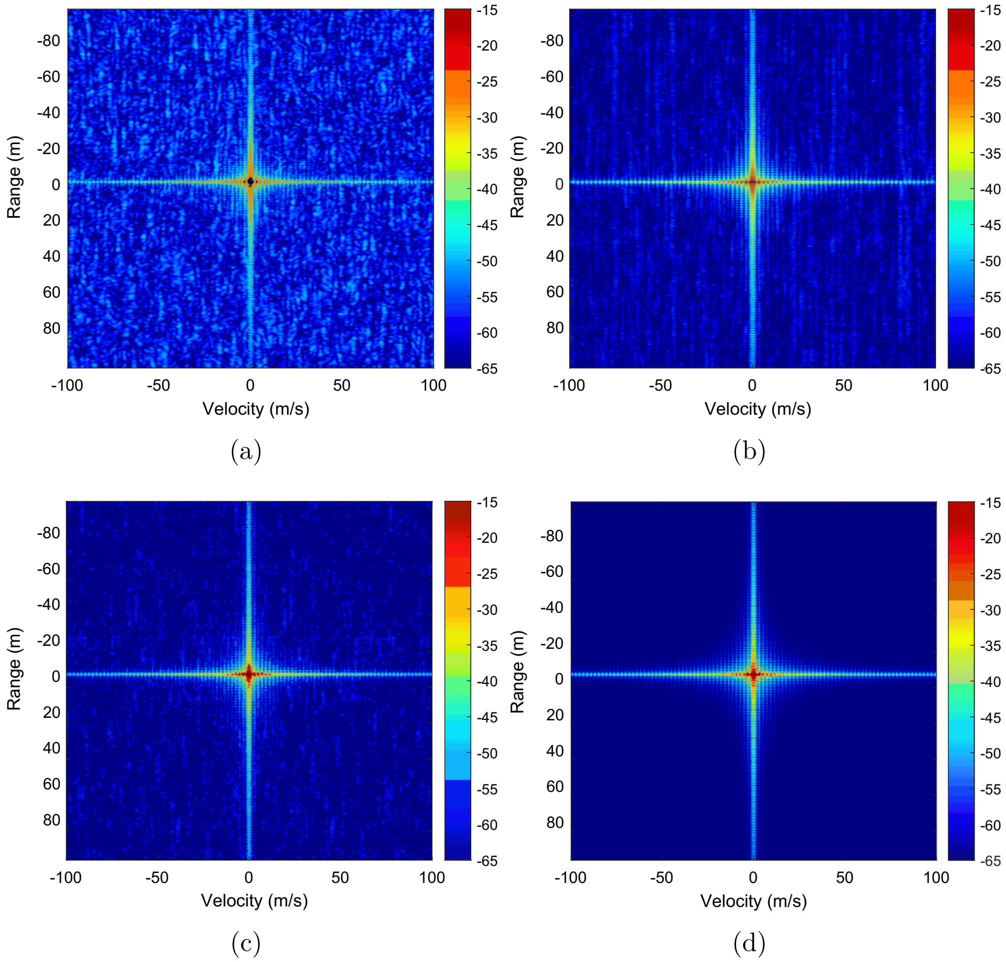

Figure 8.3: Radar image with inter-system interference for (a) OFDM, (b) UFMC, (c) GFDM and (d) FBMC

spectral efficiency. Although it has a low unambiguous range value, it is still well above the maximum target value achievable by current automotive radars, so this is not a limitation for automotive applications.

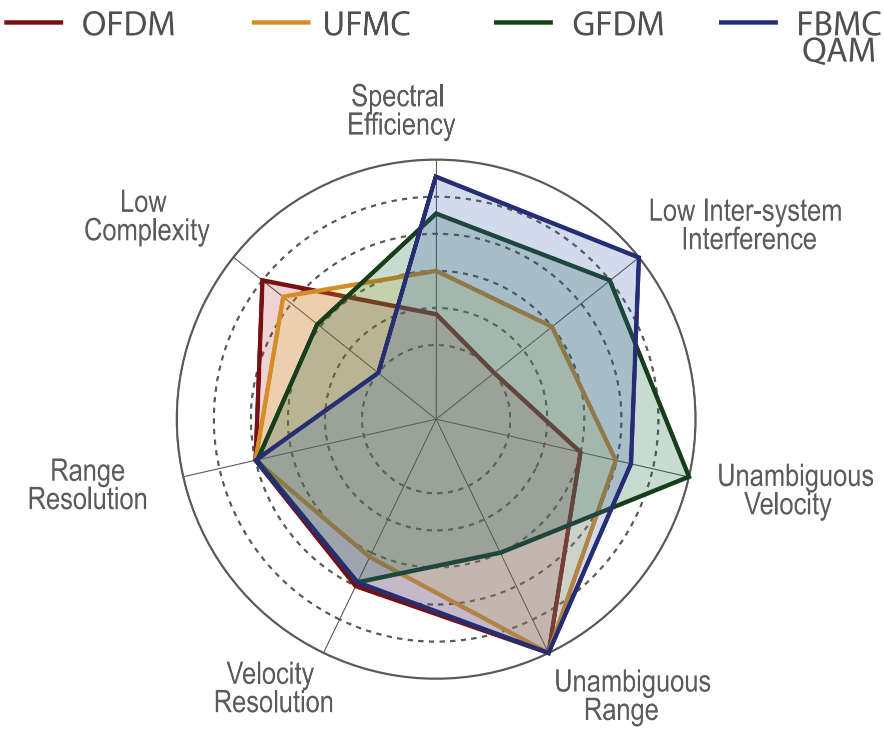

Figure 8.4: Multicarrier waveform radar comparison

PART II

RADCOM SYSTEM: ESTIMATION AND TRACKING

CHAPTER 9

Comparison of DoA Algorithms for MIMO OFDM Radar

THIS chapter presents the comparison of the DoA estimation for a MIMO OFDM radar system using some of the most popular techniques: MUSIC, ESPRIT, Min-Norm, MVDR. The performance of the algorithms is evaluated using two different metrics, namely the performance achievable in terms of resolution and the probability of target distinction, since, for example, in automotive systems, not only the resolution but also the correct distinction of the number of targets can be crucial. In Section 9.2, we present the most popular techniques to DoA estimation. In Section 9.3, we present the evaluation of the performance of DoA techniques. Finally, in Section 9.4 we present the summary.

9.1 Introduction

One important issue common to both radar and communication systems, employing multiple antennas, is the determination of the DoA of the received waveforms. While in traditional radar mechanical scanning is frequently used, for future applications, namely for the intelligent transportation system, where the angular estimate of conventional radars is not feasible due to the space limitations and also due to the velocity of the vehicle in which the radar is located. The use of MIMO for DoA estimation provides a superior performance in relation to the conventional phase array, having better resolution in DoA estimation [72].

Studies of DoA estimation techniques for OFDM radars have already been performed in [1, 72, 79]. In [1] the performance of the MUSIC technique for separation of close targets is evaluated. However, no comparative study among possible DoA estimations techniques was performed. This chapter compares the performance of MUSIC, ESPRIT, Min-Norm and MVDR [132] for DoA estimation in RadCom systems, with a focus on the evaluation of their performance for target separation. As will be shown, the MUSIC algorithm does not achieve a satisfactory performance for separation of close targets, failing to distinguish. For vehicle radar purposes this type of problem compromises the reliability of the system.

9.2 DoA estimation

Consider a MIMO radar system with M_T transmit antennas and M_R receive antennas illuminating K targets from the directions θ_k, $k = 1, 2, ..., K$. The antennas are assumed to be uniformly spaced with an inter-antenna distance of d_t for the transmitting antennas and d_r for the receiving antennas, shown in the Figure 3.9.

Considering then $\mathbf{X}(t) = [x_0(t), ..., x_{M_T-1}(t)]^T$ as the set of signals transmitted by the M_T transmitting antennas, and the set of signals $\mathbf{Y}(t) = [y_0(t), ..., y_{M_R-1}(t)]^T$ received by the M_R receiving antennas after the reflection by K targets. The signal received by the q-th receiving antenna, where $q = 0, ..., M_R - 1$,, as demonstrated in chapter 3, can be described by

$$\begin{aligned}\mathbf{Y}(t) &= \sum_{k=1}^{K} [\mathbf{a}_T(\theta_k) \otimes \mathbf{a}_R(\theta_k)]\, \mathbf{X}\left(t - \frac{2r_k}{c}\right) e^{j2\pi f_{D,k} t} + \boldsymbol{\eta}(t) \\ &= \sum_{k=1}^{K} \mathbf{A}(\theta_k)\mathbf{X}\left(t - \frac{2R_k}{c}\right) e^{j2\pi f_{D,k} t} + \boldsymbol{\eta}(t),\end{aligned}$$

with $\mathbf{A}(\theta_k) = [\mathbf{a}_T(\theta_k) \otimes \mathbf{a}_R(\theta_k)]$, where $\mathbf{a}_T(\theta_k)$ and $\mathbf{a}_R(\theta_k)$ are the steering vectors of the transmitter and receiver for the k-th target, given by

$$a_T(\theta_k) = \left[1, e^{j2\pi d_t 1 \sin\theta_k/\lambda}, \cdots, e^{j2\pi d_t (M_T-1)\sin\theta_k/\lambda}\right]^T$$
$$a_R(\theta_k) = \left[1, e^{j2\pi d_r 1 \sin\theta_k/\lambda}, \cdots, e^{j2\pi d_r (M_R-1)\sin\theta_k/\lambda}\right]^T.$$

The symbols received by the q-th receiving antenna can be described by

$$\hat{\mathbf{S}}_q(m, p + n_\mu M_T) = \sum_{k=1}^{K} e^{j2\pi d_t p \sin\theta_k/\lambda} e^{j2\pi d_r q \sin\theta_k/\lambda}$$
$$\mathbf{S}(m, p + n_\mu M_T) e^{j2\pi f_{D,k} m T} e^{-j2\pi n \Delta f \frac{2r_k}{c}} + \eta_q(m, n).$$

For the radar processing, the estimation of the channel information matrix $\mathbf{D}$ of the q-th receiving antenna is given by

$$\mathbf{D}_q(m, p + n_\mu M_T) = \frac{\hat{\mathbf{S}}_\mathbf{q}(m, p + n_\mu M_T)}{\mathbf{S}(m, p + n_\mu M_T)},$$

where $p = 0, \ldots, M_T - 1$, $n_\mu = 0, \ldots, N_{M_T} - 1$ and $N_{M_T} = N/M_T$.

For the processing of the DoA estimation techniques, the signal processing can be applied directly to the channel information matrix $\mathbf{D}$.

Using only the range profile of the channel information matrix ($m = 0$), and regrouping the channel information for each existing MIMO channel ($M_T \times M_R$), we have the matrix $\mathbf{D}_{DoA}$, represented by

$$\mathbf{D}_{DoA}(n_\mu) = [\mathbf{D}_0(0, 0 + n_\mu M_T), \ldots,$$
$$\mathbf{D}_{M_R-1}(0, 0 + n_\mu M_T), \ldots, \mathbf{D}_{M_R-1}(0, M_T - 1 + n_\mu M_T)], \tag{9.1}$$

where $n_\mu = 0, \ldots, N_{M_T} - 1$.

The covariance matrix is defined as

$$\mathbf{R} = \frac{1}{M} \sum_{n_\mu=0}^{N_{M_T}-1} \{\mathbf{D}_{DoA}(n_\mu) \mathbf{D}_{DoA}(n_\mu)^H\}. \tag{9.2}$$

$\mathbf{R}$ can also be written as

$$\mathbf{R} = \mathbf{U}_s \mathbf{\Lambda}_s \mathbf{U}_s^H + \mathbf{U}_n \mathbf{\Lambda}_n \mathbf{U}_n^H, \tag{9.3}$$

where $\mathbf{U}_s$ represents the signal subspace consisting of the largest K eigenvalues of $\mathbf{R}$ and $\mathbf{U}_n$ represents the noise subspace with the remaining $M_R \times M_R - K$ eigenvectors. $\mathbf{\Lambda}_s$ and $\mathbf{\Lambda}_n$ are diagonal matrices containing their corresponding eigenvalues. The DoA are defined by maximum values in the spectrum using these subspaces and the correlation matrix, as defined below.

9.2.1 MVDR

MVDR uses the signal correlation matrix for DoA estimation. The technique attempts to minimize the power contributed by noise and unwanted interference, while maintaining a fixed gain in the look direction, and the nulls in other directions to reject other signals [132]. The peaks in the MVDR spectrum occur whenever the direction vector is orthogonal to the noise subspace. The angular spectrum MVDR is defined by

$$P_{MVDR} = \frac{1}{\mathbf{A}(\theta)^H \mathbf{R}^{-1} \mathbf{A}(\theta)}. \tag{9.4}$$

9.2.2 MUSIC

MUSIC is one of the most recent methods proposed and a very popular method for estimation of arrival direction based on subspace techniques. The spectrum of MUSIC is given by

$$P_{MUSIC} = \frac{1}{\mathbf{A}(\theta)^H \mathbf{U}_n {\mathbf{U}_n}^H \mathbf{A}(\theta)}. \tag{9.5}$$

MUSIC estimates all possible direction vectors $\mathbf{A}(\theta)$ to find those that are perpendicular to the space covered by the noise eigenvectors, since the direction vectors corresponding to the DoA are in the subspace of the signal and are orthogonal to the noise subspace.

9.2.3 Min-Norm

The Min-Norm algorithm can improve the performace of the MUSIC algorithm. The estimation function uses the new noise subspace which is a linear combination of the noise subspace $\mathbf{U}_n$, therefore, the new noise subspace is orthogonal to the signal subspace. Its spectrum [132] is given by

$$P_{MN} = \frac{1}{\mathbf{A}(\theta)^H \mathbf{U}_n {\mathbf{U}_n}^H \mathbf{W} \mathbf{U}_n {\mathbf{U}_n}^H \mathbf{A}(\theta)}, \tag{9.6}$$

with the vector $\mathbf{W} = ww^T$ where w is equal to the first column of an identity matrix $M_T M_R \times M_T M_R$.

9.2.4 ESPRIT

ESPRIT is another subspace-based DoA estimation algorithm, but it does not perform a search on all possible direction vectors to estimate DoA, which reduces processing and memory usage. ESPRIT is based on the rotational invariance of the subspace of the incident signals expanded by two responses shifted from each other by the $\mathbf{\Phi}$ matrix. The system response is then composed of two subsets whose values are related to each other by the displacement vector, so there must be a unique nonsingular matrix $\mathbf{T}$ such that $\mathbf{U}_s$ [132] can be decomposed into two subspaces $\mathbf{U}_1$ and $\mathbf{U}_2$:

$$\mathbf{U}_s = \begin{bmatrix} \mathbf{U}_1 \\ \mathbf{U}_2 \end{bmatrix} = \begin{bmatrix} \mathbf{AT} \\ \mathbf{A\Phi T} \end{bmatrix} \tag{9.7}$$

and

$$\mathbf{U}_1\mathbf{\Psi} = \mathbf{U}_2 \Longrightarrow \mathbf{AT\Psi} = \mathbf{A}\Phi, \tag{9.8}$$

$\mathbf{\Phi}$ and $\mathbf{\Psi}$ are related via an eigenvalue-preserving similarity transformation:

$$\mathbf{\Psi} = \mathbf{T}^{-1}\mathbf{\Phi T}. \tag{9.9}$$

The diagonal elements (or eigenvalues) of $\mathbf{\Phi}$ are equal to the eigenvalues of the transformation matrix $\mathbf{\Psi}$ that relates $\mathbf{U}_1$ and $\mathbf{U}_2$. then the arrival angles can be estimated by the eigenvalues (λ_Φ) of $\mathbf{\Phi}$:

$$\theta_k = \sin^{-1}\left(\frac{\lambda}{2\pi d}\arg(\lambda_{\Phi k})\right), \tag{9.10}$$

where $\arg(\xi)$ is the function that returns the argument of the complex number ξ.

9.3 DoA algorithms - analysis of results

Numerical simulations were performed to compare the performance of DoA techniques: MVDR, MUSIC, Min-Norm and ESPRIT. The estimation capacity of these techniques was evaluated for a single target and for two targets (target A and target B) with a difference of 3 degrees in the presence of white Gaussian noise. Note that in this chapter, we suppose that K is already known. The performances are measured by the Root Mean Square Error (RMSE).

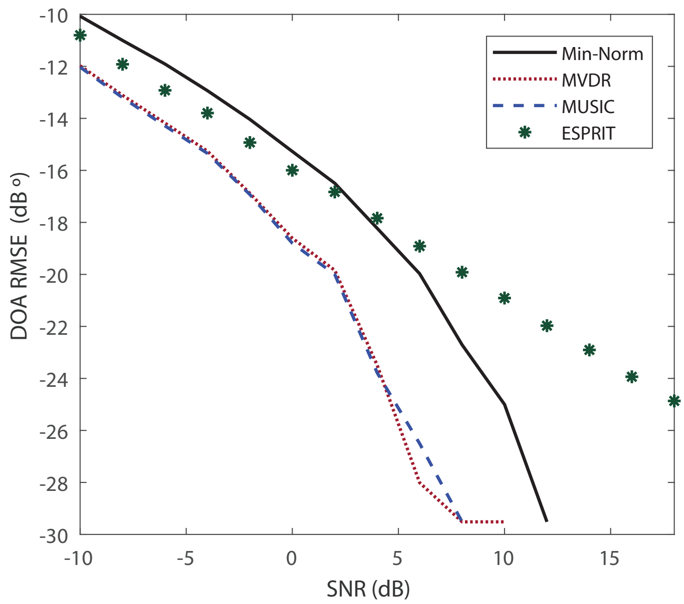

Figure 9.1: RMSE for the resolution of one target versus SNR.

The simulated radar system has a carrier frequency of 24 GHz, bandwidth of 93.1 MHz, with 1024 subcarriers spaced by 90.909 kHz. The simulation evaluates 256 4-PSK symbols with a duration per symbol of 12.375 μs. The system has 3 transmitting antennas and 3 receiving antennas spaced by $d = \lambda/2$. Details of the system parameterization are shown in [58]. In the simulations, the angles are random. The velocity and position of targets A and B are v_A = 7 m/s v_B = 6 m/s, r_A = 10 m and r_B = 10 m respectively. Figure 9.1 shows the DoA RMSE performance of the algorithms with respect to the signal-to-noise ratio for the scenario with one target. The Monte Carlo estimations were performed through 8000 simulations. With the results presented it is possible to verify that the MUSIC technique has the best performance, together with the MVDR technique. The Min-Norm technique and ESPRIT are the ones that present the worst resolution. The ESPRIT technique is the worst for values above 10 dB.

In the simulation shown in Figure 9.2 we present the results for DoA RMSE for the scenario with two targets with a difference of 3°. The angles of the two targets were randomly varied from $-75°$ to $75°$, always remaining 3 degrees between the two targets. In the case where the angle was not determined we consider as a

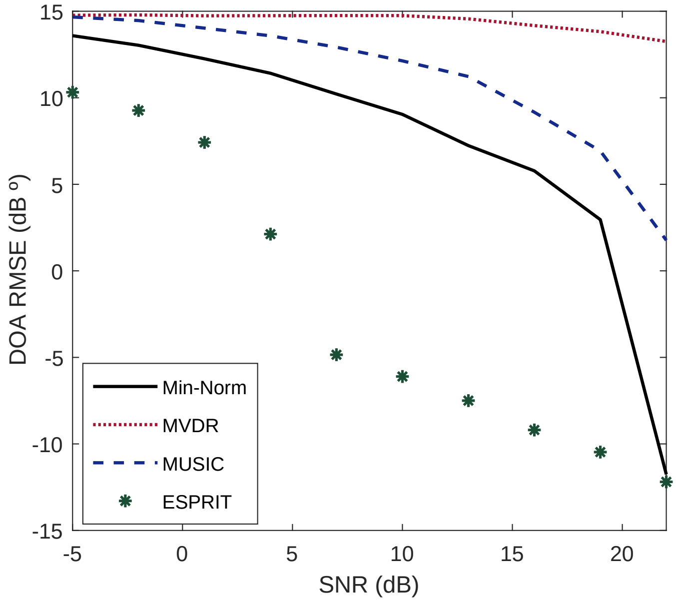

Figure 9.2: RMSE for the resolution of two target versus SNR.

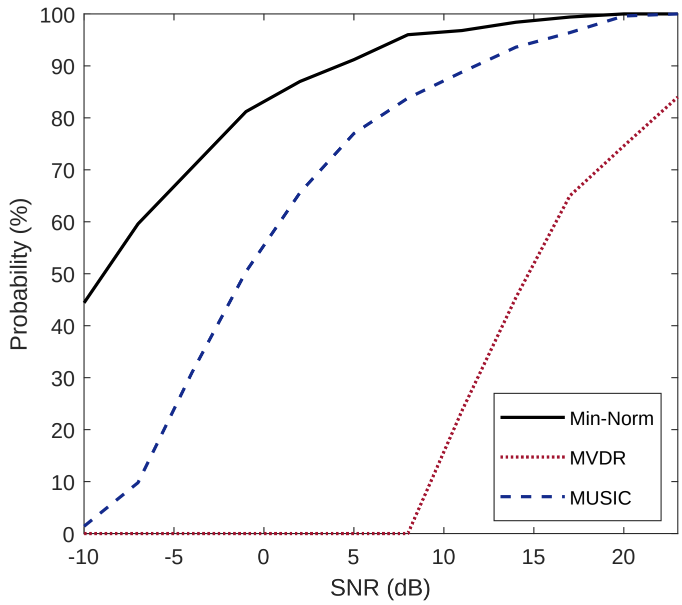

Figure 9.3: Distinction probability versus SNR.

straight line the direction of the unknown target (0°). The figure clearly shows that the performance of the MUSIC and MVDR algorithm is compromised, with the Min-Norm and ESPRIT algorithms now having the best performance.

To evaluate the ability to distinguish targets by the algorithms, the Figure 9.3 is presented, where the probability of correct distinction of the number of sources

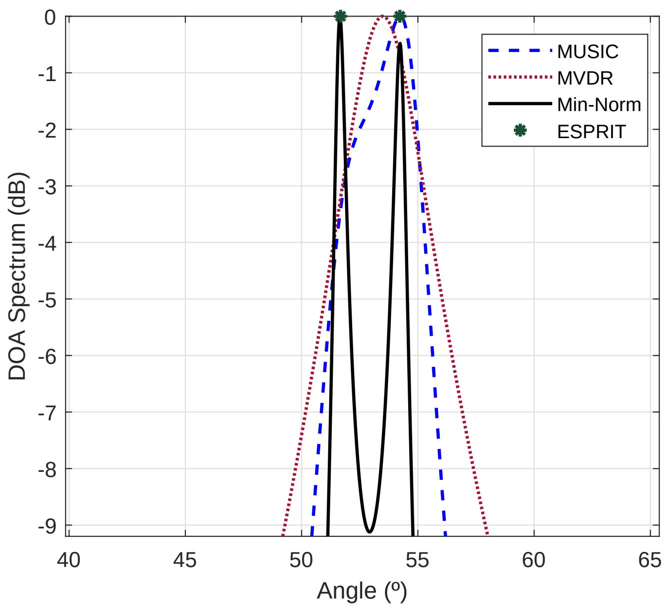

Figure 9.4: DoA spectrum with two closely located targets

is presented. The figure shows the results of the MVDR, MUSIC and Min-norm techniques; since the ESPRIT technique always provides the number of angle estimates equal to the number of targets reported, different from the other three methods which may show divergence, its results were not taken into account here. The results of this simulation show that the Min-Norm technique has a much higher resolution capability than other methods, for example having a target discrimination probability of 60% at an SNR of -5 dB against 10% of MUSIC and 0% of MVDR.

Figure 9.4 shows the comparison of the results of DoA spectrum with two closely located targets. In this simulation, the SNR is 0 dB and the angles are 51 and 54 degrees. It is possible to see that only the Min-Norm technique was able to distinguish the two targets, while MUSIC and MVDR presented only one DoA estimation peak.

9.4 Summary

This chapter presents the results of the direction-of-arrival estimation based on a MIMO OFDM radar system using some of the most popular techniques for estimation of DoA: MVDR, MUSIC, Min-Norm and ESPRIT. The results of the simulation showed that the method that presents the best resolution in determining a target is the MUSIC algorithm, followed by Min-norm and ESPRIT, and the one with the worst resolution is the MVDR. However, in the simulations performed with two separate sources at a small angular distance, we showed that the Min-Norm technique presents a much better estimation probability than the other techniques, having a much greater capacity to distinguish the two targets, followed by ESPRIT. The MUSIC and MVDR techniques do not present a good performance for the distinction of the two targets, presenting a much lower probability of estimation when compared to Min-Norm, with exception only for situations with high SNRs.

CHAPTER 10

High-Resolution DoA Estimation of Closely-Spaced and Correlated Targets

This chapter presents a new concept of high-resolution DoA estimation in orthogonal frequency division multiplexing (OFDM) MIMO radar with integrated communication system (RadCom) for automotive applications. High-resolution DoA estimation is an important requirement for automotive radar systems, especially in multi-target scenarios that require higher target separation performance. This chapter introduces a subspace-based procedure for high-resolution DoA estimation for closely spaced targets in uncorrelated and partially correlated signals. This procedure integrates the use of the radar signal together with the communication signal received from another user (one of the targets to be estimated). In Section 10.2, we provide a brief outline of DoA estimation used in this chapter. In Section 10.3, the method for high-resolution DoA estimation is presented. In Section 10.4, the performance evaluation of our method in simulation scenario is presented. Finally, in Section 10.5, we present the summary.

10.1 Introduction

The use of RadCom based in MIMO systems was first considered in [72]. These systems take advantage of the use of various transmitting antennas and various receiving antennas to exploit the spatial properties of the radio channel, thus increasing the channel capacity and reducing multi-user interference in the communication system and allowing for the determination of the DoA in the radar system [19, 36, 81].

The use of MIMO provides better resolution for DoA estimation in relation to the conventional phased array [72]. Studies of DoA estimation techniques for OFDM radars have already been performed in [1, 72, 79, 81, 133]. In [1] and [133], the performance of a subspace-based technique for the DoA estimation of closely spaced targets is evaluated and it is concluded that conventional subspace-based techniques are not able to distinguish targets whose angle of separation is very small. We present a new DoA estimation approach for automotive scenarios based on the MIMO OFDM RadCom system which allows for the differentiation of closely spaced targets in uncorrelated or partially correlated signals and allows for the estimation of DoA in coherent signals.

The new method integrates the use of the radar signal with the received signal from the targets to be estimated. The algorithm comprises two stages. In the first stage, the radar channel transfer matrix and the channel transfer matrix of the received communication signal are determined. In the second stage, the covariance differencing is performed [134] (from the covariance matrices of the radar with the communication signal received from one of the targets to be separated) and then the MUSIC [135] algorithm is applied. The simulation results show that the algorithm allows the distinction of closely spaced targets in environments with low SNR from uncorrelated and partially correlated signals, and the estimation of DoA from coherent signals. The performance of the algorithm is evaluated in simulation in terms of resolution and the probability of target discrimination.

10.2 DoA estimation

In this chapter we will use the MUSIC method presented in the chapter 9 for DoA estimation. MUSIC is a popular method for DoA estimation using subspace-based techniques. AS present in the chapter 9, MUSIC is defined as

$$\mathbf{P} = \frac{1}{\mathbf{A}(\theta)^H \mathbf{U}_n \mathbf{U}_n{}^H \mathbf{A}(\theta)},$$

where $\mathbf{U}_n$ represents the noise subspace with the smallest $M_R \times M_R - K$ eigenvectors of the signal correlation matrix. MUSIC estimates all possible direction vectors $\mathbf{A}(\theta)$ to find those that are orthogonal to the space covered by the noise eigenvectors, thus minimizing the denominator and giving rise to peaks in the spectrum of MUSIC at the correct angles [135]. The estimated DoAs are defined as the angles where the spectrum has its peak values. The direction vectors corresponding to the DoAs are in the subspace of the signal and are orthogonal to the noise subspace.

10.3 The new method: MIMO RadCom DoA estimation

As presented in [1, 133], the performance of the MUSIC algorithm is compromised when trying to distinguish closely spaced targets, having a worse performance when trying to detect highly correlated signals. To solve this problem, a high-resolution DoA estimation technique based on the covariance differencing is presented. The covariance differencing is done between the covariance matrix of the radar channel information and the covariance matrix of the communication channel information.

This technique uses the received communication signal from one of the targets to be detected (represented in Figure 10.1), estimating the channel information matrix through the pilots $\mathbf{D}_{DoA}{}^{com}(n_\rho) = [\mathbf{D}_0(0, 0 + n_\rho N_{pilot}), \ldots, \mathbf{D}_{M_R-1}(0, 0 + n\rho N_{pilot}), \ldots, \mathbf{D}_{M_R-1}(0, M_T - 1 + n\rho N_{pilot})]$, where $n_\rho = 0, ..., NP - 1$, NP is the number of pilots in each transmission antenna, and $N_{pilot} = N/NP$. The covariance matrix is calculated as shown in the previous section. Note that for the covariance matrix of the communication signal only the subcarriers with pilots are considered, although it is possible to use all subcarriers through some process of estimation of the complete channel matrix.

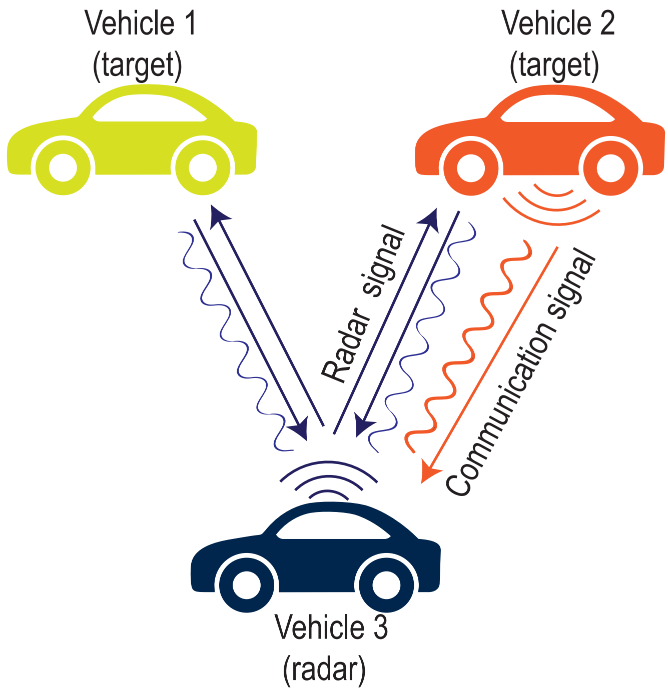

Figure 10.1: Example scenario with vehicles equipped with RadCom systems operating as radar and transmitting communication signals. In this representation, vehicle 3 receives the radar signal reflected by the targets and the communication signal transmitted by vehicle 2.

After the estimation of the radar ($\mathbf{R}_{radar}$) and communication ($\mathbf{R}_{com}$) covariance matrices, the covariance differencing of $\mathbf{R}_{radar}$ and $\mathbf{R}_{com}$ is performed, generating a new $\mathbf{R}_{radcom}$ matrix

$$\mathbf{R}_{radcom} = \mathbf{R}_{radar} - \mathbf{R}_{com}. \tag{10.1}$$

The conventional MUSIC algorithm is then applied to $\mathbf{R}_{radcom}$ and also to $\mathbf{R}_{com}$, generating the respective spectrum estimates $\mathbf{P}_{radcom}$ and $\mathbf{P}_{com}$. These two spectral estimates are normalized ($\overline{\mathbf{P}}_{radcom}$ and $\overline{\mathbf{P}}_{com}$) and then combined to form a single spectrum with the DoA information of all targets, as follows:

$$P(\theta) = \max\left(\bar{P}_{radcom}(\theta), \bar{P}_{com}(\theta)\right), \tag{10.2}$$

where $\overline{P}(\theta) = \text{abs}(P(\theta))/\max(\text{abs}(\mathbf{P}))$ is the normalization operation, with $\text{abs}(\mathbf{x})$ denoting the element-wise absolute value function, $\max(\mathbf{x})$ denoting the maximum-value element of vector $\mathbf{x}$ and $\max(\mathbf{x}, \mathbf{y})$ denoting a vector with the largest elements taken from $\mathbf{x}$ or $\mathbf{y}$.

10.4 Simulation and analysis of results

In this section, we compare the performance of the MIMO RadCom DoA estimation method with the conventional MUSIC technique. We consider an environment with a radar (vehicle 3) and two mobile targets (vehicle 1 and vehicle 2), scenario shown in Figure 10.1. We consider that only one of the targets (2) is communicating with vehicle 3 (radar). All vehicles are equipped with a RadCom system with a uniform linear arrangement of $M_T = 2$ antennas ($d_t = 2\lambda$) for transmission, and another array of $M_R = 4$ antennas for reception ($d_r = \lambda/2$).

The search range is performed over $-45°$ to $45°$ with the scanning interval equal to $0.1°$. The number of pilot subcarriers per antenna is 64 (total pilot subcarriers $NP = 128$). For the correlation matrix of the conventional technique, all subcarriers were considered; for the proposed method, only pilots were considered in order to compensate the additional computational complexity in the calculation of two matrices (R_{radar} and R_{com}). The power of all received signals is equal. The number of pilots used was 128 (spaced equally across the 1024 subcarriers) in each OFDM symbol. Further details about the parameters used in the simulations can be seen in Table 4.1 [4].

Simulations were done with two targets (vehicle 1 and vehicle 2) in the presence of AWGN. Note that in this chapter we suppose that the number of signals K is already known. The performance is measured as the RMSE, defined as:

$$RMSE = \frac{1}{K}\sum_{k=1}^{K}\sqrt{\frac{1}{L}\sum_{l=1}^{L}[(\hat{\theta}_{k,l} - \theta_{k,l})^2]}, \tag{10.3}$$

where $\hat{\theta}_{k,l}$ is an estimate of the angle, $\theta_{k,l}$ is the correct value and L=10000 is the number of Monte Carlo simulations performed. In the simulations, the angles are random. The velocity and position of vehicle 1 are v_1 and r_1 and of vehicle 2 are v_2 and r_2 respectively.

For RMSE evaluation, we considered three different scenarios. In the first scenario, the signals are uncorrelated (r_1 =1 m, r_2 =6m, v_1 =2 m/s and v_2 =5 m/s). In the second scenario, the signals are partially correlated with a correlation factor of 0.8 (R_1 =1 m, R_2 =1.55m, v_1 =2 m/s and v_2 =2 m/s). In the third scenario, the signals are fully correlated, i.e., coherent (r_1 =1 m, r_2 =1, v_1 =2 m/s and v_2 =2 m/s). In the first and second scenarios the targets have a DoA difference that varies randomly from 2° to 12°, and in the third scenario the targets have a DoA difference that varies randomly from 5° to 20°.

In Figure 10.2, the RMSE of the DoA versus input SNR is shown. Figure 10.2 demonstrates that the performance of the conventional MUSIC method is compromised. The DoA estimation of the proposed method for uncorrelated, partially correlated, and coherent signals is more accurate than that of the method, especially at low SNRs. Figure 10.3 shows the probability of correct detection of the number of targets versus SNR. This figure demonstrates that the performance of the proposed method is much higher than that of the conventional method, even at low SNRs and with correlated signals.

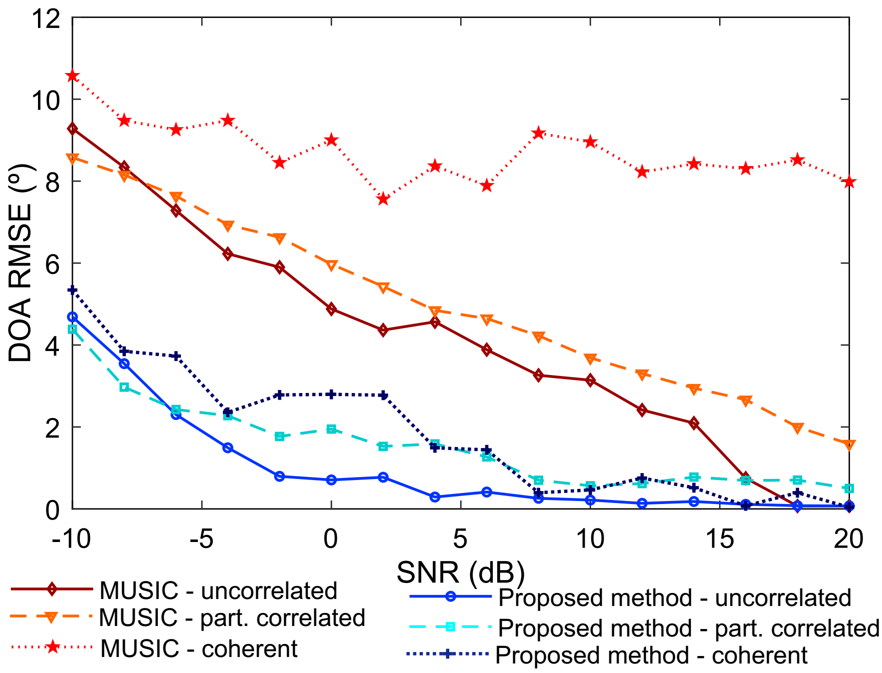

Figure 10.2: RMSE for the estimation of two target versus SNR for uncorrelated, partially correlated, and coherent signals.

The reason why the method proposed more accurately distinguishes targets is the use of an additional source of information: the communication signal from one of the targets. Due to its nature, this new source of information is not correlated to the other targets even if they have exactly the same range and velocity. With the application of the proposed method, noise interference and signal correlation can be minimized in DoA estimation.

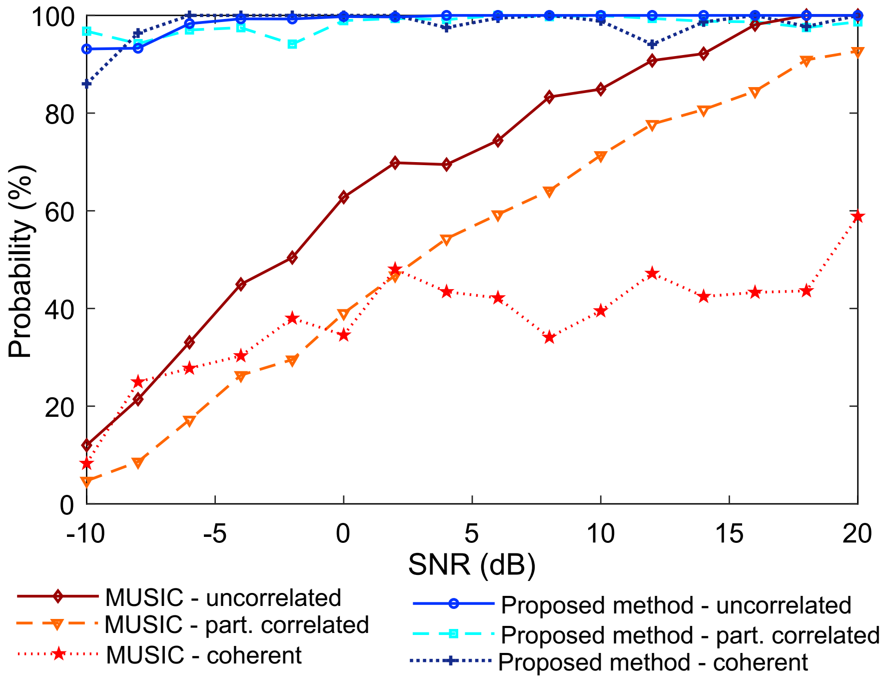

Figure 10.3: Detection probability versus SNR for uncorrelated, partially correlated, and coherent signals.

For a better visualization of the performance of the method, Figure 10.4 compares the results of DoA spectrum estimation for two targets with coherent signals (r_1 =1 m, r_2 =1, v_1 =2 m/s and v_2 =2 m/s). In this simulation, the SNR is 5 dB and the angles of the two targets are 0° and 10° in Figure 10.4(a) and 5° and 8° in Figure 10.4(b). It can be seen that the peaks are detected in the correct DoAs for the proposed technique (−0.3° and 10.3° for the scenario of Figure 10.4(a) and 7.5° and 5.8° for the Figure 10.4(b). In the conventional algorithm only a single estimation peak is present, and the two targets cannot be distinguished.

10.5 Summary

This chapter presents a novel method for DoA estimation in MIMO RadCom systems that integrates the use of the radar signal together with incoming communication signals. Simulations showed that the DoA estimation performance for multiple targets of the method present in this chapter is much superior to that of the conventional MUSIC technique, achieving a better RMSE and a much greater ability to distinguish closely spaced targets. The method also proved to be much

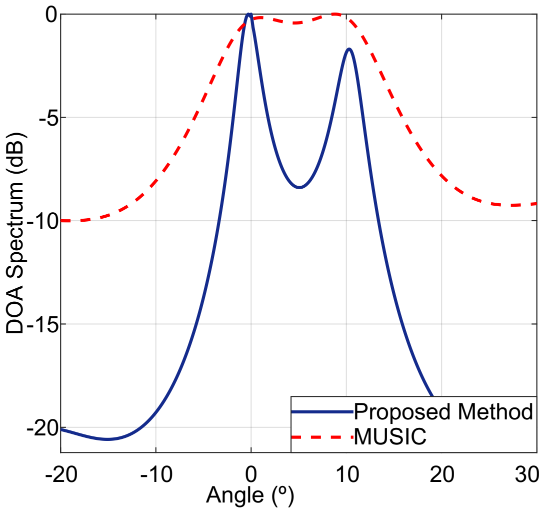

(a)

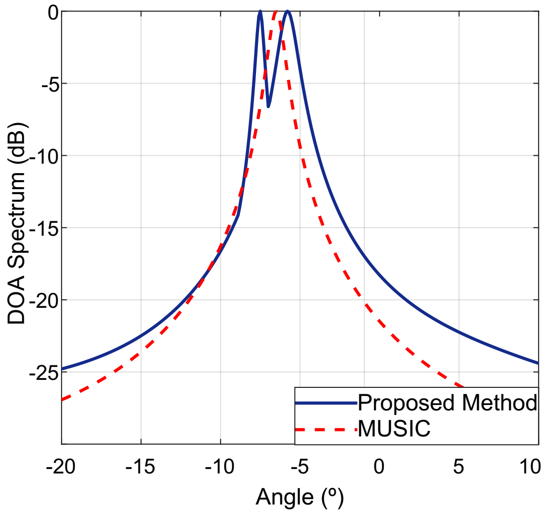

(b)

Figure 10.4: DoA spectra for two targets with coherent signals.

superior for the estimation of coherent signals, with an even higher performance gain for low SNR, even though it had a lesser number of snapshots than the conventional MUSIC technique. In conclusion, the method that is described in this chapter can be applicable to complex DoA detection scenarios with a large number of targets where uncorrelated, partially correlated and coherent signals are mixed.

CHAPTER 11

High-Resolution Delay-Doppler Estimation Using Communication Signal

High-resolution delay-Doppler estimation is an important requirement for automotive radar systems, especially in multi-target scenarios that require better target separation performance. Exploring the dual functionality enabled by OFDM in RadCom system, this chapter presents a new cooperative method for high-resolution delay-Doppler estimation. The new subspace-based method exploits the combination of both the radar and received communication signals to estimate target parameters. The procedure achieves high-resolution delay-Doppler estimation for both uncorrelated, partially correlated and coherent signals, and enables a significant reduction in the required bandwidth when compared to previous approaches which did not exploit the knowledge of the communication signals. In Section 11.2, we establish a system model for the processing of the OFDM radar and the problem formulation for OFDM radar is described. In Section 11.3, the method for radar processing using the communication signals transmitted by the targets is presented. In Section 11.4, we present the formulation of the technique fo 2D delay-doppler estimation. After this, in Section 11.5, the measurements setup and the radar measurements are presented. In Section 11.6, the performance evaluation of our method in simulation scenario is presented. Finally, in Section 11.7, we present the summary.

11.1 Introduction

The most commonly used radar processing technique for OFDM-based RadCom systems is described in [20]. In this technique, a demodulation stage that eliminates the communication data of the received signal is followed by two DFT to perform range and velocity estimation. However, this estimation has low resolution and requires wide signal bandwidths to achieve high resolution, which may be not available in most practical scenarios. High-resolution subspace-based methods for the joint estimation of target range and DoA using OFDM radar are proposed in [72, 136, 137], however these do not perform high-resolution velocity estimation. In [128] a high-resolution method for velocity and range estimation based on MUSIC and CS is proposed, but it fails to work in situations where multiple targets reflect coherent or highly correlated signals. A compressed sensing-based algorithm that exploits the sparsity of the multipath signal components is proposed in [138], but its performance is also limited in radar estimation in the presence of coherent signals. In general, the performance of subspace-based methods is severely degraded when coherent or highly correlated signals are present. For this reason, several alternatives have been proposed to solve the estimation problems in the presence of coherent or highly correlated signals [139–143], with different levels of success.

The definition of signal coherence addressed in the chapter is related to the range and velocity dimensions and is linked to the radar resolution. The signals stemming from the two or more targets are said to be coherent if the targets have the same velocity (range), and their range (velocity) relatively to the radar is less than the radar resolution. The highly correlated signals in this chapter are defined as signals from targets with velocity and range relative to the radar, less than the resolution.

This chapter presents a high-resolution method for simultaneously estimating the range and velocity of multiple targets in RadCom OFDM systems, even in the presence of coherent signals. The method presents a new approach to radar estimation: the combined use of the radar signal and received communications signals to estimate target parameters. The major contributions of this method is takes advantage of OFDM radar technology to include communication functions in the radar system and enable the combined passive- and active-radar for high-resolution estimation of targets. In situations where it would not be possible to distinguish two targets (e.g., if their differences in range and velocity are lower than the radar resolution), the communication signal transmitted by one of these targets is processed in conjunction with the received radar signals reflected by the targets, allowing the two targets to be distinguished.

In this chapter the problem of estimating coherent or highly correlated targets is exposed, then the method is formulated showing how it allows high resolution estimation of the range and velocity of multiple targets, even in the presence of signal coherency. The method estimates simultaneously the range and velocity of the target with high resolution in a single radar frame. The increase in resolution obtained by our method contributes to a significant reduction in the bandwidth required for the radar system, presenting only the cost of an additional stage in the processing of the received signal in the radar.

The method present in this chapter exploits the combination of both the radar and received communication signals to estimate target parameters. The radar channel transfer matrix and communication channel transfer matrix are combined using the covariance differencing technique [134]. Then, the delay-Doppler estimation is performed using the 2D MUSIC algorithm. In this we demonstrate by simulation with experimental validation at 24 GHz that the method performs well at low SNR even in the presence of coherent signals.

11.2 System model

In this chapter we consider a RadCom system in which the information to be transmitted is encoded by a digital complex-modulation technique, e.g., QAM. The encoded data is transmitted by the RadCom system using OFDM modulation. The transmitted signal is then reflected by the targets and received back by the same RadCom system. Since this is a RadCom system, the same signal is used to perform both radar and communication functions simultaneously. The system

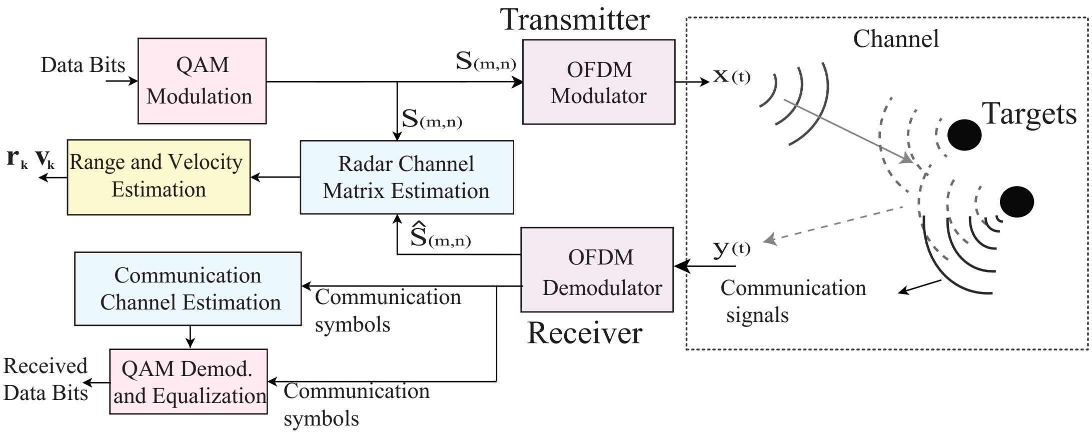

Figure 11.1: Simplified block representation of the RadCom system structure.

also receives communication signals from other devices (e.g., other vehicles).

The RadCom system receive two types of signals: (1) the OFDM radar signal transmitted by itself and reflected by the targets, and (2) the communication signals transmited by some targets which have transmission capabilities. As far as radar functionality is concerned—i.e., when the RadCom system transmits a signal and this same signal reflects on the targets and returns back to the RadCom system—, the received data sequence is known in advance because it was originally transmitted by the RadCom system itself. For the communication functionality of the RadCom system—i.e., when the RadCom system receives a communication signal that was transmitted (not reflected) by the targets (e.g., another RadCom-equipped vehicle)—, the pilot sequences of other transmitting devices are known. A block diagram depicting the operation of a RadCom system is shown in Figure 11.1. An example scenario with vehicles equipped with and without RadCom systems is depicted in Figure 11.2. Vehicles equipped with RadCom systems transmit their RadCom signals and receives their RadCom signals reflected by the targets, and also communication signals transmitted by other devices. We assume that all noise sources in this scenario are uncorrelated between themselves and with the received signals.

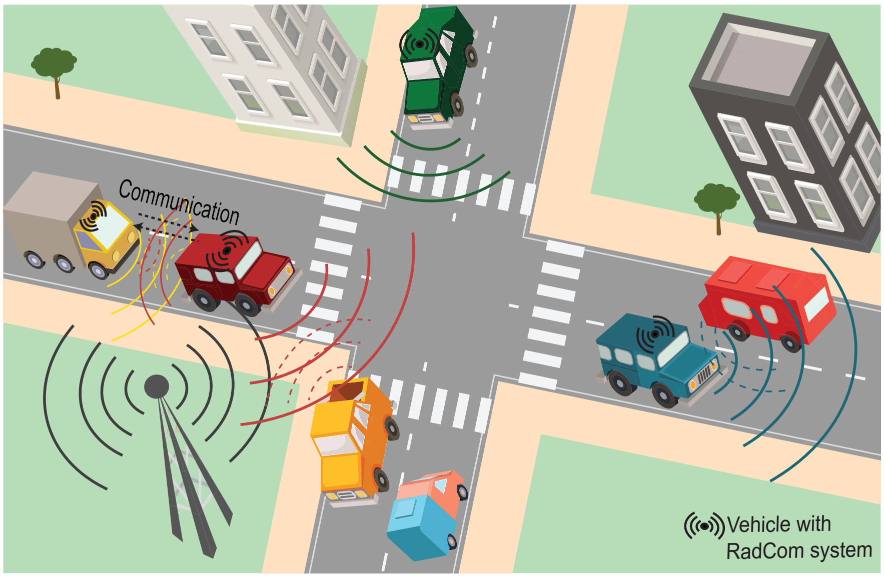

Figure 11.2: Example scenario with vehicles equipped with and without RadCom systems (reflected/transmitted wave - dashed/undashed curve).

11.2.1 Signal model

In order to obtain a simple representation the channel matrix $\mathbf{D}$ presented in the chapter 3, we have defined the vectors $\mathbf{b}_{f_{D,k}}$ and $\mathbf{a}_{\tau_k}$ as below

$$\mathbf{a}_{\tau_k} = [1, e^{-j2\pi\Delta f\tau_k}, ..., e^{-j2\pi(N-1)\Delta f\tau_k}]^T \tag{11.1}$$
$$\mathbf{b}_{f_{D,k}} = [1, e^{j2\pi T f_{D,k}}, ..., e^{j2\pi T f_{D,k}(M-1)}]^T, \tag{11.2}$$

and defined also the matrices $\mathbf{A} = [\mathbf{a}_{\tau_1}, ..., \mathbf{a}_{\tau_K}]^T$, $\mathbf{B} = [\mathbf{b}_{f_{D,1}}, ..., \mathbf{b}_{f_{D,K}}]$ and $\mathbf{G} = \text{diag}(g_1, ..., g_K)$. The new matrix $\mathbf{D_r}$ can be rewritten in the form:

$$\mathbf{D_r} = \sum_{k=1}^{K} g_k \mathbf{b}_{f_{D,k}} \mathbf{a}_{\tau_k}^T + \mathfrak{N} = \mathbf{BGA} + \mathfrak{N}, \tag{11.3}$$

where the matrix $\mathfrak{N}$ is the $M \times N$ noise matrix. The communication signals are received by the RadCom system at a different carrier frequency than the transmitted RadCom signal, and are thus processed separately from the radar signal using standard communication signal processing techniques. Other duplexing schemes may be considered in the system, such as frequency-division multiplexing and time-division multiplexing.

11.2.2 Estimation methods

2D-DFT method

From matrix $\mathbf{D_r}$ the range and velocity of each target may be estimated. The most commonly used technique for the range and velocity estimation is based on a 2D-DFT, presented in the chapter 3, where a DFT of size M is applied to each row and an IDFT of size N is applied to each column of $\mathbf{D_r}$, resulting in a matrix $\mathbf{Z} = \text{IDFT}[\text{DFT}[\mathbf{D_r}]]$ containing the range and velocity estimates [20]. These estimates have the following limitations: a range resolution limit of $\Delta r = \frac{c}{2B_W}$, a velocity resolution of $\Delta v = \frac{c}{2Mf_cT}$, a maximum unambiguous velocity of $V_{max} = \frac{c}{2f_cT}$, and a maximum measurement distance of $R_{max} = \frac{c}{2\Delta f}$ [58]. $B_W = N\Delta f$ is the bandwidth of the signal. In [20, 58, 130, 144–146] it is possible to see examples of OFDM radar implementation based on this estimation method.

Subspace-based methods

Subspace-based methods are high-resolution estimation methods. These techniques are commonly used for DoA estimation in radar systems, but can also be extended for velocity and range estimation [128, 138, 147–150]. Subspace-based methods use the spatial correlation (or covariance) matrix of the signal. The covariance matrix $\mathbf{R}$ can be decomposed as

$$\mathbf{R} = \mathbf{U}_s\mathbf{\Lambda}_s\mathbf{U}_s^H + \mathbf{U}_n\mathbf{\Lambda}_n\mathbf{U}_n^H$$

where $\mathbf{U}_s$ represents the signal subspace consisting of the K eigenvectors related to largest K eigenvalues of $\mathbf{R}$ and $\mathbf{U}_n$ represents the noise subspace with the remaining eigenvectors. $\mathbf{\Lambda}_s$ and $\mathbf{\Lambda}_n$ are diagonal matrices containing the corresponding eigenvalues.

The parameter estimation is performed by a search procedure defined by maximum values in the spectrum. The spectrum is calculated using the subspaces of the correlation matrix. MUSIC [135], ESPRIT [151] and Min-Norm [152] are some examples of subspace-based methods. The most popular subspace-based method is the MUSIC algorithm. Its attractiveness is due to providing good resolution with a single-dimensional search for each parameter to be estimated, which greatly reduces computational complexity when compared, for example, with maximum likelihood techniques, which use a K-dimensional estimate for the

K sources [153].

11.2.3 Problem Formulation

The 2D-DFT technique is the most commonly used in OFDM radar for range and velocity estimation. However, with the use of the 2D-DFT technique, the range resolution limitation is directly related to the signal bandwidth, meaning that some applications require large bandwidths in order to be able to properly estimate targets. High-resolution subspace-based techniques for OFDM radar have been proposed previously [128, 138]. However, these techniques fail to correctly distinguish between targets that reflect coherent signals. For example, two targets with the same velocity and at similar distances to the radar—i.e $v_1 = v_2$ and $|r_1 - r_2| < \Delta r$—produce coherent signals from the point of view of range estimation and are difficult to distinguish even with the use of high-resolution techniques. In the spectral estimation of these targets, the spectrum estimate of each target is added, generating only a single peak instead of two. In situations with highly correlated signals—i.e targets with $(|v_1 - v_2| < \Delta v$ and $|r_1 - r_2| < \Delta r$—the estimation problem also occurs. For simplicity, we initially consider radar estimation in the range estimation problem, but the same applies to velocity estimation (for the latter, replace the matrix $\mathbf{A}$ with the matrix $\mathbf{B}$, and vice versa).

The radar covariance matrix is defined as

$$\begin{aligned}\mathbf{R_r} &= \frac{1}{M}\mathbf{D_r}^H\mathbf{D_r} = \frac{1}{M}(\mathbf{BGA})^H(\mathbf{BGA}) + \sigma_n \mathbf{I}_N \\ &= \frac{1}{M}\mathbf{A}^H\mathbf{G}^H(\mathbf{B}^H\mathbf{B})\mathbf{GA} + \sigma_n \mathbf{I}_N,\end{aligned} \tag{11.4}$$

Since $\mathbf{G}$ is a diagonal matrix, and assuming that the columns of $\mathbf{A}$ are all different and linearly independent, then $\mathbf{G}$ and $\mathbf{A}$ have full rank.

For $\mathbf{B}^H\mathbf{B}$ to be diagonal and thus have full rank it is necessary that the signals be uncorrelated. In practice this means that the difference in speed values between targets must be greater than the minimum system speed resolution. The result of $\mathbf{B}^H\mathbf{B}$ will be nondiagonal and nonsingular when the signals are partially correlated (difference in velocity values between targets approximately equal to the resolution), and nondiagonal but singular when some signals are coherent (same velocities). So the matrix $\mathbf{R_r}$ remains as nonsingular (full rank) while the sources are at most partially correlated.

Thus, if $\mathbf{B}^H\mathbf{B}$ has full rank, then $\mathbf{R_r}$ has full rank with rank K (number of targets). The signal subspace method uses a set of eigenvectors of the matrix $\mathbf{R_r}$ to estimate the steering vectors. Unfortunately, subspace estimation techniques do not estimate satisfactorily when the $\mathbf{R_r}$ matrix does not have full rank [154].

Consider, for simplicity, that of K targets only two are coherent (same velocity). This implies that $\mathbf{b}_{f_{D,2}} = \mathbf{b}_{f_{D,1}}$, with only one gain between the two coherent signals [140]. In this case, $\mathbf{G} = \mathrm{diag}(1, g_3, ...g_K)$ with size $(K-1) \times (K-1)$, and we can rewrite (11.1) and (11.2) as

$$\mathbf{A} = [g_1\mathbf{a}_{\tau_1} + g_2\mathbf{a}_{\tau_2}, \mathbf{a}_{\tau_3}, ..., \mathbf{a}_{\tau_K}]^T \tag{11.5}$$

$$\mathbf{B} = [\mathbf{b}_{f_{D,1}}, \mathbf{b}_{f_{D,3}}, \mathbf{b}_{f_{D,K}}], \tag{11.6}$$

where $\mathbf{A}$ has size $(K-1) \times N$ and $\mathbf{B}$ has size $M \times (K-1)$.

In this situation, the rank of $\mathbf{R_r}$ is $K-1$. Due to the Vandermonde structure, the first column of $\mathbf{A}$ is no longer a legitimate targeting vector, since no linear combination of two spanning vectors can generate another targeting vector [155]. Since the number of the eigenvalues largen than σ_n of $\mathbf{R_r}$ is now $K-1$, the detection step will give $K-1$ as the number of targets. In general, if K_h signals reflected by the K targets are coherent, the application of the conventional subspaces technique will result in an estimation of $K - K_h + 1$ targets.

11.3 Delay-Doppler Estimation Using Communication Signal Method

To overcome the need for a large bandwidth for a high range resolution, it is necessary to develop methods that allow the reduction of the necessary bandwidth while maintaining the required resolution. To solve this problem, we present a new high-resolution delay-Doppler estimation technique where communication signals received from the targets are used in conjunction with the received radar signals reflected by the targets, as depicted in Figure 11.3. Essentially, in one single and unified RadCom system, there are two distinct modes of radar operation: one that is of the active-radar type, and another that is, in a broad sense, of the passive-radar type. In the active-radar mode of operation, the processing is performed on the signals that are transmitted by the RadCom system, reflected by the targets, and finally received by the RadCom system itself. In the passive-radar mode of operation, the processing is performed on the communication signals that are transmitted by the targets themselves (targets equipped with communications devices), and which are directly received by the RadCom system.

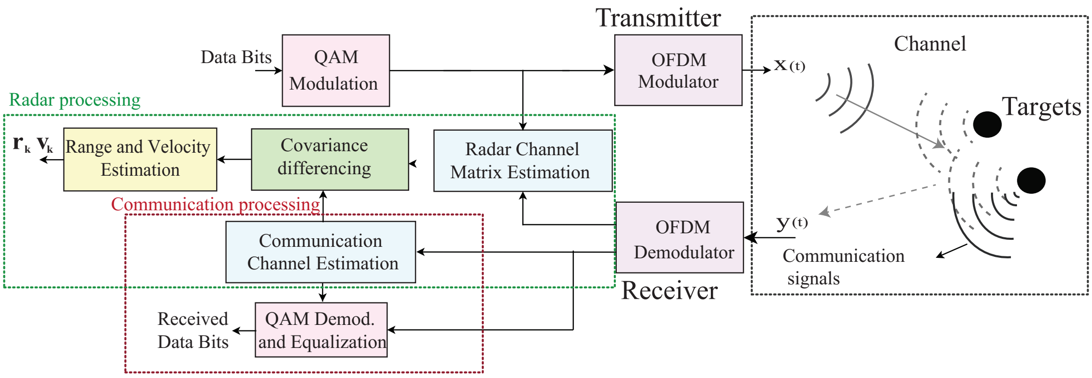

Figure 11.3: Simplified block representation of the method for RadCom system.

In the new method, covariance differencing is done between the radar covariance matrix and the communication covariance matrices. Then, the subspace-based technique MUSIC is applied. For simplicity, we will continue to consider range estimation in the radar estimation problem, however, the application of our method enables the best estimation of both parameters simultaneously. The same derivation shown here applies to the velocity estimation (to verify this, replace the matrix $\mathbf{A}$ with the matrix $\mathbf{B}$, and vice versa).

Radar covariance matrix

The matrix $\mathbf{D_r}$ is defined as

$$\mathbf{D_r} = \sum_{k=1}^{K} g_k \mathbf{b}_k \mathbf{a}_k^T + \mathfrak{N}. \tag{11.7}$$

Assume that the $\mathbf{D_r}$ matrix is composed of K_u targets with uncorrelated signals and of $K_h = K - K_u$ targets with coherent or highly correlated signals. The K_h targets are divided into Q groups of $K_{\rho,q}$ signals ($K_{\rho,q} \geq 2$ and $\sum_q K_{\rho,q} = K_h$), where $q = 1, ..., Q$.

Each group q is formed by coherent or highly correlated signals between the signals in that group. Suppose that uncorrelated signals and coherent signals in different groups are not correlated with each other. The matrix $\mathbf{D_r}$ is now given by

$$\mathbf{D_r} = \sum_{k_u=1}^{K_u} g_{k_u} \mathbf{b}_{f_{D,k_u}} \mathbf{a}_{\tau_{k_u}}^T + \sum_{q=1}^{Q} \sum_{k_\rho=1}^{K_{\rho,q}} g_{k_\rho,q} \mathbf{b}_{f_{Dk_\rho},q} \mathbf{a}_{\tau_{k_\rho},q}^T + \mathfrak{N}, \tag{11.8}$$

where the pair of indices (k_ρ, q) represents the target k_ρ present in the group q with $(k_\rho, q) \in K_h$. The covariance matrix is defined as

$$\mathbf{R_r} = \frac{1}{M} \mathbf{D_r}^H \mathbf{D_r}. \tag{11.9}$$

For simplicity, we define the vector of the amplitude of the uncorrelated radar signals as $\mathbf{g}_u = [g_1, ..., g_{K_u}]^T$ and the coherent or highly correlated radar signals in each group q as $\mathbf{g}_q = [g_{1,q}, ..., g_{K_\rho,q}]^T$. We also define the $K_u \times N$ matrix $\mathbf{A_u} = [\mathbf{a}_{\tau_1}, ..., \mathbf{a}_{\tau_{K_u}}]^T$ and the $M \times K_u$ matrix $\mathbf{B_u} = [\mathbf{b}_{f_{D,1}}, ..., \mathbf{b}_{f_{D,K_u}}]$ for the uncorrelated radar signals. For the coherent or highly correlated radar signals in each group q we define the $K_{\rho,q} \times N$ matrix $\mathbf{A}_q = [\mathbf{a}_{\tau_1,q}, ..., \mathbf{a}_{\tau_{K_\rho},q}]^T$ and the $M \times K_{\rho,q}$ matrix $\mathbf{B}_q = [\mathbf{b}_{f_{D,1},q}, ..., \mathbf{b}_{f_{D,K_\rho},q}]$. Since the estimation considered in this demonstration is only for the range, all vectors in the matrix $\mathbf{B}_q$ of the coherent or highly correlated signals will have equal or approximately equal values. We will then consider $\mathbf{b}_{f_{D,1},q} = \mathbf{b}_{f_{D,2},q} = ... = \mathbf{b}_{f_{D,K_u},q}$. The matrix $\mathbf{G_u}$ is defined as $\mathbf{G_u} = \mathrm{diag}(\mathbf{g}_u)$.

The radar channel matrix can be rewritten as

$$\mathbf{D_r} = \mathbf{B_u G_u A_u} + \sum_{q=1}^{Q} \mathbf{b}_{f_{D,1},q} \mathbf{g}_q^T \mathbf{A}_q + \mathfrak{N}. \tag{11.10}$$

The covariance matrix of the radar signal is given by

$$\mathbf{R_r} = \frac{1}{M} \mathbf{D_r}^H \mathbf{D_r} = \mathbf{R_u} + \sum_{q=1}^{Q} \mathbf{R}_q + \sigma_n \mathbf{I}_N, \tag{11.11}$$

with

$$\begin{aligned} \mathbf{R}_q &= \frac{1}{M} (\mathbf{b}_{f_{D,1},q} \mathbf{g}_q^T \mathbf{A}_q)^H (\mathbf{b}_{f_{D,1},q} \mathbf{g}_q^T \mathbf{A}_q) \\ &= \frac{\mathbf{b}_{f_{D1},q}^H \mathbf{b}_{f_{D1},q}}{M} \mathbf{A}_q^H \mathbf{g}_q^* \mathbf{g}_q^T \mathbf{A}_q, \end{aligned} \tag{11.12}$$

where $\mathbf{R_u}$ is the covariance matrix of uncorrelated radar signals and $\mathbf{R}_q$ is the covariance matrix of coherent or highly correlated radar signals in each group q.

Communication signal covariance matrix

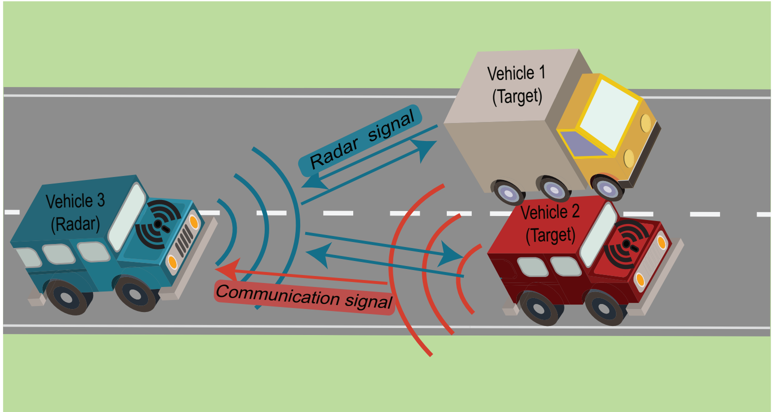

Figure 11.4: Example scenario with one group of vehicles equipped with RadCom systems. In this representation, vehicle 3 receives the radar signal reflected by the targets and the communication signal transmitted by vehicle 2.

The purpose of the use of the communication channel matrix is to enable the estimation of highly correlated or coherent targets. For this to be realized, the matrix of the communication channel of $K_{\rho,q}-1$ targets of each group q is required. Figure 11.4 shows an example of one group with two targets with correlated signals, where the communication signal of only one of the targets is used. The channel information matrix $\mathbf{D}_{k_c,q}$ of the communication signal of an arbitrary target k_c in group q is defined by

$$\begin{aligned}\mathbf{D}_{k_c,q}(m,n) &= \left(\frac{\hat{\mathbf{S}}_{\mathbf{pilot}}(m,n)}{\mathbf{S}_{\mathbf{pilot}}(m,n)}\right)^2 \\ &= \left(g^c_{k_c,q} e^{j\pi T f_{Dk_{k_c,q}} m} e^{-j2\pi n\Delta f \frac{R_{k_c,q}}{c}} + \tilde{\eta}_c\right)^2,\end{aligned} \tag{11.13}$$

where $\tilde{\eta}_c$ is AWGN with zero mean and variance σ_{n_c}, $\mathbf{S}_{\mathbf{pilot}}$ are the pilot symbols transmitted, $\hat{\mathbf{S}}_{\mathbf{pilot}}$ are the pilot symbols received, and $g^c_{k_c,q}$ is the amplitude of the communication signal transmitted by the target k_c of the group q. Note that since the signal is transmitted directly by the target, it travels half the distance of the signal sent from the radar, so to be equivalent a power of 2 is necessary. Thus, velocity and range values in this matrix are equivalent to that of the radar channel matrix. The covariance matrix is calculated as

$$\begin{aligned}\mathbf{R}_{k_c,q} &= \frac{1}{M}\mathbf{D}^{H}_{k_c,q}\mathbf{D}_{k_c,q}\\ &= \frac{1}{M}(\mathbf{b}_{f_{D1},q}g^{c}_{k_c,q}\mathbf{a}_{\tau_{k_c},q}))^{H}(\mathbf{b}_{f_{D1},q}g^{c}_{k_c,q}\mathbf{a}_{\tau_{k_c},q})) + \sigma_{n_c}\mathbf{I}_N\\ &= \frac{\mathbf{b}^{H}_{f_{D1},q}\mathbf{b}_{f_{D1},q}}{M}\mathbf{a}^{H}_{\tau_{k_c},q}g^{c}_{k_c,q}g^{c}_{k_c,q}\mathbf{a}_{\tau_{k_c},q} + \sigma_{n_c}\mathbf{I}_N.\end{aligned} \tag{11.14}$$

Note that, for the covariance matrix of the communication signal, only the subcarriers with pilots are known for the channel matrix estimation. However, there are methods of estimating the complete channel matrix. For simplicity, we consider in this mathematical demonstration the use of all subcarriers (N subcarriers) and symbols (M symbols) as pilots, so in this demonstration $\mathbf{S_{pilot}}$ has size of $M \times N$.

The vector of the amplitude of the communication signal $g^{c}_{k_c,q}$ with size $K_{\rho,q} \times 1$ of each group q for arbitrary targets k_c is defined as

$$\mathbf{g^c}_{k_c,q}(i) = \begin{cases} g^{c}_{k_c,q}, & \text{for } i = k_c\\ 0, & \text{others,}\end{cases} \tag{11.15}$$

with $k_\rho = 1, ...K_{\rho,q}$. The covariance matrix of all received communication signals in group q is given by

$$\mathbf{R^c}_q = \sum_{k_c=1}^{K_{\rho,q}-1}\mathbf{R}_{k_c,q}, \tag{11.16}$$

Then, using $\mathbf{G^c}_q = [\mathbf{g^c}_{1,q}, ..., \mathbf{g^c}_{K_\rho-1,q}]^T$, $\mathbf{R^c}_q$ can be rewritten as

$$\mathbf{R^c}_q = \frac{\mathbf{b}^{H}_{f_{D1},q}\mathbf{b}_{f_{D1},q}}{M}\mathbf{A}^{H}_{q}\mathbf{G^c}^{H}_{q}\mathbf{G^c}_q\mathbf{A}_q + \sum_{k_c=1}^{K_{\rho,q}-1}\sigma_{n_c}\mathbf{I}_N. \tag{11.17}$$

Constructed differencing matrix

Since the matrix $\mathbf{R_u}$ is composed only of uncorrelated signals, it is guaranteed to have rank K_u, making possible the estimation of all K_u targets. However, the matrices $\mathbf{R}_q$ do not have full rank because the signals are highly correlated or coherent, and from this it follows that the matrix $\mathbf{R_r}$ does not have full rank either. To transform $\mathbf{R_r}$ into a full-rank matrix, the differencing of $\mathbf{R_r}$ with the covariance matrices $\mathbf{R^c}_q$ of all communication signals in each group q is performed, obtaining the full-rank matrix for each group q, as will be demonstrated below. This finally results in the new full-rank matrix $\mathbf{R}_{\mathbf{RadCom}}$ defined as

$$\mathbf{R}_{\mathbf{RadCom}} = \mathbf{R}_{\mathbf{r}} - \sum_{q=1}^{Q} \mathbf{R^c}_q. \tag{11.18}$$

For the demonstration of how to obtain full rank in $\mathbf{R}_{\mathbf{RadCom}}$, the noise covariance matrix is disregarded. In this method, each matrix $\mathbf{R}_q$ is differenced by each $\mathbf{R^c}_q$ matrix, obtaining the full-rank matrix for each group q with rank $K_{\rho,q}$ as

$$\begin{aligned}
&\mathbf{R}_q - \mathbf{R^c}_q = \\
&\frac{\mathbf{b}_{f_{D1},q}^H \mathbf{b}_{f_{D1},q}}{M} \mathbf{A}_q^H \mathbf{g}_q^* \mathbf{g}_q^T \mathbf{A}_q - \frac{\mathbf{b}_{f_{D1},q}^H \mathbf{b}_{f_{D1},q}}{M} \mathbf{A}_q^H \mathbf{G^c}_q^H \mathbf{G^c}_q \mathbf{A}_q \\
&= \frac{\mathbf{b}_{f_{D1},q}^H \mathbf{b}_{f_{D1},q}}{M} \mathbf{A}_q^H (\mathbf{g}_q^* \mathbf{g}_q^T - \mathbf{G^c}_q^H \mathbf{G^c}_q) \mathbf{A}_q \\
&= \frac{\mathbf{b}_{f_{D1},q}^H \mathbf{b}_{f_{D1},q}}{M} \mathbf{A}_q^H [\mathbf{g}_q^* \mathbf{G^c}_q^H] \begin{bmatrix} 1 & 0 \\ 0 & -\mathbf{I}_{K_{\rho,q}-1} \end{bmatrix} [\mathbf{g}_q^T \mathbf{G^c}_q] \mathbf{A}_q.
\end{aligned} \tag{11.19}$$

Thus, $\mathbf{R}_{\mathbf{RadCom}}$ is given by

$$\begin{aligned}
\mathbf{R}_{\mathbf{radcom}} &= \mathbf{A_u}^H \mathbf{G_u} (\mathbf{B_u}^H \mathbf{B_u}) \mathbf{G_u} \mathbf{A_u} \\
&+ \sum_{q=1}^{Q} \frac{\mathbf{b}_{f_{D1},q}^H \mathbf{b}_{f_{D1},q}}{M} \mathbf{A}_q^H [\mathbf{g}_q^* \mathbf{G^c}_q^H] \begin{bmatrix} 1 & 0 \\ 0 & -\mathbf{I}_{K_{\rho,q}-1} \end{bmatrix} [\mathbf{g}_q^T \mathbf{G^c}_q] \mathbf{A}_q.
\end{aligned} \tag{11.20}$$

The prior knowledge of the number of Q groups and the number of targets pertaining to each q group was placed only for mathematical demonstration. In a realistic application, prior knowledge of these factors is not necessary. In the method, communication with a target would be performed during a tracking process or a continuous target estimation procedure—whenever a target approaches one or more targets, the communication process would start with the required number of targets. At most, it would be necessary to know the number of targets that were nearby. In any case, all communication signals can be used constantly to improve estimates in general.

11.4 2D-MUSIC delay-doppler estimation

In order to avoid the need for multiple snapshots for the estimation of range and velocity, the covariance matrix is calculated using a single snapshot (OFDM frame) by a spatial smoothing technique [138]. Consider the $N \times M$ channel transformation matrix $\mathbf{D_r}$ of a single OFDM frame. The data in this matrix are rearranged into sub-matrices $\overline{\mathbf{D}}_{\mathbf{r}_{\mathbf{p_n},\mathbf{p_m}}}$ of size $N_s \times M_s$ [128], where each submatrix is formed by samples decimated at intervals of ln and lm for the columns and rows of the matrix $\mathbf{D_r}$ respectively. A total of $P_n P_m$ submatrices are formed for all possible positions of $\mathbf{D_r}$, where $P_n = N - (N_s - 1)ln$, $P_m = M - (M_s - 1)lm$, $p_n = 1, ..., P_n$ and $p_m = 1, ..., P_m$. The decimation intervals of the elements in the matrix are $ln = M/M_s$ and $lm = N/N_s$. We also consider the vectors

$$\begin{aligned}\bar{\mathbf{a}}_{\tau_k} =& [1, e^{-j2\pi(ln+1)\Delta f \tau_k}, \\ & e^{-j2\pi(2*ln+1)\Delta f \tau_k}, ..., e^{-j2\pi((N_s-1)*ln+1)\Delta f \tau_k}]^T \ ,\end{aligned} \tag{11.21}$$

$$\begin{aligned}\bar{\mathbf{b}}_{f_{D,k}} =& [1, e^{j2\pi T f_{D,k}(lm+1)}, \\ & e^{j2\pi T f_{D,k}(2*lm+1)}, ..., e^{j2\pi T f_{D,k}((M_s-1)*lm+1)}]^T,\end{aligned} \tag{11.22}$$

and the two rotation factors $\mathcal{A}(k) = e^{-j2\pi\Delta f \tau_k}$ and $\mathcal{B}(k) = e^{j2\pi f_{D,k} T}$. The submatrices $\overline{\mathbf{D}}_{\mathbf{r}_{p_n,p_m}}$ are defined as

$$\overline{\mathbf{D}}_{\mathbf{r}_{p_n,p_m}} = \sum_{k=1}^{K} \mathcal{A}(k)^{p_n} \mathcal{B}(k)^{p_m} \bar{\mathbf{b}}_{f_{D,k}} \bar{\mathbf{a}}_{\tau_k}^T + \mathfrak{N}_{p_n,p_m}. \tag{11.23}$$

These submatrices are vectorized, and then the covariance matrix for each of these vectors is computed, $\overline{\mathbf{R}}_{\mathbf{r}_{p_n,p_m}}$. The two-dimensional radar covariance matrix ${}^{2D}\mathbf{R_r}$ is obtained through a weighted average of these covariances, given by

$${}^{2D}\mathbf{R_r} = \frac{1}{P_n P_m} \sum_{p_n=1}^{P_n} \sum_{p_m=1}^{P_m} \overline{\mathbf{R}}_{\mathbf{r}_{p_n,p_m}}. \tag{11.24}$$

The same procedure is applied to the covariance matrix of the received communication signals $\mathbf{R^c}_q$, thus obtaining a 2D $\mathbf{R_{RadCom}}$ matrix ${}^{2D}\mathbf{R_{RadCom}}$. The conventional MUSIC algorithm [135] is then applied to ${}^{2D}\mathbf{R}_{\mathbf{RadCom}}$ as

$$\mathbf{P}_{\tau,\mathbf{f_D}} = \frac{1}{(\bar{\mathbf{a}}_\tau \otimes \bar{\mathbf{b}}_{f_D})^H \mathbf{U}_n {\mathbf{U}_n}^H (\bar{\mathbf{a}}_\tau \otimes \bar{\mathbf{b}}_{f_D})}, \tag{11.25}$$

where $\otimes$ represents the Kronecker product and $\mathbf{U}_n$ represents the noise subspace with $N_s M_s \times N_s M_s - K$ eigenvectors of ${}^{2D}\mathbf{R}_{\mathbf{RadCom}}$. The estimation of the range and velocity is done by detecting the peaks in the spectrum $\mathbf{P}_{\tau,\mathbf{f_D}}$.

11.5 Radar measurements

In this section, we evaluate the performance of our method under coherent signals through laboratory measurements of a 24 GHz RadCom system. In Section VII we present further results obtained through simulation environments including multiple targets with uncorrelated, highly correlated, and coherent signals.

The OFDM radar was implemented with Modulation 4-QAM and the parameters are presented in Table 4.3. The range and velocity resolution is 1.33 m and 2.4 m/s respectively, the unambiguous range is 1358 m and unambiguous velocity is 306 m/s for OFDM standard radar, and 169 m and 306 m/s for our method radar. This decrease in unambiguous range is due to the low number of pilots used in the communication system; we note, however, that it can be increased through the estimation of the complete transformation matrix using channel estimation techniques. For the correlation matrix, only pilots (both radar and communications signals) were considered. The other symbols were ignored when estimating the channel matrix, for both signals, radar and received communication signal. The number of pilots used was 128 (spaced equally across the 1024 subcarriers) in each OFDM symbol. Note that in this chapter we assume that the number of the targets K is already known. The parameters of our method are N_s=12, M_s=12, ln=8 and lm=14. The radar system is considered operating at the carrier frequency $f_c = 24$ GHz and the target with communication capabilities operated at 24.157 GHz.

11.5.1 Measurement setup

The measurement setup and scenario for the 24 GHz RadCom system is illustrated in Figure 11.5 and pictured in Figure 11.6. The scenario included a RadCom system employing its radar functionalities to estimate two targets, one of which

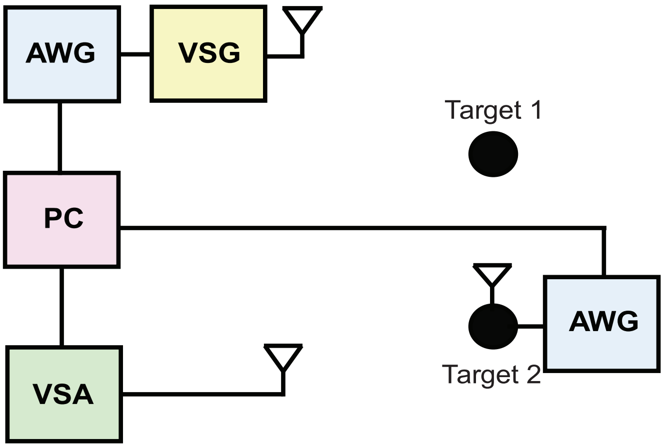

Figure 11.5: Diagram of the measurement setup.

was equipped with a transmitting antenna to simulate another RadCom system employing its communication functionalities. The radar transmits and receives its own signal and receives also the communication signal transmitted by the target equipped with another antenna.

The radar front-end consisted of an Ocean Microwave OLB-28-10 horn antenna for the transmission and an A-Info LB-180400-KF horn antenna for the reception; the communicating target was equipped with an A-Info LB-180400-KF antenna to transmit its communication signal.

The transmissions of the two systems (the radar and the communicating target) were simultaneous. Signals were generated randomly with a 4-QAM constellation. The data transmitted by the radar had a bandwidth of 113.92 MHz and was synthesized in the baseband, at a sample rate of 911.36 MSa/s, using a Keysight M8190A AWG. The AWG outputs the in-phase (I) and quadrature (Q) components of the waveform in a differential-pair configuration ($I/\bar{I}$ and $Q/\bar{Q}$). The baseband waveform was then converted to the 24 GHz band using a Keysight E8267D PSG VSG. The signal at the output of the VSG had an average power of 2 dBm and was fed to the transmitting antenna.

The signal transmitted by the antenna on the target also had a bandwidth of 113.92 MHz and was synthesized at 24.157 GHz with a sample rate of 61.97 GSa/s, using a Keysight M8195A aAWG. The AWG output had an average power of 0 dBm and was fed to the transmitting antenna.

Both signals were received by the radar antenna, and were measured using a Keysight N9041B UXA VSA. For greater accuracy of measurement, the 10 MHz oscillator of the VSA was used as a reference to synchronize the clocks of all h] 

Figure 11.6: Photograph of the scenario with measurement setup and two targets, where the target 2 was equipped with an antenna transmitter.

instruments (the two AWGs, the VSG, and the VSA), and a baseband trigger signal was provided by the M8190A AWG to the VSA and to M8195A AWG.

The AWG was connected via USB to a personal computer (PC) and the other instruments were connected through a local area network to the same computer. All instruments were controlled via Matlab, where all signals were generated and processed.

The measurement scenario is shown in Figure 11.6. In the scenario we have two steel sheet targets with 50×50 cm dimensions, at a distance of 2 m (target 1) and 1.3 m (target 2) from the radar. Only static targets were considered in these scenarios because no moving targets were available.

The two AWGs were synchronized and the total group delay of the radar hardware (instruments, cables, antennas) was measured; this delay was then calibrated out during radar processing.

11.5.2 Measurements

All measurements were done according to the modulation parameters presented in Table 4.3. Figure 11.7 shows the resulting radar images for the scenario in Figure 11.6 for 2 targets at a distance of 2 m and 1.3 m respectively. Figure 11.7(a) refers to the conventional 2D-DFT technique, Figure 11.7(b) refers to the 2D-

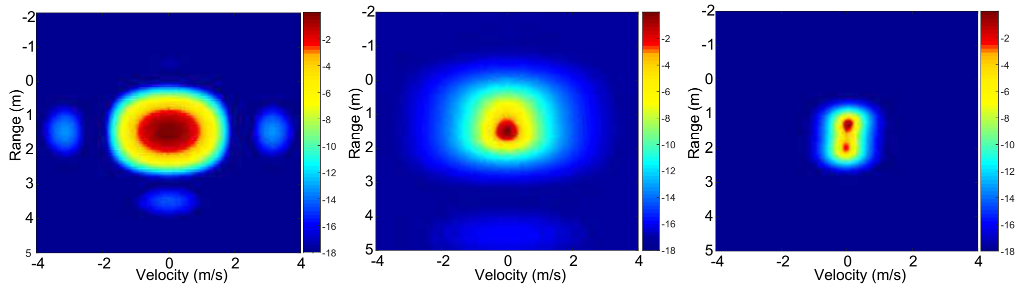

(a) (b) (c)

Figure 11.7: Radar image for (a) 2D-DFT technique, (b) the 2D-MUSIC technique (without the communication signal) and (c) proposed method (2D-MUSIC using the communication signal).

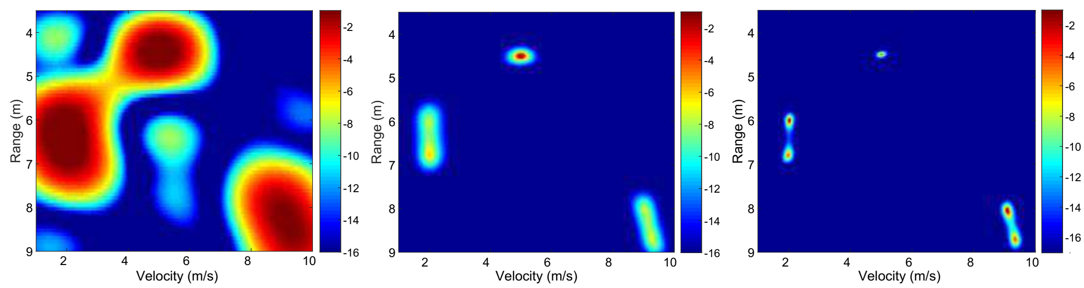

(a) (b) (c)

Figure 11.8: Radar image for (a) 2D-DFT technique, (b) the 2D-MUSIC technique (without the communication signal) and (c) proposed method (2D-MUSIC using the communication signal).

MUSIC estimation without the communication signal [128], and Figure 11.7(c) refers to our method where covariance differencing of the communication signal transmitted by one of the targets is followed by 2D-MUSIC.

In Figure 11.7 it is evident that only our method was able to detect and distinguish two targets. The 2D-DFT and 2D-MUSIC method without the communication signal failed to detect the two targets: only a single estimation peak is present. The 2D-DFT method estimated a range of 1.44 m and the 2D-MUSIC method without the communication signal estimated a range of 1.51 m. Our method yielded two range estimates, 1.97 m and 1.28 m, which were very close to the distances between the radar and the targets (2 m and 1.3 m). From Figure 11.7 we verify that our method was the only one able to estimate the position of both targets. Since our estimation method was able to distinguish the two targets despite them having a difference in range smaller than the range resolution of the conventional 2D-DFT method, our method can be classified as a high-resolution method.

11.6 Performance evaluation

In this section, we compare the performance of our method under various simulation environments with the parameters in Table 4.3. First, we consider an environment with five targets with different velocities and ranges, where the targets reflect uncorrelated, highly correlated, and coherent signals. Then, we consider a environment with two targets with equal velocities and random ranges to evaluate the RMSE and the probability of detection of the targets. As in the previous section, here we also only consider the equally spaced 128 pilot subcarriers out of the total 1024 subcarriers for both radar and communication signals. The parameters of our method are $N_s = 12$, $M_s = 12$, $ln = 8$ and $lm = 14$. The radar system has a carrier frequency $f_c = 24$ GHz and the other targets have a carrier frequency of $f_c + k * (100\text{MHz} + B/2)$. The RMSE is defined as:

$$\text{RMSE} = \frac{1}{K}\sum_{k=1}^{K}\sqrt{\frac{1}{L}\sum_{l=1}^{L}[(\hat{r}_{k,l} - r_{k,l})^2]}, \tag{11.26}$$

where $\hat{r}_{k,l}$ is an estimate of the range, $r_{k,l}$ is the correct value and $L = 6000$ is the number of Monte Carlo simulations performed. Note that to avoid discrepancies in estimated error values for high range values, in situations where only one target is detected in place of two, the estimated value is used in the error calculation for the two targets.

In the first scenario, five targets were considered with velocities of $v_1 = 2$ m/s, $v_2 = 2$ m/s, $v_3 = 9$ m/s $v_4 = 9.3$ m/s $v_5 = 5$ m/s, ranges of $r_1 = 6$ m, $r_2 = 6.8$ m, $r_3 = 8$ m, $r_4 = 8.7$ m and $r_5 = 4.5$ m. The power of all received signals was equal. The targets were divided into two groups of correlated signals and one single target with an uncorrelated signal. The first group was composed of two coherent signals (target 1 and 2) and the other group was composed of two highly correlated signals (target 3 and 4). The two groups and the fifth target (target 5) present in the scenario were uncorrelated with each other. The communication signals transmitted by targets 1 and 3 were received by the radar system. The simulation was performed in the presence of AWGN at an SNR of 0 dB.

The results of the estimation of the five targets are presented in Figure 11.8.

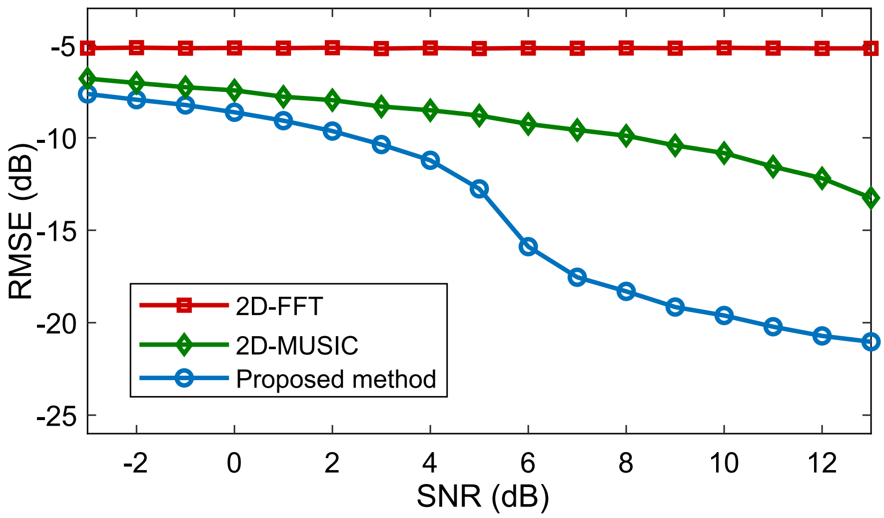

Figure 11.9: RMSE of the range estimation of two targets versus SNR.

Based on the results shown in this figure, it is possible to verify that our method can detect and correctly distinguish the five targets, and the 2D-DFT method detects only 3 targets, not being able to distinguish the targets with correlated signals. While the 2D-MUSIC method does present a better target-estimation resolution than the 2D-DFT method, Figure 11.8(b) demonstrates that it is still not enough for the distinction of the coherent and highly-correlated targets. Our method is, thus, the only method capable of accurately estimating and distinguishing all five targets. With the results presented in Figure 11.8, we see that our method operates well in environments that include multiple targets with uncorrelated, highly correlated, and coherent signals.

In the second scenario, for RMSE evaluation, we considered two targets with coherent signals, equal velocities, and random ranges that differed from 0.5m up to Δr (1.32 m). The range and velocities of the two targets were also randomized from 0 m to 100 m and 0 m/s to 100 m/s respectively. The communication signal from one of the targets was received by the radar. The simulation was performed under the presence of AWGN.

Figure11.9 shows the resulting RMSE of the range estimation as a function of SNR for 2D-DFT, 2D-MUSIC (without the communication signal) and our method. Figure 11.9 demonstrates that the performance of the conventional 2D-DFT method is compromised in the presence of coherent signals regardless of SNR. The 2D-MUSIC method failed to correctly detect and distinguish the targets at low SNRs. Moreover, our method has greater accuracy even at low SNRs. The 2D-DFT method also presents no performance gain with the increase

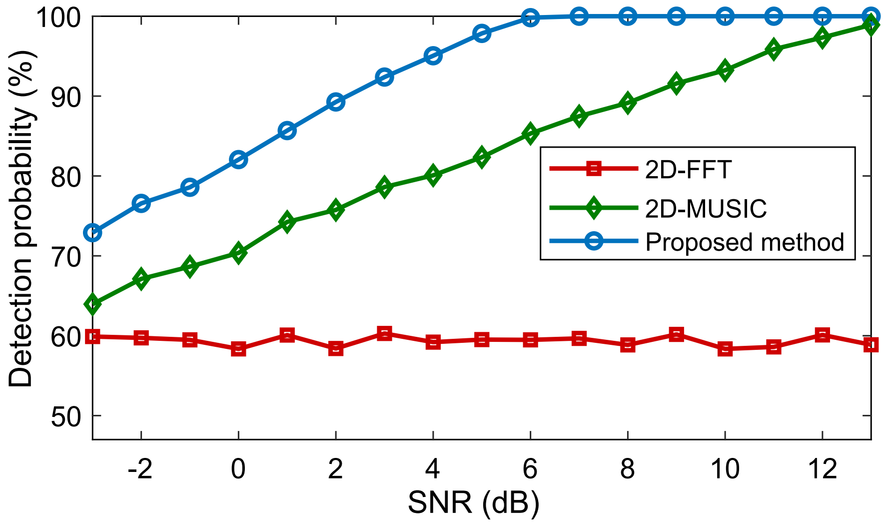

Figure 11.10: Probability of detection of all targets versus SNR.

of the SNR, which was already expected, since the limitation in this method is the range resolution (proportional to the signal bandwidth). Since two targets are separated by a distance smaller than the radar resolution, the 2D-DFT method cannot estimate them correctly.

Figure 11.10 shows that the probability of detection and correct distinction of all targets achieved by our method is much higher than that of the conventional 2D-DFT method regardless of SNR.

The reason why the method is able to distinguish targets more accurately is the use of an additional source of information: the communication signal from one of the targets. Due to its nature, this new source of information is not correlated with the other targets. With the application of our method, noise interference and signal correlation can be minimized in the radar estimation.

11.7 Summary

This chapter presents a method for improving Delay-Doppler resolution estimation for RadCom system. This new concept integrates the use of the reflected radar signal together with incoming communication signals transmitted by the targets. Measurements and simulations showed that our method is not only more effective distinguishing targets than the conventional 2D-DFT method, it also does so with increased accuracy. This holds true regardless of SNR and whether the signals reflected by targets are uncorrelated, highly correlated, or even coherent. The results show that the use of the communication signal received by the radar can be used to improve the estimation in the radar system. It is concluded that our method for radar processing with the use of incoming communication signals enables the use of lower bandwidth values to distinguish and estimate targets when compared to the conventional 2D-DFT technique, presenting high resolution even in the presence of coherent signals. Our method can also be used as a complement to 2D-DFT, being used in situations where the detection and distinction of two or more targets using 2D-DFT is not possible. Future research can expand the method for target tracking applications, taking advantage of the dual functionality of RadCom systems and exploring cooperation between vehicles to improve safety and accuracy during tracking.

CHAPTER 12

Cooperative Method for Distributed Target Tracking with Fusion Information

In this chapter we present a cooperative method for distributed target tracking for MIMO OFDM radar systems. The method employs a cascading information-fusion approach. First, the ego-vehicle performs a multi-target estimation by fusing the radar signals reflected by the targets with the communication signals it receives. Then, the ego-vehicle performs a tracking process, fusing its estimates with the estimates made by other in-network vehicles. By exploring the cooperation between vehicles, the proposed method enables the distributed tracking of targets. The result is a highly accurate multi-target tracking across the entire cooperative vehicle network, leading to improvements in transport reliability and safety. This chapter is organized as follows. In Section 12.2, the system model for the processing of the RadCom system is established and the target tracking model is introduced. In Section 12.3, the method for tracking based on the fusion of radar signal, communication signals and estimates from the vehicular network is presented. In Section 12.4, the measurement setup, measurement results, and performance evaluation thought simulation are presented. Finally, in Section 12.5, we present the summary.

12.1 Introduction

Radar is an important technology in automotive driver assistance systems because radar estimates are independent of ambient light and climate conditions, unlike those of Light Detection And Ranging (LIDAR) and camera systems [156]. Future radar systems for automotive applications will require a broad field of view and accurate tracking [157]. One rapidly evolving technology for automotive radar is RadCom. RadCom systems combine, in one single device, the ability to perform both radar functions and data communication functions [6]. The OFDM waveform can be used to perform radar and communication functions without degrading the performance of any of the RadCom subsystems [21, 127–131, 158, 159].

The dual functionality of RadCom may be an enabler of intelligent transportation systems which simultaneously reap the benefits of autonomous detection of the driving environment (through radar) and cooperative information exchange (in the form of vehicle-to-vehicle and vehicle-to-infrastructure communications) [17]. However, in conventional OFDM radar systems, target estimation requires wide signal bandwidths to achieve high resolution, which may not be available in most practical scenarios [58]. Furthermore, the ability of conventional OFDM radar systems to estimate targets is severely degraded in multi-target scenarios. In automotive systems, the distances from objects of interest can be in the order of less than one meter. Thus, the radar resolution offered by OFDM radars is typically insufficient for an accurate target estimation. Target tracking is a possible solution to improve target estimation with OFDM radar, mainly for automotive scenarios[157, 160].

Several automotive radar algorithms with information fusion from different sources have been proposed for target detection [161–165]. In [161], the authors present a vehicular network as a matrix of sensors to adapt their detection resolution, in order to better respond to the signal in the presence of noise. In [162], the authors present a multi-object detection methodology that utilizes the complementarity of three-dimensional LIDAR and camera data to identify multiple objects around an autonomous vehicle. In [163], the authors analyze the impact of fusing LIDAR, radar and camera estimates for target detection in vehicle systems. The authors show that the fusion of estimates improved target estimation and reduced incorrect detection during the tracking process. In [164], the authors present a new method for tracking and predicting paths for cooperative vehicular systems. This method takes into account velocity and acceleration sensor data from other vehicles (via wireless communications) and measurements made by the vehicle' radar system. In [165], to overcome the problem of radar resolution in target estimation and tracking, the authors propose a model of a radar sensor that describes the spatial distribution of vehicle detections, as well as a probabilistic description of the number of vehicle detections. The proposed model also considers the effects of fusing a general number of target reflections (limited resolution). An analysis of vehicle detection techniques, comparing the performance of sensors and tracking techniques in automotive systems, can be found in [166–168].

The aforementioned studies did not consider the use of RadCom based systems, therefore no additional advantages arising from its use were evaluated. In this chapter we present a technique for target tracking in MIMO RadCom systems, enabling the simultaneous tracking of target velocity, range, and direction. This method takes advantage of the ability of the vehicles to communicate with each other, thus creating an ad-hoc RadCom network where each vehicle broadcasts to neighboring vehicles the target estimates obtained by its own radar sensor. A method for determining a weight for each measure is also presented, allowing for the increased weighing of the better-conditioned measures on the final target estimation. In order to validate the method, laboratory RadCom measurements at 24 GHz were used for the Single-Input Single-Output (SISO) scenario, and simulations are performed for the MIMO RadCom network scenario.

12.2 System model

In this chapter, we consider a RadCom system in which the information to be transmitted is encoded by a digital complex-modulation technique, e.g., QAM. The encoded data is transmitted using OFDM modulation. The same signal is used to perform both radar and communication functions simultaneously, since a RadCom system is considered. The system also receives communication signals from other devices (e.g., other vehicles). The communication signals are received

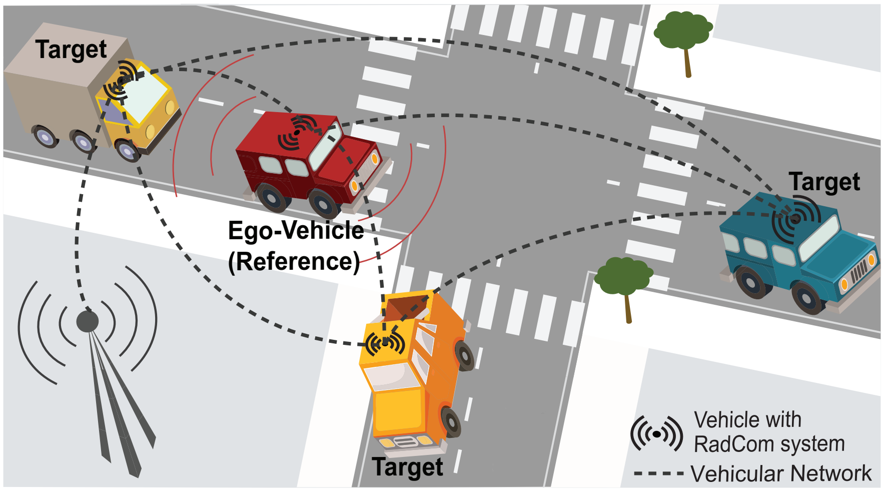

Figure 12.1: Example scenario with vehicles equipped with RadCom systems connected to a vehicle network.

by the RadCom system at a different carrier frequency or a different time than the transmitted signal, and are thus processed separately from the radar signal using standard communication signal processing techniques. The term ego-vehicle is used in this thesis to refer to the reference vehicle (RadCom) for target estimation. We also consider in this chapter that the ego-vehicle is connected to a vehicle network, as shown in Figure 12.1. Vehicles connected to the ego-vehicle are equipped with RadCom systems and transmit their target estimates to the ego-vehicle for the collaborative tracking of targets, forming a network of distributed radars. A block diagram depicting the operation of a RadCom system is shown in Fig. 12.2.

12.2.1 Radar target tracking

In automotive radar systems, the position of a target is reported in polar coordinates as the range and direction (azimuth angle) with respect to the sensor location. In target tracking, the target motion can be modeled in Cartesian coordinates [169]. The transformation of the position of the target in range and direction information to cartesian coordinates is given by

$$x_l = r_l cos(\theta_l), \tag{12.1}$$

$$y_l = r_l sin(\theta_l). \tag{12.2}$$

The state model used in this chapter is described in [170]. This model considers information on the position (x_l, y_l) and relative velocity $(\dot{x}_l, \dot{y}_l)$ of a target l at

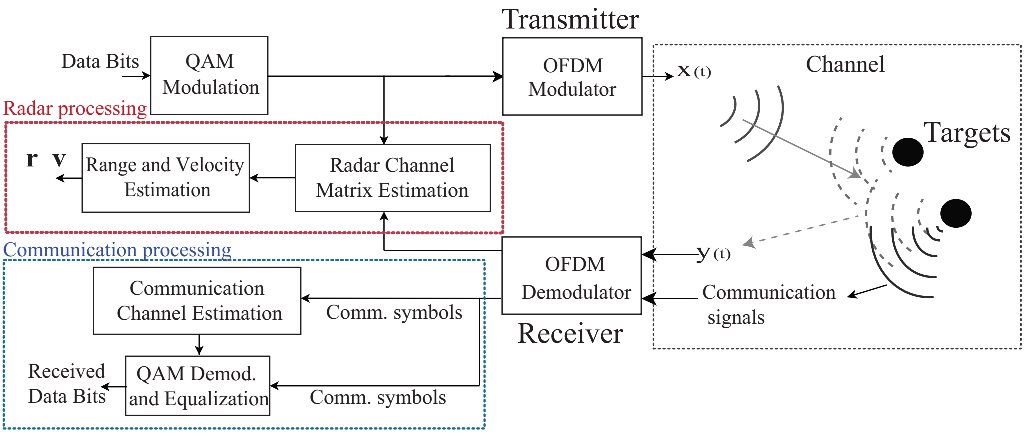

Figure 12.2: Simplified block representation of the RadCom system structure. The encoded data is transmitted by the RadCom system using OFDM modulation. The transmitted signal is then reflected by the targets and received back by the same RadCom system to estimate the range and velocity of targets. The system also receives and processes communication signals transmitted from other devices (e.g., other vehicles).

the instant k. The state model is represented by $\mathbf{X} = [x_l, y_l, \dot{x}_l, \dot{y}_l]^T$. A nearly constant velocity model with discretized continuous-time white noise acceleration [100] was considered for the target movement, so the prediction of the state based on the previous state can be described by

$$\mathbf{X}_k = \mathbf{F}\mathbf{X}_{k-1} + \mathbf{G}\mathbf{w}_{k-1}, \tag{12.3}$$

where

$$\mathbf{F} = \begin{bmatrix} 1 & 0 & \Delta_t & 0 \\ 0 & 1 & 0 & \Delta_t \\ 0 & 0 & 1 & 0 \\ 0 & 0 & 0 & 1 \end{bmatrix}, \tag{12.4}$$

$$\mathbf{G} = \begin{bmatrix} \frac{1}{2\sqrt{3}}\Delta_t^3 & 0 & \frac{1}{2}\sqrt{\Delta_t}^3 & 0 \\ 0 & \frac{1}{2\sqrt{3}}\sqrt{\Delta_t}^3 & 0 & \frac{1}{2}\sqrt{\Delta_t}^3 \\ 0 & 0 & \sqrt{\Delta_t} & 0 \\ 0 & 0 & 0 & \sqrt{\Delta_t} \end{bmatrix}. \tag{12.5}$$

The measurement period is denoted by Δ_t and $\mathbf{w}_k$ is the sensor measurement error white noise with covariance matrix $\mathbf{R_w}$. The measurement equation is written as:

$$\tilde{\mathbf{X}}_k = \mathbf{H}\mathbf{X}_k + \mathbf{n}_k, \tag{12.6}$$

where $\tilde{\mathbf{X}}_k$ is the sensor measurement, $\mathbf{n}_k$ is the sensor measurement error with $\mathbf{R_n}$ covariance matrix and $\mathbf{H}$ is an identity matrix of size 4×4. The Kalman filter [100] algorithm that describes the prediction of the current state $(\overline{\mathbf{X}}_{k+1})$ and the state estimation $(\mathbf{X}_{k+1})$ are given by

$$\overline{\mathbf{X}}_k = \mathbf{F}\mathbf{X}_{k-1}, \tag{12.7}$$

$$\overline{\mathbf{P}}_k = \mathbf{F}\mathbf{P}_k\mathbf{F}^T + \mathbf{G}\mathbf{R_w}\mathbf{G}^T, \tag{12.8}$$

$$\mathbf{K}_k = \overline{\mathbf{P}}_k\mathbf{H}^T[\mathbf{H}\overline{\mathbf{P}}_k\mathbf{H}^T + \mathbf{R_n}]. \tag{12.9}$$

$$\mathbf{X}_k = \overline{\mathbf{X}}_k + \mathbf{K}_k[\tilde{\mathbf{X}}_k - \mathbf{H}\overline{\mathbf{X}}_k], \tag{12.10}$$

$$\mathbf{P}_k = [\mathbf{I} - \mathbf{K}_k\mathbf{H}]\overline{\mathbf{P}}_k, \tag{12.11}$$

where $\mathbf{K}_k$ is referred to as the Kalman filter gain, $\overline{\mathbf{P}}_k$ is the predicted covariance matrix of the error, $\mathbf{P}_k$ is the covariance matrix of the state estimation error and $\mathbf{I}$ is an identity matrix. In this chapter for relative velocity $\dot{x}_l$ and $\dot{y}_l$ of the targets, only the velocity estimation obtained by the filter itself is used, the radar measurements of velocity are not considered.

12.3 Fusion of radar and communication information method

The essence of the method is to take advantage of the dual functionality of RadCom systems. The method employs a cascading information-fusion approach: initially, for the target estimates made by the ego-vehicle, the radar signal reflected by the targets is merged with the received communication signals. Then, information relating to the target estimates made by the ego-vehicle is merged with target estimates made by all vehicles connected to the ego-vehicle.

In the first stage, three different sources are used for target estimates in the RadCom system, as depicted in Figure 12.3: estimates using the radar signal; estimates obtained by processing the communication signals received; and

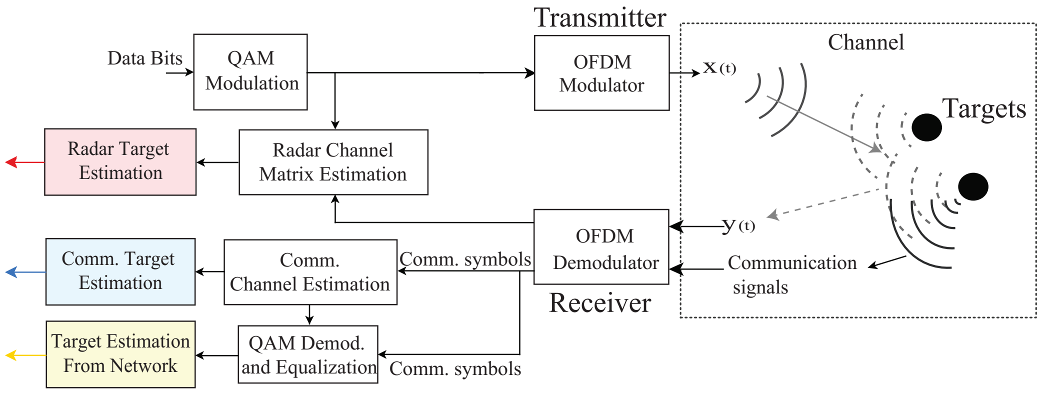

Figure 12.3: Simplified block representation of the proposed method in a RadCom system, where three independent target estimates are obtained for further processing (information fusion and tracking).

estimates from the joint processing of radar and communication signals.

After this, in a second stage, a new fusion of information using the radar estimates transmitted by the vehicles that are connected to the network and communicate with the ego-vehicle is performed as depicted in Figure 12.3. This second fusion stage enables a RadCom network where target estimation is performed in a cooperative distributed fashion. The target association with all different sources of estimates is then performed and a fusion of these estimates is finally realised in a target tracking stage, as depicted in Figure 12.4.

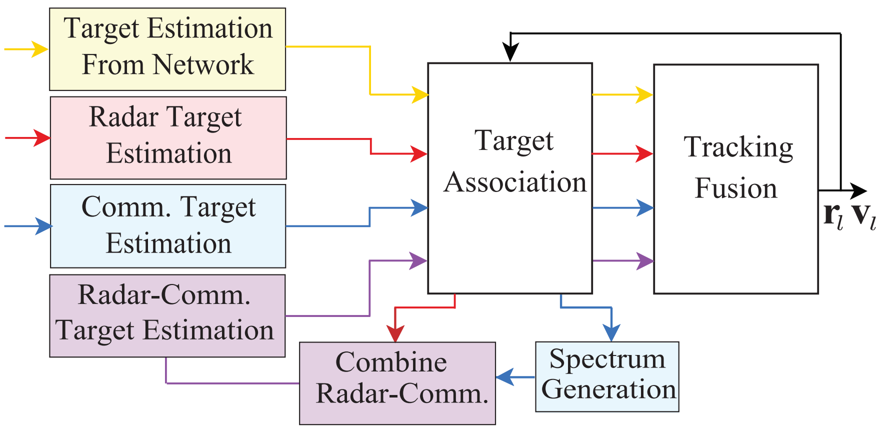

Figure 12.4: Simplified block representation of the proposed method for target tracking in RadCom system.

12.3.1 Fusion of radar and communication information

This stage consists of three distinct target estimation phases: a multi-target estimation using the radar signal; a single target estimation using the communications signals of each transmitting target; and a third target estimation that combines the two signal spectra (radar and received communication signals) as depicted in Figure 12.4.

Radar target estimation

In a first processing step, a 2D range and velocity spectrum of the targets is estimated, as discussed in section II-A and described in [20]. In a second step for target estimation, targets are identified by comparing the magnitude of each spectrum cell with a set of decision boundaries. The decision limiting value is calculated by averaging and scaling the magnitude of the neighboring cells of the current cell [100]. The peak values of the spectrum for each target are recorded. A target measurement is considered a valid target after it has been confirmed by four consecutive measurements. For the DoA estimation, the MUSIC method is applied; the measurements of a target's position are then reported in Cartesian coordinates. The correct association of the direction of the targets with the estimate of range and velocity is considered known. The detected targets are associated with previous estimates by the Nearest Neighbor (NN) algorithm [100].

Communication signal target estimation

For each received communication signal, target estimation is performed as in the radar. This is possible because of the pilot symbols are known a priori, so target information can be extracted from the pilot subcarriers. Moreover, there are methods for the complete channel estimation [171] that could be used to improve the target estimation. The range and velocity of the target are estimated at the peak of the 2D spectrum and the DoA estimation using the MUSIC method.

Radar-communication fusion target estimation

In this processing step, the targets estimated from the communication signals are removed from the radar spectrum. This procedure is performed as follows. First, using the NN algorithm, each target estimated from the communication signals is associated with one of the targets estimated from the radar signal. Then, a new 2D (range and velocity) spectrum ($\mathbf{Z}_{com}$) is generated with velocity and range information of the target from the communication signals. A maximum peak value is defined for each of these new spectra according to the previously estimated peak value for the same radar target. For situations where the correct association of radar targets and communication signal targets is not possible (such as insufficient radar targets detected), an estimated value is used for the peak value associated with the target. This estimated peak value is given by the sum of the averaging gradient of the last 4 radar measurements available with the last peak value defined.

The generated spectra are then subtracted from the estimated radar spectrum ($\mathbf{Z}_{radar}$), and the combined radar-communications spectrum $\mathbf{Z}_{radcom}$ is obtained,

$$\mathbf{Z}_{radcom} = \mathbf{Z}_{radar} - \mathbf{Z}_{com}. \tag{12.12}$$

Finally, a new target estimation is performed using the $\mathbf{Z}_{radcom}$ spectrum (using the same procedure as in the radar estimation).

For the DoA estimation of targets, a technique based on covariance differencing is applied as detailed in chapter 10. The covariance differencing is done between the covariance matrix of the radar ($\mathbf{R}_{radar}$) and the covariance matrix of the communication signal ($\mathbf{R}_{com}$). The covariance matrix is calculated as shown in the previous section. After the estimation of the covariance matrices, the covariance differencing is performed, generating a new $\mathbf{R}_{radcom}$ matrix

$$\mathbf{R}_{radcom} = \mathbf{R}_{radar} - \mathbf{R}_{com}. \tag{12.13}$$

The conventional MUSIC algorithm is then applied to $\mathbf{R}_{radcom}$, generating the respective DoA estimates.

12.3.2 Cooperative distributed target estimation

In this phase of the method, we consider that the vehicles that are connected to the ego-vehicle, form a network of distributed radars. The example scenario of Figure 12.5 represents this process. In Figure 12.5 we consider vehicle 0 as the ego-vehicle, and the other vehicles as targets (vehicle 1, 2 and 3). All vehicles are considered to be equipped with RadCom systems, though, at the illustrated instant in time, only vehicle 1 is communicating with the ego-vehicle. Vehicle 1 sends to the ego-vehicle its target estimates related to the other neighboring

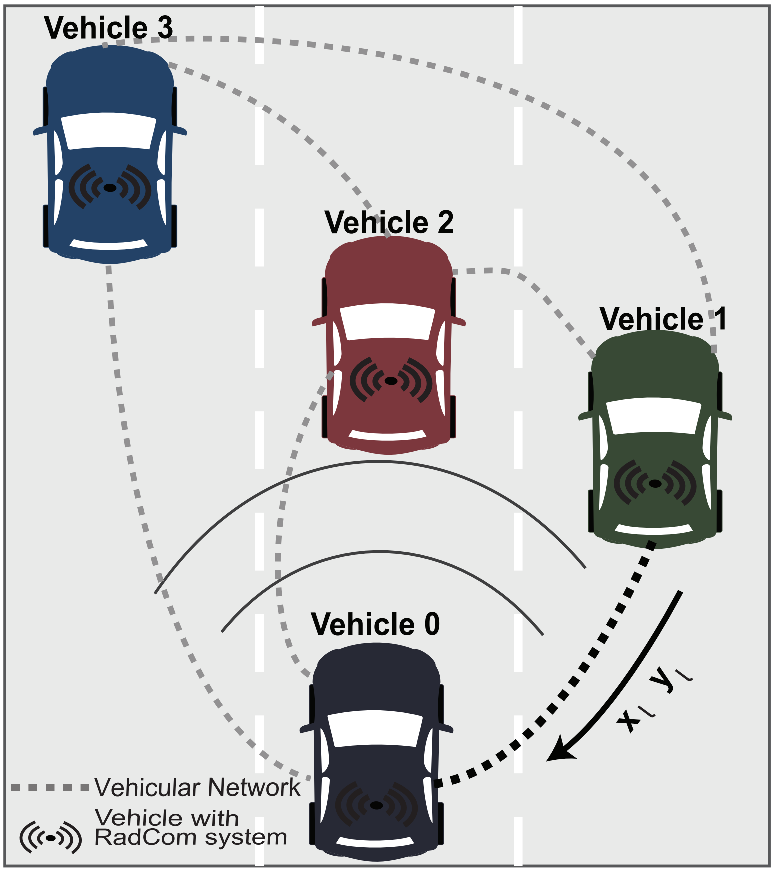

Figure 12.5: Example scenario with vehicles equipped with RadCom systems. The vehicles are connected to form a network of distributed radars. In this scenario, the vehicle 1 is communicating with the ego-vehicle (vehicle 0).

vehicles, that is, the target estimates related to vehicle 2, 3 and 0 (ego-vehicle). The ego-vehicle uses these estimates together with its own estimates in the process of tracking targets.

During this stage, the association of target estimates made by the different vehicles connected to the vehicle network is performed. The first step in associating the different estimates mentioned above is the spatial alignment. Spatial alignment is performed by translating the received estimates into the ego-vehicle coordinate system. These estimates then go through a validation procedure, where unlikely estimates and associations are removed from processing.

12.3.3 Information fusion and target tracking

The first step is to start the tracking process with Kalman filtering using the equations (12.7), (12.8) and (12.9). The second step is the association of the all estimates mentioned above, which is solved with the NN algorithm. All estimates (radar, communication, combined radar-communication and vehicular-network) are fused using a method based on the work in [100], given by

$$\mathbf{P}_k = [\overline{\mathbf{P}}_k^{-1} + \sum_{s=1}^{S} \mathbf{H}_s^T(\mathbf{W}_{s,k} + \mathbf{R}_{\mathbf{n}s})^{-1}\mathbf{H}_s]^{-1}, \tag{12.14}$$

$$\mathbf{X}_k = \mathbf{P}_k[\overline{\mathbf{P}}_k^{-1}[\overline{\mathbf{X}}_k + \sum_{s=1}^{S} \mathbf{H}_s^T(\mathbf{W}_{s,k} + \mathbf{R}_{\mathbf{n}s})^{-1}\tilde{\mathbf{X}}_{s,k}]^{-1}, \tag{12.15}$$

where S is the number of sources used to collect measurements and $\mathbf{W}_{s,k}$ is the weighted-fusion matrix, related to the measured reliability for each source s in the instant k, which is defined as

$$\mathbf{W}_{s,k} = w_{s,k}\mathbf{I}, \tag{12.16}$$

$$w_{s,k} = \frac{1}{L}[\rho_k^a\delta_a + \rho_k^r\delta_r + \frac{\delta_d}{\Delta r}\sum_{l=1}^{L}\xi_{l,k}], \tag{12.17}$$

where ρ_k^a is the number of targets coming from the same direction, ρ_k^r is the number of pairs of targets with differences in range and velocity between them, less than the resolution of the radar. δ_a, δ_r and δ_d are the weights parameters define by the user, relative to estimation error for DoA, range and relative distance respectively. $\xi_{l,k}$ is the relative distance between the estimates obtained by the measurements of the system with the estimates obtained by the Kalman filter, defined as

$$\xi_{l,k} = |\tilde{x}_{l,k} - \bar{x}_{l,k-1}| + |\tilde{y}_{l,k} - \bar{y}_{l,k-1}|, \tag{12.18}$$

where $\tilde{x}_l$ and $\tilde{y}_l$ are the position of the target l for the estimations k and $\bar{x}_l$ and $\bar{y}_l$ are the position of the target l for Kalman estimation $k-1$. The weighted-fusion matrix proposed in this chapter adds adaptability to the algorithm, allowing it to weigh more the better-conditioned measurements on the final estimate of the target.

For SISO scenarios the parameter $\delta_a = 0$ and $\xi_{l,k} = |\tilde{r}_{l,k} - \bar{r}_{l,k}|$, where $\tilde{r}_l$ is the range of target l for the measurement k, and $\bar{r}_l$ is the range of target l for the Kalman estimation $k-1$.

Furthermore, in SISO systems, only the range and velocity measurements of the radar, communication signal and radar-communication fusion are used in the tracking, since the target direction is not provided. Also, estimates received by the network are not considered, since it is not possible to determine the estimates received in relation to the ego-vehicle (DoA estimation inaccessible in OFDM SISO system).

The method with distributed radar network and cooperative estimation is described in Algorithm 1.

Algorithm 1 Tracking algorithm with distributed radar network and cooperative estimation

For every time instant k:

1: Estimate the 2-dimensional range and velocity spectra $\mathbf{Z}_{radar}$ and $\mathbf{Z}_{com}$.
2: Calculate combined radar-communication spectrum:

$$\mathbf{Z}_{radcom} = \mathbf{Z}_{radar} - \mathbf{Z}_{com}.$$

3: Estimate the covariance matrix $\mathbf{R}_{radar}$ and $\mathbf{R}_{com}$
4: Calculate the radar-communication covariance matrix:

$$\mathbf{R}_{radcom} = \mathbf{R}_{radar} - \mathbf{R}_{com}.$$

5: Apply MUSIC method to $\mathbf{R}_{radcom}$, $\mathbf{R}_{radar}$ and $\mathbf{R}_{com}$.
6: Estimate the range and DoA of the targets for all sources (radar, communication signals and combined radar-communication).
7: Calculate the cartesian position $x_{s,l}$ and $y_{s,l}$ for each target l of each source s:

$$x_{s,l} = r_{s,l} cos(\theta_{s,l}),$$

$$y_{s,l} = r_{s,l} sin(\theta_{s,l}),$$

8: Transmit to vehicular network the $x_{s,l}$ and $y_{s,l}$ estimations.
9: Receive from the vehicular network the $x_{s,l}$ and $y_{s,l}$ estimations of others vehicles.
10: Translate the received $x_{s,l}$ and $y_{s,l}$ estimates into the ego-vehicle's reference coordinate system.
11: Associate the targets with NN algorithm.
12: Start the Kalman filter stage.

$$\overline{\mathbf{X}}_k = \mathbf{F}\mathbf{X}_{k-1},$$

$$\overline{\mathbf{P}}_k = \mathbf{F}\mathbf{P}_k\mathbf{F}^T + \mathbf{G}\mathbf{R}_{\mathbf{w}}\mathbf{G}^T,$$

$$\mathbf{K}_k = \overline{\mathbf{P}}_k\mathbf{H}^T[\mathbf{H}\overline{\mathbf{P}}_k\mathbf{H}^T + \mathbf{R}_{\mathbf{n}}].$$

13: Start the fusion filter stage.

$$\mathbf{P}_k = [\overline{\mathbf{P}}_k^{-1} + \sum_{s=1}^{S} \mathbf{H}_s^T(\mathbf{W}_{s,k} + \mathbf{R}_{\mathbf{n}s})^{-1}\mathbf{H}_s]^{-1},$$

$$\mathbf{X}_k = \mathbf{P}_k[\overline{\mathbf{P}}_k^{-1}[\overline{\mathbf{X}}_k + \sum_{s=1}^{S} \mathbf{H}_s^T(\mathbf{W}_{s,k} + \mathbf{R}_{\mathbf{n}s})^{-1}\tilde{\mathbf{X}}_{s,k}]^{-1},$$

12.4 Results

In this section, we present the results for the fusion of radar and communication information method for two different scenarios. In the first scenario, a SISO system is considered for laboratory measurements at 24 GHz for tracking two targets. In the second scenario, a MIMO system with a vehicular network is considered in a simulation environment for tracking three targets. In both scenarios, the RadCom system communicates with only one of the targets. Moreover, in both scenarios, the RadCom system has the parameters presented in Table 4.3. The number of pilot subcarriers is 128. The MIMO RadCom system includes a uniform linear arrangement of $M_T = 4$ antennas ($d_t = 2\lambda$) for transmission, and another array of $M_R = 4$ antennas for reception ($d_r = \lambda/2$). The RadCom system is considered to be operating at 24 GHz and the target with communication capabilities at 23.8 GHz. The weighted target-association parameters are defined as $\delta_a = 0$ for the SISO RadCom system,$\delta_a = 0.1$ for the MIMO RadCom system and $\delta_r = 0.05$, and $\delta_d = 0.2$ for both systems.

12.4.1 Measurement setup

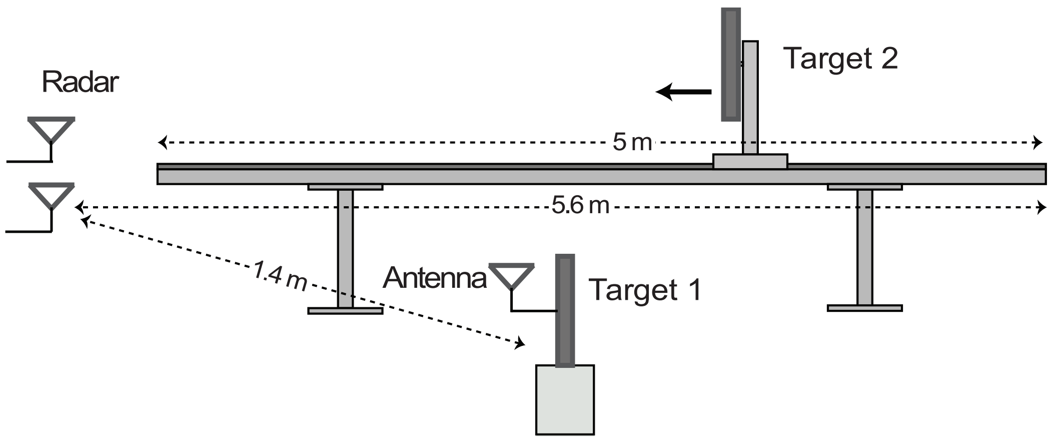

Figure 12.6: Diagram of the scenario of measurement.

The measurement setup and scenario for the 24 GHz RadCom system are illustrated in Figure 12.6 and pictured in Figure 12.7. The scenario included a RadCom system employing its radar functionalities to estimate two targets, one of which was equipped with a transmitting antenna to simulate another RadCom system employing its communication functionalities. The radar transmits and receives its own signal (through target reflection), and also receives also the communication signal transmitted by the target equipped with another antenna.

(a) (b)

Figure 12.7: Photograph of the (a) measurement setup, (b) scenario with two targets.

Target 1 was a stationary 50 × 50 cm steel plate, and target 2 was a moving 50 × 50 cm steel plate mounted on a motorized linear track with a length of 5 m. Target 1 was placed 1.4 m away from the radar. Target 2 started at 5.6 m away from the radar, accelerated for 2 m of track length up to a velocity of 2.3 m/s, maintained this velocity constant for 2 m, and then decelerated for the remaining 1 m of track length until it stopped at 0.6 m away from the radar.

In target 1, a transmit antenna was installed to simulate another RadCom system employing its communication functionalities. For practical reasons, the same 24 GHz signal generator was used for both the radar and target 1. This required repeating the same measurements, changing the position of the transmitting antenna from the radar to the target. The received signals (radar and communication) were synchronized in post-processing. Measurements for target tracking are made for a total of 3 s, with a measurement interval of 52 ms.

The transmitting and receiving antennas were A-Info LB-180400-KF 15 dBi horn antennas. The transmitted waveform had a bandwidth of 113.92 MHz and was synthesized in the baseband, at a sample rate of 256 MSa/s, using a Keysight M8190A AWG. The AWG outputs the in-phase (I) and quadrature (Q)

components of the waveform in a differential-pair configuration ($I/\bar{I}$ and $Q/\bar{Q}$). The baseband waveform was then converted to the 24 GHz band using a Keysight E8267D PSG VSG. The signal at the output of the VSG had an average power of 12 dBm and was fed to the transmitting antenna.

Both signals were received by the radar antenna and were measured using a Keysight N9041B UXA VSA. For greater accuracy of measurement, the 10 MHz oscillator of the VSA was used as a reference to synchronize the clocks of all instruments (the AWG, the VSG, and the VSA), and a baseband trigger signal was provided by the AWG to the VSA. The AWG was connected via USB to a personal computer (PC) and the other instruments were connected through a local area network to the same computer. All instruments were controlled via Matlab, where all signals were generated and processed. The total group delay of the radar hardware (instruments, cables, antennas) was measured; this delay was then calibrated out during radar processing.

12.4.2 Radar measurements

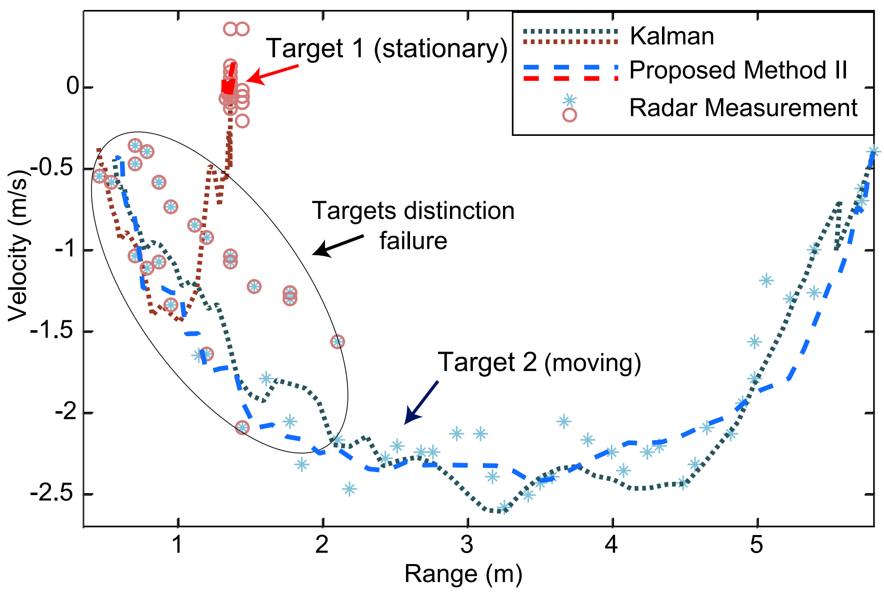

Figure 12.8: Velocity and range tracking for two targets.

In Figure 12.8 the results of the tracking of the two targets using laboratory measurements in the scenario represented in Figure 12.7 are shown. Note that target 1 was stationary at 1.4 m away from the radar and target 2 moved from 5.6 m to 0.6 m away from the radar; thus, a chronological analysis of Figure 12.8 requires the examination of the plotted lines from right to left.

It can be seen in Figure 12.8 that our method allowed the correct estimation of both targets, even in situations where the speed and range measurements provided by the radar were not correct. When the radar was unable to distinguish the two targets (insufficient radar resolution), the Kalman method failed to correctly estimate the targets (the estimate of target 1 should have been stationary, but it is incorrectly estimated with movement. However, our method was able to estimate both targets correctly during the whole duration of the test, concentrating all estimates of target 1 at the 1.4 m, 0 m/s point while target 2 moved toward the radar.

The reason why the method is able to distinguish targets more accurately is the use of an additional source of information: the communication signal of one of the targets. With the application of the first fusion stage of our method, the combined radar-communications spectrum is generated; this spectrum contains the information of the other targets that are in the radar view (the target that transmitted the communication signal is removed). Thus, this preliminary fusion stage allows for the accurate separation of two targets, even when the radar resolution is insufficient.

To better illustrate how the method operates, we have the examples of Figure 12.9 and Figure 12.10 which show the resulting radar images for the scenario in Figure 12.7 at two different times. For a first moment (Figure 12.9), when both targets are at a distance between them greater than the radar resolution (1.31 m), Figure 12.9(a) shows that the radar correctly estimates two peaks (two targets) with a range of 1.36 m and velocity of 0.09 m/s for the target 1, and range of 4.32 m and velocity of -2.20 m/s for the target 2. In Figure 12.9(b) we have the radar image obtained using the communication signal, where we see a single estimated target, as expected, with the measurement of 1.36 m and 0.09 m/s. In Figure 12.9(c), we have the radar image with the radar-communication fusion estimation; in this Figure, it is possible to see the other estimated targets, as was also expected, with position 4.32 m and velocity -2.2 m/s. As shown, the fusion of the radar and communication signal removes the target that transmitted the communication signal from the radar image, leaving the other target isolated.

Let us now consider another example where the application of this technique becomes absolutely necessary: when the radar cannot correctly distinguish the two targets due to its limited resolution. In a second moment (Figure 12.10), we have the targets close to each other (less than 1 m distance between them). Figure 12.10(a) shows that at this moment the radar cannot correctly distinguish

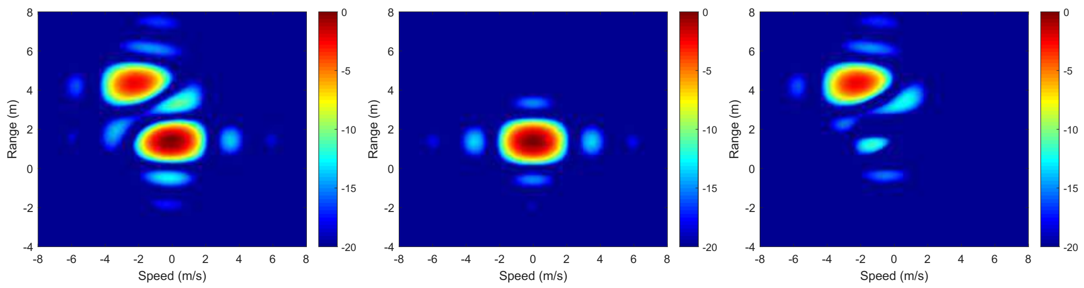

(a) (b) (c)

Figure 12.9: Radar image for the measurement scenario with two targets at a distance between them greater than the radar resolution for (a) the radar estimation, (b) the communication signal estimation (c) the radar-communication fusion estimation.

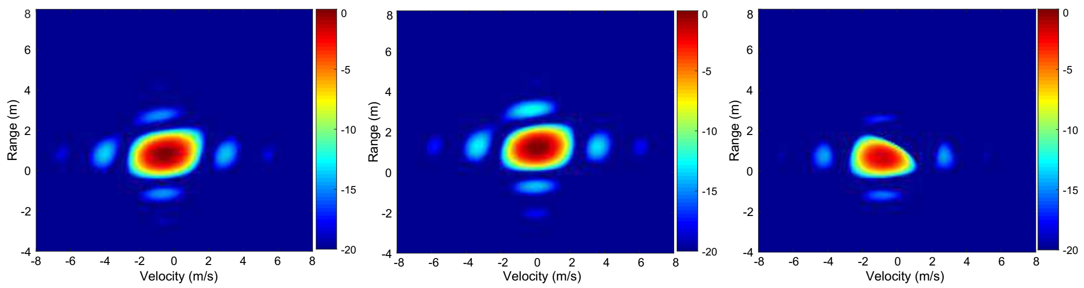

(a) (b) (c)

Figure 12.10: Radar image for the measurement scenario with the two targets at a distance between them less than the radar resolution for (a) the radar estimation, (b) the communication signal estimation (c) the radar-communication fusion estimation.

the two targets, presenting a single peak with a range of 0.86 m and a velocity of -0.58 m/s. In Figure 12.10(b) we have the radar image obtained using the communication signal, where we see a single estimated target, with a range of 1.43 m and velocity of 0.05 m/s. Finally, in Figure 12.10(c), we have the radar image of the radar-communication fusion estimation. In this Figure, it is possible to see a single target, estimated with a range of 0.69 m and a velocity of -0.73 m/s (target 2). Thus, using the radar-communication fusion method, the two targets were able to be separated and their range and velocity were able to be estimated. As shown in Figure 12.10(a), this would have been impossible using just the radar because of its limited resolution.

12.4.3 Performance evaluation

In environments with a large number of targets close to each other, only the communication signal of a target may not be sufficient to guarantee a correct estimate of all the nearby targets. That is why in this section we show how distributed estimation and cooperative processing in the method improves the tracking of multiple targets. For this, we evaluate by simulation the performance of the proposed method for a MIMO RadCom system connected in a vehicular network.

We consider the scenario in Figure 12.5 with RadCom-equipped vehicle (vehicle 0) and three mobile targets (vehicle 1, vehicle 2 and vehicle 3).In this scenario, only one of the targets (vehicle 1) is communicating with the ego-vehicle (vehicle 0), at the illustrated instant in time. Vehicle 1 transmits to the ego-vehicle its target estimates related to the other neighboring vehicles, that is, the target estimates related to vehicle 0, 2, 3. The ego-vehicle uses these estimates together with its own estimates in the process of tracking targets. Both radar systems (vehicle 0 and vehicle 1) are simulated with target estimation with radar signals, communication signals, and radar-communication fusion. Only in vehicle 0 are estimates coming from the vehicle network, and only the final target estimates of vehicle 0 are shown in the results.

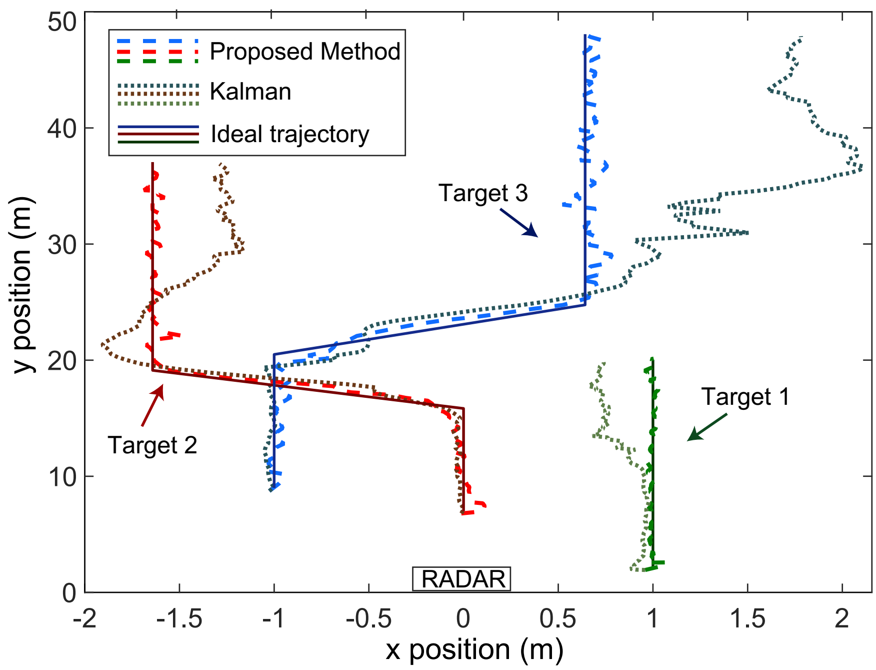

Figure 12.11: Position tracking for three targets.

The initial relative range and velocity in Cartesian coordinates of the targets relatively to the ego-vehicle are: ranges of $x_1 = 1$ m and $y_1 = 2$ m, $x_2 = 0$ m/s and $y_2 = 7$ m, $x_3 = -1$ m and $y_3 = 9$ m; velocities of $\dot{x}_1 = 0$ m/s and $\dot{y}_1 = 0.6$ m/s, $\dot{x}_2 = 0$ m/s and $\dot{y}_2 = 1$ m/s, $\dot{x}_3 = 0$ m/s and $\dot{y}_3 = 1.3$ m/s; After 9.25 s, the velocities $\dot{x}_2$ and $\dot{x}_2$ change to $\dot{x}_2$=-0.5 m/s and $\dot{x}_3 = 0.5$ m/s for 3.25 s, and change back to 0 m/s in the remaining time. The normalized average power of the received signal is $P_l = 1$. One measurement is made every 250 ms, with a total of 120 measurements being performed for 30 s. The estimation error is defined as the RMSE. The RMSE is calculated by

$$\text{RMSE} = \frac{1}{L}\sum_{l=1}^{L}\sqrt{\frac{1}{\Psi}\sum_{\psi=1}^{\Psi}[(\bar{x}_{\psi,l} - x_{\psi,l})^2 + (\bar{y}_{\psi,l} - y_{\psi,l})^2]}, \tag{12.19}$$

where L is the number of targets, $\bar{x}_{\psi,l}$ and $\bar{y}_{\psi,l}$ is the estimate of the position, $x_{\psi,l}$ and $y_{\psi,l}$ is the correct value of the target and $\Psi = 50$ is the number of Monte Carlo simulations performed.

Figure 12.11 shows the tracking results with simulation of our method for a RadCom MIMO system comparing with the Kalman algorithm (presented in Section II-B) and radar measurements without tracking. The channel was considered flat without attenuation and with a SNR of -5 dB. It is possible to verify that our method greatly improves the target estimation in the RadCom system. As it is possible to visualize in Figure 12.11, when the targets are moving away from the ego-vehicle, the angular difference between the targets decreases, thus decreasing the accuracy in the estimation of the targets by the radar system.

Figure 12.12 presents the RMSE of estimates for different SNR values. Figure 12.12 demonstrates that radar measurements and target tracking using the Kalman method suffer greater losses with increased noise in the system. Moreover, this Figure demonstrates that the proposed method achieves, for all SNR cases, an RMSE that is better than that of the radar measurements or Kalman tracking estimates. Figure 12.12 also reveals a higher RMSE in the radar measurements and Kalman estimates at the moment relative to the crossing of target 2 with target 3 in Figure 12.11. Our method, however, presents low and stable RMSE values in the same region, offering better tracking accuracy even in situations where targets are very close to each other. This is due to the fact that the proposed method uses information from more than one source (target estimates from the vehicular network and from communication signals) for the target tracking process, thus

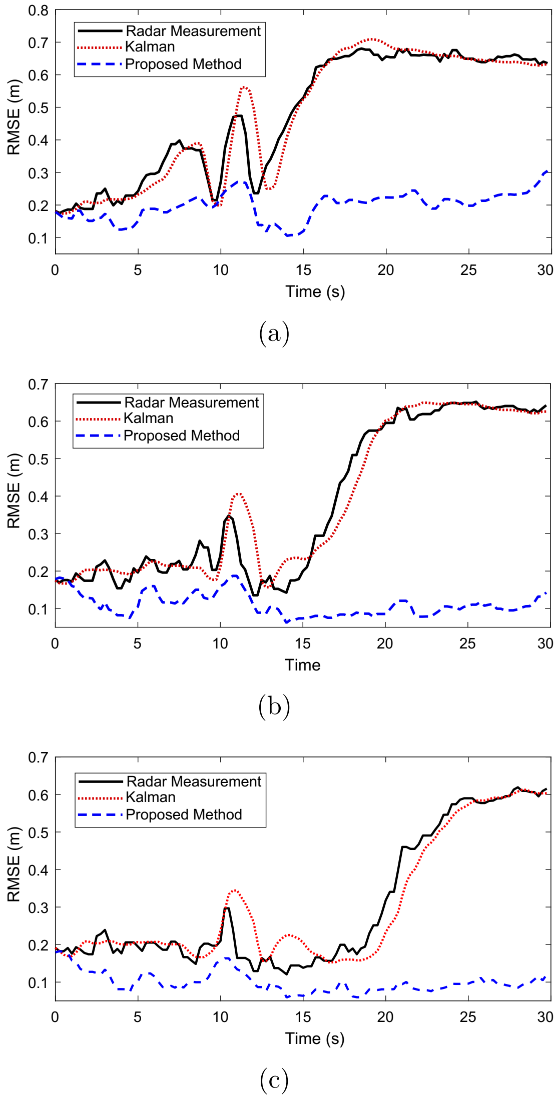

Figure 12.12: RMSE for target tracking with SNR of (a) 0 dB, (b) 5 dB and (c)10 dB.

increasing the reliability and stability of the estimates.

12.5 Summary

In this chapter, the fusion of radar and communication information method for distributed target tracking using RadCom systems in automotive applications is presented. The method employs a cascading information fusion approach to improve the accuracy of target estimation and tracking. The method combines the radar and communications functions of RadCom systems to enable the distributed estimation of multiple targets and greatly improve multi-target tracking accuracy, especially in situations where the radar resolution is insufficient. Laboratory RadCom measurements at 24 GHz and simulations demonstrate that our method has a higher accuracy, a greater ability to distinguish targets and much more stability in target tracking when compared to other methods that use only the estimates provided by the radar.

CHAPTER 13

Conclusions

THE results obtained in this thesis, show that multicarrier waveforms are a viable option for radar and can compete with other waveforms. The dual functionality of the muticarrier waveforms is an innovative advantage, the two functions (radar and communication) can operate cooperatively in the same device. To conclude this thesis, in this chapter the main contributions will be recapitulated and a brief discussion on future research directions will be outlined.

13.1 Summary of Key Contributions

In this thesis, the basic concepts of communication systems and OFDM radar were discussed. The implementation aspects using multicarrier waveforms as well parameter estimation methods were presented and analysed. The choice of an appropriate parametrization in the waveform design was also discussed, considering communication and radar requirements.

One of the research topics in this thesis was the proposal of the adaptation of the other multicarrier waveforms in addition to OFDM, such as FBMC, GFDM and UFMC, for radar functions. These alternative waveforms were compared performance-wise regarding achievable target parameter estimation performance, amount of residual background noise in the radar image, impact of intersystem interference and flexibility of parametrization.

The analysis shows that both UFMC, GFDM and FBMC can be used to mitigate inter-system interference problems—since the OOB emission is reduced—and increase the effective bandwidth of the system, thus improving the resolution of the radar. Inter-system interference is a problem in automotive applications, where a large volume of sensing and communication devices is present. FBMC shows the greatest reduction in inter-system interference, followed by GFDM and UFMC. Regarding the complexity of implementation, we have the opposite order, with UFMC being the simplest and FBMC being the most complex for implementation, thus GFDM being the intermediate trade-off between performance and implementation viability of the proposed waveforms. An in-depth discussion on the choice of waveform for RadCom systems was carried out in Chapter 8. We also demonstrated that, with correct processing, non-orthogonality in multicarrier waveforms is not a problem for radar estimation.

In a second part of the work, the problem of estimating and tracking targets was considered. During the thesis, DoA estimation algorithms were studied. Among them, the MUSIC and Min-Norm algorithms proved to be the most promising. Also in this research, techniques were proposed to improve the estimation and tracking of targets based on the cooperation of the radar and communication functions of the RadCom system.

We developed a novel high-resolution method for DoA estimation in MIMO RadCom systems that integrates the use of the radar signal together with incoming communication signals in the radar processing. The proposed DoA estimation method achieves performance improvements in RMSE and has a greater ability to distinguish closely spaced targets. The method can be applied to complex DoA detection scenarios with a large number of targets where uncorrelated, partially correlated and coherent signals are mixed.

We also developed a method for improving delay-Doppler resolution estimation for RadCom system. This method is based on the same idea of our high-resolution method for DoA estimation: the integration of the reflected radar signal together with incoming communication signals transmitted by the targets. The communication signal received by the radar can be used to improve the estimation in the radar system.

The proposed method for radar processing when combined with the incoming communication signals allows to reduce the bandwidth required to distinguish multiple targets. The method can also be used as a complement to conventional methods, in situations where the detection and distinction of two or more targets is not possible.

Finally, during this thesis, the target tracking problem is discussed, and a new method of fusing radar and communication information for distributed target tracking is presented. The method uses the approach considered in our high-resolution methods for DoA, delay and Doppler—the communication between the targets and the radar is used to improve the tracking of the targets. The method combines the radar and communication functions of RadCom systems to allow distributed estimation of multiple targets and significantly improve the accuracy of target tracking, especially in situations where radar resolution is insufficient. Laboratory measurements and simulations demonstrate that our method has a higher accuracy, a greater ability to distinguish targets and much more stability in target tracking when compared to other methods that use only the estimates provided by the radar.

13.2 Future research

Future research can expand our method for high-resolution delay-Doppler estimation in target tracking applications for multipath scenarios, where the dual functionality of RadCom systems and cooperation between vehicles can improve safety and accuracy during tracking.

We demonstrate in this thesis that, with correct processing, non-orthogonality in multicarrier waveforms is not a problem for radar estimation. This opens the door to further investigations with other non-orthogonal waveforms for RadCom systems. Research with multicarrier waveforms that optimize performance on both integrated functions (radar and data communication) can be performed.

The communication-aided concept i.e. the usage of communication signals as a tool to improve the RadCom system's radar function can be further expanded. In automotive networks the concept can be the basis of generalized distributed processing, where local data is exchanged and combined, improving the security and reliability of the system. Another topic for future research may be the dual of the previous one, where the radar estimates are used to improve the communication function by facilitated per example the channel tracking, beamforming, etc.. The final goal is to provide a dual system with both functions operating cooperatively.

Appendix

The proposed method was based on the mathematics of the techniques demonstrated in [172–174]. The parameters Δf and T for GFDM radar are chosen so that the channel can be considered slow-fading in time and frequency, that is, constant during the duration of a symbol and the bandwidth of a subcarrier. We assume that the prototype filter $p(q)$ has a length much longer than the maximum delay spread of the channel, and is well-localized in time and frequency domains [174]. The channel frequency response at the n-th subcarrier and m-th symbol is denoted by $H_{n,m}$. The transmitted GFDM signal can be represented as

$$x(q) = \sum_{m=0}^{M-1} \sum_{n=0}^{N-1} S(n,m) p_{n,m}[q]. \tag{13.1}$$

and the received signal $y(q)$ as [172]

$$y(q) \approx \sum_{m=0}^{M-1} \sum_{n=0}^{N-1} H_{n,m} S(n,m) p_{n,m}[q] + \eta(q). \tag{13.2}$$

In the receiver, to demodulate the signal, a matched filtering is performed. Let n_0 be the index of a given subcarrier and m_0 the index of a given symbol, Then since $\{p_{n,m}[q] \circledast p^*_{n_0,m_0}[-q]\}|_{q=0} = (\mathbf{p}_{n_0,m_0})^H \mathbf{p}_{n,m}$, the received data symbol $\hat{\mathbf{S}}$ at the (n_0, m_0) position is

$$\hat{S}(n_0, m_0) = \{y(q) \circledast p^*_{n_0,m_0}[-q]\}|_{q=0}. \tag{13.3}$$

Because of the non-orthogonality of GFDM, intercarrier and intersymbol interference is present at the output of the GFDM demodulator when using matched filtering. The self-interference induced from N subcarriers and M

symbols on the n_0-th subcarrier of the m_0-th symbol can be expressed as

$$\zeta(n_0, m_0) = \sum_{m=0}^{M-1} \sum_{n=0}^{N-1} S(n,m)\{p_{n,m}[q] \circledast p^*_{n_0,m_0}[-q]\}|_{q=0},$$
$$\text{for } (n,m) \neq (m_0, n_0). \tag{13.4}$$

Then, the received data symbol at the (m_0, n_0) position can be rewritten as [174]

$$\hat{S}(n_0, m_0) = H_{n_0,m_0} \{S(n_0, m_0) + \zeta(n_0, m_0)\} + \tilde{\eta}(n_0, m_0). \tag{13.5}$$

In GFDM-PMF, considering $\hat{S}^\dagger_{PMF}(n_0, m_0) = \hat{S}(n_0, m_0)$, the element (n_0, m_0) of the channel transfer matrix $\mathbf{D}$ is estimated as $D(n_0, m_0) = \hat{S}^\dagger_{PMF}(m_0, n_0)/S^\dagger_{PMF}(m_0, n_0)$, where $S^\dagger_{PMF}(n_0, n_0)$ is defined as

$$S^\dagger_{PMF}(n_0, m_0) = \left\{\left(\sum_{m=0}^{M-1} \sum_{n=0}^{N-1} S(n,m) p_{n,m}[q]\right) \circledast p^*_{n_0,m_0}[-q]\right\}|_{q=0} \tag{13.6}$$

$$= S(n_0, m_0) + \sum_{m=0}^{M-1} \sum_{n=0}^{N-1} S(n,m)\{p_{n,m}[q] * p^*_{n_0,m_0}[-q]\}|_{q=0}$$
$$= S(n_0, m_0) + \zeta(n_0, m_0). \tag{13.7}$$

Thus, when performing the elementary division, we compensate the self-interference in the radar transfer matrix:

$$D(n_0, m_0) = \frac{\hat{S}^\dagger_{PMF}(n_0, m_0)}{S^\dagger_{PMF}(n_0, m_0)} = \frac{H_{n_0,m_0} (S(n_0, m_0) + \zeta(n_0, m_0)) + \tilde{\eta}(n_0, m_0)}{S(n_0, m_0) + \zeta(n_0, m_0)}. \tag{13.8}$$

Bibliography

[1] SIT, Y. L., STURM, C., BAIER, J., et al. "Direction of arrival estimation using the MUSIC algorithm for a MIMO OFDM radar". In: *IEEE Radar Conference*, pp. 0226–0229, May 2012.

[2] MAHAFZA, B. *Radar Systems Analysis and Design Using MATLAB Third Edition*. Taylor & Francis, 2013.

[3] LELLOUCH, G. *Waveform desing and processing techniques in OFDM radar*. Ph.D., Department of Electrical Engineering, UNIVERSITY OF CAPE TOWN.

[4] STURM, C., WIESBECK, W. "Waveform Design and Signal Processing Aspects for Fusion of Wireless Communications and Radar Sensing", *Proceedings of the IEEE*, v. 99, n. 7, pp. 1236–1259, July 2011.

[5] BRAUN, M., STURM, C., NIETHAMMER, A., et al. "Parametrization of joint OFDM-based radar and communication systems for vehicular applications". In: *IEEE 20th Int. Symp. on Personal, Indoor and Mobile Radio Communications*, pp. 3020–3024, Sep. 2009.

[6] KUMARI, P., GONZALEZ-PRELCIC, N., HEATH, R. W. "Investigating the IEEE 802.11ad Standard for Millimeter Wave Automotive Radar". In: *IEEE Vehicular Technology Conference*, pp. 1–5, Sept 2015.

[7] SIT, Y. L., NUSS, B., BASAK, S., et al. "Demonstration of interference cancellation in a multiple-user access OFDM MIMO Radar-Communication network using USRPs". In: *2016 IEEE MTT-S International Conference on Microwaves for Intelligent Mobility (ICMIM)*, pp. 1–4, May 2016.

[8] PALMER, J. E., HARMS, H. A., SEARLE, S. J., et al. "DVB-T passive radar signal processing", *IEEE Transactions on Signal Processing*, v. 61, n. 8, pp. 2116–2126, Apr. 2013.

[9] BACZYK, M. K., SAMCZYNSKI, P., KRYSIK, P., et al. "Traffic density monitoring using passive radars", *IEEE Aerospace and Electronic Systems Magazine*, v. 32, n. 2, pp. 14–21, Feb. 2017.

[10] DANIEL, L., HRISTOV, S., LYU, X., et al. "Design and Validation of a Passive Radar Concept for Ship Detection Using Communication Satellite Signals", *IEEE Transactions on Aerospace and Electronic Systems*, v. 53, n. 6, pp. 3115–3134, Dec. 2017.

[11] GARMATYUK, D., SCHUERGER, J., KAUFFMAN, K. "Multifunctional software-defined radar sensor and data communication system", *IEEE Sensors Journal*, v. 11, n. 1, pp. 99–106, Jan. 2011.

[12] GUTIERREZ DEL ARROYO, J. R., JACKSON, J. A. "WiMAX OFDM for Passive SAR Ground Imaging", *IEEE Transactions on Aerospace and Electronic Systems*, v. 49, n. 2, pp. 945–959, Apr. 2013.

[13] CIUONZO, D., DE MAIO, A., FOGLIA, G., et al. "Intrapulse radar-embedded communications via multiobjective optimization", *IEEE Transactions on Aerospace and Electronic Systems*, v. 51, n. 4, pp. 2960–2974, Oct. 2015.

[14] BLUNT, S. D., YATHAM, P., STILES, J. "Intrapulse Radar-Embedded Communications", *IEEE Transactions on Aerospace and Electronic Systems*, v. 46, n. 3, pp. 1185–1200, Jul. 2010.

[15] CIUONZO, D., DE MAIO, A., FOGLIA, G., et al. "Pareto-theory for enabling covert intrapulse radar-embedded communications". In: *2015 IEEE Radar Conference (RadarCon)*, pp. 0292–0297, May 2015.

[16] GUIDI, F., GUERRA, A., DARDARI, D. "Personal mobile radars with millimeter-wave massive arrays for indoor mapping", *IEEE Transactions on Mobile Computing*, v. 15, n. 6, pp. 1471–1484, Jun. 2016.

[17] KUMARI, P., CHOI, J., GONZALEZ-PRELCIC, N., et al. "IEEE 802.11ad-Based Radar: An Approach to Joint Vehicular Communication-Radar

System", *IEEE Transactions on Vehicular Technology*, v. 67, n. 4, pp. 3012–3027, Apr. 2018.

[18] LEVANON, N. "Multifrequency complementary phase-coded radar signal", *IEE Proceedings - Radar, Sonar and Navigation*, v. 147, n. 6, pp. 276–284, Dec. 2000.

[19] DONNET, B. J., LONGSTAFF, I. D. "Combining MIMO radar with OFDM communications". In: *European Radar Conf.*, pp. 37–40, Sep. 2006.

[20] STURM, C., WIESBECK, W. "Waveform design and signal processing aspects for fusion of wireless communications and radar sensing", *Proceedings of the IEEE*, v. 99, n. 7, pp. 1236–1259, Jul. 2011.

[21] GAMEIRO, A., CASTANHEIRA, D., **J. SANSON**, et al. "Research challenges, trends and applications for future joint radar communications systems", *Wireless Personal Communications*, v. 100, n. 1, pp. 81–96, May 2018.

[22] GARMATYUK, D., SCHUERGER, J., MORTON, Y. T., et al. "Feasibility study of a multi-carrier dual-use imaging radar and communication system". In: *European Radar Conf.*, pp. 194–197, Oct. 2007.

[23] GARMATYUK, D., SCHUERGER, J. "Conceptual design of a dual-use radar/communication system based on OFDM". In: *MILCOM 2008 - 2008 IEEE Military Communications Conference*, pp. 1–7, Nov 2008. doi: 10.1109/MILCOM.2008.4753063.

[24] GARMATYUK, D., SCHUERGER, J., KAUFFMAN, K., et al. "Wideband OFDM system for radar and communications". In: *2009 IEEE Radar Conference*, pp. 1–6, May 2009.

[25] GARMATYUK, D., KAUFFMAN, K. "Radar and data communication fusion with UWB-OFDM software-defined system". In: *2009 IEEE International Conference on Ultra-Wideband*, pp. 454–458, Sept 2009.

[26] FALCONE, P., COLONE, F., BONGIOANNI, C., et al. "Experimental results for OFDM WiFi-based passive bistatic radar". In: *2010 IEEE Radar Conference*, pp. 516–521, May 2010.

[27] STURM, C., ZWICK, T., WIESBECK, W., et al. “Performance verification of symbol-based OFDM radar processing”. In: *2010 IEEE Radar Conference*, pp. 60–63, May 2010.

[28] REICHARDT, L., STURM, C., GRÜNHAUPT, F., et al. “Demonstrating the use of the IEEE 802.11P Car-to-Car communication standard for automotive radar”. In: *2012 6th European Conference on Antennas and Propagation (EUCAP)*, pp. 1576–1580, March 2012.

[29] SHI, C., WANG, F., SELLATHURAI, M., et al. “Low Probability of Intercept-Based Optimal Power Allocation Scheme for an Integrated Multistatic Radar and Communication System”, *IEEE Systems Journal*, v. 14, n. 1, pp. 983–994, Mar. 2020.

[30] SHI, C., WANG, F., SALOUS, S., et al. “Joint Subcarrier Assignment and Power Allocation Strategy for Integrated Radar and Communications System Based on Power Minimization”, *IEEE Sensors Journal*, v. 19, n. 23, pp. 11167–11179, Dec. 2019.

[31] ZHOU, Y., ZHOU, H., ZHOU, F., et al. “Resource Allocation for a Wireless Powered Integrated Radar and Communication System”, *IEEE Wireless Communications Letters*, v. 8, n. 1, pp. 253–256, Feb. 2019.

[32] LIU, Y., LIAO, G., XU, J., et al. “Adaptive OFDM Integrated Radar and Communications Waveform Design Based on Information Theory”, *IEEE Communications Letters*, v. 21, n. 10, pp. 2174–2177, Oct 2017.

[33] HU, L., DU, Z., XUE, G. “Radar-communication integration based on OFDM signal”. In: *2014 IEEE International Conference on Signal Processing, Communications and Computing (ICSPCC)*, pp. 442–445, Aug 2014.

[34] Y. L. SIT, C. STURM, L. R. T. Z. W. W. “The OFDM joint radar-communication system: an overview”, *in Proc. 3rd Int. Conf. SPACOMM*, pp. 69–74, Apr. 2011.

[35] SIT, Y. L., ZWICK, T. “MIMO OFDM radar with communication and interference cancellation features”. In: *2014 IEEE Radar Conference*, pp. 0265–0268, May 2014.

[36] LI, B., PETROPULU, A. P., TRAPPE, W. "Optimum Co-Design for Spectrum Sharing between Matrix Completion Based MIMO Radars and a MIMO Communication System", *IEEE Transactions on Signal Processing*, v. 64, n. 17, pp. 4562–4575, Sep. 2016.

[37] XU, R., PENG, L., ZHAO, W., et al. "Radar mutual information and communication channel capacity of integrated radar-communication system using {MIMO}", {*ICT*} *Express*, v. 1, n. 3, pp. 102 – 105, 2015.

[38] QUIJADA, R. *Joint Radar and Communication Application for Traffic Safety System*. Ph.D. dissertation, Kungliga Tekniska Högskolan, Stockholm, Sweden, 2011.

[39] FRANKEN, G. E. A., NIKOOKAR, H., GENDEREN, P. V. "Doppler Tolerance of OFDM-coded Radar Signals". In: *2006 European Radar Conference*, pp. 108–111, Sept 2006.

[40] HARA, S., PRASAD, R. *Multicarrier Techniques for 4G Mobile Communications*. Norwood, MA, USA, Artech House, Inc., 2003. ISBN: 1580534821.

[41] RUCK, G. *Radar cross section handbook*. N. vol. 1. Plenum Press, 1970.

[42] SIT, Y. L., REICHARDT, L., STURM, C., et al. "Extension of the OFDM joint radar-communication system for a multipath, multiuser scenario". In: *IEEE RadarCon* , pp. 718–723, May 2011.

[43] XIA, Y., SONG, Z., LU, Z., et al. "A novel range-Doppler imaging algorithm with {OFDM} radar", *Chinese Journal of Aeronautics*, v. 29, n. 2, pp. 492 – 501, 2016.

[44] ZHENG, L., WANG, X. "Super-Resolution Delay-Doppler Estimation for OFDM Passive Radar", *IEEE Transactions on Signal Processing*, v. 65, n. 9, pp. 2197–2210, May 2017.

[45] GU, J. F., MOGHADDASI, J., WU, K. "Delay and Doppler shift estimation for OFDM-based radar-radio (RadCom) system". In: *2015 IEEE International Wireless Symposium (IWS 2015)*, pp. 1–4, March 2015.

[46] SIT, Y. L., STURM, C., ZWICK, T. "Doppler estimation in an OFDM joint radar and communication system". In: *2011 German Microwave Conference*, pp. 1–4, March 2011.

[47] KOSLOWSKI, S., BRAUN, M., JONDRAL, F. K. "Using Filter Bank Multicarrier signals for radar imaging". In: *IEEE/ION Position, Location and Navigation Symp.*, pp. 152–157, May 2014.

[48] CHEN, K., LIU, Y., ZHANG, W. "Study on integrated radar-communication signal of OFDM-LFM based on FRFT". In: *IET International Radar Conference 2015*, pp. 1–6, Oct 2015.

[49] SIT, Y. L., NUSS, B., BASAK, S., et al. "Demonstration of interference cancellation in a multiple-user access OFDM MIMO Radar-Communication network using USRPs". In: *2016 IEEE MTT-S International Conference on Microwaves for Intelligent Mobility (ICMIM)*, pp. 1–4, May 2016. doi: 10.1109/ICMIM.2016.7533927.

[50] HUI, S. Y., YEUNG, K. H. "Challenges in the migration to 4G mobile systems", *IEEE Communications Magazine*, v. 41, n. 12, pp. 54–59, Dec 2003.

[51] BOUDREAU, G., PANICKER, J., GUO, N., et al. "Interference coordination and cancellation for 4G networks", *IEEE Communications Magazine*, v. 47, n. 4, pp. 74–81, April 2009.

[52] I, C. L., ROWELL, C., HAN, S., et al. "Toward green and soft: a 5G perspective", *IEEE Communications Magazine*, v. 52, n. 2, pp. 66–73, February 2014.

[53] RAPPAPORT, T. S., SUN, S., MAYZUS, R., et al. "Millimeter Wave Mobile Communications for 5G Cellular: It Will Work!" *IEEE Access*, v. 1, pp. 335–349, 2013.

[54] BOCCARDI, F., HEATH, R. W., LOZANO, A., et al. "Five disruptive technology directions for 5G", *IEEE Communications Magazine*, v. 52, n. 2, pp. 74–80, February 2014.

[55] GUINARD, D., TRIFA, V., KARNOUSKOS, S., et al. "Interacting with the SOA-Based Internet of Things: Discovery, Query, Selection, and On-

Demand Provisioning of Web Services", *IEEE Transactions on Services Computing*, v. 3, n. 3, pp. 223–235, July 2010.

[56] KAREN ROSE, SCOTT ELDRIDGE, L. C. "The Internet of Things (IoT): An Overview". out. 2015. Disponível em: <http://www.internetsociety.org/sites/default/files/ISOC-IoT-Overview-20151022.pdf>.

[57] LEVANON, N. "Multifrequency complementary phase-coded radar signal", *IEEE Proc. Radar, Sonar and Navigation*, v. 147, n. 6, pp. 276–284, Dec. 2000.

[58] STURM, C., ZWICK, T., WIESBECK, W. "An OFDM system concept for joint radar and communications operations". In: *IEEE 69th Vehicular Technology Conf.*, pp. 1–5, Apr. 2009.

[59] ZHENG, L., WANG, X. "Super-Resolution Delay-Doppler Estimation for OFDM Passive Radar", *IEEE Transactions on Signal Processing*, v. 65, n. 9, pp. 2197–2210, May 2017.

[60] WEIB, M. "Single frequency surveillance radar network using an adapted; minimization approach for extended targets". In: *2016 4th International Workshop on Compressed Sensing Theory and its Applications to Radar, Sonar and Remote Sensing (CoSeRa)*, pp. 153–157, Sept 2016.

[61] PALMER, J. E., HARMS, H. A., SEARLE, S. J., et al. "DVB-T Passive Radar Signal Processing", *IEEE Transactions on Signal Processing*, v. 61, n. 8, pp. 2116–2126, April 2013.

[62] YANG, X., HUO, K., JIANG, W., et al. "A passive radar system for detecting UAV based on the OFDM communication signal". In: *Progress in Electromagnetic Research Symp.*, pp. 2757–2762, Aug, 2016.

[63] TIAN, X., SONG, Z. "On radar and communication integrated system using OFDM signal". In: *2017 IEEE Radar Conf.*

[64] BISHOP, R. *Intelligent Vehicle Technology and Trends*. Artech House, 2005.

[65] MEINEL, H. H. "Evolving automotive radar 2014; From the very beginnings into the future". In: *The 8th European Conf. on Antennas and Propagation*, pp. 3107–3114, Apr. 2014.

[66] JONES, W. D. "Keeping cars from crashing", *IEEE Spectrum*, v. 38, n. 9, pp. 40–45, Sep 2001.

[67] ETSI. *Intelligent Transport Systems (ITS); Vehicular Communications; C2C-CC Demonstrator 2008; Use Cases and Technical Specifications*. ETSI TR 102 698 V1.1.2, 2010.

[68] "IEEE Draft Standard for Information Technology - Telecommunications and information exchange between systems - Local and metropolitan area networks - Specific requirements - Part 11: Wireless LAN Medium Access Control (MAC) and Physical Layer (PHY) specifications Amendment : Wireless Access in Vehicular Environments", *IEEE Unapproved Draft Std P802.11p /D11.0, Mar 2010*, Mar 2010.

[69] FINK, J., BRAUN, M., JONDRAL, F. K. "Effects of Arbitrarily Spaced Subcarriers on Detection Performance in OFDM Radar". In: *2012 IEEE Vehicular Technology Conference (VTC Fall)*, pp. 1–5, Sept 2012.

[70] NUSS, B., SIT, L., ZWICK, T. "A novel technique for interference mitigation in OFDM radar using compressed sensing". In: *2017 IEEE MTT-S International Conference on Microwaves for Intelligent Mobility (ICMIM)*, pp. 143–146, March 2017.

[71] FISHLER, E., HAIMOVICH, A., BLUM, R., et al. "MIMO radar: an idea whose time has come". In: *Proceedings of the 2004 IEEE Radar Conference (IEEE Cat. No.04CH37509)*, pp. 71–78, April 2004.

[72] WU, X. H., KISHK, A. A., GLISSON, A. W. "MIMO-OFDM radar for direction estimation", *IET Radar, Sonar Navigation*, v. 4, n. 1, pp. 28–36, February 2010.

[73] LI, J., STOICA, P. "MIMO Radar with Colocated Antennas", *IEEE Signal Processing Magazine*, v. 24, n. 5, pp. 106–114, Sept 2007.

[74] HAIMOVICH, A. M., BLUM, R. S., CIMINI, L. J. "MIMO Radar with Widely Separated Antennas", *IEEE Signal Processing Magazine*, v. 25, n. 1, pp. 116–129, 2008.

[75] CONTU, M., LOMBARDO, P. "Sidelobe control for a MIMO radar virtual array". In: *2013 IEEE Radar Conference (RadarCon13)*, pp. 1–6, April 2013.

[76] LI, J., STOICA, P. *MIMO Radar Signal Processing*. Wiley - IEEE. Wiley, 2008.

[77] SIT, Y. L., NGUYEN, T. T., ZWICK, T. "3D Radar imaging with a MIMO OFDM-based radar". In: *2013 Asia-Pacific Microwave Conference Proceedings (APMC)*, pp. 68–70, Nov. 2013.

[78] NUSS, B., SIT, Y. L., ZWICK, T. "3D radar image fusion using OFDM-based MIMO radar". In: *2016 German Microwave Conference (GeMiC)*, pp. 209–212, March 2016.

[79] AUER, G. "3D MIMO-OFDM Channel Estimation", *IEEE Transactions on Communications*, v. 60, n. 4, pp. 972–985, April 2012.

[80] KETPAN, W., SELLATHURAI, M. "Compressive sensing-based 3D signal extraction for MIMO passive radar using OFDM waveforms". In: *2016 IEEE International Conference on Communications (ICC)*, pp. 1–6, May 2016.

[81] SIT, Y. L., ZWICK, T. "Automotive MIMO OFDM radar: Subcarrier allocation techniques for multiple-user access and DOA estimation". In: *European Radar Conference*, pp. 153–156, Oct. 2014.

[82] HAKOBYAN, G., YANG, B. "A novel OFDM-MIMO radar with non-equidistant dynamic subcarrier interleaving". In: *2016 European Radar Conference (EuRAD)*, pp. 45–48, Oct 2016.

[83] GERZAGUET, R., BARTZOUDIS, N., BALTAR, L. G., et al. "The 5G candidate waveform race: a comparison of complexity and performance", *EURASIP J. on Wireless Communications and Networking*, v. 2017, n. 1, pp. 13, Jan. 2017.

[84] SCHAICH, F., WILD, T. "Waveform contenders for 5G 2014; OFDM vs. FBMC vs. UFMC". In: *2014 6th International Symposium on Communications, Control and Signal Processing (ISCCSP)*, pp. 457–460, May 2014.

[85] FARHANG-BOROUJENY, B. "OFDM Versus Filter Bank Multicarrier", *IEEE Signal Processing Magazine*, v. 28, n. 3, pp. 92–112, May 2011.

[86] SAIDEH, M., BERBINEAU, M., DAYOUB, I. “5G waveforms for Railway”. In: *2017 15th International Conference on ITS Telecommunications (ITST)*, pp. 1–5, May 2017.

[87] RIDENOUR, L. N. *Radar system engineering / edited by Louis N. Ridenour*. McGraw-Hill New York, 1947.

[88] SKOLNIK, M. *Introduction to Radar Systems*. Electrical engineering series. McGraw-Hill, 2001.

[89] PATOLE, S. M., TORLAK, M., WANG, D., et al. “Automotive radars: A review of signal processing techniques”, *IEEE Signal Processing Magazine*, v. 34, n. 2, pp. 22–35, March 2017.

[90] PRASAD, R. *OFDM for Wireless Communications Systems*. Artech House universal personal communications series. Artech House, 2004.

[91] VAN NEE, R., PRASAD, R. *OFDM for Wireless Multimedia Communications*. Artech House universal personal communications series. Artech House, 2000.

[92] LELLOUCH, G., NIKOOKAR, H. “On the capability of a radar network to support communications”. In: *14th IEEE Symp. on Communications and Vehicular Technology in the Benelux*, pp. 1–5, Nov. 2007.

[93] NGUYEN, T. T. *Design and Analysis of Superresolution Algorithm and Signal Separation Technique for an OFDM-based MIMO Radar*. Ph.D. dissertation, Karlsruhe Institute of Technology (KIT), Karlsruhe, 2012.

[94] STURM, C., SIT, L., BRAUN, M., et al. “Spectrally interleaved multi-carrier signals for radar network applications and MIMO-radar”, *Radar, Sonar Navigation, IET*, v. 7, pp. 261–269, 03 2013.

[95] SIT, Y. L., NGUYEN, T. T., STURM, C., et al. “2D radar imaging with velocity estimation using a MIMO OFDM-based radar for automotive applications”. In: *European Radar Conference*, pp. 145–148, Oct. 2013.

[96] CHENG, L., HENTY, B. E., COOPER, R., et al. “A Measurement Study of Time-Scaled 802.11a Waveforms Over The Mobile-to-Mobile Vehicular Channel at 5.9 GHz”, *IEEE Communications Magazine*, v. 46, n. 5, pp. 84–91, May 2008.

[97] BRAUN, M. *OFDM Radar Algorithms in Mobile Communication Networks*. Ph.D. dissertation, Karlsruhe Institute of Technology (KIT), Karlsruhe, 2014.

[98] ROHLING, H. *OFDM: concepts for future communication systems*. Signals and Communication Technology. Springer Berlin Heidelberg, 2011.

[99] KOROWAJCZUK, L. *LTE, WiMAX and WLAN Network Design, Optimization and Performance Analysis*. Wiley, 2011.

[100] RICHARDS, M., HOLM, W., SCHEER, J. *Principles of Modern Radar: Basic Principles*. Electromagnetics and Radar. Institution of Engineering and Technology, 2010.

[101] WANG, W. *Multi-antenna Synthetic Aperture Radar*. CRC Press, Taylor & Francis, 2013.

[102] KARTHIK RAMASUBRAMANIAN, K. R., AGINSKIY, A. *Moving from legacy 24 GHz to state-of-the-art 77 GHz radar*. Relatório técnico, Texas Instruments, oct 2017.

[103] SIT, Y. L., ZWICK, T. "MIMO OFDM radar networks: Inter- & intra-system interference handling". In: *2014 Asia-Pacific Microwave Conference*, pp. 1318–1320, Nov. 2014.

[104] YUN, Y. H., KIM, C., KIM, K., et al. "A new waveform enabling enhanced QAM-FBMC systems". In: *IEEE 16th International Workshop on Signal Processing Advances in Wireless Communications*, pp. 116–120, Jun. 2015.

[105] QI, Y., AL-IMARI, M. "An enabling waveform for 5G QAM-FBMC: Initial analysis". In: *IEEE Conference on Standards for Communications and Networking* , pp. 1–6, Oct. 2016.

[106] M. BELLANGER, E. A. "FBMC physical layer : a primer ". 2010. Disponível em: <http://www.ict-phydyas.org/teamspace/internal-folder/FBMC-Primer-06-2010.pdf>.

[107] HO, Z., KIM, K., KIM, C., et al. "A QAM-FBMC Space-Time Block Code System with Linear Equalizers". In: *IEEE Globecom Workshops*, pp. 1–5, Dec 2015.

[108] BELLANGER, M., DAGUET, J. “TDM-FDM Transmultiplexer: Digital Polyphase and FFT”, *IEEE Transactions on Communications*, v. 22, n. 9, pp. 1199–1205, Sep 1974.

[109] BELLANGER, M. “FS-FBMC: An alternative scheme for filter bank based multicarrier transmission”. In: *5th International Symposium on Communications, Control and Signal Processing*, pp. 1–4, May 2012.

[110] KIM, C., KIM, K., YUN, Y. H., et al. “QAM-FBMC: A new multi-carrier system for post-OFDM wireless communications”. In: *IEEE Global Communications Conference* , pp. 1–6, Dec. 2015.

[111] ZHANG, X., CHEN, L., QIU, J., et al. “On the Waveform for 5G”, *IEEE Communications Magazine*, v. 54, n. 11, pp. 74–80, Nov. 2016.

[112] BANELLI, P., BUZZI, S., COLAVOLPE, G., et al. “Modulation Formats and Waveforms for 5G Networks: Who Will Be the Heir of OFDM?: An overview of alternative modulation schemes for improved spectral efficiency”, *IEEE Signal Processing Magazine*, v. 31, n. 6, pp. 80–93, Nov. 2014.

[113] A. FARHANG AND N. MARCHETTI AND L. E. DOYLE. “Low-complexity modem design for GFDM”, *IEEE Transactions on Signal Processing*, v. 64, n. 6, pp. 1507–1518, Mar. 2016.

[114] FETTWEIS, G., KRONDORF, M., BITTNER, S. “GFDM - Generalized Frequency Division Multiplexing”. In: *IEEE 69th Vehicular Technology Conf.*, pp. 1–4, Apr. .

[115] ZHANG, D., MATTHÉ, M., MENDES, L. L., et al. “A study on the link level performance of advanced multicarrier waveforms under MIMO wireless communication channels”, *IEEE Transactions on Wireless Communications*, v. 16, n. 4, pp. 2350–2365, Apr. 2017.

[116] MICHAILOW, N., GASPAR, I., KRONE, S., et al. “Generalized Frequency Division Multiplexing: Analysis of an alternative multi-carrier technique for next generation cellular systems”. In: *Int. Symp. on Wireless Communication Systems (ISWCS)*, pp. 171–175, Aug. 2012.

[117] MICHAILOW, N., MATTHÉ, M., GASPAR, I. S., et al. "Generalized Frequency Division Multiplexing for 5th generation cellular networks", *IEEE Transactions on Communications*, v. 62, n. 9, pp. 3045–3061, Sep. 2014.

[118] MATTHE, M., MICHAILOW, N., GASPAR, I., et al. "Influence of pulse shaping on bit error rate performance and out of band radiation of Generalized Frequency Division Multiplexing". In: *IEEE Int. Conf. on Communications Workshops*, pp. 43–48, Jun. 2014.

[119] ZHANG, D., MENDES, L. L., MATTHÉ, M., et al. "Expectation propagation for near-optimum detection of MIMO-GFDM signals", *IEEE Transactions on Wireless Communications*, v. 15, n. 2, pp. 1045–1062, Feb. 2016.

[120] MATTHE, M., MENDES, L. L., MICHAILOW, N., et al. "Widely linear estimation for space-time-coded GFDM in low-latency applications", *IEEE Transactions on Communications*, v. 63, n. 11, pp. 4501–4509, Nov. 2015.

[121] ZHANG, D., FESTAG, A., FETTWEIS, G. P. "Performance of Generalized Frequency Division Multiplexing based physical layer in vehicular communications", *IEEE Transactions on Vehicular Technology*, v. 66, n. 11, pp. 9809–9824, Nov. 2017.

[122] AL-HASAANI, N. A., NAMDAR, M., ILHAN, H. "Energy detection of spectrum sensing for cognitive radio networks using GFDM modulation". In: *10th Int. Conf. on Electrical and Electronics Engineering*, pp. 690–694, Nov. 2017.

[123] GARCIA-ROGER, D., DE VALGAS, J. F., MONSERRAT, J. F., et al. "Hardware testbed for sidelink transmission of 5G waveforms without synchronization". In: *IEEE 27th Annual International Symposium on Personal, Indoor, and Mobile Radio Communications (PIMRC)*, pp. 1–6, Sept 2016.

[124] VAKILIAN, V., WILD, T., SCHAICH, F., et al. "Universal-filtered multicarrier technique for wireless systems beyond LTE". In: *IEEE Globecom Workshops (GC Wkshps)*, pp. 223–228, Dec 2013.

[125] ZAYANI, R., MEDJAHDI, Y., SHAIEK, H., et al. "WOLA-OFDM: A Potential Candidate for Asynchronous 5G". In: *2016 IEEE Globecom Workshops (GC Wkshps)*, pp. 1–5, Dec 2016.

[126] KNOPP, R., KALTENBERGER, F., VITIELLO, C., et al. "Universal filtered multicarrier for machine type communications in 5G". In: *European Conference on Networks and Communications*, 06 2016.

[127] SHI, C., WANG, F., SELLATHURAI, M., et al. "Power minimization-based robust OFDM radar waveform design for radar and communication systems in coexistence", *IEEE Transactions on Signal Processing*, v. 66, n. 5, pp. 1316–1330, Mar. 2018.

[128] BERGER, C. R., DEMISSIE, B., HECKENBACH, J., et al. "Signal processing for passive radar using OFDM waveforms", *IEEE Journal of Selected Topics in Signal Processing*, v. 4, n. 1, pp. 226–238, Feb. 2010.

[129] SEN, S., NEHORAI, A. "Adaptive OFDM radar for target detection in multipath scenarios", *IEEE Transactions on Signal Processing*, v. 59, n. 1, pp. 78–90, Jan. 2011.

[130] LELLOUCH, G., MISHRA, A. K., INGGS, M. "Stepped OFDM radar technique to resolve range and doppler simultaneously", *IEEE Transactions on Aerospace and Electronic Systems*, v. 51, n. 2, pp. 937–950, Apr. 2015.

[131] SEN, S., NEHORAI, A. "OFDM MIMO radar with mutual-information waveform dsign for low-grazing angle tracking", *IEEE Transactions on Signal Processing*, v. 58, n. 6, pp. 3152–3162, Jun. 2010.

[132] CHEN, Z., GOKEDA, G., YU, Y. *Introduction to Direction-of-arrival Estimation*. Artech House, 2010.

[133] **J. SANSON**, GAMEIRO, A., CASTANHEIRA, D., et al. "Comparison of DoA algorithms for MIMO OFDM radar". In: *European Radar Conference*, Set. 2018.

[134] M. AL-ARDI, E., SHUBAIR, R., AL-MUALLA, M. "Direction of arrival estimation in a multipath environment: An overview and a new contribution", *Applied Computational Electromagnetics Society Journal*, v. 21, pp. 226–238, 11 2006.

[135] SCHMIDT, R. "Multiple emitter location and signal parameter estimation", *IEEE Transactions on Antennas and Propagation*, v. 34, n. 3, pp. 276–280, Mar. 1986.

[136] R. ZHANG, Y. QUAN, S. Z. L. Y. Y. L., XING, M. "Joint High-Resolution Range and DOA Estimation via MUSIC Method Based on Virtual Two-Dimensional Spatial Smoothing for OFDMRadar", *International Journal of Antennas and Propagation*, v. 2018, pp. 9, Nov. 2018.

[137] SIT, Y. L., NGUYEN, T. T., STURM, C., et al. "2D radar imaging with velocity estimation using a MIMO OFDM-based radar for automotive applications". In: *2013 European Radar Conference*, pp. 145–148, Oct. 2013.

[138] ZHENG, L., WANG, X. "Super-Resolution Delay-Doppler Estimation for OFDM Passive Radar", *IEEE Transactions on Signal Processing*, v. 65, n. 9, pp. 2197–2210, May. 2017.

[139] THAKRE, A., HAARDT, M., GIRIDHAR, K. "Single Snapshot Spatial Smoothing With Improved Effective Array Aperture", *IEEE Signal Processing Letters*, v. 16, n. 6, pp. 505–508, June 2009.

[140] FRIEDLANDER, B., WEISS, A. J. "Direction finding using spatial smoothing with interpolated arrays", *IEEE Transactions on Aerospace and Electronic Systems*, v. 28, n. 2, pp. 574–587, Apr. 1992.

[141] DU, W., KIRLIN, R. L. "Improved spatial smoothing techniques for DOA estimation of coherent signals", *IEEE Transactions on Signal Processing*, v. 39, n. 5, pp. 1208–1210, May 1991.

[142] XU, H., WANG, D., BA, B., et al. "Direction-of-Arrival Estimation for Both Uncorrelated and Coherent Signals in Coprime Array", *IEEE Access*, v. 7, pp. 18590–18600, Feb. 2019.

[143] PRASAD, S., WILLIAMS, R. T., MAHALANABIS, A. K., et al. "A transform-based covariance differencing approach for some classes of parameter estimation problems", *IEEE Transactions on Acoustics, Speech, and Signal Processing*, v. 36, n. 5, pp. 631–641, May 1988.

[144] **J. SANSON**, GAMEIRO, A., CASTANHEIRA, D., et al. "24 GHz QAM-FBMC radar with communication system (RadCom)". In: *Asia-Pacific Microwave Conference*, pp. 1318–1320, Aug. 2018.

[145] HAKOBYAN, G., YANG, B. "High-Performance Automotive Radar: A review of signal processing algorithms and modulation schemes", *IEEE Signal Processing Magazine*, v. 36, n. 5, pp. 32–44, Sep. 2019.

[146] **J. SANSON**, CASTANHEIRA, D., GAMEIRO, A., et al. "Non-Orthogonal Multicarrier Waveform for Radar With Communications Systems: 24 GHz GFDM RadCom", *IEEE Access*, v. 7, pp. 128694–128705, Set. 2019.

[147] KIM, K. ., SEO, D. ., KIM, H. . "Radar target identification using one-dimensional scattering centres", *IEE Proceedings - Radar, Sonar and Navigation*, v. 148, n. 5, pp. 285–296, Oct. 2001.

[148] LI, X., MA, X., YAN, S., et al. "Super-resolution time delay estimation for narrowband signal", *IET Radar, Sonar Navigation*, v. 6, n. 8, pp. 781–787, Oct. 2012.

[149] URAZGHILDIIEV, I., RAGNARSSON, R., RYDBERG, A. "High-Resolution Estimation of Ranges Using Multiple-Frequency CW Radar", *IEEE Transactions on Intelligent Transportation Systems*, v. 8, n. 2, pp. 332–339, Jun. 2007.

[150] JAKOBSSON, A., SWINDLEHURST, A. L., STOICA, P. "Subspace-based estimation of time delays and Doppler shifts", *IEEE Transactions on Signal Processing*, v. 46, n. 9, pp. 2472–2483, Sep. 1998.

[151] ROY, R., PAULRAJ, A., KAILATH, T. "Estimation of Signal Parameters via Rotational Invariance Techniques - ESPRIT". In: *Military Communications Conference - Communications-Computers: Teamed for the 90's, 1986. MILCOM 1986. IEEE*, v. 3, pp. 41.6.1–41.6.5, Oct 1986.

[152] KUMARESAN, R., TUFTS, D. W. "Estimating the Angles of Arrival of Multiple Plane Waves", *IEEE Transactions on Aerospace and Electronic Systems*, v. AES-19, n. 1, pp. 134–139, Jan 1983.

[153] THOMPSON, J. S., GRANT, P. M., MULGREW, B. "Performance of spatial smoothing algorithms for correlated sources", *IEEE Transactions on Signal Processing*, v. 44, n. 4, pp. 1040–1046, April 1996.

[154] SCHMIDT, R. "Multiple emitter location and signal parameter estimation", *IEEE Transactions on Antennas and Propagation*, v. 34, n. 3, pp. 276–280, Mar. 1986.

[155] TIE-JUN SHAN, WAX, M., KAILATH, T. "On spatial smoothing for direction-of-arrival estimation of coherent signals", *IEEE Transactions on Acoustics, Speech, and Signal Processing*, v. 33, n. 4, pp. 806–811, Aug. 1985.

[156] RUSSELL, M. E., CRAIN, A., CURRAN, A., et al. "Millimeter-wave radar sensor for automotive intelligent cruise control (ICC)", *IEEE Transactions on Microwave Theory and Techniques*, v. 45, n. 12, pp. 2444–2453, Dec. 1997.

[157] WU, S., DECKER, S., CHANG, P., et al. "Collision Sensing by Stereo Vision and Radar Sensor Fusion", *IEEE Transactions on Intelligent Transportation Systems*, v. 10, n. 4, pp. 606–614, Dec. 2009.

[158] COLONE, F., FALCONE, P., BONGIOANNI, C., et al. "WiFi-Based Passive Bistatic Radar: Data Processing Schemes and Experimental Results", *IEEE Transactions on Aerospace and Electronic Systems*, v. 48, n. 2, pp. 1061–1079, Apr. 2012.

[159] SEN, S., NEHORAI, A. "Adaptive Design of OFDM Radar Signal With Improved Wideband Ambiguity Function", *IEEE Transactions on Signal Processing*, v. 58, n. 2, pp. 928–933, Feb. 2010.

[160] FOLSTER, F., ROHLING, H. "Data association and tracking for automotive radar networks", *IEEE Transactions on Intelligent Transportation Systems*, v. 6, n. 4, pp. 370–377, Dec 2005.

[161] OGREN, P., FIORELLI, E., LEONARD, N. E. "Cooperative control of mobile sensor networks:Adaptive gradient climbing in a distributed environment", *IEEE Transactions on Automatic Control*, v. 49, n. 8, pp. 1292–1302, Aug. 2004.

[162] ZHAO, X., SUN, P., XU, Z., et al. “Fusion of 3D LIDAR and Camera Data for Object Detection in Autonomous Vehicle Applications”, *IEEE Sensors Journal*, pp. 1–1, Jan. 2020.

[163] CHAVEZ-GARCIA, R. O., AYCARD, O. “Multiple Sensor Fusion and Classification for Moving Object Detection and Tracking”, *IEEE Transactions on Intelligent Transportation Systems*, v. 17, n. 2, pp. 525–534, Feb. 2016.

[164] LYTRIVIS, P., THOMAIDIS, G., TSOGAS, M., et al. “An Advanced Cooperative Path Prediction Algorithm for Safety Applications in Vehicular Networks”, *IEEE Transactions on Intelligent Transportation Systems*, v. 12, n. 3, pp. 669–679, Sep. 2011.

[165] HAMMARSTRAND, L., SVENSSON, L., SANDBLOM, F., et al. “Extended Object Tracking using a Radar Resolution Model”, *IEEE Transactions on Aerospace and Electronic Systems*, v. 48, n. 3, pp. 2371–2386, Jul. 2012.

[166] CAVENEY, D. “Cooperative Vehicular Safety Applications”, *IEEE Control Systems Magazine*, v. 30, n. 4, pp. 38–53, Aug. 2010.

[167] STEINBAECK, J., STEGER, C., HOLWEG, G., et al. “Next generation radar sensors in automotive sensor fusion systems”. In: *2017 Sensor Data Fusion: Trends, Solutions, Applications (SDF)*, pp. 1–6, Oct. 2017.

[168] WANG, Z., WU, Y., NIU, Q. “Multi-Sensor Fusion in Automated Driving: A Survey”, *IEEE Access*, v. 8, pp. 2847–2868, Jan. 2020.

[169] LERRO, D., BAR-SHALOM, Y. “Tracking with debiased consistent converted measurements versus EKF”, *IEEE Transactions on Aerospace and Electronic Systems*, v. 29, n. 3, pp. 1015–1022, Jul. 1993.

[170] RAMACHANDRA, K. *Kalman Filtering Techniques for Radar Tracking*. Taylor & Francis, 2000.

[171] COLERI, S., ERGEN, M., PURI, A., et al. “Channel estimation techniques based on pilot arrangement in OFDM systems”, *IEEE Transactions on Broadcasting*, v. 48, n. 3, pp. 223–229, Sep. 2002.

[172] JAVAUDIN, J., LACROIX, D., ROUXEL, A. “Pilot-aided channel estimation for OFDM/OQAM”. In: *The 57th IEEE Semiannual Vehicular Technology Conference*, v. 3, pp. 1581–1585 vol.3, Apr. 2003.

[173] C. LELE, J. P. JAVAUDIN, R. L. A. S. P. S. “Channel estimation methods for preamble-based OFDM/OQAM modulations”, *European Transactions on Telecommunications*, v. 19, n. 7, pp. 741–750, Nov. 2008.

[174] CHOI, J., OH, Y., LEE, H., et al. “Pilot-Aided channel estimation utilizing intrinsic interference for FBMC/OQAM Systems”, *IEEE Transactions on Broadcasting*, v. 63, n. 4, pp. 644–655, Dec. 2017.